UNIVERSIDADE DE BRASÍLIA - UNB

INSTITUTO DE GEOCIÊNCIAS – IG

PROGRAMA DE PÓS-GRADUAÇÃO EM GEOLOGIA – PPGG/IG

CARACTERIZAÇÃO E METALOGÊNESE DO DEPÓSITO DE NI DO JAGUAR, PROVÍNCIA MINERAL DE CARAJÁS.

Dissertação de Mestrado

Mariana Mota Ferraz de Oliveira

Orientador: Prof. Dr. Cesar Fonseca Ferreira Filho (IG-UnB)

Coorientadora: Profª. Drª. Maria Emilia Schutesky Della Giustina (IG-UnB)

Examinadores: Prof. Dr. Nilson Francisquini Botelho (IG-UnB)

Prof. Dr. Roberto Perez Xavier (IG-Unicamp)

Brasília – DF

Fevereiro 2017

AGRADECIMENTOS

À Universidade de Brasília (UnB) e ao Programa de Pós-Graduação em Geologia (PPGG) pela infraestrutura disponibilizada para a realização desta pesquisa;

À Coordenação de Aperfeiçoamento de Pessoal de Nível Superior (CAPES) pela concessão da bolsa de estudos durante o período de realização da pesquisa;

À Vale S.A. por ter disponibilizado os dados e testemunhos de sondagem, pelo suporte em trabalhos de campo e pelo apoio financeiro para análises químicas. Gostaria de agradecer particularmente aos meus antigos gestores, os geólogos e amigos queridos Fernando Greco (Gerente de Exploração Brasil) e Fernando Matos (Especialista Técnico em Geologia), por todo o apoio que deram ao meu trabalho. Um agradecimento mais que especial vai para o geólogo e amigo Wolney Rosa (Gerente de Integração e Geração de Projetos), pela disponibilidade para participar das discussões geológicas, pelo apoio nos trabalhos de campo, por ter sempre disponibilizado os dados prontamente, pelo ajuda na redação do texto, enfim, muito grata por tudo, Wolney!

Ao meu orientador, Prof. Cesar Fonseca Ferreira Filho, pela orientação sempre dedicada, pelo comprometimento com o trabalho de qualidade e pela vontade de transmitir seu conhecimento (e pela paciência, é claro!);

À minha coorientadora Prof. Maria Emilia Schutesky Della Giustina, pela participação no trabalho e pela amizade e animação de sempre;

A todos os meus antigos colegas de trabalho que de alguma forma participaram da pesquisa, em especial ao Leandro José de Oliveira, Denis Costa, Sergio Huhn, Rogerio Kiwitko e Denise Rocha;

Ao pessoal do Laboratório de Microssonda Eletrônica (UnB): Isabela, Iris e Jaqueline pela assistência durante a realização das análises;

Aos meus colegas de pós-graduação pelo companheirismo, amizade, animação e pelo suporte geológico/tecnológico: Alan, Betão, Felipe, Simone, Mara, Daniel, Claudia, Fifty, Eduardo, Alisson, Ana, Karen, Hammel, Carol, Alanna, Max, Marcos e Nivia. Um agradecimento mais que especial vai para minha colega de pós e amiga querida Chris Fianco, pela contribuição no momento final de entrega (<3), ao Vitor (Dalit) pelas boas risadas, à Prof. Julia Curto Ma-Ra (que não é colega da pós mas foi da graduação) e à Lolo, pelas longas discussões geológicas no horário do almoço;

Ao meu namorado, Jérémie, meu fornecedor oficial de material bibliográfico, por ter se aventurado no mundo dos IOCGs e por ter sido parceiro nessa jornada, me incentivando e inspirando sempre (merci :*);

Aos meus pais, Geraldo e Rosangela, pelo apoio incondicional nas minhas decisões, por providenciarem todas as condições necessárias para o desenvolvimento da minha vida acadêmica e pela paciência e carinho ao longo deste período e de toda a vida <3.

Índice

Índice de Figuras

Índice de Tabelas

RESUMO

O depósito Jaguar representa uma descoberta importante de Ni de origem hidrotermal e está localizado na porção sudoeste da Província Mineral de Carajás no estado do Pará. Depósitos hidrotermais de Ni são raros e geralmente possuem menor importância econômica, quando comparados com depósitos de Ni-Cu-PGE de origem magmática. No entanto, o depósito Jaguar possui recursos preliminares de 92 Mt @ 0.65 % Ni (*cut-off* 0.4% Ni) e possui potencial para se tornar um depósito de classe mundial. O depósito possui muitas características comuns aos depósitos IOCG de Carajás. O depósito Jaguar está hospedado em rochas granito-gnáissicas da Suíte Plaquê e Complexo Xingu, na porção norte e em rochas subvulcânicas félsicas do Supergrupo Itacaiúnas, na porção sul. Encontra-se encaixado ao longo de zonas de alteração hidrotermal, controladas estruturalmente por falhamentos regionais, de direção W-NW, e por zonas de cisalhamento dúcteis-rúpteis. Estas zonas de alteração estão principalmente confinadas ao contato entre as rochas granito-gnáissicas e as rochas subvulcânicas félsicas e formam corpos lenticulares, alongados na direção W-NW e subverticais. Rochas encaixantes sem alteração ou fracamente alteradas gradam para corpos de alteração pervasiva, em que a alteração é crescente em direção aos corpos de minério. O sistema hidrotermal desenvolvido no depósito é complexo e pode ser caracterizado por estágios de alterações superimpostas que se inicia com alteração a biotita-clorita (± quartzo, magnetita, apatita, alanita, titanita, fluorita, zircão, turmalina e epidoto). Esta alteração ocorre de forma expansiva e está associada a um regime de deformação dúctil. Neste estágio ocorre forte enriquecimento em FeO e MgO, acompanhado de enriquecimento leve em K_2O e depleção em Na_2O. Localmente ocorre cloritização, formando bandas ricas em clorita, principalmente na porção norte do depósito. Alteração a anfibólio-biotita ocorre de forma localizada e se sobrepõe aos estágios de alteração iniciais. Este tipo de alteração é restrito e ocorre principalmente associado à mineralização. O conteúdo de CaO aumenta neste estágio. Alteração a magnetita-apatita-quartzo (± anfibólio, clorita, e biotita) segue os estágios iniciais e é caracterizada por forte enriquecimento em FeO, P_2O_5 e F. Este tipo de alteração ocorre em regime deformacional predominantemente rúptil e formas corpos brechados. O ultimo estágio significativo do sistema hidrotermal é o evento mineralizante, o qual forma corpos subverticais, de direção W-NW, que se sobrepõem ou cortam as zonas de alteração. O principal sulfeto é pirita, seguida por milerita, pentlandita, calcopirita, pirrotita, e esfalerita. A mineralização mais abundante ocorre na forma de veios ou disseminada e hospeda os mais baixos teores de Ni. Brechas e sulfetos maciços ocorrem de forma subordinada e hospedam os mais altos teores. Veios tardios de fluorita, carbonatos, quartzo, e clorita (subordinada) ocorrem cortando os corpos mineralizados. Os produtos de alteração hidrotermal do depósito Jaguar são enriquecidos em ETRL, Fe, U, P, Pb, Ni e Co, uma característica comum nos depósitos IOCG de Carajás. Uma feição importante no depósito Jaguar é o enriquecimento anômalo em F que contrasta com os valores mais baixos de Cl. Esta feição difere do que é encontrado normalmente nos depósitos IOCG, os quais são normalmente mais enriquecidos em Cl do que em F. Umas das possibilidades apresentadas neste trabalho para a fonte do Ni são as rochas máfica-ultramáficas, de ampla ocorrência principalmente na porção sul do Domínio Carajás. Os teores de Pt-Pd do depósito Jaguar são baixos, normalmente abaixo do limite de detecção. Se estas rochas máfico-ultramáficas forem pobres em PGE, é razoável dizer que o depósito Jaguar teve origem em um modelo que envolve mobilização de Ni e Cu por fluidos hidrotermais de rochas máfica-ultramáficas em

profundidade abaixo do depósito. A falta de associação direta da mineralização do depósito Jaguar com rochas máfica-ultramáficas contrasta com o que é encontrado na maioria dos depósitos de Ni hidrotermal descritos na literatura e com todos os depósitos de Ni de origem magmática. Esta feição representa um aspecto importante para prospecção de Ni. A possibilidade de associar a mineralização hidrotermal de Ni com os depósitos de Cu-Au de Carajás pode aumentar a abrangência prospectiva de depósitos de Ni em escala mundial. A abundância de rochas máfica-ultramáficas na porção sul do Domínio Carajás somados a presença de um sistema hidrotermal eficiente na província pode indicar possibilidades de mobilização de Ni por fluidos hidrotermais e posterior mineralização.

ABSTRACT

The Jaguar deposit represents an important hydrothermal Ni sulfide discovery in recent years. It is located in the southwestern portion of the Carajás Mineral Province, one of the most important Cu-Au districts in the world. Hydrothermal Ni deposits are rare and have minor economic significance compared to magmatic Ni-Cu-PGE deposits. However, the Jaguar deposit has preliminary resources of 92 Mt @ 0.65% Ni (cut-off 0.4% Ni), with potential for world-class. Many characteristics of the deposit are comparable to those found in IOCG deposits from the Carajás Mineral Province. The Jaguar deposit is hosted by felsic subvolcanic rocks from the Itacaiunas Supergroup in the southern portion and granitic-gneissic rocks from the Plaquê Suite and Xingú Complex in the northern portion. It is located along hydrothermal alteration zones, structurally controlled by W-NW regional-scale faults and brittle-ductile shear zones. Alteration zones are mainly confined to the contact between the granitic-gneissic rocks and felsic subvolcanic rocks, and they form W-NW striking, lens-shaped, steeply dipping bodies. Unaltered to poorly altered host rocks grade to pervasively altered bodies with increasing hydrothermal alteration towards the mineralized zones. A complex hydrothermal system characterized by overlapping stages begins with pervasive biotite-chlorite (± quartz, magnetite, apatite, allanite, titanite, fluorite, zircon, tourmaline and epidote) alteration. This alteration type is the most widespread and occurs under ductile conditions. FeO and MgO enrichment, matched with mild K_2O enrichment and decrease in Na_2O, occur in this stage. Chloritization can locally form chlorite-rich bands, mostly in the northern part of the deposit. Amphibole-biotite alteration locally overprints early alteration zones. This alteration type is restricted and occurs mainly associated to the mineralized zones. CaO contents increase in this stage. The early alteration stages are followed by magnetite-apatite-quartz (± amphibole, chlorite and biotite) alteration, characterized by strong FeO, P_2O_5 and F enrichment. This alteration type takes place under a brittle regime and forms brecciated bodies. The mineralizing event is the last stage of the hydrothermal system and forms W-NW striking, steeply dipping bodies, overprinting and crosscutting alteration zones. Pyrite is the main sulfide, followed by millerite, pentlandite and minor chalcopyrite, pyrrhotite and sphalerite. Vein and disseminated mineralization style are more common and host lower Ni grades whereas subordinate breccia and massive mineralization style hosts the highest Ni grades. Post-mineralization alteration is represented by late veins of fluorite, carbonate, quartz and minor chlorite that crosscut the mineralized bodies. The hydrothermal alteration products from the Jaguar deposit are enriched in LREE, Fe, U, P, Pb, Ni and Co, as occurs in most IOCG deposits in Carajás. An important feature in the Jaguar deposit is the unusually high F content, contrasting with the lower Cl contents, differing from IOCG deposits in Carajás that have higher Cl contents when compared to F contents. A possible source of Ni for the Jaguar deposit is the Ni present in mafic-ultramafic rocks, fairly abundant in the southern portion of the Carajás Domain. Pt-Pd contents in the Jaguar deposit are very low, normally below the detection limits. If these mafic-ultramafic rocks are PGE-poor, it seems suitable that Ni mineralization from the Jaguar deposit was originated in a model that involves mobilization of Ni and Cu by hydrothermal fluids from mafic-ultramafic rocks at depth below the deposit. The lack of direct association between the Jaguar deposit and mafic-ultramafic rocks contrasts with most hydrothermal Ni deposits described in literature and with all magmatic Ni deposits. This feature represents an important prospective highlight for Ni exploration. The possible association of hydrothermal Ni sulfide

mineralization with Cu-Au deposits in Carajás provides a significant venue for research, which may enlarge the scope of hydrothermal deposits worldwide. The abundance of mafic-ultramafic rocks in the southern portion of the Carajás Domain and the presence of a widespread hydrothermal system can indicate possibilities of Ni leaching by hydrothermal fluids and later mineralization.

CONSIDERAÇÕES GERAIS

1. Introdução

A presente dissertação de mestrado consiste na primeira caracterização geológica e geoquímica do depósito de níquel Jaguar, localizado na Província Mineral de Carajás (PMC), próximo ao Complexo Máfico-Ultramáfico Serra do Puma (Ferreira Filho et al., 2007; Rosa, 2014). Diferente do que ocorre em depósitos magmáticos de Ni-Cu-PGE, a mineralização sulfetada no depósito Jaguar está hospedada em rochas subvulcânicas félsicas e graníticas e está encaixada ao longo de zonas de alteração hidrotermal com características dúcteis-rúpteis. Estas feições sugerem que o depósito Jaguar representa uma descoberta rara e significativa de depósito de níquel de origem hidrotermal.

Depósitos hidrotermais de níquel são relativamente raros e de menor importância econômica, ocorrendo geralmente associados a remobilização de depósitos magmáticos em rochas máfico-ultramáficas ou em depósitos polimetálicos (Cu-Ni-Co-Au) em folhelhos negros (Gonzalez-Álvarez et al., 2013). A solubilidade relativamente baixa de sulfetos de Ni comparada com outros metais (e.g. Cu, Co, Au) em sistemas hidrotermais é apontada como justificativa para a pouca importância dos depósitos de Ni hidrotermal (Liu et al., 2012). Os estudos desenvolvidos no depósito Jaguar indicaram a existência de mineralizações de Ni em um sistema hidrotermal com características semelhantes aquelas observadas nos depósitos IOCG da região.

A PMC contem a maior concentração conhecida no mundo de depósitos de grande tonelagem do tipo IOCG (100–789 Mt @ 0.77–1.40 wt.% Cu e 0.28–0.86 g/t Au; Xavier et al., 2012;), representada principalmente pelos depósitos Salobo (789 Mt; Souza and Vieira, 2000), Gameleira (100 Mt), Igarapé Bahia/Alemão (219 Mt; Tallarico et al., 2005), Sossego (245 Mt; Lancaster Olivera et al., 2000), Cristalino (500 Mt; Huhn et al., 1999) e Alvo 118 (170 Mt; Rigon et al., 2000). O depósito Jaguar possui várias características semelhantes aos depósitos do tipo IOCG de Carajás que incluem a associação espacial com sequencias metavulcano-sedimentares, alteração hidrotermal rica em Fe, localização ao longo de zonas de cisalhamentos regionais e mineralização associada a brechas de ocorrência tardia.

A possibilidade de associação da mineralização hidrotermal de Ni do depósito

Jaguar com os depósitos de Cu-Au de Carajás pode aumentar o escopo de depósitos hidrotermais em escala mundial. Este trabalho apresenta uma descrição detalhada do depósito Jaguar, baseada nos dados adquiridos ao longo dos anos de exploração pela Vale S.A. Dados complementares adquiridos neste estudo, como descrições geológicas e petrográficas, resultados analíticos adicionais, incluindo litogeoquímica e química mineral, providenciaram o embasamento para a origem da mineralização de níquel. O depósito Jaguar é interpretado neste estudo como pertencendo a uma classe importante, porem pouco conhecida, de depósitos de Ni de origem hidrotermal. Os resultados proporcionam maior conhecimento para exploração de Ni e guias prospectivos em um ambiente geológico diferente.

2. Localização e aspectos fisiográficos

O depósito Jaguar está situado na porção leste do município de São Félix do Xingu, no sudeste do Estado do Pará, a cerca de 50 km a norte das cidades de Tucumã e Ourilândia do Norte e a 10 km a norte do depósito de níquel laterítico localizado no Complexo Máfico-Ultramáfico Serra da Onça. A partir de Ourilândia, o acesso principal à área do depósito é feito pela estrada pavimentada que leva à planta da Mineração Onça-Puma (25 km), seguindo por uma estrada não pavimentada na direção norte, passando pela Serra Arqueada, em percurso de cerca de 25 km até a área do depósito.

A geomorfologia da área é caracterizada por um relevo de serras isoladas que se destacam sobre extensa superfície aplainada, com cotas entre 250 e 300 m acima do nível do mar. As Serras do Puma, da Onça e Arqueada (localizada entre as duas primeiras) dominam o relevo regional. Dentre estas serras, destaca-se a Serra Arqueada, de direção aproximadamente EW, cuja encosta norte hospeda a porção sul do depósito. A cota de topo está em torno de 650 m. A vegetação predominante é classificada como Floresta Tropical do tipo pluvial, integrada à zona de transição entre a Floresta Amazônica e os cerrados. Grande parte desta floresta deu lugar a áreas de pastagem. A região do depósito é drenada pela bacia do Rio Carapanã e Rio Fresco, afluentes do Rio Xingú que estão inseridos na bacia hidrográfica Amazônica. O clima da região é do tipo tropical, caracterizado por duas estações: chuvosa, de novembro a maio, com mais de 90% das precipitações; e seca, de junho a outubro. A média pluviométrica anual é de aproximadamente 2.000 mm e a umidade relativa do ar é bastante elevada, com média de 76%. A temperatura média anual é de 26°C.

3. Justificativa e objetivos

Depósitos de níquel formados por processos essencialmente hidrotermais, não associados a remobilização de depósitos magmáticos, são raros, e o conhecimento sobre este tipo de mineralização na PMC está limitado a apenas um prospecto reportado na literatura, o GT34 (Siepierski, 2008). O objetivo deste estudo é fazer a primeira caracterização geológica do depósito Jaguar, incluindo dados petrológicos, litogeoquímicos e de química mineral, que permitam caracterizar o depósito no contexto dos depósitos de Cu-Au hidrotermais da PMC. Este trabalho também tem como objetivo comparar o depósito Jaguar com outros depósitos de origem hidrotermal descritos na literatura. Adicionalmente, em vista das características geológicas peculiares que o depósito Jaguar apresenta, a sua caracterização geológica e geoquímica pode evidenciar uma nova tipologia de depósito de Ni. Os resultados destes estudos são relevantes para a exploração mineral em Carajás e sugerem possibilidades de avançar o conhecimento científico sobre o comportamento do níquel em processos hidrotermais.

4. Métodos

A fase inicial deste trabalho teve enfoque na revisão bibliográfica e integração de resultados (mapas, seções, descrições e litogeoquímica de testemunhos de sondagem, lâminas polidas, relatórios internos, etc) adquiridos em trabalhos de exploração desenvolvidos no depósito pela Vale S.A. Mapas de detalhe (1:10.000, com algumas regiões detalhadas em 1:5.000) foram confeccionados pela empresa durante os trabalhos de exploração na região (2007 a 2010). A empresa disponibilizou 7534 resultados analíticos de 32 furos de sondagem diamantada realizados no depósito ao longos dos anos de pesquisa.

O trabalho de campo foi realizado em fevereiro de 2015 e consistiu no reconhecimento regional, descrição de afloramentos e coleta de amostras de rocha (3 amostras), amostragem sistemática de 2 testemunhos de sondagem do depósito Jaguar (32 amostras), amostragem localizada de um furo de sondagem do depósito Serra Arqueada (4 amostras), totalizando 39 amostras. O trabalho contou com o apoio e participação de geólogos da Vale S.A, incluindo apresentações, discussões sobre o contexto geológico e alteração hidrotermal, dados de litogeoquímica e descrições de testemunhos.

Estudos petrográficos foram desenvolvidos em lâminas polidas de 35 amostras, abarcando a rocha hospedeira parcialmente preservada, o produto da alteração hidrotermal em diferentes estágios e a mineralização. Estudos petrográficos permitiram reconhecer diferentes estilos de alteração hidrotermal e intensidade, desde alteração parcial até rochas com alteração pervasiva. A partir destas informações, foram selecionadas 32 lâminas para o estudo de química mineral.

As análises de química mineral foram realizadas por microssonda electronica JEOL JXA-8230, em modo de dispersão por comprimentos de onda (WDS – Wavelength Dispersive Spectrometry), no Laboratório de Microssonda Eletrônica da Universidade de Brasília (ver item *Materials and Methods* do artigo anexo para informações mais detalhadas). Os minerais selecionados para análise química foram: anfibólio, biotita, clorita, apatita, magnetita, feldspatos e sulfetos (pirita, milerita, pentlandita, calcopirita e esfalerita). Durante as análises foram utlizados padrões naturais e sintéticos, e o mesmo procedimento foi mantido durante todo o processo analítico. O tratamento dos dados foi feito por meio de planilha electronica Excel e os resultados se encontram no Anexo I.

Os resultados de litogeoquímica fornecidos pela Vale S.A. foram realizados pelo laboratório SGS GEOSOL. Para estudos complementares, 25 amostras de testemunhos de sondagem foram selecionadas (DH127 e DH132) para análise no laboratório ALS Chemex (Canadá). Os resultados para estas amostras são apresentados na Tabela 01. A descrição detalhada das técnicas analíticas utilizadas se encontra no item *Materials and Methods* do artigo anexo.

5. Escopo do estudo

Conforme previsto no regulamento do curso de Pós-Graduação em Geologia da Universidade de Brasília, esta dissertação de mestrado foi estruturada na forma de artigo, intitulado "***The Jaguar Deposit: A Hydrothermal Nickel Sulfide Deposit in the Carajás Mineral Province, Brazil"***. O artigo é apresentado na forma que será submetido à revista *Economic Geology* mantendo o estilo e o formato previstos no periódico.

Referências

Ferreira Filho, C.F., Cançado, F., Correa, C., Macambira, E.M.B., Siepierski, L., and Brod, T.C.J., 2007, Mineralizações estratiformes de EGP-Ni associadas a complexos acamadados em Carajás: os exemplos de Luanga e Serra da Onça, in Contribuições à Geologia da Amazônia, Publitec Gráfica & Editora, v. 5, p. 01-14.

González-Álvarez, I., Pirajno, F., and Kerrich, R., 2013, Hydrothermal nickel deposits: Secular variation and diversity: Ore Geology Reviews, v. 52, p. 1–3.

Huhn, S.R.B., Souza, C.I.J., Albuquerque, M.C., Leal, E.D., and Brustolin, V., 1999, Descoberta do depósito Cu-(Au) Cristalino: Geologia e mineralização associada região da Serra do Rabo, Carajás, PA: Simpósio de Geologia da Amazônia, 6th, Belém, Sociedade Brasileira de Geologia, Proceedings, p. 140−143.

Lancaster Oliveira, J., Fanton, J., Almeida, A.J., Leveille, R.A., and Vieira, S., 2000, Discovery and geology of the Sossego copper-gold deposit, Carajás district, Pará State, Brazil: International Geology Congress, 31st, Rio de Janeiro, 6−17 August, Proceedings [CD-ROM].

Liu, W., Migdisov, A., and Williams-Jones, A., 2012, The stability of aqueous nickel (II) chloride complexes in hydrothermal solutions: results of UV–visible spectroscopic experiments: Geochimica et Cosmochimica Acta, v. 94, p. 276–290.

Rigon, J.C., Munaro, P., Santos, L.A., Nascimento, J.A.S., and Barreira, C.F., 2000, Alvo 118 copper-gold deposit: Geology and mineralization, Serra dos Carajás, Pará, Brazil [abs.]: International Geological Congress, 31st, Rio de Janeiro, Sociedade Brasileira de Geologia, International Union of Geological Sciences, Abstract Volume [CD-ROM].

Rosa, W.D., 2014, Complexos acamadados da Serra da Onça e Serra do Puma: geologia e petrologia de duas intrusões máfico-ultramáficas com sequência de cristalização distinta na Província Arqueana de Carajás, Brasil: Unpublished M.Sc. thesis, Brasilia, Brazil, Universidade de Brasilia, 65 p.

Siepierski, L., Geologia e petrologia do prospecto gt-34: evidência de metassomatismo de alta temperatura e baixa fo2, Província Mineral Carajás, Brasil, Unpublished M.Sc. thesis, Brasilia, Brazil, Universidade de Brasília, 72 p.

Souza, L.H., and Vieira, E.A.P., 2000, Salobo 3 Alpha deposit: Geology and mineralization, in Porter, T.M., ed., Hydrothermal iron-oxide copper-gold and related deposits: A global perspective: Adelaide, PGC Publishing, v. 1, p. 213−224.

Tallarico, F.H.B., Figueiredo, B.R., Groves, D.I., Kositcin, N., McNaughton, N.J., Fletcher I.R., and Rego J.L., 2005, Geology and SHRIMP U-Pb geochronology of the Igarapé Bahia deposit, Carajás copper-gold belt, Brazil: An Archean (2.57 Ga) example of iron-oxide Cu-Au-(U-REE) mineralization: Economic Geology, v. 100, p. 7−28.

Xavier, R.P., Monteiro, L.V.S., Moreto, C.P.N., Pestilho, A.L.S., Melo, G.H.C., Silva, M.A.D., Aires, B., Ribeiro, C., and Silva, F.H.F., 2012, The iron oxide copper-gold systems of the Carajás mineral province, Brazil: Society of Economic Geologists, Special Publication no. 16, p. 433–454.

To be submitted to the ECONOMIC GEOLOGY

The Jaguar Deposit: A Hydrothermal Nickel Sulfide Deposit in the Carajás Mineral Province, Brazil

Mariana Mota Ferraz de Oliveira[1]; Cesar Fonseca Ferreira Filho[1]; Maria Emilia Schutesky Della Giustina[1]; Wolney Dutra Rosa[2]

1 Instituto de Geociências, Universidade de Brasília, Brasília – DF, 70910-900, Brazil
2 Vale S.A., Rodovia BR 381, Santa Luzia – MG, 33040-900, Brazil

Abstract

The Jaguar deposit represents an important hydrothermal Ni sulfide discovery in recent years. It is located in the southwestern portion of the Carajás Mineral Province, one of the most important Cu-Au districts in the world. The Jaguar deposit has preliminary resources of 92 Mt @ 0.65% Ni (cut-off 0.4% Ni), with potential for world-class. Many characteristics of the deposit are comparable to those found in IOCG deposits from the Carajás Mineral Province. The Jaguar deposit is hosted by granitic-gneissic rocks in the northern portion and by felsic subvolcanic rocks in the southern portion. It is located along hydrothermal alteration zones, structurally controlled by W-NW regional-scale faults and ductile-brittle shear zones. Alteration zones are mainly confined to the contact between the granitic-gneissic rocks and felsic subvolcanic rocks, and they form W-NW striking, lens-shaped, steeply dipping bodies. The hydrothermal system begins with pervasive, widespread biotite-chlorite alteration under ductile conditions. Amphibole-biotite alteration locally overprints early alteration zones. The early alteration stages are followed by magnetite-apatite-quartz (± amphibole, chlorite and biotite) alteration, under a brittle regime. The late-stage mineralization forms W-NW striking, steeply dipping bodies, overprinting and crosscutting alteration zones. Pyrite is the main sulfide, followed by millerite, pentlandite and minor chalcopyrite, pyrrhotite and sphalerite. This mineral assemblage is always associated with abundant magnetite, suggesting oxidizing conditions of the hydrothermal system. Vein and disseminated mineralization style are more common and host lower Ni grades whereas subordinate breccia and massive mineralization style hosts the highest Ni grades. The hydrothermal alteration products from the Jaguar deposit are enriched in LREE, Fe, U, P, Pb, Ni and Co, as occurs in most IOCG deposits in Carajás. An important feature in the Jaguar deposit is the unusually high F content, contrasting with lower Cl contents, differing from most IOCG deposits in Carajás that usually have higher Cl than F contents. A possible source of Ni for the Jaguar deposit is the Ni present in mafic-ultramafic rocks, fairly abundant in the southern portion of the Carajás Domain. The lack of direct association between the Jaguar deposit and mafic-ultramafic rocks contrasts with what occurs in most hydrothermal Ni deposits described in literature and with all magmatic Ni deposits. This feature represents an important prospective highlight for Ni exploration. The possible association of hydrothermal Ni sulfide mineralization with Cu-Au deposits in Carajás provides a significant venue for research, which may enlarge the scope of hydrothermal deposits worldwide.

Key words: Hydrothermal Ni deposit, Carajás, Ni-Cu sulfides, hydrothermal alteration, IOCG.

Introduction

The Jaguar nickel sulfide deposit, located in the Carajás Mineral Province (CMP) in southeastern Brazil, was discovered by Vale S.A. in 2007. The deposit has preliminary resources of 92 Mt @ 0.65% Ni (cut-off 0.4% Ni) and the discovery resulted from a regional exploration program for Ni-PGE developed by Vale S.A. in the CMP. Different from magmatic Ni-Cu-PGE deposits, Ni sulfide mineralization in the Jaguar deposit is hosted by felsic subvolcanic and granitic rocks and located along ductile-brittle hydrothermal alteration zones. These features led to the suggestion that it represents a significant new discovery of a hydrothermal deposit (Vale S.A., internal report).

Hydrothermal nickel deposits are relatively rare and have minor economic significance compared to magmatic Ni-Cu-PGE deposits. They commonly occur associated with Ni remobilization in magmatic deposits or mafic-ultramafic rocks, as well as in polymetallic deposits (Cu-Ni-Co-Au) in black shales (González-Álvarez et al., 2013). The relatively low solubility of nickel sulfides when compared to other metals (e.g., Cu, Zn, Au) in hydrothermal systems is pointed out as the reason for the small importance of hydrothermal nickel deposits (Liu et al., 2012).

Recent studies in the CMP have indicated the occurrence of Ni mineralization in a hydrothermal system with similar characteristics as the IOCG deposits located in the region. The Jaguar deposit and the GT34 prospect (Siepierski, 2008) are examples of this mineralization type. The CMP contains the largest known concentration of large-tonnage (100–789 Mt at 0.77–1.40 wt.% Cu and 0.28–0.86 g/t Au) IOCG deposits in the world (Xavier et al., 2012). The Salobo (789 Mt; Souza and Vieira, 2000), Gameleira (100 Mt), and Igarapé Bahia/Alemão (219 Mt; Tallarico et al., 2005), Sossego (245 Mt; Lancaster Oliveira et al., 2000), Cristalino (500 Mt; Huhn et al., 1999a), and Alvo 118 (170 Mt; Rigon et al., 2000) deposits are the main examples of IOCG mineralization in the province (Fig. 1B). The Jaguar deposit shares a number of similarities with IOCG deposits in Carajás, including the common association with metavolcanic-sedimentary sequences, intense Fe hydrothermal alteration, location along major fault systems and late stage ore related breccias. The possible association of hydrothermal Ni sulfide mineralization with Cu-Au deposits in Carajás provides a significant venue for research, which may enlarge the scope of hydrothermal deposits

worldwide.

In this study we present a description of the Jaguar deposit based upon extensive exploration data acquired by Vale S.A. Geological descriptions, together with geochemical results from this study, including lithogeochemistry and mineral compositions provide a basic framework to constraint the origin of the Ni sulfide mineralization. The Jaguar deposit is interpreted in this study to belong to a significant but yet poorly investigated class of hydrothermal Ni deposits. Our findings provide insights for nickel exploration and prospective guides in different geological environments.

Discovery History

The Jaguar deposit is located nearby two world-class deposits, 2 km north of the Serra Arqueada Fe deposit and 10 km SW of the Serra do Puma Complex. These deposits are part of the first round of discoveries in the Carajás Mineral Province in the 60s. Strong magnetic anomalies, coincident with ultramafic rocks of the Serra do Puma Complex and banded iron formations of the Serra Arqueada, were indicated by regional airborne magnetic and radiometric surveys in the Carajás region, carried out by the Brazilian Geological Survey in the 70s and 80s. Vale S.A. carried out an additional and more detailed regional airborne magnetic and radiometric survey during the late 90s. This survey attested the strong and large magnetic anomalies previously identified, as well as less expressive and smaller anomalies located between the Serra do Puma and Serra Arqueada deposits. Discrete U and K anomalies were also identified, partly coincident with the magnetic anomalies. Based on the regional data available, Vale S.A. decided to verify these smaller and less expressive anomalies with high-resolution magnetic and electromagnetic airborne surveys in GEOTEM system, in the early 2000s. The GEOTEM data showed that they are characterized by high conductivity anomalies associated with strong magnetic anomalies. In 2005 an extensive soil geochemistry survey carried by Vale S.A. targeted both Ni-Cu-PGE deposits in the western portion of the Serra do Puma Complex and the geophysical anomalies indicated by the GEOTEM survey. Geochemical results indicated significant geochemical Ni anomalies within domains of felsic subvolcanic rocks. These unusual anomalies, disconnected from mafic-ultramafic rocks, were characterized by high nickel (up to 900 ppm) associated

with low Cr contents (< 50 ppm). Additional soil geochemistry surveys outlined a 4.5 km E-W trending zone of Ni anomalies. Induced polarization and ground time-domain electromagnetic data were acquired over 2D profiles to detail these anomalies and support the drilling program. The first hole drilled in 2007 (DH0001) intersected 79 m of sulfide mineralization grading 0.87 wt.% Ni. Following this result, a major drilling program totaling 55,000 m was completed in 2008-2010. The drilling results lead to the preliminary resource definition of 92 Mt @ 0.65 wt.% Ni (cut-off 0.4 wt.% Ni).

Geological Setting

The Carajás Mineral Province is one of the best-preserved cratonic areas in the world. It is located in the southeastern margin of the Archean Amazon Craton in Brazil (Fig. 1A) and is limited to the east and south by the Neoproterozoic Araguaia Fold Belt and to the west by overlying Proterozoic sequences of the Uatumã Supergroup (DOCEGEO, 1988; Araújo and Maia, 1991). To the north, it is limited by the Bacajá Domain, which includes reworked Archean terrains and juvenile Paleoproterozoic units (Vasquez et al., 2008a). The Carajás Mineral Province is divided into two Archean tectonic domains (Fig. 1B): the southern Rio Maria Domain and the northern Carajás Domain (Araújo et al., 1988; Araújo and Maia, 1991; Vasquez et al., 2008a). A poorly defined zone characterized by regional EW faults, designated as the Transition Subdomain (Feio et al., 2013), separates these two domains.

The Rio Maria Domain is a granite–greenstone terrain comprising greenstone belt sequences and meta-sedimentary rocks of the 2.97 to 2.90 Ga Andorinhas Supergroup (DOCEGEO, 1988; Macambira and Lancelot, 1996; Souza et al., 2001). Several Archean granitic suites with different composition and ages intruded the greenstone belt sequences. This domain is characterized by hosting orogenic lode-gold deposit (Grainger et al., 2008).

The Carajás Domain basement units consist of gneisses and migmatites of the Xingu Complex and mafic to felsic ortho-granulites of the Pium Complex (DOCEGEO, 1988; Machado et al., 1991; Pidgeon et al., 2000). Overlying the basement units is the Neoarchean Carajás Basin. It comprises the ca. 2.73 to 2.76 Ga metavolcanic-sedimentary units of the Rio Novo Group (Hirata et al., 1982) and the Itacaiúnas Supergroup (DOCEGEO, 1988; Machado et al., 1991). The Itacaiúnas Supergroup

encompasses the Grão Pará, Salobo, Igarapé Bahia and Igarapé Pojuca groups (Wirth et al., 1986; DOCEGEO, 1988; Machado et al., 1991). The Grão Pará Group is the dominant volcanic-sedimentary sequence in the Carajás Basin and contains the giant iron deposits such as Serra Norte, Serra Sul, Serra Leste and Serra São Felix, that contain total resources of 17.3 Gt @ 66% Fe (Tolbert et al., 1971; Gibbs and Wirth, 1990). The Itacaiúnas Supergroup also hosts several IOCG deposits such as Cristalino, Igarapé Bahia-Alemão, Salobo and Sossego. The Itacaiúnas Supergroup is overlain by an extensive succession of low-grade meta-sedimentary units known as the Águas Claras Formation (Nogueira, 1985; Araújo et al., 1988) or the Rio Fresco Group (DOCEGEO, 1988). These units cover large areas in the Carajás Mineral Province where it hosts the Azul manganese deposit (Costa et al., 2005), the Águas Claras and Breves Cu-Au deposits (Silva and Villas, 1998; Tallarico et al., 2004), and the Serra Pelada/Serra Leste Au–PGE deposits (Tallarico et al., 2000; Moroni et al., 2001).

Granitic magmatism crosscuts the Carajás Mineral Province comprising magmas of distinct ages and compositions, essentially correlated to three episodes: (1) Neoarchean intrusions (ca. 2.75 - 2.70) include syn-orogenic foliated alkaline granites and are widespread through the Carajás Domain; (2) Younger intrusions (ca. 2.5 Ga) are restricted to the north part of the Carajás Domain and include peralkaline to meta-aluminous granites, coeval with the Carajás and Cinzento transcurrent fault systems and (3) Paleoproterozoic episodes (ca. 1.88 Ga) of A-type alkaline granite formation are widespread in the CMP.

Several mafic-ultramafic complexes intrude the Xingu Complex and the Itacaiúnas Supergroup (DOCEGEO, 1988; Ferreira Filho et al., 2007) and were ascribed as part of the Cateté Intrusive Suite (e.g., Macambira and Ferreira Filho, 2002) and the Serra Leste Magmatic Suite (Ferreira Filho et al., 2007). The former is represented by the Serra da Onça, Serra do Puma, Jacaré-Jacarezinho, and Carapanã Complexes and the later by the Luanga and Lago Grande Complexes. Cr and Ni-PGE deposits (e.g., Luanga and Lago Grande Complexes; Ferreira Filho et al., 2007; Teixeira et al., 2015; Mansur and Ferreira Filho, 2016) and lateritic Ni deposits (e.g., Jacaré-Jacarezinho, Vermelho and Puma-Onça; Ferreira Filho et al., 2007; Rosa, 2014) are associated to these mafic-ultramafic complexes.

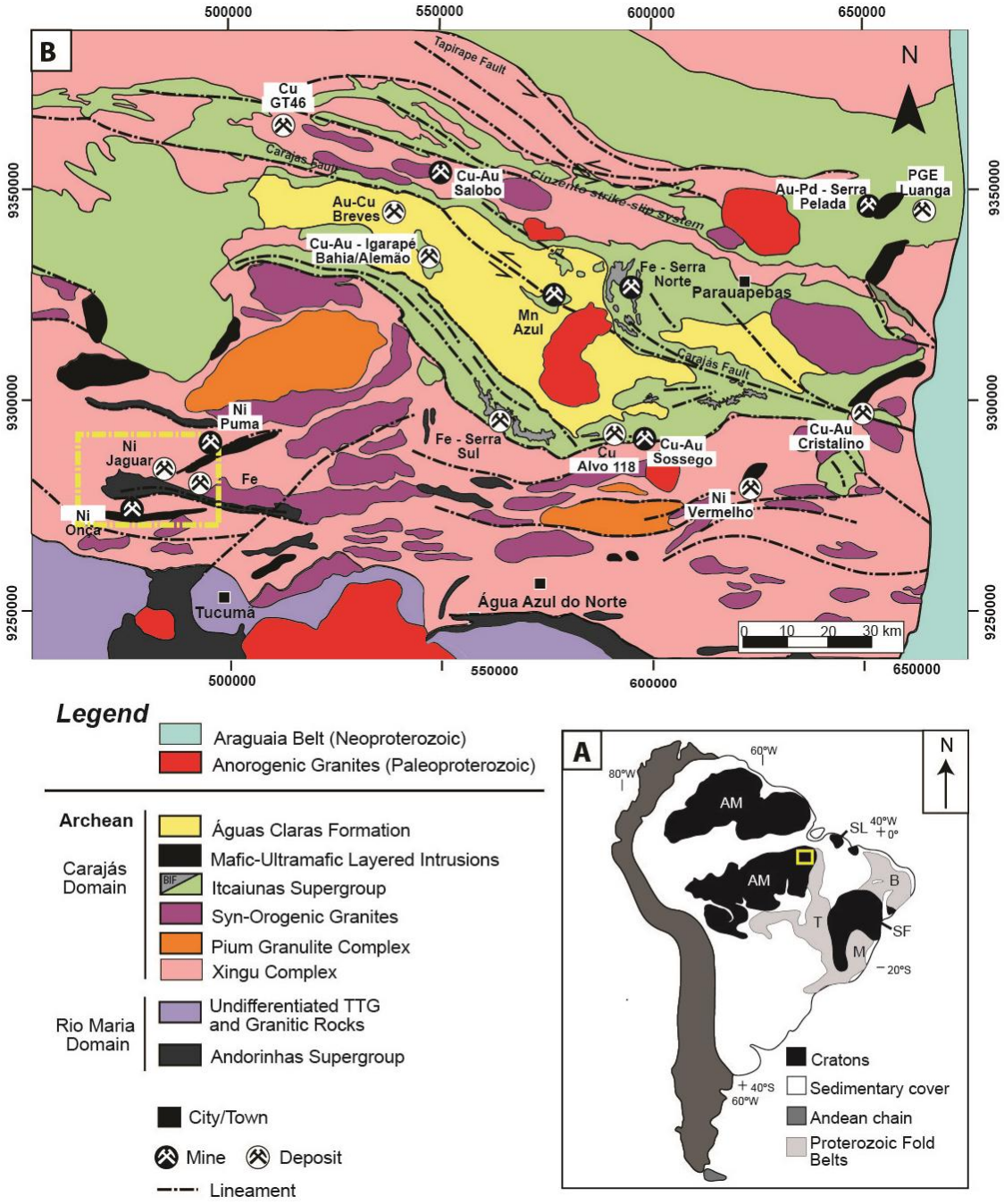

Fig. 1. A) Location of the Carajás Mineral Province. AM - Amazonian Craton; B - Borborema Province; M - Mantiqueira Province; SF - São Francisco Craton; T - Tocantins Province. B) Geology and mineral deposits of the Carajás Mineral Province (partially modified from Vasquez et al., 2008). The dashed rectangle indicates the position of Fig. 2.

The tectonic setting of the Carajás Basin is still a matter of debate. Interpretation of geologic, geochemical, and isotopic data for the mafic rocks of the Itacaiúnas Supergroup has resulted in two models for its tectonic setting including a continental extensional basin (Gibbs et al., 1986; DOCEGEO, 1988; Araújo and Maia, 1991), related to mantle plume activity (Tallarico, 2003) and a compressional orogenic setting

(e.g., fore- or back-arc basin; Lobato et al., 2005; Silva et al., 2005; Zuchetti, 2007) suggested by high potassium calc-alkaline basalt of the Itacaiúnas Supergroup.

IOCG Deposits in the Carajás Mineral Province

The IOCG deposits of the Carajás Mineral Province are located along or close to regional shear zones, in the contact of the units of the Itacaiúnas Supergroup and the basement rocks of the Xingu Complex (Machado et al., 1991; Feio, 2011; Moreto et al., 2011). They are mainly located in two sectors: the northern copper belt and the southern copper belt. The northern copper belt occurs along the W-NW- striking Cinzento shear zone and hosts the Salobo (789 Mt @ 0.96% Cu, 0.52 g/t Au, 55 g/t Ag; Vieira et al., 1988; Souza and Vieira, 2000), Igarapé Bahia-Alemão (219 Mt @ 1.4 % Cu, 0.86 g/t Au; Tallarico et al., 2005) and Alvo GT46 deposits, as well as several other satellite deposits (e.g., Grota Funda, Paulo Afonso, Gameleira). The southern copper belt occurs along a W-NW- striking, 60 km long shear zone and includes the Sossego (245 Mt @ 1.1 % Cu, 0.28 g/t Au; Lancaster Oliveira et al., 2000), Cristalino (500 Mt @ 1.0 % Cu; 0.3 g/t Au; Huhn et al., 1999a), Alvo 118 (170 Mt @ 1.0 % Cu, 0.3 g/t Au; Rigon et al., 2000) deposits, as well as several other satellite deposits (e.g., Visconde, Castanha, Bacaba, Jatobá and Bacuri). IOCG deposits from the northern and southern belts share several geological and geochemical characteristics. These similar characteristics are indicated in the following description, while major differences are pointed out together at the end.

The host rocks are variable and include felsic and mafic intrusive rocks and metavolcanic-sedimentary units of the Itacaiúnas Supergroup. The formation environment of the deposits and the nature of the host rocks define specific sub-types of hydrothermal alteration (Monteiro et al., 2008a) and the development and amplitude of the hydrothermal alteration zones in individual deposits are dependent upon fluid-rock interactions at different structural levels (Xavier et al., 2012).

Distinct hydrothermal alteration assemblages have been identified along the shear zones (e.g., Xavier et al., 2012). IOCG deposits in Carajás commonly display an early high-temperature (>500°C) sodic-calcic alteration controlled by ductile structures and mylonitic fabrics. This sodic-calcic alteration is characterized by hydrothermal rocks containing variable amounts of albite, scapolite and actinolite (e.g., Sequeirinho

ore body in the Sossego deposit; Monteiro et al., 2008a, b; Xavier et al., 2012). Following this early stage, potassic (K-feldspar and biotite) alteration is generally present and is subsequently overprinted by lower temperature (<300°C) chlorite, carbonate-epidote, or sericite-hematite alteration and Cu-Au mineralization, all controlled by brittle structures (e.g., Sossego ore body at Sossego; Monteiro et al., 2008a,b; and Alvo 118; Torresi et al., 2011). High temperature alteration assemblages in the Salobo deposit (fayalite and garnet; Lindenmayer, 2003; Réquia et al., 2003) were used to suggest emplacement at relatively deep crustal levels. On the other hand, potassic, chlorite, silica, and carbonate alteration are important in deposits formed under brittle-ductile conditions at shallower crustal levels (e.g., Igarapé Bahia, Cristalino, Sossego, and Alvo 118; Xavier et al., 2012).

The geochemical ore signature of the IOCG deposits of the CMP is strongly dependent on the chemistry of the leached host rocks and it is defined by Fe-Cu-Au-LREE-P and variables contents of U-Ni-Co-Pd-Y-Sn-Bi-Be-Pb-Ag-Te (Xavier et al., 2010).

The copper-gold mineralization occurrence form is generally dependent on the crustal depth: lens-shaped and massive replacement bodies parallel to the mylonitic foliation at deeper crustal levels occur in Salobo (Souza and Vieira, 2000), while breccia bodies (e.g., Sossego; Morais and Alkmim, 2005; Carvalho, 2009; Domingos, 2009) and vein stockworks (e.g., Alvo 118; Xavier et al., 2012) are the dominant styles in the shallower IOCG systems.

Ore mineral assemblages were invariably introduced during the late stages of all of the IOCG systems of the Carajás Domain (Xavier et al., 2012). They are indicative of different sulfidation states of the source fluids: chalcopyrite-chalcocite-bornite-magnetite at Salobo (Lindenmayer, 1990; Réquia et al., 1995); chalcopyrite ± chalcocite-digenite-covellite-magnetite at Igarapé Bahia (Tazava et al., 1999; Dreher et al., 2008); chalcopyrite-pyrite-magnetite at Sossego (Xavier et al., 2012) and Cristalino (Huhn et al., 1999a); and chalcopyrite-bornite-hematite at Alvo 118 (Torresi et al., 2011).

Geological and chronological relationship between intrusions and IOCG ore bodies are not clearly defined in the CMP. The genesis of the IOCG mineralization in

Carajás was related to two granitogenesis events (Tallarico et al., 2005; Grainger et al., 2008): (1) a major Archean event at ca. 2.57 Ga (Salobo, Igarapé Bahia-Alemão, Cristalino and Sossego deposits), related to the Old Salobo and Itacaiúnas granites and (2) a major Paleoproterozoic event at ca. 1.88 Ga (Alvo 118 deposit), related to the Central de Carajás, Young Salobo, Cigano, Pojuca, and Breves granites. However, recent studies suggest that the southern copper belt endured episodic and multiple IOCG hydrothermal systems over an extended period between the Neoarchean and the Paleoproterozoic (Moreto et al., 2015a). According to the authors, several deposits of the southern belt (e.g., Bacaba, Bacuri, and possibly the Castanha, Cristalino, and Visconde) record the Neoarchean hydrothermal evolution and share a common metallogenic history with the ca. 2.72–2.68-Ga Sequeirinho-Baiano-Pista ore bodies of the Sossego deposit. Robust geochronological data in the northern copper belt (Salobo and Igarapé Bahia-Alemão deposits) pointed out an important metallogenetic event at 2.57 Ga (Réquia et al., 2003; Tallarico et al., 2005), which correlates to reported late Archean magmatism in Carajás (Old Salobo and Itacaiúnas granites). However, granites of this age only occur close to the Cinzento shear zone (Machado et al., 1991; Souza et al., 1996).

The younger reported episode of IOCG deposit formation in the Carajás Province is coeval with the 1.90-1.88 Ga anorogenic magmatism and is represented by Alvo 118 (Tallarico, 2003) and the Sossego-Curral ore bodies (Moreto et al., 2015b). Geochronological data in Moreto et al. (2014) do not support a common evolution for the IOCG deposits in the southern copper belt and those in the northern copper belt. Evidence for the 2.57 Ga hydrothermal event, widely recognized in the northern copper belt, was not identified in the southern copper belt by these authors. The authors refute the hypothesis that IOCG deposits in the southern and northern copper belts of the CMP were formed during a single IOCG hydrothermal event.

Materials and Methods

Several results presented in this study were based on exploration data developed by Vale S.A., such as geologic maps, sections, drill cores, geochemistry and geophysical surveys. Two representative drill holes were described in detail and 32 thin sections were produced for petrographic studies.

Thirty-two drill holes were available comprising 7534 whole-rock assay results from Vale S.A. database. Half core was sampled continuously at approximately 1-m intervals, respecting geologic contacts. Analyses were carried out at SGS GEOSOL in Brazil, using inductively coupled plasma optical emission spectroscopy (ICP-OES) and Atomic Absorption (for Cu, Ni and Zn) with four acid digestion. The flowchart for preparation includes crushing (95 wt. % < 4mm) and pulverizing (95 wt. % < 0.105mm). F and Cl were measured by specific ion electrode after alkaline fusion and S analyses were performed by infrared.

For detailed studies, 25 samples from 2 drill holes (DH127 and DH132) were assayed in ALS Chemex by the complete characterization package (ALS code CCP-PKG03). This package includes a whole rock package plus LOI (code ME-ICP06), total S plus total C (code ME-IR08), base metals by four acid digestion (codes ME-4ACD81) and 39 elements by ICP-MS (codes ME-MS81 and ME-MS42). For several samples, Ni and Cu were also analysed by aqua regia digestion with ICP-AES (code OG-46). A complete description of analytical methods is available in ALS Chemex Home Page (www.alsglobal.com). Results are shown in Table 1.

Mineral chemistry analyses were performed on polished thin sections using a 5-spectrometer JEOL JXA-8230 SuperProbe at the Electron Microprobe Laboratory of the University of Brasília (Brazil). The wavelength dispersive (WDS) analyses were performed at an accelerating voltage of 15 kV and a beam current of 10 nA. Both synthetic and natural mineral standards were used for the analyses and the same standards and procedure were retained throughout the analytical work. Systematic WDS analyses were obtained for amphibole, biotite, chlorite, magnetite, apatite, plagioclase and sulfides.

Results

Local Geology

The Jaguar deposit is located in the southwestern portion of the Carajás Domain, close to the contact with the Rio Maria Domain (Fig. 1B). It occurs along the Canaan fault system, close to the intersection with the NE-SW McCandless fault (Fig. 2A). The former consists in an important regional EW tectonic feature (DOCEGEO, 1988) that extends discontinuously to the limit of the CMP with the Araguaia Belt, more than 190

km to the east of the Jaguar deposit. Geological units mapped in the area of the Jaguar deposit include basement rocks of the Xingu Complex, granitic and mafic-ultramafic intrusions, a volcanic-sedimentary sequence, and younger dolerite dikes (Fig. 2B). This region was mapped in detail during several exploration programs by VALE, which included soil geochemistry and geophysical surveys. On the other hand, detailed academic studies in the investigated area are restricted to the mafic-ultramafic intrusions and associated mineral deposits.

The Xingu Complex consists of banded gneisses and migmatites outcropping in flat areas. Large granitic intrusions and mafic-ultramafic complexes are intrusive in the Xingu Complex and they occur as smooth hills or elongated ridges. Granitic intrusions consist of massive to weakly foliated medium-grained rocks likely to be part of the Neoarchean Plaquê Suite (Leite, 2001).

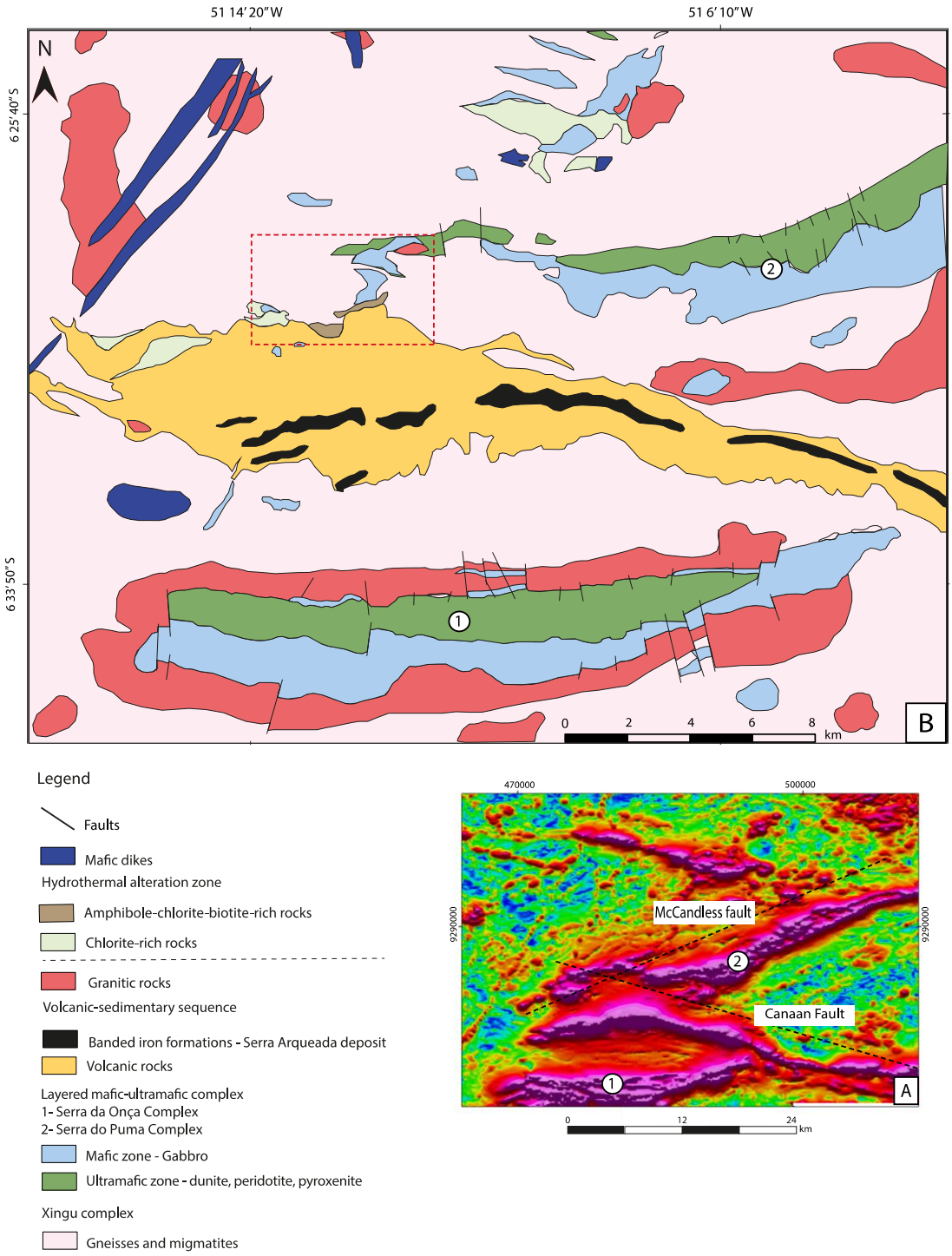

Fig. 2. A) Airborne magnetic total gradient map of the area indicated in the dashed rectangle in Fig. 1. B) Geological map of the region where the Jaguar deposit is located. The dashed rectangle indicates the position of Fig. 3. Geological and analytical signal maps were partially modified from unpublished reports of VALE**.**

Their compositions include granite and granodiorite but none of these bodies were investigated in detail during exploration work in the investigated area. Mafic and ultramafic intrusions include the Serra do Puma and Serra da Onça Complexes

(Macambira and Ferreira Filho, 2002; Ferreira Filho et al., 2007; Rosa, 2014). These layered complexes are intrusive into gneiss-migmatite of the Xingu Complex or weakly foliated granitic intrusions. These large layered intrusions host the world-class Puma-Onça lateritic nickel deposit (198.7 Mt @ 1.36% Ni - Vale 2013 Annual Report; in www.vale.com).

The Serra do Puma Complex (Macambira and Ferreira Filho, 2002; Rosa, 2014) is located along the McCandless fault (Fig. 2A) and comprises an NE-SW structure constituted by ultramafic rocks to the north (dunite, peridotite and pyroxenite) and mafic rocks (leucogabro and gabbro) to the south. The Serra da Onça Complex (Ferreira Filho et al., 2007; Rosa, 2014) is located along the Canaan fault and comprises an E-W structure constituted by ultramafic rocks to the north (dunite and pyroxenite) and mafic rocks to the south (gabbronorite and norite). Magmatic layering in the Serra da Onça and Serra do Puma Complexes has consistent moderate dip to the south. Pristine magmatic textures and minerals are largely preserved in both complexes. However, primary magmatic structures are disrupted and igneous minerals are extensively replaced within sheared zones, as illustrated in the western portion of the Serra do Puma Complex where the Canaan and McCandless faults intersect.

The most prominent geomorphologic feature in the investigated area is an arc-shaped ridge up to 300 meters higher than surrounded areas (Fig. 2B). This ridge is sustained by banded iron formations of the Serra Arqueada iron ore deposit (VALE internal report). The banded iron formation is associated with a volcanic-sedimentary sequence consisting mainly of mafic and felsic metavolcanics. Although this volcanic-sedimentary sequence is ascribed as a greenstone belt of the Andorinhas Supergroup in regional maps (see Fig. 1B; Vasquez et al., 2008a), it may as well be part of the Neoproterozoic Itacaiúnas Supergroup, as indicated by ca. 2.74 Ga U-Pb zircon ages (unpublished results from VALE internal report).

Granitic intrusions, layered complexes, volcanic-sedimentary rocks and gneiss-migmatite from the Xingu Complex are variably affected by hydrothermal alteration in the investigated area. Alteration products are extensively developed within the Jaguar deposit and will be described in the following section. Several dolerite dikes cross cut the alteration products and its host rocks. These dikes are up to several meters wide and belong to a regional swarm of mafic dikes.

Geology of the Jaguar deposit

The Jaguar deposit consists of a 3 km long corridor of WNW-ESE discontinuous lens-shaped ore bodies enveloped by hydrothermal alteration rocks or hydrothermally altered host rocks (Fig. 3). Ore bodies and associated hydrothermal alteration occur along the intersection of two major fault zones, the Canaan and McCandless faults (Fig. 2A). The deposits occurs within a complex domain comprising gneissic rocks of the Xingu Complex, fragments of layered rocks from the western portion of the Serra do Puma Complex, granitic intrusions and felsic subvolcanics of the northern portion of the volcanic-sedimentary sequence. Mineralized zones are mainly confined to the contact between the northern granitic-gneissic rocks and the southern felsic subvolcanic rocks. The host rocks in the northern portion of the deposit consist mainly of gneisses and foliated granites of tonalitic to granodioritic compositions (Fig 3). These rocks vary from isotropic to highly foliated and occur mainly as blocks and boulders. The southern portion of the deposit is mainly hosted by porphyritic felsic volcanic and subvolcanic rocks (Fig. 3). These rocks occur in large massive outcrops consisting of quartz and feldspar phenocrysts within a fine-grained quartz-feldspar matrix (Fig. 4B, C).

Mineralized zones consist in sub-vertical lens-shaped bodies of hydrothermally altered rocks that host the Ni sulfide mineralization (Fig. 3B, C). Outcrops of mineralized zones and hydrothermal alteration rocks are rare and commonly restricted to isolated blocks, except for large magnetite-rich boulders associated with variably sheared and altered felsic subvolcanic rocks located in the southern portion of the deposit (Fig. 4D). Ore bodies are up to 2 km long, with variable width (up to 80 m) and follow a WNW-ESE trend concordant with the regional structures (Fig. 3A). The contact with the host rocks is gradational and characterized by increasing hydrothermal alteration toward the mineralized zones. The following descriptions, based on representative drill core samples, provide the main petrographic features of common host rocks and alteration products associated with mineralized zones of the Jaguar deposit.

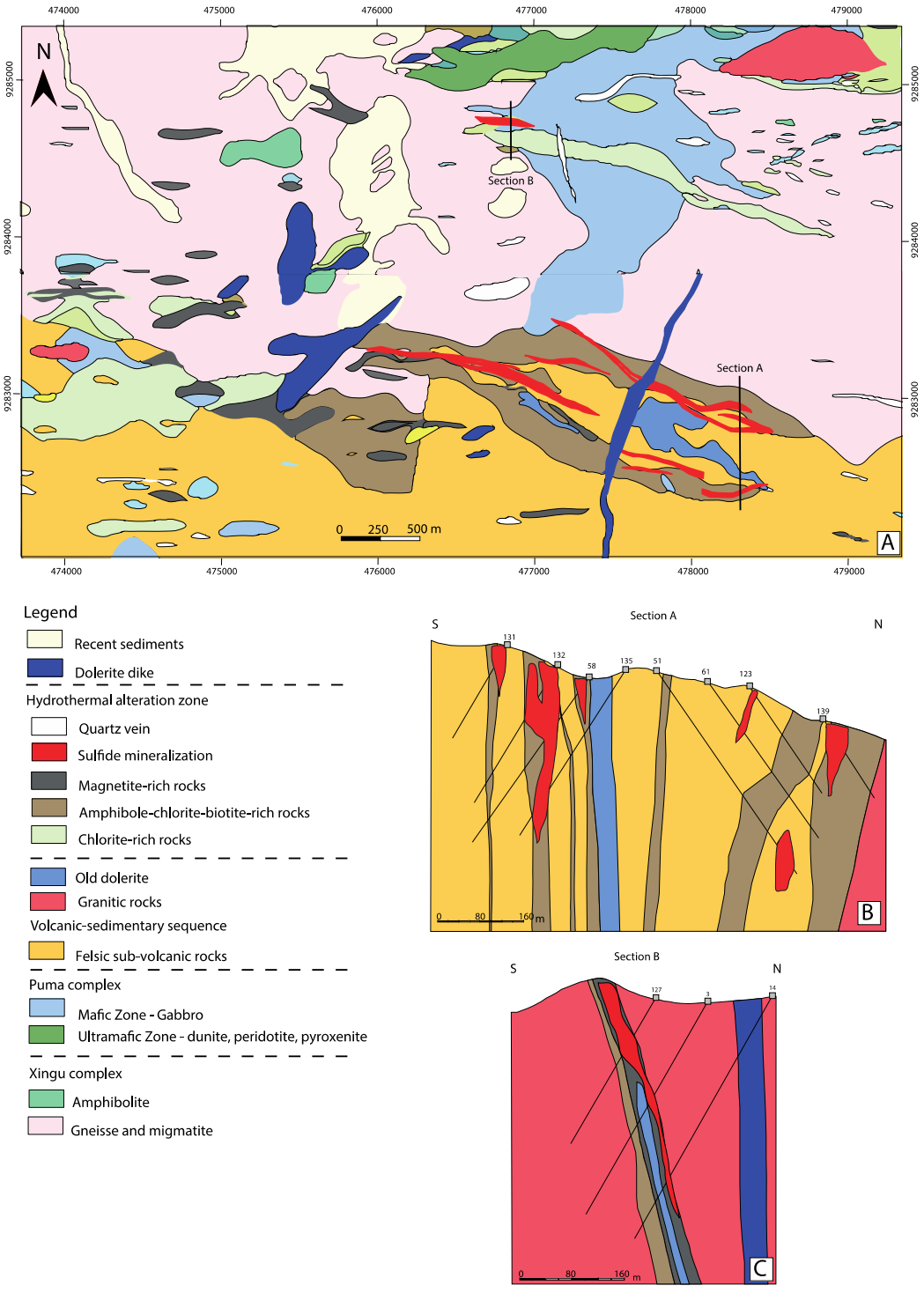

Fig. 3. A) Geological map of the Jaguar deposit. B) Representative geological section of the southern portion of the Jaguar deposit (DH132). C) Representative geological section of the northern portion of the Jaguar deposit (DH127). Note that granitic rocks intercepted in drill cores are not indicated in (A). Geological map and sections are partially modified from unpublished reports of VALE.

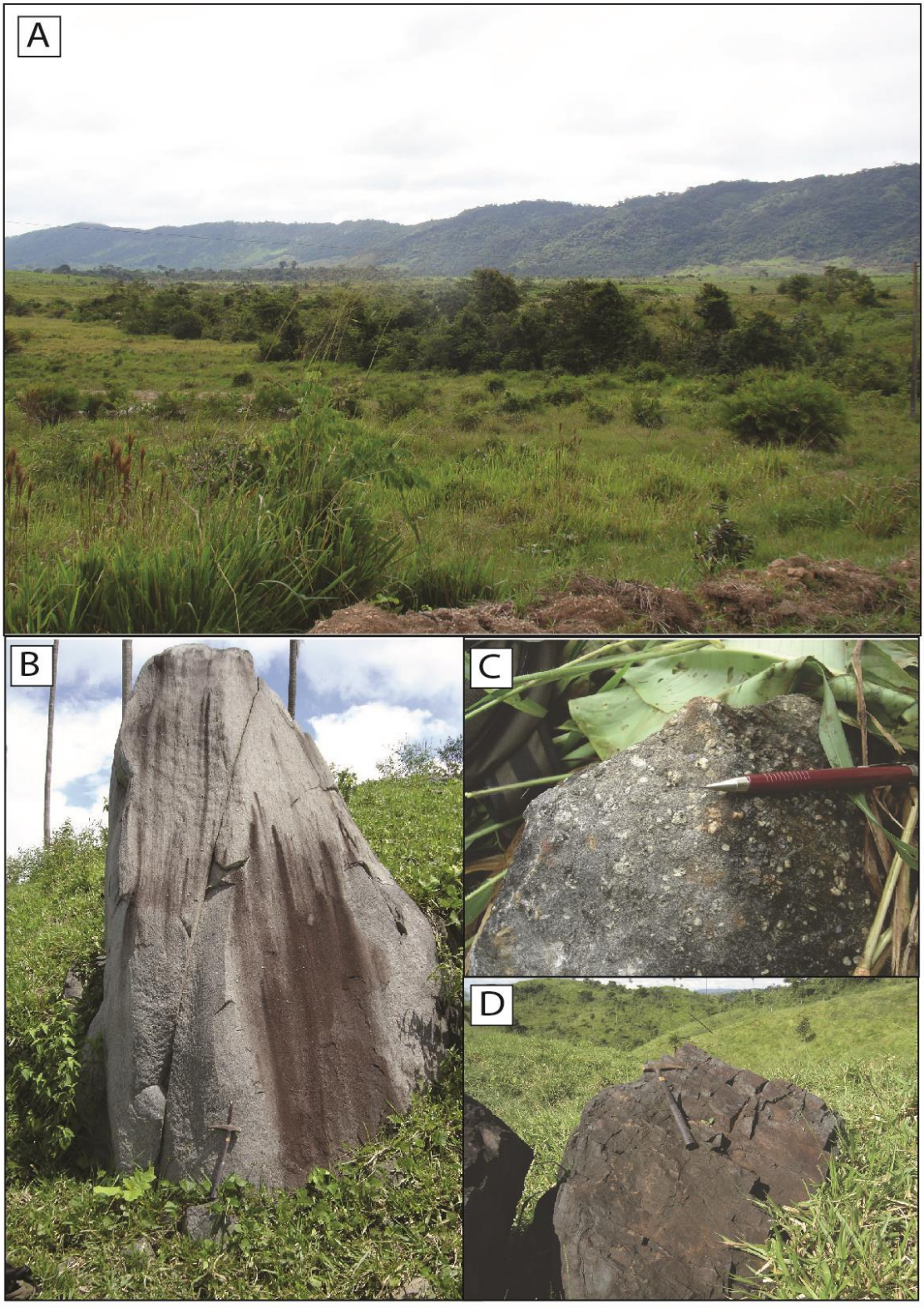

Fig. 4. Field features of the Jaguar deposit. A) Panoramic view of the southwestern portion of the Jaguar deposit. Note the contrasting relief of the flat terrain of the Jaguar deposit and the Serra Arqueada ridge in the back. The latter is sustained by banded iron formations. B) Boulder of felsic subvolcanic rock. C) Typical porphyritic texture of felsic subvolcanic rocks. D) Large block of magnetite-rich rock.

Host rocks petrography

The felsic subvolcanic rock is the most common rock hosting the Ni sulfide mineralization. They are massive dark grey porphyritic rocks characterized by blue phenocrysts of quartz in core samples (Fig. 5A). The felsic subvolcanic contains abundant euhedral to subhedral phenocrysts of plagioclase (albite), quartz and potassic feldspar within a very fine-grained matrix of quartz, plagioclase (albite) and subordinate biotite, chlorite and amphibole (Fig. 5B, C). The quartz phenocrysts are up to 5 mm and show the typical corrosion embayments (Fig. 5C) of volcanic to subvolcanic rocks. Plagioclase phenocrysts occur in tabular crystals up to 4 mm and may locally comprise more than 50 vol. % of the rock, whereas phenocrysts of potassic feldspar are less abundant. Apatite, magnetite, ilmenite, allanite, titanite and carbonates are accessory minerals. The primary mineralogy suggests a dacitic composition to this felsic rock. Subordinate minerals such as biotite, chlorite and amphibole become progressively more abundant close to ore zones, and commonly occur in slightly foliated and magnetic rocks. Locally, phenocrysts can be more abundant than what is expected for a volcanic rock, thus, these massive felsic rocks are interpreted as being subvolcanic.

Massive granitic rocks are the dominant host of the Ni sulfide mineralization in the northern portion of the Jaguar deposit. Extensive drilling has shown that these massive rocks occur frequently (Fig. 3C). However, most of the northern area is mapped as the gneissic-migmatitic domain of the Xingu Complex (Fig. 3A). Thus, drill cores show that massive granitic rocks are more abundant than indicated in the exploration maps. The granitic rocks are light grey, medium to coarse-grained massive rocks (Fig. 6A, B). They consist of quartz, plagioclase, biotite and minor potassic feldspar and magnetite, as well as carbonate filling veins (Fig. 6C). Biotite and chlorite become abundant in altered rocks close to the ore zone, where an incipient to strong foliation is developed. The primary mineralogy indicates a predominantly tonalitic composition.

Two generations of dikes intrude the subvolcanic rocks: old dolerite dikes, affected by the hydrothermal alteration, and younger non-mineralized dolerites. The older dolerite, a dark grey and moderately magnetic rock, is commonly porphyritic. The texture is defined by tabular, up to 6 mm plagioclase and aggregates of clinopyroxene (augite) crystals in a fine-grained matrix. The latter has plagioclase, clinopyroxene and

minor amphibole (actinolite) with intergranular texture. Primary igneous minerals are variably altered to fine biotite, chlorite and amphibole. Magnetite, ilmenite, carbonate, apatite and sulfides (pyrite>pyrrothite>chalcopyrite) are common accessory minerals. The younger dolerites are dark grey, isotropic and moderately magnetic rocks that crosscut the Ni mineralization and its host rocks. They have pristine igneous mineralogy and ophitic and subophitic texture.

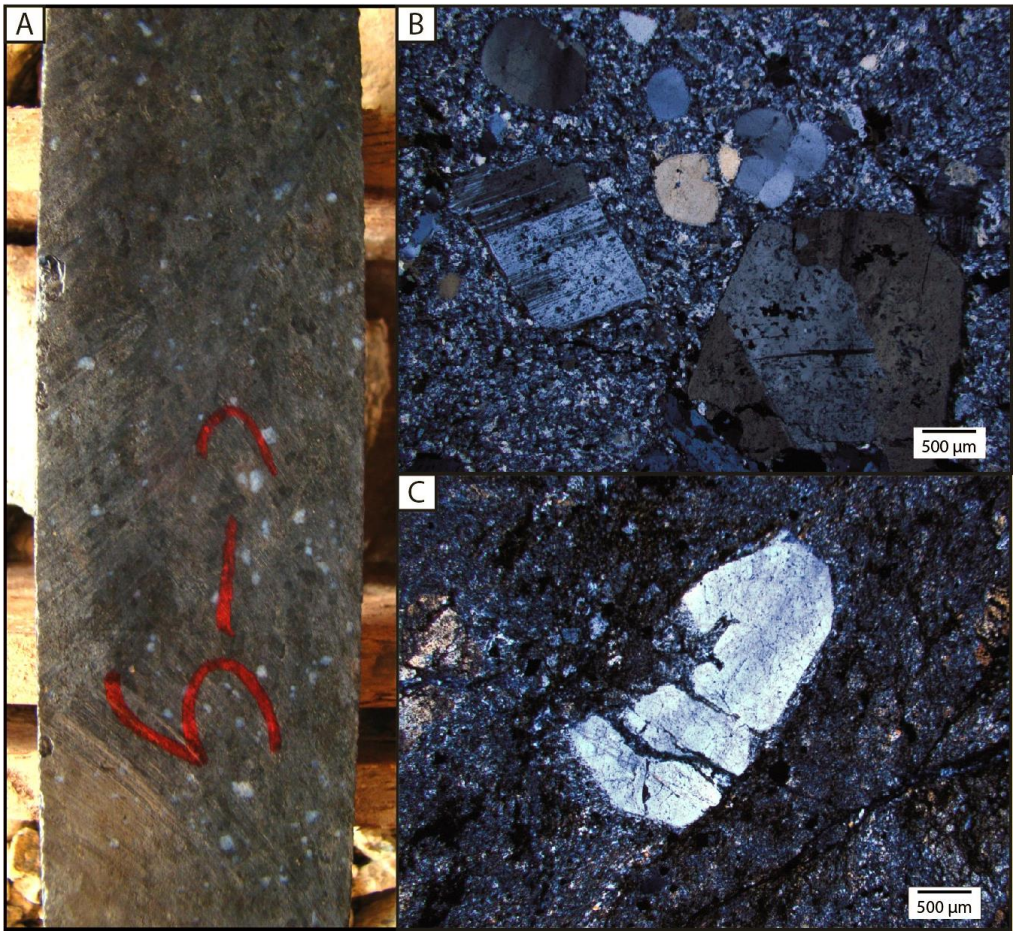

Fig 5. Representative samples of subvolcanic felsic rocks. A) Core sample with blue quartz phenocrysts; B) Photomicrograph of felsic subvolcanic rock constituted by quartz-feldspar phenocrysts in a fine-grained quartz-feldspar-rich matrix; C) Detail of a quartz phenocryst with corrosion embayment, typical of volcanic rocks.

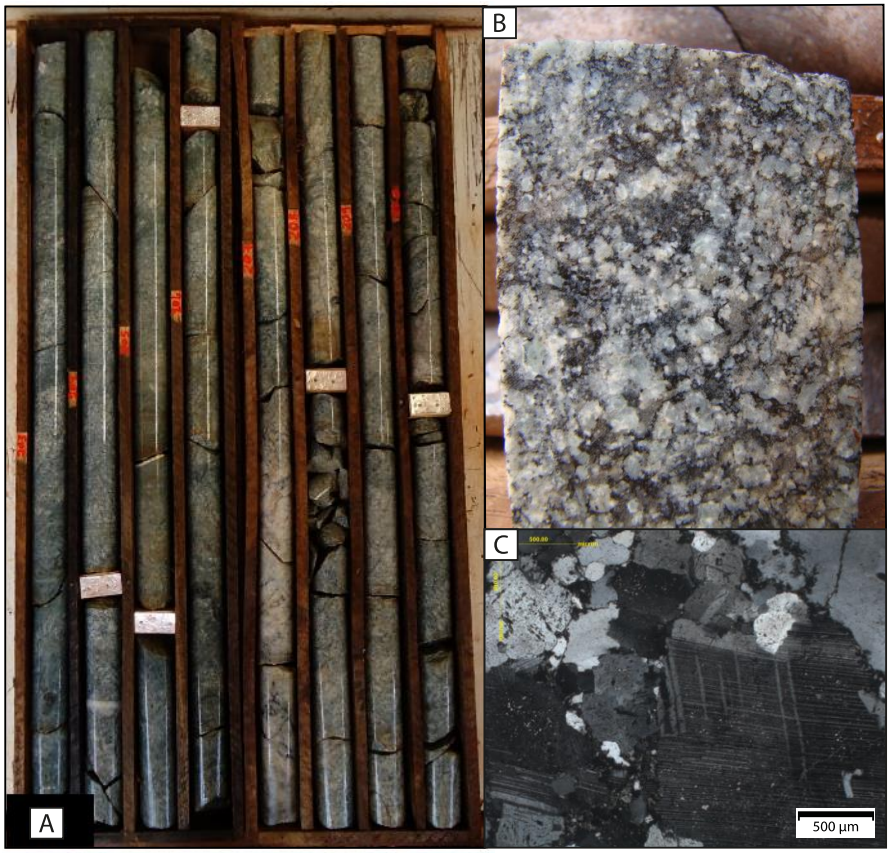

Fig 6. Representative samples of granitic host rocks from the Jaguar deposit. A) and B) Core samples of isotropic granitic rock. C) Photomicrograhp of granitic rock consisting of albite (twinned crystals) and quartz.

Hydrothernal alteration

Host rocks of the Jaguar deposit are intensely altered, with partial to total obliteration of primary igneous textures and minerals. The hydrothermal alteration and mineralization form sub-vertical to vertical bodies structurally controlled by the regional ductile-brittle shear zones. These bodies occur within poorly altered to unaltered host rocks (Fig. 3B, C). The hydrothermal alteration appears to be synchronous or pre date deformation.

Three main types of alteration assemblages are recognized in the Jaguar deposit: (a) biotite-chlorite, (b) amphibole-biotite and (c) magnetite-apatite-quartz. These hydrothermal mineral assemblages are variably developed around the mineralized bodies and influenced by the composition of the host rocks. Alteration rocks display a

range of textures from well-developed mylonitic fabrics to breccias.

Biotite-chlorite is an early alteration varying from minor to moderate replacement (~30 vol. %) of host rock (i.e., felsic subvolcanic or granitic rocks) up to pervasive alteration bodies (Fig. 7). This alteration type includes, besides a fine-grained intergrowth of biotite and chlorite, magnetite, pyrite, and minor amphibole (actinolite/hornblende) and apatite. Chlorite may occur both synchronous to biotite formation, thus in equilibrium (chlorite I – Fig. 7B), as well as a paragenetically late replacement of biotite (chlorite II – Fig. 7C). Fluorite, ilmenite, tourmaline, epidote, allanite, titanite and zircon are common accessory minerals. Weakly altered rocks commonly have a white mica (sericite) replacing plagioclase (albite) from the host rocks. Fine-grained biotite and chlorite lamellae typically define mylonitic foliated bands alternating with fine-grained quartz- and plagioclase-rich bands. Relicts of quartz phenocrysts in altered felsic subvolcanic rocks enveloped by the mylonitic foliation exhibit pressure shadow. Phenocrysts of quartz and albite are typically fractured and are completely replaced by the alteration assemblage in highly altered and sheared zones. Fine-grained magnetite grains occur as oriented ribbons along with the mylonitic foliation. Intra-foliation folds occur locally and exhibit crenulation cleavage defined by chlorite. Although biotite and chlorite are commonly associated, the modal percentage of biotite and chlorite in the alteration zones is highly variable and form alternating bands up to dozens of centimeters thick. Chlorite-rich bands occur mainly in distal portions of the mineralized bodies associated with granitic host rocks. Low grade Ni sulfide mineralization with abundant pyrite is eventually associated to the early alteration assemblage (Fig. 7C).

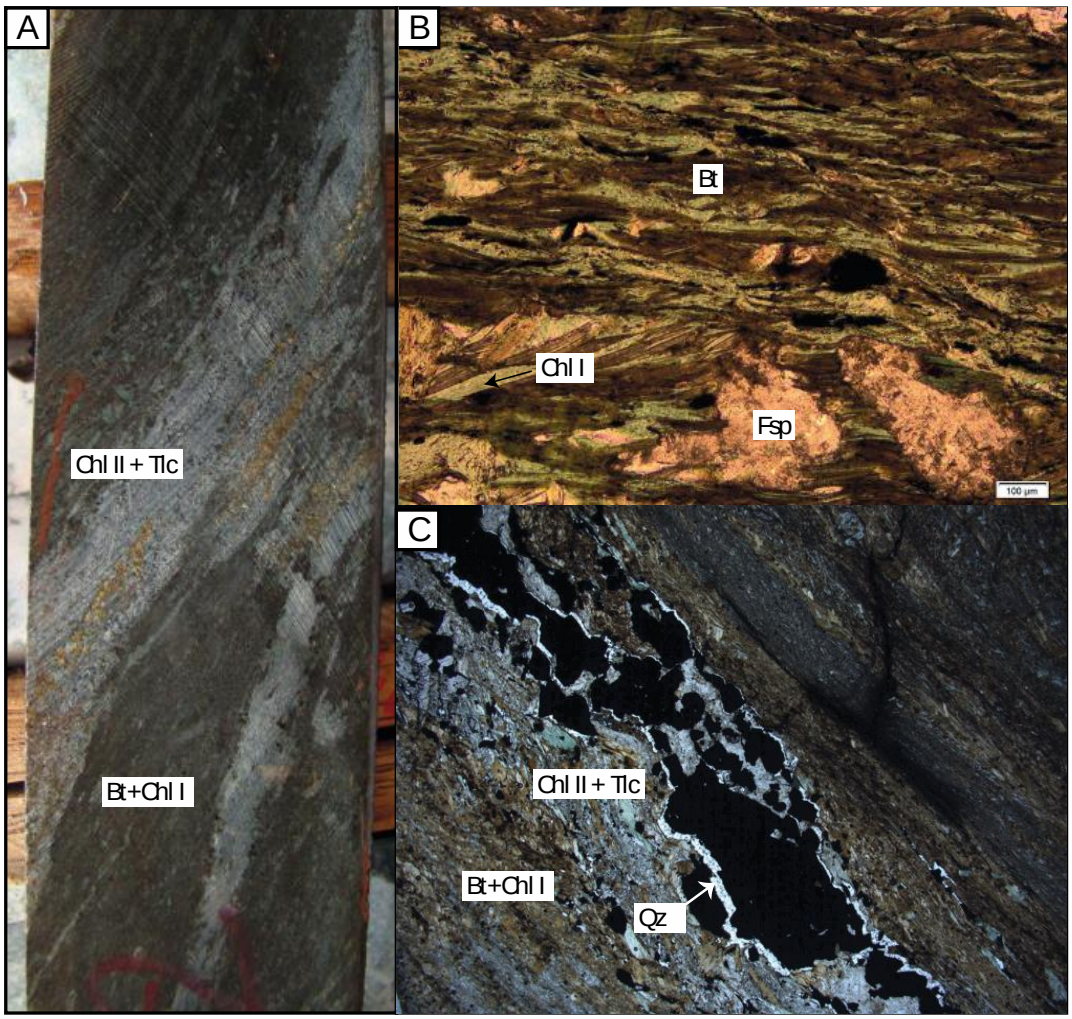

Fig 7. A) Photograph of drill core sample of a felsic subvolcanic rock extensively altered to biotite-chlorite alteration rock. Note that the early stage alteration defines a foliation comprised by biotite + chlorite I. Sulfide mineralization is concordant with folation and develops talc + chlorite II rich bands close to the contact with the early stage alteration. B) Photomicrograph of early stage biotite-chlorite alteration defining a foliation in felsic subvolcanic rock. Felspar relics are still present. C) Photomicrograph of the drill core sample showing the biotite-chlorite alteration zone with concordant Ni sulfide vein (Type 1). Note a later stage alteration of the biotite- chlorite-rich rock indicated by enrichment in chlorite and development of talc in the vein contact. Mineral abbreviations after Whitney and Evans (2010); Qz=quartz, Bt=biotite, Chl=chlorite, Fsp=feldspar, Mag=magnetite and sulf=sulfide.

The amphibole-biotite alteration type is less common and occurs associated with both biotite-chlorite or magnetite-apatite-quartz alteration zones as discontinuous lenses. Fine-grained actinolite is the main amphibole (Fig. 8A), but medium- to coarse-grained hornblende may also occur (Fig. 8C), mostly associated with magnetite-apatite-quartz alteration and mineralization. This alteration forms massive to foliated bodies and may be a late replacement of the biotite-chlorite assemblage. Towards the mineralized zone, amphibole-biotite alteration crosscuts the mylonitic fabric defined by the older biotite-chlorite alteration (Fig. 8B). Fine-grained biotite, talc, magnetite,

apatite and minor chlorite, sericite and quartz are also associated with the amphibole-biotite alteration.

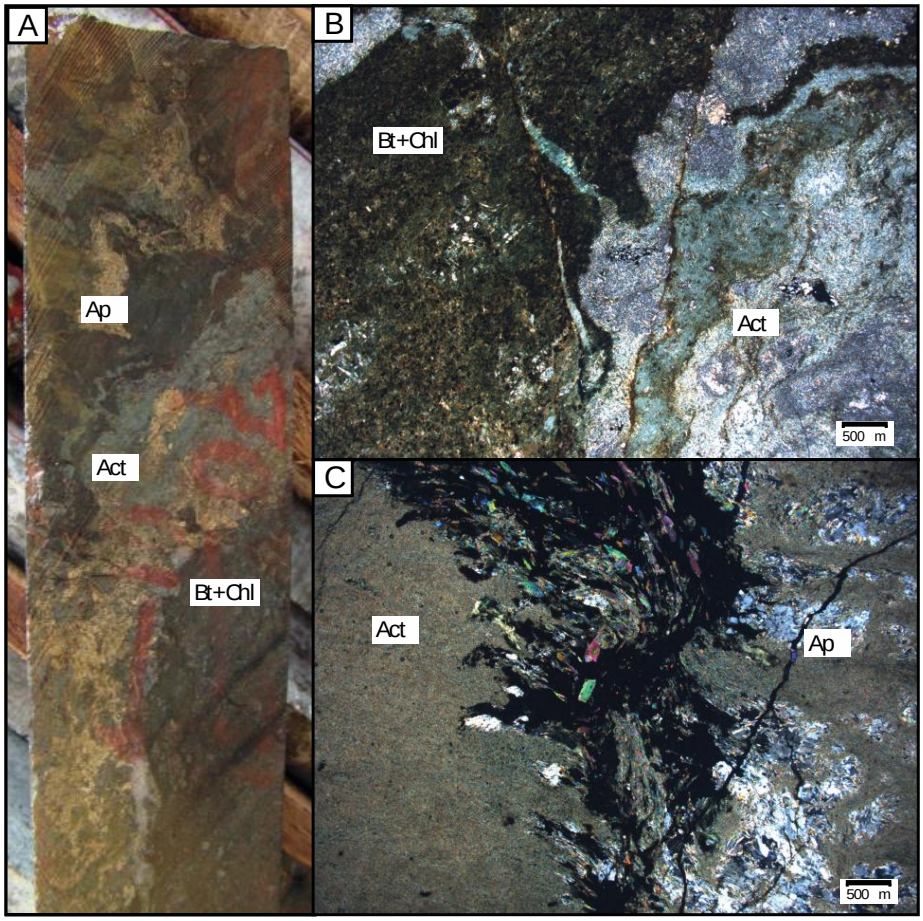

Fig 8. Representative samples of amphibole-biotite alteration. A) Core sample showing the association of the amphibole-biotite alteration and the biotite-chlorite alteration. Apatite is abundant and closely associated to the amphiboles. B) Photomicrograph showing the detail of amphibole-biotite alteration zone crosscutting the biotite-chlorite alteration. C) Sulfide vein crosscutting the fine-grained amphibole-rich alteration. Coarse-grained apatite is closely associated with the sulfide vein. The very fine-grained amphiboles are actinolites and the coarser grains, closer to the sulfides are hornblends. Mineral abbreviations after Whitney and Evans (2010); Bt=biotite, Chl=chlorite, Act=actinolite, Ap=apatite and Hbl=hornblende.

The magnetite-apatite-quartz alteration assemblage occurs in both types of host rocks (Fig. 9). It forms structurally controlled, sub-vertical breccias that host the highest ore grades in the Jaguar deposit, although mineralization is not always present. This alteration stage crosscuts and overprints the earlier stages and becomes pervasive towards the ore zone (Fig. 9A, B). Breccia bodies are commonly enveloped by the biotite-chlorite alteration rocks. Pervasive alteration results in massive bodies of magnetitite consisting mainly of coarse-grained, euhedral to subhedral magnetite. The hydrothermal alteration consists of medium-grained subhedral apatite and magnetite

with fine-grained granular quartz intergrown with sulfides. Apatite forms aggregates of crystals with interstitial sulfides (Fig 9C). Amphibole (actinolite) and biotite may be associated with magnetite-apatite-quartz alteration, although these minerals are typically less abundant than in other alteration stages. Talc is commonly associated with magnetite-apatite-quartz alteration, either as a talc-rich border developed around the sulfides and apatite in contact with biotite-chlorite alteration zones, or as talc-rich lenses in contact with magnetite-rich bodies. Talc and chlorite also occur filling fractures in apatite and magnetite crystals. Quartz is highly deformed, showing strong undulatory extinction. Monazite, ilmenite, titanite and allanite occur as accessory minerals in magnetite-apatite-quartz alteration assemblages.

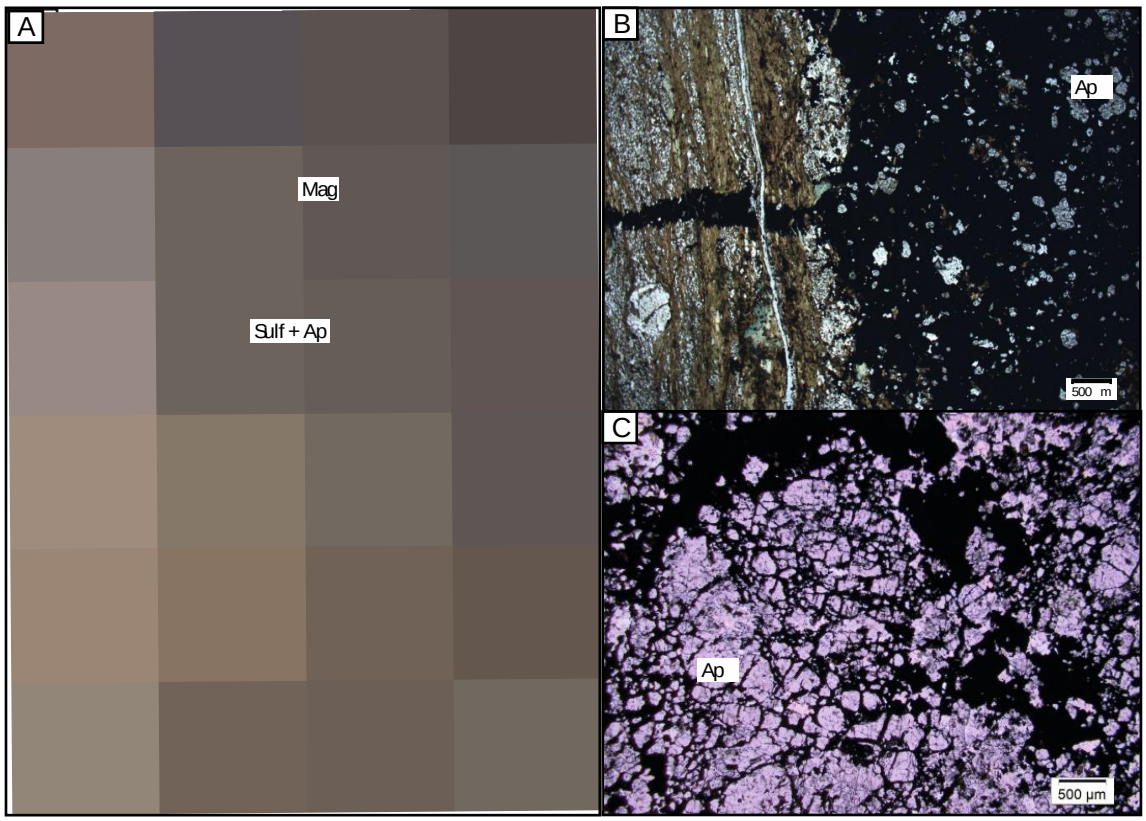

Fig 9. Representative samples of magnetite-apatite-quartz alteration. A) Core sample of mineralized magnetite-apatite-quartz alteration rock. B) Sulfides within a magnetite- apatite-quartz alteration zone crosscutting biotite- chlorite-rich rock. C) Apatite-rich band within magnetite-apatite-quartz alteration zone. Mineral abbreviations after Whitney and Evans (2010); Qz=quartz, Bt=biotite, Chl=chlorite, Ap=apatite, Mag=magnetite and sulf=sulfide.

Fe-carbonates, fluorite, titanite and quartz occur as vein fillings in fractures crosscutting all the alteration and mineralized zones. Locally abundant calcite is associated with the sulfide mineralization.

Petrography of the nickel sulfide ore

Two main types of Ni sulfide mineralization occur in the Jaguar deposit. These distinct types are closely associated and concentrated within up to 100 meters thick steeply dipping ore bodies. The most abundant type (Type I, Fig. 10A, B) comprises mainly low-grade ore and is associated with the biotite-chlorite alteration. Type I mineralization is associated to, besides biotite and chlorite, amphibole, magnetite, quartz, apatite and talc. This mineralization type comprises veins and veinlets to stringer sulfides in biotite-chlorite alteration zones. Sulfides are usually within veins concordant with the foliation but may also infill discordant fractures or occur as disseminated grains in alteration zones. Close to the contact of sulfide veins and biotite-rich altered rocks, biotite is commonly affected by later chloritization and talc formation that develops a chlorite- and talc-rich border.

The second type of Ni mineralization (Type II, Fig. 10C, D) is associated with the magnetite-apatite-quartz alteration. It is less abundant but has the highest ore grades. It occurs as breccia bodies (Fig. 10C, D) consisting of irregular fragments of extensively altered host rocks within a sulfide-, magnetite-, and apatite rich matrix. Mineralized breccias form thin to thick bodies (up to 80 meters thick) parallel to or crosscuting biotite-chlorite rich zones. The breccias are predominantly clast-supported, but matrix-supported breccias are also recognized. Type II mineralization contains, besides sulfides, magnetite, apatite and quartz, minor amphiboles, biotite and chlorite. Sulfide assemblages are similar in both ore types. The main difference relies in the sulfide modal composition and structure.

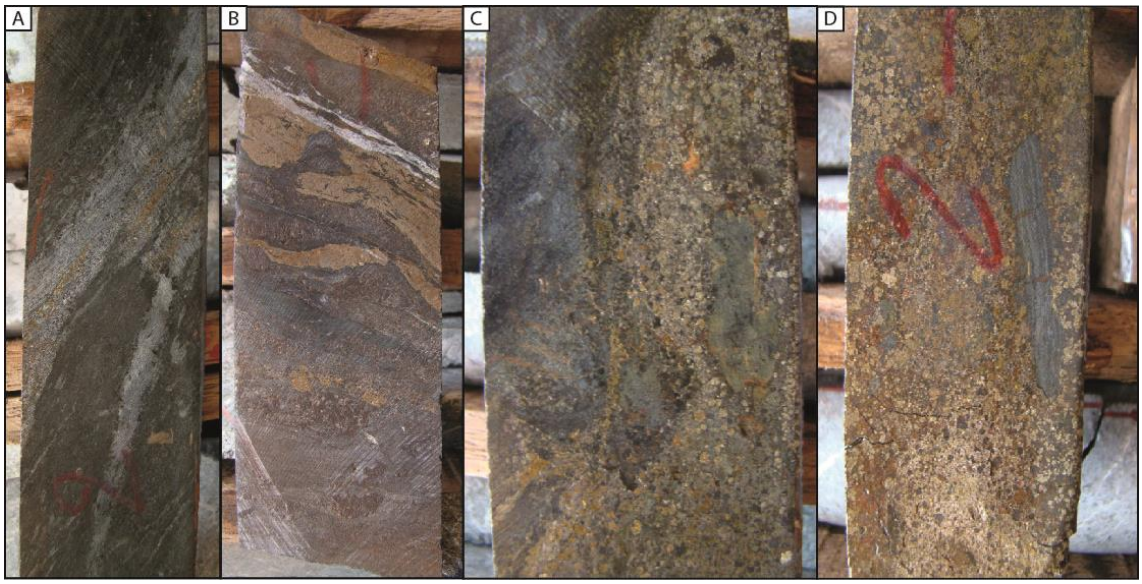

Fig. 10. Mineralization styles of the Jaguar deposit: A) Discontinuous lenses of disseminated sulfide ore (Type I) in biotite- and chlorite-rich alteration rocks. B) Vein and veinlet of sulfides (Type I) in biotite- and chlorite-rich alteration rocks. C) and D) Breccia-style, high-grade mineralization (Type II) consisting of abundant sulfides and irregular fragments of biotite-chlorite alteration rocks. Sulfides and ore grade increase from A) to D).

The main sulfide assemblage is pyrite >> millerite > pentlandite > chalcopyrite pyrrhotite > sphalerite. Pyrite forms euhedral to subhedral crystals and irregular anhedral aggregates. Millerite forms a very fine-grained intergranular network around pyrite grains and enclosing small aggregates of pyrite (Fig. 11A) and may be strongly altered to violarite (Fig. 11C, D). Millerite is more common in type 2 mineralization and occurs dominantly in the southern portion of the deposit. Chalcopyrite forms very fine-grained irregular aggregates usually associated with pyrite (Fig. 11B) but also enclosed in silicates. Sulfides are closely associated with quartz, apatite and magnetite, mainly in type II mineralization. They may surround euhedral to subhedral magnetite or magnetite aggregates, as well as apatite (Fig. 11A, B). Magnetite crystals also enclose sulfides grains or aggregates (Fig. 11B). Small grains and aggregates of magnetite, pentlandite, pyrrhotite and chalcopyrite are eventually enclosed in pyrite crystals (Fig. 11B). Pentlandite forms coarse blocky aggregates surrounded by an intergranular matrix of pyrrhotite. Pentlandite is more abundant in type II mineralization and can be moderately altered to violarite along grain boundaries and grain partings (Fig. 11E). Minor exsolution flames of pentlandite occur within pyrrhotite grains. Sphalerite also comprises the sulfide-rich matrix and commonly exhibits aligned fine-grained inclusions of chalcopyrite (Fig. 11F).

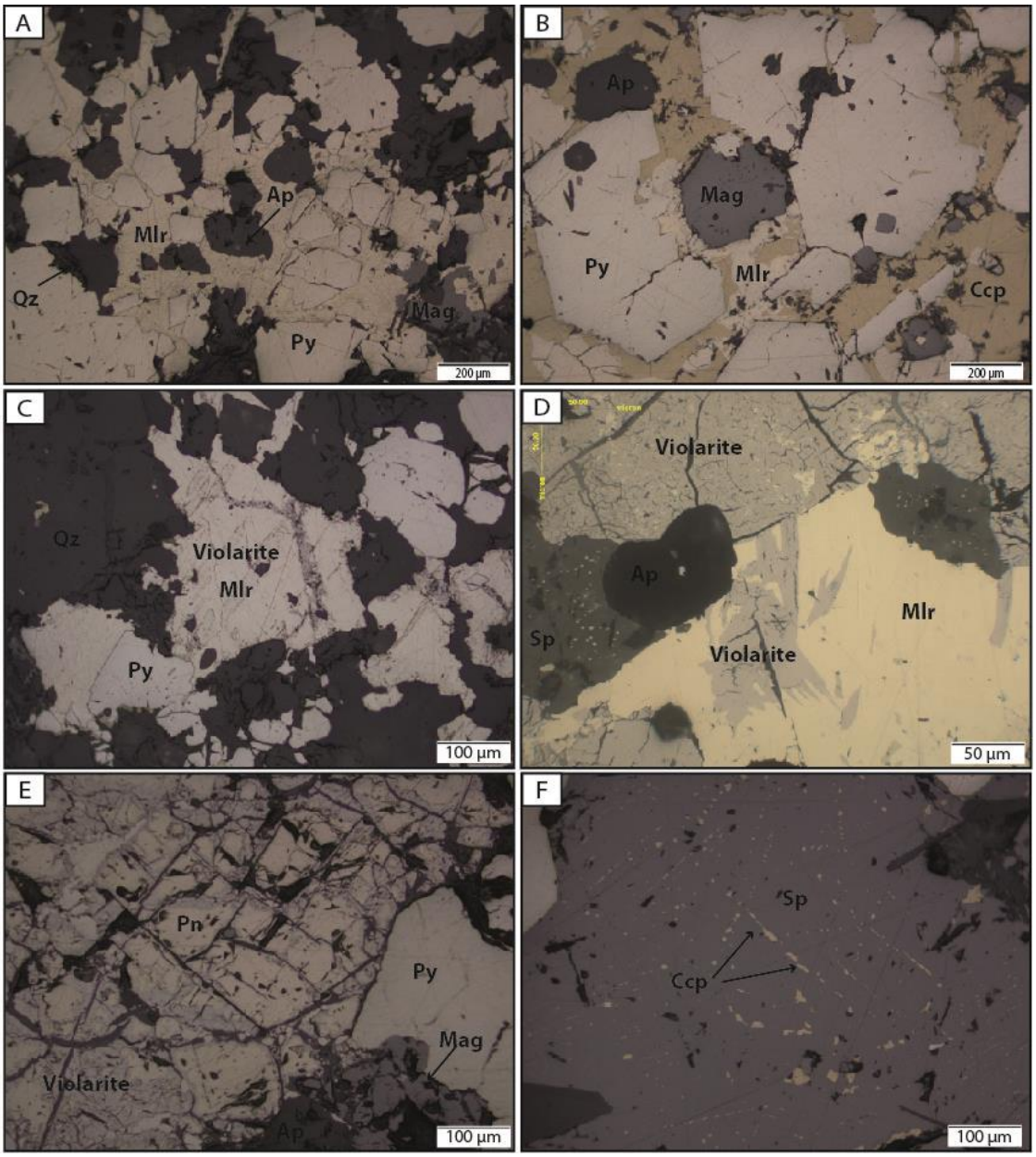

Fig. 11. Representative photomicrographs of the ore of the Jaguar deposit: Breccia type ore where coarse-grained, euhedral to subhedral, strongly fractured magnetite, apatite and pyrite are surrounded by anhedral millerite A) and chalcopyrite + minor millerite B). C) Millerite crystals altered to violarite in grain boundaries and fractures. D) Millerite crystals showing strong alteration to violarite in fractures. Sphalerite has chalcopyrite inclusions and violarite (superior part) has millerite inclusions. E) Fractured pentlandite aggregates with violarite alteration in breccia ore style. F) Detail of a sphalerite crystal with chalcopyrite exsolution. Mineral abbreviations after Whitney and Evans (2010); Qz=quartz, Mlr=millerite, Py=pyrite, Ap=apatite, Mag=magnetite, Ccp=chalcopyrite, Pn=pentlandite and Sp=sphalerite.

Lithogeochemistry of host rocks and alteration zones

Assay results from Vale S.A. database were used for a geochemical evaluation of the alteration zones and mineralization throughout the Jaguar deposit. Two representative drill holes (DH127 and DH132) were selected to illustrate critical geochemical features of the hydrothermal alteration and associated mineralization in this study (Fig. 12 and Fig. 14). Host rocks in drill holes DH127 and DH132 consist mainly of homogeneous granitic and felsic subvolcanic rocks, respectively. These host rocks provide the background for comparison with altered and mineralized zones. Hydrothermal alteration zones in the Jaguar deposit are characterized by FeO enrichment (i.e., higher FeO content compared with host rocks), which is particularly significant for the magnetite-apatite-quartz alteration zones (Fig. 12). FeO enrichment results from abundant Fe-bearing minerals (e.g., magnetite, biotite, sulfides) in the alteration zones. Apart from the chalcophyle elements that will be considered later in this section, P_2O_5, F and MgO follow the distinctive FeO enrichment in the alteration zones (Fig. 12). P_2O_5 and F are also particularly enriched in the magnetite-quartz-apatite alteration zone. P_2O_5 and F enrichment result from widespread apatite as an accessory to major mineral in the alteration zones.

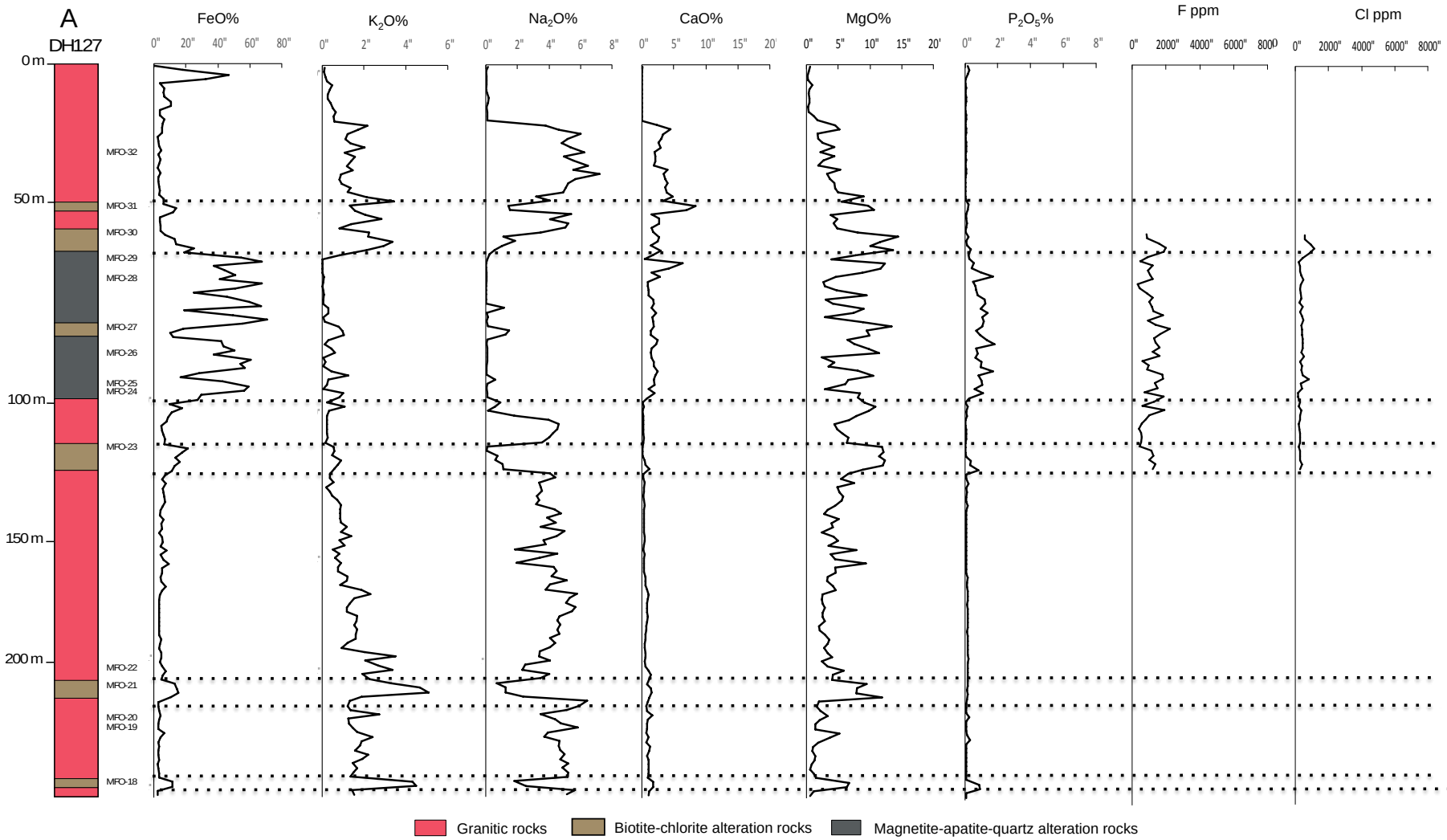

Fig. 12. DH127 A) and DH132 B) drill holes strip log and its FeO, K_2O, Na_2O, CaO, MgO, P_2O_5, F and Cl assay results. Data from Vale S.A. internal report.

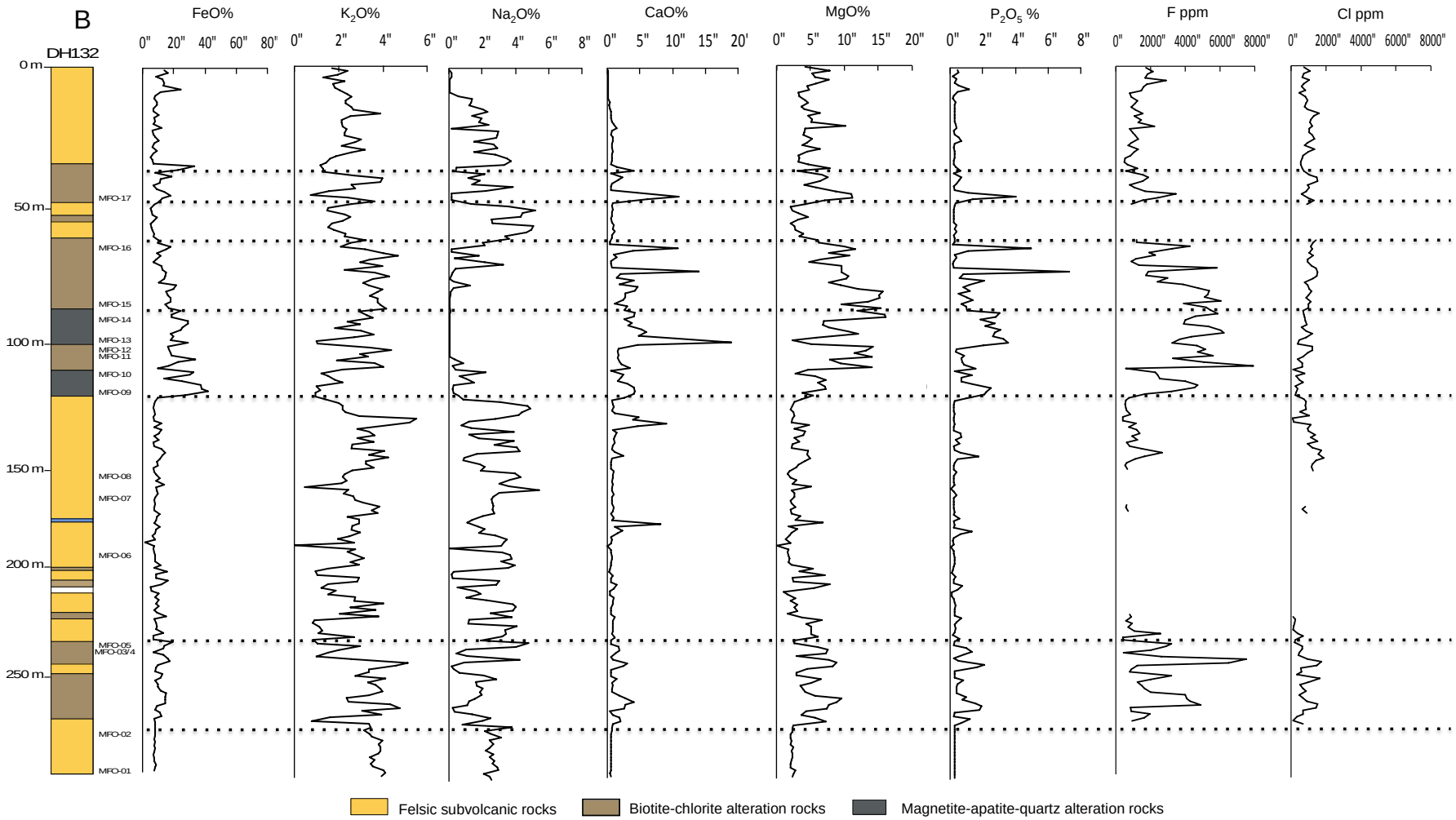

Fig. 12. (Cont.) DH127 A) and DH132 B) drill holes strip log and its FeO, K_2O, Na_2O, CaO, MgO, P_2O_5, F and Cl assay results. Data from Vale S.A. internal report.

Because F enrichment is not mirrored by Cl enrichment, which has significantly lower contents than F in the alteration zones (Fig. 12B), geochemical results suggest that F-bearing apatite prevail in the Jaguar deposit. In general, alkaline major oxides (e.g., K_2O, Na_2O, CaO) do not show significant differences from host to altered rocks, except for depletion in Na_2O (i.e., lower Na_2O content compared with host rocks) in the magnetite-quartz-apatite alteration zones (Fig. 12). Biotite-chlorite alteration zones are significantly enriched in MgO, resulting from widespread biotite as a major mineral. This alteration zone also shows mild to distinctive increase in K_2O, matched with decrease in Na_2O (Fig. 12). The enrichment in K_2O is particularly evident in few meters thick discrete zone away from the highly mineralized zones and is consistent with abundant biotite and chlorite. CaO contents are highly variable in the alteration zones (Fig. 12) with higher contents (> 6 wt. % and up to 19 wt. %) occurring in thin (< few meters thick) amphibole-biotite alteration zones. Considering that Ni sulfide mineralization in the Jaguar deposit is enveloped by wider zones of closely associated biotite-chlorite and magnetite-apatite-quartz alteration zones, the geochemical results from drill holes indicate significant and widespread Fe and Mg alteration, discrete K and Ca alteration, and no evidence for Na alteration.

Twenty-five core samples from drill holes DH127 and DH132 were analysed in detail for major, minor and trace elements (Table 1). These samples, selected based on core description supported by exploration assays (see Fig. 12 for location of the samples), comprise representative host rocks and their hydrothermal alteration products and associated sulfide ore. The plot of selected major and minor elements vs SiO_2, an oxide with a large composition range in the investigated samples, illustrates the main characteristics of these rocks (Fig. 13). They split into host rocks, unmineralized to weakly mineralized rocks from biotite-chlorite alteration and minor magnetite-apatite-quartz alteration zones, sulfide-rich (> 5 wt. % S) ore samples including rocks from both magnetite-apatite-quartz (mostly) and biotite-chlorite alteration zones, and finally one apatite-rich rock from the amphibole-biotite alteration zone (Fig. 13). Several samples have high S contents (up to 30.7 wt. %) and results for major and minor elements in these samples largely reflect a dilution effect by variable amounts of sulfides.

Table 1. Whole-rock analyses of drill core samples from the Jaguar deposit.

Sample	DH127-32	DH127-31	DH127-30	DH127-28	DH127-27	DH127-26	DH127-25	DH127-24	DH127-23	DH127-21	DH127-19	DH127-18
Depth	28.90	49.70	61.10	72.30	82.90	89.90	96.10	98.10	109.30	207.50	225.80	248.70
Rock Type	GRN	Bt-Chl	Bt-Chl	Mag	Bt-Chl	Mag	Mag	Mag	Bt-Chl	Bt-Chl	GRN	Bt-Chl
SiO2	71.40	44.90	55.60	14.75	50.50	3.72	3.75	42.90	45.70	51.50	71.30	53.70
Al2O3	14.90	10.00	19.55	1.32	12.45	0.93	0.79	10.20	8.79	14.70	15.25	12.10
Fe2O3	3.11	16.75	6.45	73.70	14.45	74.50	75.90	22.60	21.90	14.10	3.87	13.80
MnO	0.03	0.14	0.04	0.03	0.08	0.03	0.03	0.05	0.04	0.03	0.02	0.04
MgO	1.58	13.90	5.79	4.11	10.20	1.58	1.58	11.05	7.03	8.84	1.21	6.51
CaO	1.60	8.60	2.75	1.23	1.55	1.14	0.47	0.71	0.15	1.29	1.19	1.46
SrO	0.02	<0.01	0.04	<0.01	<0.01	<0.01	<0.01	<0.01	<0.01	0.02	0.03	<0.01
Na2O	6.13	0.73	5.61	0.02	0.95	0.05	0.03	0.03	0.11	1.16	5.84	1.76
K2O	1.22	1.78	2.74	0.03	0.85	0.07	0.11	1.15	0.28	2.47	1.41	4.85
BaO	0.04	0.04	0.05	0.01	0.01	0.01	0.01	0.01	0.01	0.04	0.05	0.09
Cr2O3	0.01	0.03	0.01	0.01	0.01	0.01	0.01	0.01	0.01	0.04	0.01	0.01
TiO2	0.29	0.84	0.83	0.04	2.41	0.04	0.03	0.21	0.09	0.63	0.18	2.39
P2O5	0.01	0.09	0.01	0.73	1.02	0.53	0.11	0.28	0.07	0.13	0.08	0.90
L.O.I.	1.41	3.48	2.19	2.75	5.08	7.38	2.68	11.50	11.25	4.87	0.95	1.43
Total	101.75	101.28	101.66	98.73	99.56	89.99	85.50	100.70	95.43	99.82	101.39	99.04
S	0.03	1.10	0.10	5.40	0.22	13.80	8.19	8.19	11.60	0.30	0.05	0.11
C	0.01	0.01	0.01	0.01	0.01	0.01	0.07	0.56	0.02	0.14	0.01	0.08
V	13.00	251.00	34.00	266.00	309.00	274.00	252.00	393.00	72.00	168.00	25.00	323.00
Cr	30.00	200.00	10.00	10.00	10.00	20.00	10.00	30.00	20.00	270.00	20.00	20.00
Co	23.00	170.00	32.00	664.00	112.00	1900.00	784.00	1780.00	1550.00	84.00	16.00	49.00
Ni	519.00	1650.00	466.00	6180.00	490.00	26300.00	33800.00	1660.00	1010.00	300.00	50.00	162.00
Cu	15.00	403.00	24.00	266.00	19.00	789.00	2360.00	23.00	24.00	4.00	4.00	10.00
Zn	171.00	324.00	449.00	745.00	1540.00	10000.00	10000.00	824.00	370.00	51.00	9.00	44.00
Ga	18.00	18.10	23.00	25.00	22.50	22.50	28.30	31.80	19.80	30.30	20.50	21.10
Ge	<5	<5	<5	<5	<5	<5	<5	<5	<5	<5	<5	<5
As	1.50	14.80	0.90	29.10	2.20	44.80	4.30	96.70	107.00	1.20	0.50	0.80
Rb	43.10	84.20	147.00	2.60	49.80	1.80	3.80	69.50	18.50	87.40	34.70	148.00
Sr	204.00	9.60	370.00	7.60	36.50	6.90	5.10	21.90	17.10	141.00	279.00	60.80
Y	7.10	16.70	8.90	18.00	58.00	7.60	5.30	29.10	16.80	39.90	4.30	40.50
Zr	249.00	68.00	459.00	3.00	364.00	2.00	2.00	71.00	32.00	102.00	98.00	314.00
Nb	1.10	3.30	7.10	1.00	15.50	1.60	4.10	3.90	2.60	3.60	3.10	13.10
Mo	3.00	1.00	36.00	11.00	2.00	3.00	3.00	126.00	593.00	1.00	1.00	1.00
Ag	0.50	0.60	0.50	0.50	0.50	0.70	0.90	1.10	0.50	0.50	0.50	0.50
In	0.01	0.02	0.02	0.02	0.05	0.09	0.42	0.02	0.02	0.04	0.01	0.02
Sn	1.00	4.00	3.00	2.00	3.00	2.00	3.00	3.00	3.00	4.00	1.00	6.00
Sb	0.08	0.05	0.05	0.08	0.05	0.08	0.15	0.05	0.08	0.05	0.06	0.05
Cs	0.11	0.71	1.76	0.19	1.00	0.06	0.09	1.42	0.30	0.75	0.32	1.35
Ba	353.00	372.00	445.00	8.00	121.00	10.60	23.80	87.20	27.50	335.00	497.00	813.00
La	15.80	3.90	4.00	13.70	67.40	10.40	6.60	392.00	35.70	58.90	15.90	49.40
Ce	30.60	7.70	10.30	25.40	135.50	22.00	12.80	759.00	77.50	110.50	29.90	102.00
Pr	3.34	0.79	1.32	3.04	16.00	2.41	1.40	82.40	8.21	12.20	3.13	12.10
Nd	12.00	3.40	5.70	12.40	60.50	10.00	5.80	283.00	28.90	45.20	10.70	45.70
Sm	2.11	1.32	1.66	2.98	11.90	1.98	0.98	45.80	5.33	9.66	1.67	9.05
Eu	0.55	0.39	0.46	0.78	4.40	0.48	0.23	9.13	1.19	4.16	0.56	1.92
Gd	1.89	2.33	1.73	4.29	12.55	2.13	1.06	27.00	4.81	11.20	1.18	8.94
Tb	0.36	0.42	0.28	0.61	1.87	0.28	0.17	3.24	0.73	1.74	0.19	1.39
Dy	1.73	2.63	1.83	3.11	11.35	1.46	0.81	11.55	3.99	9.13	0.98	7.89
Ho	0.32	0.60	0.33	0.68	2.14	0.29	0.17	1.31	0.88	1.54	0.19	1.63
Er	0.90	1.82	0.96	1.75	6.53	0.76	0.45	2.46	2.25	3.84	0.52	5.31
Tm	0.16	0.32	0.13	0.19	0.87	0.08	0.08	0.25	0.32	0.47	0.06	0.74
Yb	0.71	2.06	0.96	1.13	5.59	0.53	0.34	1.20	1.80	2.73	0.50	4.55
Lu	0.10	0.32	0.16	0.14	0.89	0.08	0.05	0.14	0.21	0.38	0.03	0.70
Hf	6.50	2.00	10.00	0.20	8.90	0.20	0.20	2.10	1.00	3.10	2.90	7.70
Ta	0.10	0.20	0.70	0.10	0.90	0.10	0.10	0.30	0.20	0.20	0.40	0.70
W	1.00	1.00	<1	<1	2.00	1.00	3.00	2.00	2.00	<1	<1	10.00
Tl	0.02	0.09	0.18	0.02	0.08	0.04	0.05	0.10	0.04	0.08	0.05	0.32
Pb	11.00	7.00	7.00	15.00	6.00	114.00	35.00	19.00	103.00	27.00	5.00	2.00
Bi	0.11	0.48	0.11	3.19	0.34	21.30	27.50	3.89	5.07	0.12	0.02	0.01
Th	2.20	2.01	5.79	1.92	6.24	0.71	1.59	7.27	7.11	4.30	5.66	5.31
U	1.90	1.88	3.96	26.10	4.32	2.26	4.12	69.60	148.50	4.70	0.80	3.41
Se	0.20	1.10	0.20	2.30	0.80	8.80	6.40	3.50	2.90	1.00	0.20	0.50
Te	0.01	0.25	0.03	1.69	0.03	5.32	5.21	0.35	2.82	0.02	0.01	0.01
Sc	2.00	18.00	7.00	2.00	32.00	2.00	2.00	13.00	15.00	22.00	2.00	36.00
Li	10.00	30.00	30.00	10.00	40.00	10.00	10.00	40.00	30.00	40.00	10.00	40.00
Cd	0.50	0.60	0.50	2.50	2.10	119.50	149.50	0.50	0.50	0.50	0.50	0.50
Hg	0.01	0.01	0.01	0.01	0.01	0.06	0.11	0.01	0.01	0.01	0.01	0.01
Re	0.00	0.00	0.00	0.01	0.00	0.02	0.01	0.04	0.21	0.00	0.00	0.00

Total iron reported as Fe_2O_3; LOI: Lost of ignition. Rock code: FSV = Felsic subvolcanic; GRN = Granitic rocks; Bt-Chl = Biotite-chlorite alteration rocks; Amp = Amphibole-biotite alteration rocks; Mag = Magnetite-apatite-quartz alteration rocks. Major oxides, S and C are reported in wt.% and minor elements are reported in ppm.

Table 1. (Cont.) Whole-rock analyses of drill core samples from the Jaguar deposit.

Sample	DH132-16	DH132-15	DH132-13	DH132-14	DH132-12	DH132-11	DH132-10	DH132-09	DH132-06	DH132-05	DH132-04	DH132-03	DH132-02
Depth	70.00	87.50	92.60	99.80	102.40	104.35	111.20	116.30	193.10	238.00	239.30	239.80	277.90
Rock Type	Bt-Chl	Amp	Mag	Mag	Bt-Chl	Bt-Chl	Mag	Mag	FSV	Bt-Chl	Bt-Chl	Bt-Chl	FSV
SiO2	43.90	40.00	7.53	12.40	40.30	40.90	7.71	24.80	66.50	15.05	27.80	61.80	68.10
Al2O3	9.11	1.35	0.81	2.87	11.25	9.41	1.14	5.48	12.90	2.05	6.13	12.65	13.90
Fe2O3	19.90	9.06	49.30	46.10	18.65	18.05	47.80	35.10	8.54	36.90	30.30	12.40	9.58
MnO	0.04	0.08	0.07	0.03	0.04	0.04	0.02	0.03	0.05	0.02	0.04	0.07	0.03
MgO	10.40	12.65	1.45	4.38	14.55	17.05	1.01	10.25	1.74	1.48	4.92	5.96	1.95
CaO	2.37	22.00	4.10	3.81	1.67	2.84	5.09	3.90	0.54	4.55	3.90	0.46	0.64
SrO	<0.01	<0.01	<0.01	<0.01	<0.01	<0.01	<0.01	<0.01	<0.01	<0.01	<0.01	<0.01	<0.01
Na2O	0.12	0.22	0.03	0.04	0.09	0.10	0.05	0.05	3.87	0.04	0.06	2.47	3.08
K2O	3.88	0.13	0.23	1.42	6.08	4.23	0.30	2.28	2.81	0.54	0.20	0.75	3.61
BaO	0.03	0.01	0.01	0.01	0.04	0.03	0.01	0.01	0.13	0.01	0.01	0.02	0.19
Cr2O3	0.01	0.01	0.01	0.01	0.01	0.01	0.01	0.01	0.01	0.01	0.01	0.01	0.01
TiO2	0.63	0.05	0.07	0.23	0.71	0.63	0.08	0.41	0.91	0.13	0.39	0.85	1.06
P2O5	0.33	9.56	1.39	2.62	0.45	1.01	2.93	2.00	0.27	3.36	2.83	0.29	0.28
L.O.I.	5.92	2.04	21.00	17.25	4.30	4.70	15.55	8.83	1.45	22.60	15.90	4.00	1.80
Total	96.64	97.16	86.00	91.17	98.14	99.00	81.70	93.15	99.72	86.74	92.49	101.73	104.23
S	4.11	0.31	25.70	19.10	0.92	0.47	26.20	9.79	0.14	30.70	19.60	0.06	0.04
C	0.01	0.01	1.11	0.28	0.08	0.01	0.23	0.33	0.01	0.01	0.01	0.03	0.03
V	110.00	106.00	188.00	288.00	105.00	102.00	204.00	199.00	94.00	22.00	73.00	57.00	98.00
Cr	20.00	20.00	10.00	10.00	20.00	20.00	10.00	20.00	20.00	10.00	10.00	10.00	20.00
Co	409.00	47.00	2280.00	2020.00	138.00	91.00	2470.00	763.00	28.00	2480.00	1480.00	13.00	16.00
Ni	12200.00	2980.00	93800.00	57500.00	4430.00	3390.00	71100.00	27900.00	380.00	76700.00	19000.00	1140.00	194.00
Cu	607.00	535.00	5770.00	3600.00	414.00	355.00	52260.00	5770.00	116.00	2450.00	1510.00	342.00	7.00
Zn	200.00	183.00	36.00	45.00	174.00	158.00	680.00	217.00	304.00	1200.00	10000.00	466.00	94.00
Ga	18.50	4.90	10.00	16.40	22.50	19.40	9.90	20.90	18.70	6.00	17.50	19.30	18.00
Ge	<5	<5	<5	<5	<5	<5	<5	<5	<5	<5	<5	<5	<5
As	12.20	4.90	102.50	116.50	15.70	9.70	68.10	59.10	2.80	250.00	228.00	0.40	1.60
Rb	224.00	5.90	14.90	90.50	347.00	222.00	17.90	127.00	58.10	20.90	6.80	20.20	63.80
Sr	4.00	53.70	14.90	18.80	10.80	9.20	21.40	20.60	39.20	27.90	32.10	21.50	43.80
Y	36.70	129.50	70.10	63.40	37.90	42.70	50.30	30.30	32.20	60.70	82.20	42.90	19.90
Zr	306.00	10.00	19.00	85.00	361.00	291.00	30.00	176.00	463.00	67.00	188.00	447.00	450.00
Nb	13.10	1.60	1.50	5.10	13.10	14.70	1.50	10.50	16.10	3.10	8.20	12.70	17.70
Mo	7.00	1.00	18.00	13.00	1.00	5.00	28.00	7.00	4.00	85.00	143.00	17.00	11.00
Ag	0.50	0.60	5.90	1.60	1.30	0.90	14.80	1.70	0.50	3.20	4.90	0.90	0.50
In	0.05	0.05	0.66	0.13	0.06	0.04	0.74	0.35	0.04	0.14	1.21	0.03	0.01
Sn	5.00	5.00	4.00	4.00	8.00	6.00	3.00	4.00	6.00	5.00	12.00	6.00	7.00
Sb	0.06	0.08	0.37	0.13	0.05	0.05	0.25	0.08	0.05	0.23	0.17	0.05	0.05
Cs	3.49	0.13	0.40	1.03	3.71	2.62	0.39	1.66	0.42	0.28	0.49	0.28	0.32
Ba	296.00	15.90	14.70	87.10	327.00	223.00	36.80	107.50	1230.00	90.60	35.30	158.50	1680.00
La	72.60	73.70	586.00	440.00	426.00	320.00	214.00	153.50	119.00	152.00	721.00	385.00	77.10
Ce	146.00	186.50	1085.00	832.00	775.00	598.00	433.00	295.00	227.00	296.00	1265.00	687.00	151.50
Pr	15.90	24.90	104.50	79.10	71.80	58.70	46.10	30.50	24.60	31.50	128.50	67.50	16.90
Nd	61.50	121.00	347.00	255.00	235.00	204.00	171.00	108.50	84.30	106.00	403.00	202.00	60.00
Sm	10.70	28.60	37.00	32.70	27.20	24.70	26.20	14.55	13.35	18.50	52.70	26.30	9.74
Eu	1.48	2.05	4.46	4.50	3.65	3.25	3.01	1.61	2.32	2.72	10.70	6.55	2.04
Gd	9.23	28.30	24.30	22.80	16.30	15.15	19.85	10.65	9.27	15.70	33.90	16.05	7.16
Tb	1.40	4.24	3.08	2.49	1.96	1.94	2.61	1.21	1.20	2.26	4.18	2.18	0.86
Dy	7.44	25.60	15.75	13.15	9.87	9.86	12.55	6.58	6.68	12.70	20.30	10.40	4.51
Ho	1.50	5.20	2.99	2.43	1.71	1.80	2.27	1.28	1.27	2.51	3.46	1.86	0.88
Er	3.99	14.50	7.39	6.04	4.32	4.60	5.51	2.98	3.67	7.09	8.71	4.97	2.28
Tm	0.56	1.81	0.97	0.71	0.60	0.75	0.58	0.37	0.55	0.75	0.93	0.65	0.43
Yb	3.84	10.90	6.10	4.18	4.07	4.76	3.50	2.23	3.51	3.55	5.05	4.19	2.86
Lu	0.56	1.35	0.90	0.57	0.67	0.64	0.40	0.34	0.57	0.47	0.69	0.65	0.51
Hf	8.00	0.40	0.50	2.10	9.50	7.80	0.80	4.60	11.40	1.60	4.60	10.70	11.20
Ta	0.60	0.10	0.10	0.20	0.60	0.60	0.10	0.50	0.90	0.10	0.40	0.80	1.00
W	1.00	2.00	2.00	2.00	1.00	1.00	2.00	1.00	3.00	1.00	1.00	<1	3.00
Tl	0.42	0.02	0.61	0.36	0.48	0.32	0.39	0.41	0.06	0.08	0.07	0.02	0.05
Pb	3.00	2.00	10.00	11.00	3.00	2.00	52.00	11.00	6.00	131.00	45.00	5.00	8.00
Bi	0.56	0.13	13.35	11.10	0.51	0.28	9.96	5.98	0.20	13.50	16.80	0.03	0.04
Th	6.79	7.16	5.31	9.48	10.70	9.16	2.63	6.00	11.50	2.17	7.59	13.65	12.40
U	7.10	4.10	17.40	8.40	12.95	5.42	10.90	27.00	6.88	22.20	38.30	10.15	5.66
Se	4.20	2.50	27.10	22.70	1.30	1.10	26.00	9.70	0.70	30.10	18.30	0.40	0.20
Te	1.00	0.10	9.47	8.30	0.16	0.10	8.26	3.20	0.06	9.66	8.09	0.01	0.01
Sc	14.00	16.00	4.00	6.00	10.00	19.00	2.00	8.00	15.00	2.00	7.00	13.00	13.00
Li	20.00	10.00	10.00	10.00	20.00	20.00	10.00	20.00	10.00	10.00	40.00	20.00	10.00
Cd	0.50	0.50	1.00	1.40	0.50	0.50	2.50	0.70	0.50	2.40	50.50	0.50	0.50
Hg	0.01	0.01	0.02	0.01	0.01	0.01	0.02	0.01	0.01	0.01	0.13	0.01	0.01
Re	0.03	0.00	0.14	0.10	0.01	0.03	0.14	0.06	0.00	0.13	0.15	0.00	0.00

Total iron reported as Fe_2O_3; LOI: Lost of ignition. Rock code: FSV = Felsic subvolcanic; GRN = Granitic rocks; Bt-Chl = Biotite-chlorite alteration rocks; Amp = Amphibole-biotite alteration rocks; Mag = Magnetite-apatite-quartz alteration rocks. Major oxides, S and C are reported in wt.% and minor elements are reported in ppm.

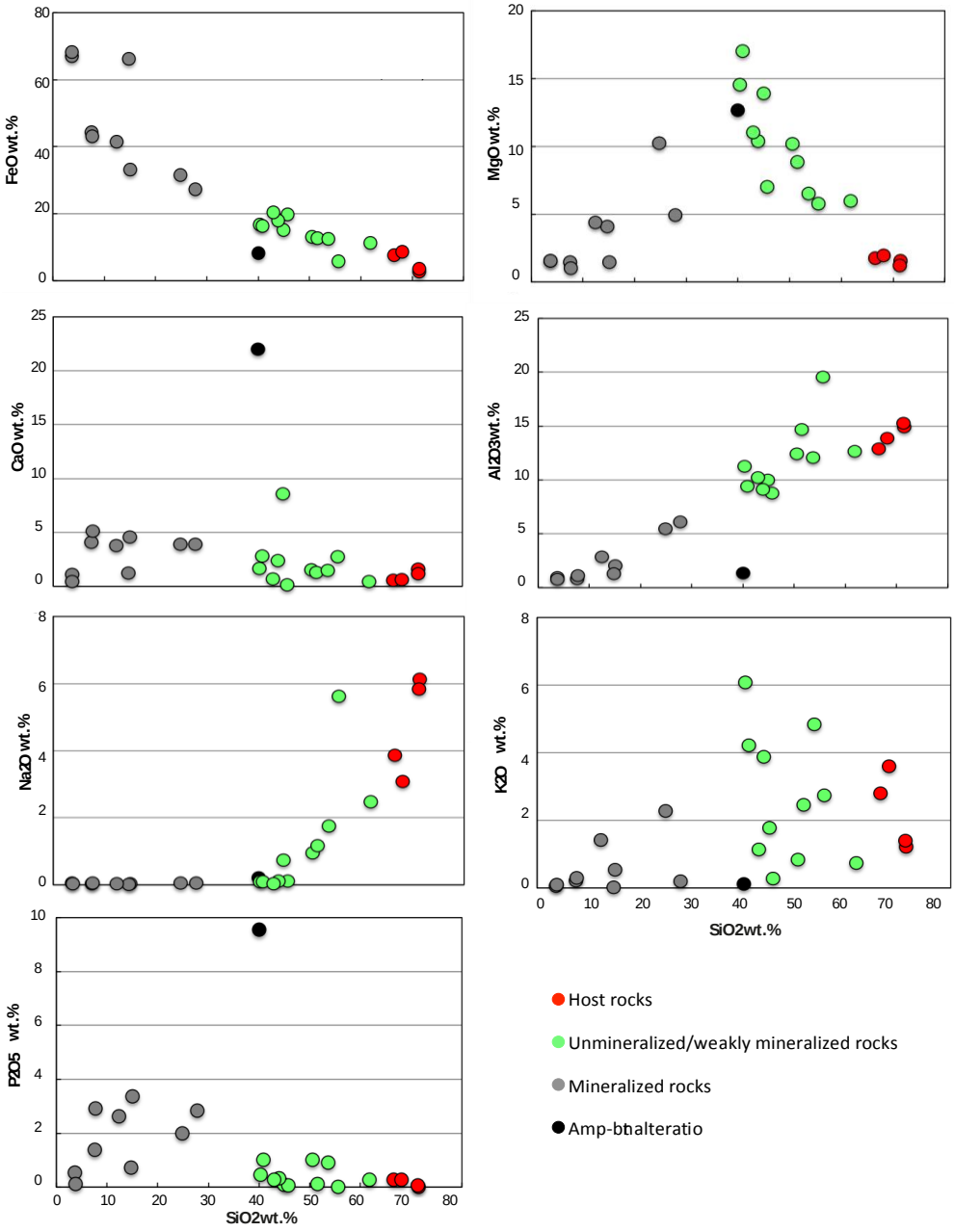

Fig. 13. Plot of SiO2 vs major and minor elements. Data from Table 1.

For sulfide-rich samples the recalculation of total Fe as an oxide (e.g., Fig. 13) is obviously inappropriate and has been provided in this study just for comparison with unmineralized samples.

Both granitic and felsic subvolcanic host rocks are characterized by high SiO_2 (66.5-71.4 wt. %), Al_2O_3 (12.9-15.2 wt. %) and alkalis contents (Fig. 13). These features, together with low MgO (1.2-1.9 wt. %) and Cr (< 30 ppm) contents, are characteristic of acid igneous rocks consisting mainly of quartz and feldspars. Petrographic studies indicate that minor biotite and chlorite in granitic and felsic

subvolcanic rocks result from mild hydrothermal alteration, which is supported by variable and relatively high FeO (2.8-8.6 wt. %) and LOI (0.9-1.8 wt. %) contents for acid igneous rocks. Differences in composition between two granitic and two felsic subvolcanic rocks indicated in this study (e.g., SiO_2, Na_2O, P_2O_5) do not impact the significant geochemical changes, in major elements, promoted by hydrothermal alteration. Therefore, compositions from both rock types are grouped as a broad reference for original host rocks affected by hydrothermal alteration in the Jaguar deposit.

Compared with host rocks, baren to weakly mineralized rocks are highly enriched in FeO and MgO, with moderate enrichment in P_2O_5 and CaO (Fig. 13). On the other hand, K_2O enrichment is restricted to a few samples while Na_2O is highly depleted (Fig. 13). The apatite- and amphibole-rich rock from the amphibole-biotite alteration zone has a distinctively different composition, characterized by high P_2O_5 (9.5 wt. %) and CaO (22.0 wt. %) contents (Fig. 13). Sulfide-rich (> 5 wt. % S) ore samples, including rocks from both magnetite-apatite-quartz and biotite-chlorite alteration zones, are highly enriched in FeO and P_2O_5, and depleted in most major and minor elements due to a dilution effect by variable amounts of sulfides (Fig. 13).

Nickel sulfide mineralization is more intense in Fe alteration zones where FeO enrichment matches the intervals with higher contents of S, Ni, Co and Cu (Fig. 14). A plot of S vs chalcophile elements illustrates the main characteristics of the sulfide ore in the Jaguar deposit (Fig. 15). Figure 15 indicates that sulfur has strong positive correlation with Ni (0.83) and Co (0.87). Consistently high Ni (Ni/S ~ 0.15-0.30) and Co (Co/S ~ 0.005-0.015) contents, high Ni/Cu ratios (~ 5-25) and generally low (< 500 ppm) but eventually high (up to ~ 5.00 wt. %) Zn contents characterize the sulfide mineralization. Results for precious metals (e.g., Au, Ag, Pt, Pd) are usually below their detection limits and were not systematically assayed during exploration. Even though these elements were assayed just in a few drill holes, results indicate that they are not significantly enriched in the sulfide mineralized intervals.

Bulk rock analyses also provide evidence for strong positive correlation of S with Te, As, Bi and Sb (Fig. 15). These chalcophyle elements, usually designated as TABS, are enriched in mineralized samples (S > 5.0 wt. %) of the Jaguar deposit. Our data indicate significant contents for TABS (e.g., Te = 0.3-9.6 ppm, As = 4.3-250.0

ppm, Bi = 3.2-27.5 ppm, Sb = 0.05-0.37 ppm), a group of elements usually disregarded during exploration.

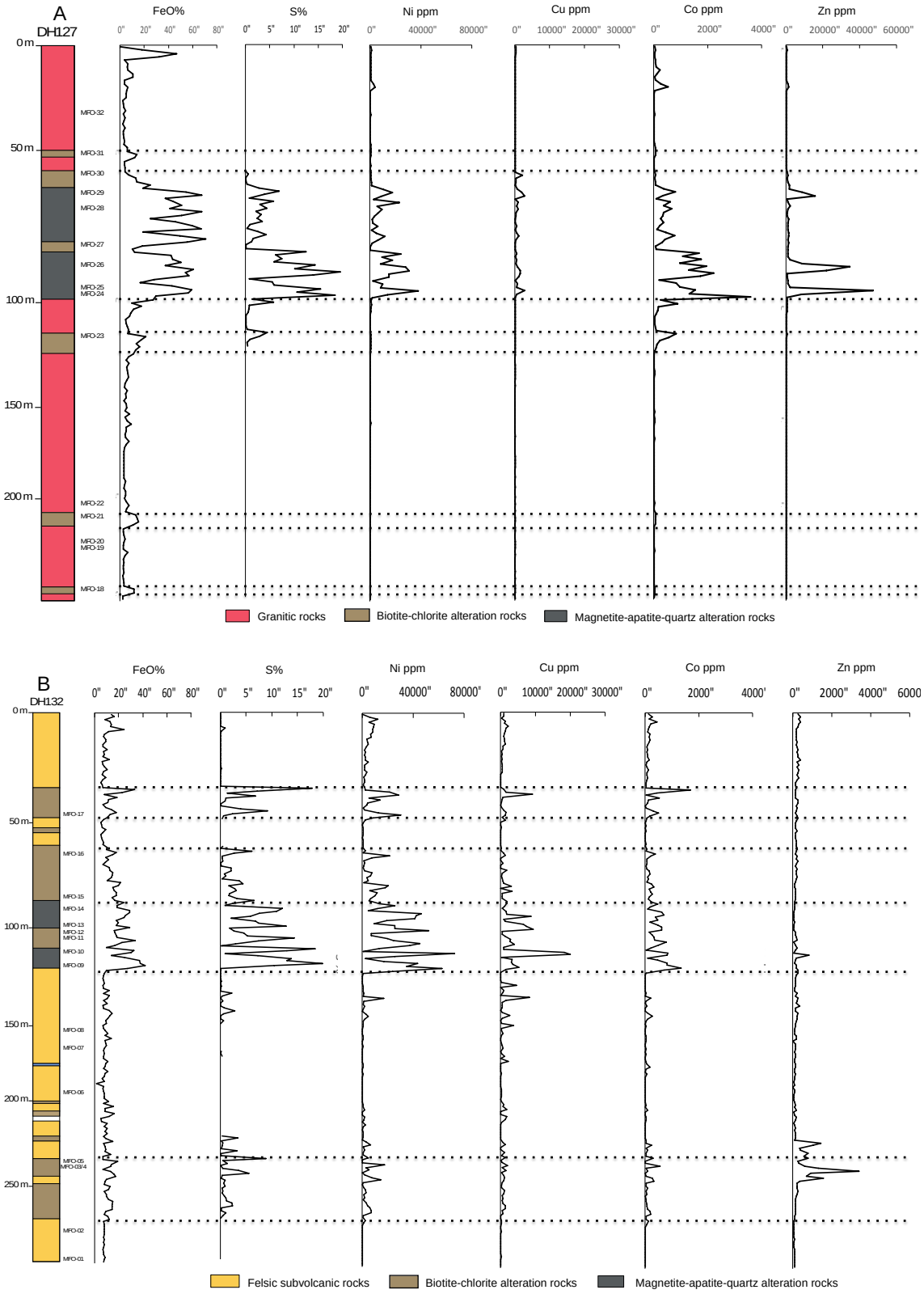

Fig. 14. DH127 A) and DH132 B) drill holes strip log and its FeO, S, Ni, Cu, Co and Zn assay results. Data from Vale S.A. internal report.

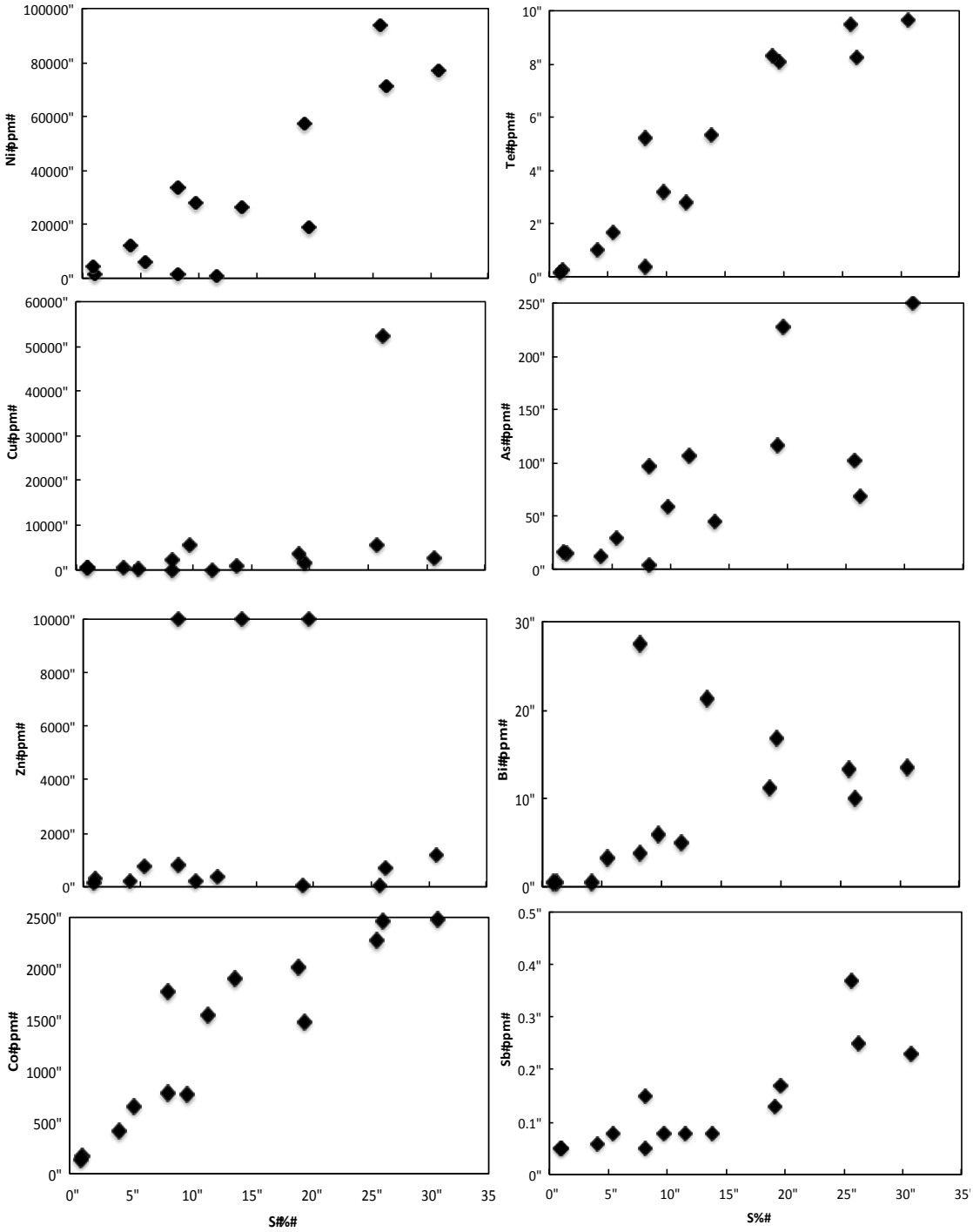

Fig. 15. Plot of S vs Ni, Cu, Co, Zn, Te, As, Bi and Sb. Data from Table 1.

Trace-elements

Distinct mantle-normalized rare earth element (REE) profiles characterize each host rock (i.e., granitic and felsic subvolcanic) and their respective alteration rocks (Fig 16). Therefore, the results for trace elements were considered separately for different

types of alteration rocks depending on their host rock. The plot of primitive mantle normalized (PMN) REE contents for different group of rocks from samples from the northern (granitic host rocks) and southern portions (felsic subvolcanic rock) of the Jaguar deposit are shown in Fig. 16A and 16B respectively. The REE contents of hydrothermally altered rocks of the Jaguar deposit are generally higher than their host rocks.

Granitic rocks have REE profiles characterized by progressive LREE and HREE enrichment (La/Sm_{PMN} = 4.84-6.15; Gd/Yb_{PMN} = 1.95-2.20), with slightly negative to positive Eu anomalies (Eu/Eu* = 0.84-1.22). These rocks have relatively low total REE contents (66-71 ppm). Unmineralized to weakly mineralized alteration rocks from the northern portion (six samples from biotite-chlorite alteration zones; one sample from a magnetite-apatite-quartz alteration zone) have variable total REE abundances (28-1618 ppm). The samples exhibit LREE fractionation, with positive slopes for LREE (La/Sm_{PMN} = 1.56-5.53) and HREE (Gd/Yb_{PMN} = 0.94-18.61) and variable Eu anomalies (Eu/Eu* = 0.65-1.23). Different contents of REE result from distinct proportions of hydrothermal minerals (allanite, biotite, chlorite and apatite). The magnetite-apatite-quartz rich rock has the highest contents, while the chlorite-rich rocks have the lowest REE abundances. Mineralized rocks (S > 5 wt. %) from the northern portion have lower total REE abundances when compared to alteration rocks from the same drill hole (31-70 ppm). These samples also exhibit LREE fractionation, with positive slopes for LREE (La/Sm_{PMN} = 2.97-4.35) and HREE (Gd/Yb_{PMN} = 2.58-3.32) and negative Eu anomalies (Eu/Eu* = 0.67-0.72).

Felsic subvolcanic rocks from the southern portion of the deposit have REE profiles characterized by LREE and HREE enrichment (La/Sm_{PMN} = 5.12-5.76; Gd/Yb_{PMN} = 2.07-2.18), with slightly negative Eu anomaly (Eu/Eu* = 0.63-0.74). The total REE contents are much higher than the granitic rocks and vary from 337 to 497 ppm. As occurs in the northern portion, unmineralized or weakly mineralized rocks associated to felsic subvolcanic host rocks of the southern portion (5 samples from biotite-chlorite alteration zones) have highly variable total REE abundances (337-1578 ppm), also reflecting different modal proportions of hydrothermal minerals. The samples exhibit strong LREE fractionation, with positive slopes for LREE (La/Sm_{PMN} = 4.39-10.12) and HREE (Gd/Yb_{PMN} = 1.99-3.31) and slightly variable Eu anomalies (Eu/Eu* = 0.46-0.98). The apatite-rich rock from the amphibole-biotite alteration zone

has minor LREE enrichment (La/Sm_{PMN} = 1.67) and HREE (Gd/Yb_{PMN} = 2.15) and negative Eu anomaly (Eu/Eu* = 0.22). Mineralized rocks from the southern portion have generally higher total REE abundances (629-2658 ppm) when compared with unmineralized to weakly mineralized alteration samples with the same host rock and mineralized rocks from the northern portion. The mineralized rocks have all very similar REE patterns characterized by progressive LREE enrichment (La/Sm_{PMN} = 5.28-10.24) and HREE (Gd/Yb_{PMN} = 3.30-5.55), as well as pronounced negative Eu anomalies (Eu/Eu* = 0.40-0.80).

The incompatible trace-element variations are summarized on primitive mantle-normalized diagrams (Fig. 17). Granitic host rocks and felsic subvolcanic rocks have similar trace-element patterns characterized by relative enrichment in all elements regarding the primitive mantle, where felsic subvolcanic rocks have slightly higher values. Nb, Ta, P and Ti have negative anomalies in both host rocks. Granitic rocks are slightly enriched in Pb and the felsic subvolcanics have strong Sr negative anomaly.

Patterns for hydrothermally altered rocks from biotite-chlorite or amphibole-chlorite alteration zones are similar for both host rocks. They are generally enriched in trace-elements compared with the primitive mantle, with lower contents in chlorite-rich rocks. Rocks from these alteration zones are also characterized by variable positive U anomalies, negative Sr, Ti, Ba, Nb and Ta anomalies. Pb and Zr have negative and positive anomalies reflecting variable amounts of zircon, whereas P contents are variable and correlate with apatite abundance.

Samples from mineralized rocks from the southern portion have higher overall trace elements contents when compared with samples from the northern portion. However, trace elements patterns are similar in the northern and southern portions of the deposit and comparable to the unmineralized to weakly mineralized rocks showing strong Ba, Sr, Zr and Ti negative anomalies and high positive U anomalies. Pb varies from strong positive to negative anomalies. Nb, Ta, La, Ce and Eu values are variable, but always higher when compared with the primitive mantle.

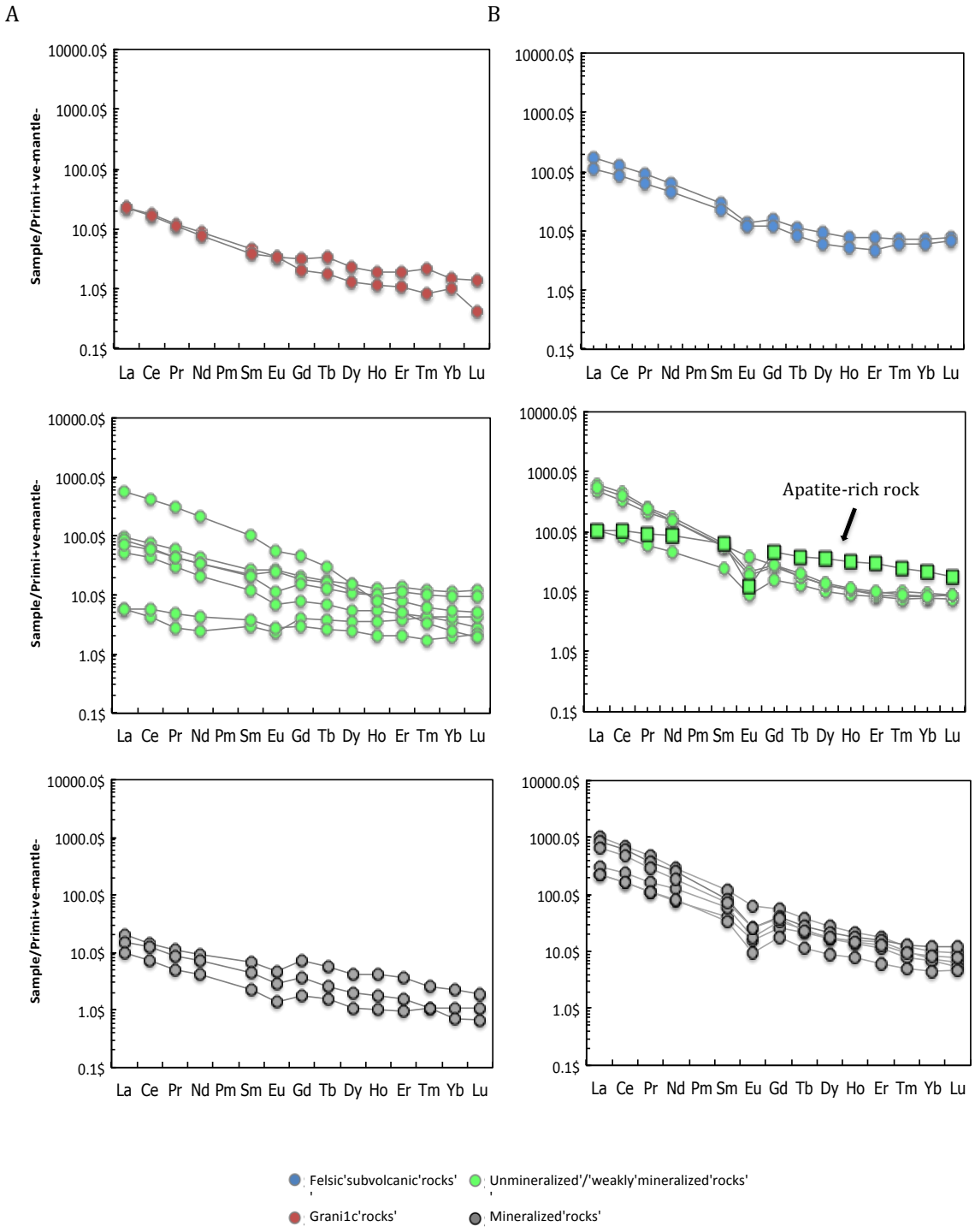

Fig. 16. Primitive mantle-normalized REE patterns for samples of the Jaguar deposit. A) DH127 and B) DH132. Normalization data from Sun and McDonough (1989). Data from Table 1.

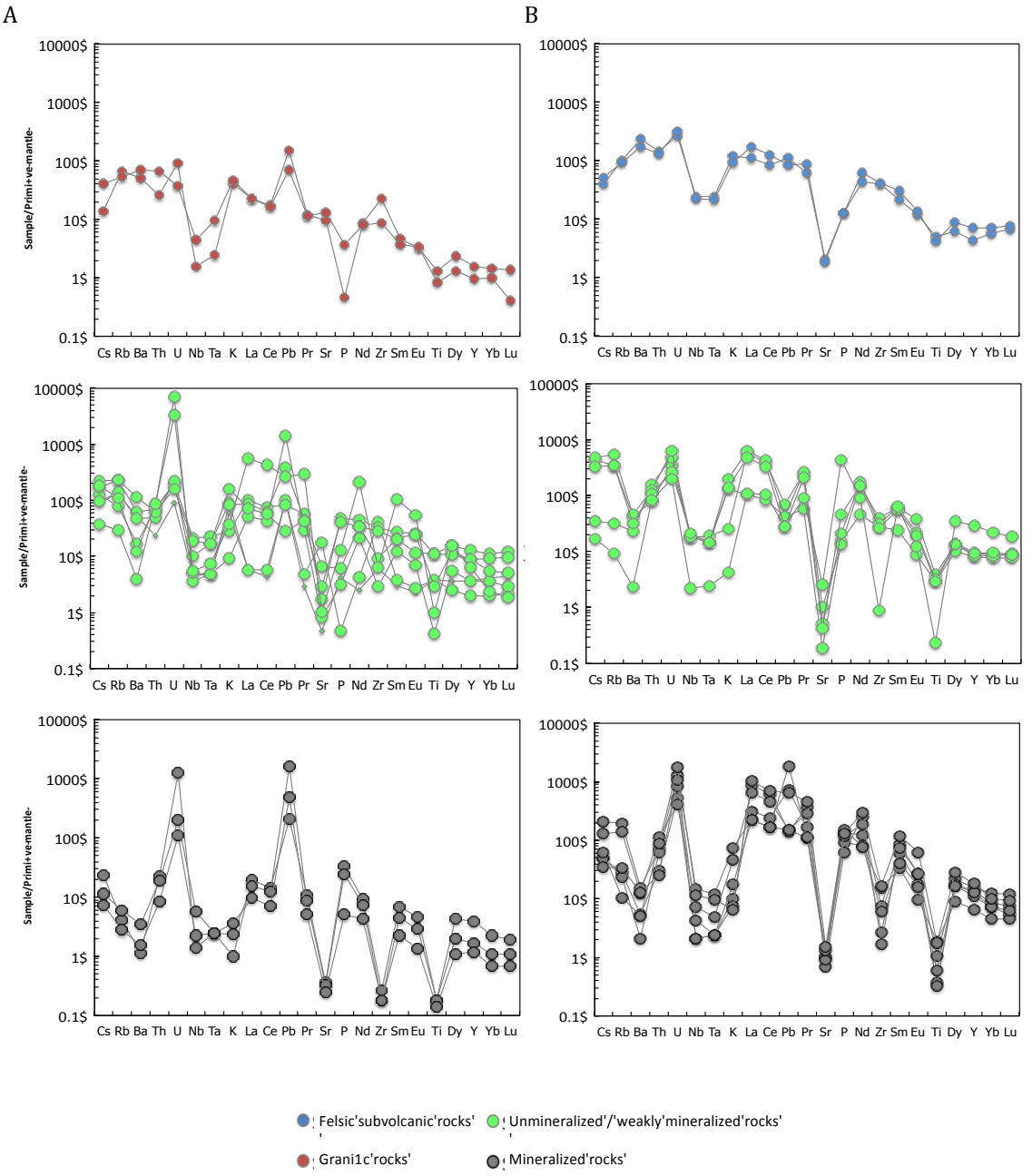

Fig. 17. Primitive mantle-normalized incompatible trace-element diagrams for representative samples of the Jaguar deposit. A) DH127 and B) DH132. Data from Table 1. Normalization data from Sun and McDonough (1989).

Mineral Chemistry

Amphibole

Representative compositions of amphiboles from hydrothermal alteration and mineralization zones are shown in Table 2. Following IMA 2012, the formula $AB_2C_5T_8O_{22}W_2$ was normalized on the basis of 24 anions (O, OH, F, Cl), with assumption of (OH, F, Cl) = 2 pfu at W, which is equivalent in charge to 23O pfu (23 O-equivalent). Amphibole classification followed Hawthorne et al. (2012).

Amphibole associated with biotite-chlorite alteration zones occurs in later veins commonly associated with sulfides. Rocks from biotite-chlorite and amphibole-biotite alteration zones have amphiboles consisting mainly of very fine-grained crystals with colorless to pale green pleochroism (Fig. 8D, E), and minor larger crystals (up to 1 mm) with darker green color and distinct pleochroism. The latter are commonly closely associated with the sulfide-bearing portions of the veins in rocks from biotite-chlorite alteration zones. The amphiboles in these rocks have variable compositions that range mainly from actinolite to magnesio-ferri-hornblende. The plot of Al^{IV} vs Na_2O illustrates the compositional variation of amphiboles in biotite-chlorite and amphibole-biotite alteration zones (Fig. 18A). Except for sample MFO-31, their compositions are characterized by low $(Na + K)_A$ contents (< 0.18 pfu), #Mg values of 0.7-0.9, CaO contents from 11.2 to 12.4 wt.% and generally low Al_2O_3 contents (< 6.3 wt.%). They also have relatively low contents of F (< 0.17 wt.%), Cl (< 0.21%), Ti (< 0.07 wt.%) and NiO (< 0.31 wt.%). Analyses for individual samples (i.e., individual thin sections) show significant compositional variations that follow the compositional range of the whole group of samples (Fig. 18A). Sample MFO-31 has amphiboles with distinct habit and more variable composition than the previously described samples.

Table 2. Representative microprobe analyses of amphiboles. Rock code: Bt-Chl = Biotite-chlorite alteration rocks; Amp = Amphibole-biotite alteration rocks; Mag = Magnetite-apatite-quartz alteration rocks.

Rock Type	Amp	Bt-Chl	Bt-Chl	Bt-Chl	Mag	Mag	Mag	Bt-Chl	Bt-Chl	Bt-Chl
Sample	MFO15	MFO12	MFO16	MFO11	MFO26	MFO25	MFO28	MFO31	MFO30	MFO30
Analysis (wt%)	C2 anf 2	C4 anf 2	C4 anf 1	C4 anf 1.2	C1 anf 1	C1 anf 4	C3 anf 3	C1 anf 4.2	C1 anf 1	C3 anf 2
SiO2	53.25	56.31	55.34	54.93	52.18	56.17	52.93	45.69	51.27	54.83
TiO2	0.02	0.18	0.00	0.36	0.15	0.00	0.00	0.22	0.64	0.15
Al2O3	3.46	1.77	2.04	1.38	5.64	1.59	4.95	10.87	4.23	1.85
Cr2O3	0.05	0.00	0.00	0.02	0.01	0.06	0.02	0.05	0.00	0.00
FeO	11.38	9.42	10.43	8.38	11.23	6.42	10.98	14.34	9.94	8.32
MnO	0.03	0.07	0.14	0.04	0.07	0.06	0.02	0.07	0.18	0.09
MgO	17.34	19.05	17.73	18.89	16.71	20.39	16.94	12.86	17.50	19.15
CaO	12.14	12.06	12.02	11.97	11.57	12.73	11.47	11.57	12.44	12.28
Na2O	0.49	0.39	0.39	0.43	1.02	0.34	0.83	1.29	0.57	0.25
K2O	0.05	0.07	0.05	0.14	0.08	0.03	0.05	0.25	0.18	0.07
NiO	0.14	0.28	0.14	0.19	0.16	0.15	0.14	0.03	0.11	0.22
V2O3	0.00	0.00	0.00	0.00	0.00	0.00	0.02	0.10	0.00	0.04
P2O5	0.03	0.00	0.00	0.13	0.02	0.05	0.01	0.00	0.00	0.04
SrO	0.01	0.00	0.03	0.17	0.00	0.00	0.00	0.08	0.07	0.00
F	0.09	0.12	0.00	0.17	0.13	0.18	0.14	0.00	0.02	0.00
Cl	0.01	0.02	0.06	0.07	0.03	0.01	0.03	0.17	0.13	0.04
Total	98.45	99.69	98.36	97.17	98.94	98.09	98.48	97.54	97.23	97.33
Number of ions on the basis of 24 (O, F, Cl, OH)										
TSi	7.51	7.79	7.79	7.79	7.30	7.80	7.45	6.64	7.32	7.73
TAl (IV)	0.49	0.22	0.21	0.20	0.70	0.20	0.55	1.36	0.68	0.26
TP	0.00			0.02	0.00	0.01	0.00			0.01
CAl (VI)	0.09	0.07	0.13	0.03	0.23	0.06	0.27	0.51	0.03	0.05
CCr	0.01			0.00	0.00	0.01	0.00	0.01		
CFe3+	0.38	0.12	0.11	0.10	0.52	0.13	0.30	0.58	0.42	0.16
CTi	0.00	0.02		0.04	0.02			0.02	0.07	0.02
CMg	3.65	3.93	3.72	3.99	3.49	4.22	3.55	2.79	3.72	4.03
CFe2+	0.87	0.83	1.03	0.82	0.73	0.57	0.86	1.09	0.74	0.72
CNi	0.02	0.03	0.02	0.02	0.02	0.02	0.02	0.00	0.01	0.03
CV							0.00	0.01		0.01
BCa	1.83	1.79	1.81	1.82	1.73	1.89	1.73	1.80	1.90	1.86
BNa	0.07	0.07	0.07	0.09	0.19	0.05	0.13	0.10	0.05	0.03
BFe2+	0.10	0.14	0.10	0.08	0.07	0.05	0.14	0.08	0.02	0.10
BMn2+	0.00	0.01	0.02	0.01	0.01	0.01	0.00	0.01	0.02	0.01
BSr			0.00	0.01				0.01	0.01	
ANa	0.07	0.04	0.04	0.03	0.09	0.04	0.10	0.26	0.11	0.04
AK	0.01	0.01	0.01	0.03	0.01	0.01	0.01	0.05	0.03	0.01
Cations	15.08	15.05	15.05	15.06	15.10	15.05	15.11	15.31	15.14	15.05
WF	0.04	0.05		0.08	0.06	0.08	0.06		0.01	
WCl	0.00	0.00	0.02	0.02	0.01	0.00	0.01	0.04	0.03	0.01
WOH	1.96	1.94	1.99	1.91	1.93	1.92	1.93	1.96	1.96	1.99

Amphiboles in sample MFO-31 consist of dark green large (up to 3 mm) euhedral prismatic strongly zoned crystals. These amphiboles are randomly oriented and occur within irregular biotite-rich bands (up to 1 cm thick) alternated with chlorite-rich bands. Within the chlorite-rich bands the prismatic amphiboles are extensively replaced by chlorite and/or actinolite. Euhedral dark colored amphiboles in sample MFO-31 have compositions that range mainly from magnesio-hornblende to magnesio-ferri-hornblende, characterized by higher $(Na + K)_A$ contents (0.2-0.4 pfu), similar #Mg values of 0.6-0.8, CaO contents from 11.2 to 12.8 wt.% and higher Al_2O_3 contents (1.7-11.4 wt.%). They also have relatively low contents of F (< 0.07 wt.%), Cl (< 0.21%), Ti (usually < 0.07 wt.%) and NiO (< 0.31 wt.%).

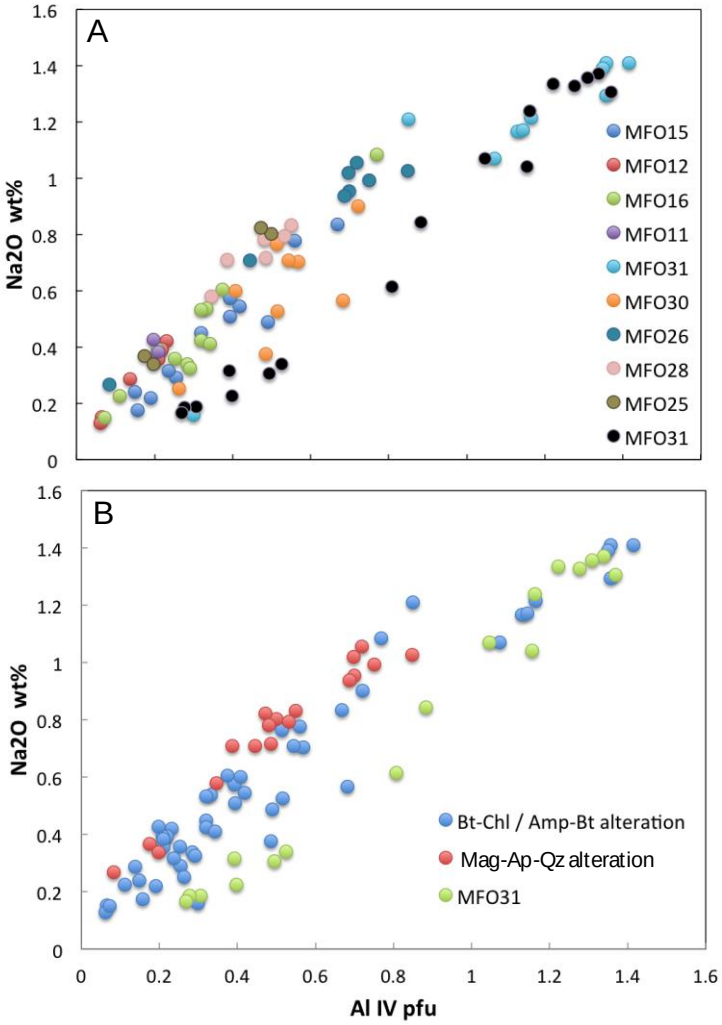

Fig. 18. Plot of Al^{IV} (pfu) vs Na_2O (wt.%) for amphiboles of the Jaguar deposit. A) Amphiboles are separated by samples. The black circles represent the analysis of one individual zoned amphibole from MFO31. B) Amphiboles from rocks of the biotite-chlorite/amphibole-biotite alteration zones and magnetite-apatite-quartz alteration zones. The green circles represent the analysis of one individual zoned amphibole from MFO31.

Amphibole is also a common hydrothermal mineral in magnetite-apatite-quartz alteration rocks in mineralized breccias. Amphiboles in these rocks are coarser-grained (up to 5 mm) and dark green (Fig. 8F). Their compositions range from magnesio-ferri-hornblende to subordinate magnesio-hornblende and minor actinolite, largely overlapping with the compositional range of amphiboles from rocks of the biotite-chlorite and amphibole-biotite alteration zones (Fig. 18B). However, the average composition is characterized by higher $(Na + K)_A$ and Al_2O_3 contents (Fig. 18B), as well as relatively higher F (up to 0.15 wt.%) and NiO (0.10-0.54 wt.%) contents. Higher F and NiO contents are consistent with lithogeochemical results indicating a positive correlation of Ni and F in mineralized rocks.

Feldspars

Potassic feldspars in granitic rocks are less common than plagioclase and have orthoclase composition (Or_{88-99} and Ab_{1-11}). Plagioclase in felsic subvolcanic rocks occurs as euhedral to subhedral tabular phenocrysts or comprising a very fine-grained matrix. Plagioclase phenocrysts are variably altered to fine-grained aggregates of chlorite, epidote and sericite as indicated by total oxides commonly below the expected 100 wt.%. Analyses recalculated to 100 wt.% indicate mainly albite composition with a narrow compositional range ($An_{0.4-1.8}$ and Ab_{89-99}). Plagioclase in hydrothermally altered rocks (chlorite-rich bands from biotite-chlorite alteration) is very fine-grained and is mainly associated with biotite and chlorite. Few analyses of plagioclase from one sample (MFO-30) have highly variable compositions that range from albite to oligoclase (An_{6-28} and Ab_{55-93}) and commonly total oxides below 100 wt.%. These results suggest severe restrictions for a systematic EMP study of the very fine-grained feldspars of the hydrothermal rocks of the Jaguar deposit.

Magnetite

Representative compositions of magnetite from the Jaguar deposit are shown in Table 3. The composition of magnetite was systematically analysed in variably mineralized drill core rocks from magnetite-apatite-quartz alteration zones (8 samples). Additional magnetite analyses were carried on in outcrop samples of magnetite-rich rocks in hydrothermal zones within felsic subvolcanic domains (3 samples), disseminated magnetite in drill core samples from biotite-chlorite alteration zones (2 samples) and drill core samples of banded iron formations from the Serra Arqueada iron deposit (3 samples).

Hydrothermal magnetite is abundant in the mineralized breccias within magnetite-apatite-quartz alteration zones in drill core samples from the northern and southern portions of the deposit, where it occurs in fine- to medium-grained aggregates. Magnetite in samples from both portions has low TiO_2 contents (< 0.28 wt.%). Scattered TiO_2 contents in individual samples and crystals suggest that higher contents are associated with small inclusions. The plot of V_2O_3 vs NiO indicate that magnetite from the northern portion (DH127) has largely overlapping to slightly higher NiO contents but distinctively lower V_2O_3 contents compared with magnetite from the southern portion (DH132; Fig. 19A). Distinct V_2O_3 contents were not expected considering the very similar mineral assemblages and bulk rock compositions of

magnetite-apatite-quartz-rich rocks. However, distinct V_2O_3 contents in magnetite are consistent with different V_2O_3 contents of host rocks in the alteration zones of the northern and southern portions (granitic rocks; 13-15 ppm and felsic subvolcanic rocks; 65-130 ppm, respectively).

Table 3. Representative microprobe analyses of magnetite.

Rock Type	Mag	Mag	Mag	Mag	Bt-Chl	Bt-Chl	Mag	Mag	Mag RS	Mag RS	Arqueada
Sample	MFO13	MFO14	MFO26	MFO28	MFO23	MFO27	MFO25	MFO10	MFO102AB	MFO102AB	MFO50
Analysis (wt%	C3 Mag 2	C3 Mag 1	C3 Mag 2	C1 Mag 3	C2 Mag 2	C3 Mag 1.1	C1 Mag 2.1	C4 Mag 1	C2 Mag 2	C2 Mag 1	C1 Mag 1
SiO2	0.05	0.01	0.40	0.13	0.15	0.08	0.04	0.00	0.04	0.16	2.29
TiO2	0.00	0.00	0.25	0.12	0.09	0.00	0.19	0.16	0.02	0.19	0.01
Al2O3	0.02	0.00	0.16	0.05	0.08	0.11	0.07	0.04	0.08	0.08	0.00
Fe2O3	68.25	68.11	66.94	67.30	68.43	69.20	67.39	68.13	68.20	68.31	64.20
FeO	30.62	30.40	30.94	30.74	31.18	31.10	30.62	30.81	30.57	31.04	34.15
MnO	0.12	0.00	0.09	0.00	0.00	0.06	0.05	0.10	0.00	0.13	0.04
MgO	0.00	0.03	0.07	0.01	0.05	0.01	0.00	0.03	0.08	0.13	0.02
CaO	0.00	0.06	0.07	0.00	0.00	0.01	0.00	0.02	0.01	0.02	0.01
Na2O	0.00	0.03	0.05	0.00	0.04	0.07	0.00	0.01	0.03	0.00	0.03
Cr2O3	0.04	0.04	0.04	0.03	0.08	0.10	0.00	0.03	0.06	0.00	0.05
V2O3	0.16	0.16	0.05	0.06	0.22	0.41	0.02	0.10	0.16	0.07	0.00
NiO	0.19	0.06	0.15	0.12	0.03	0.04	0.15	0.02	0.11	0.13	0.00
Total	99.46	98.91	99.19	98.56	100.33	101.18	98.53	99.43	99.34	100.26	100.79
Number of cations per 4 oxygens											
Ni	0.01	0.00	0.00	0.00	0.00	0.00	0.00	0.00	0.00	0.00	0.00
Si	0.00	0.00	0.02	0.00	0.01	0.00	0.00	0.00	0.00	0.01	0.09
Ti	0.00	0.00	0.01	0.00	0.00	0.00	0.01	0.00	0.00	0.01	0.00
Al	0.00	0.00	0.01	0.00	0.00	0.00	0.00	0.00	0.00	0.00	0.00
Cr	0.00	0.00	0.00	0.00	0.00	0.00	0.00	0.00	0.00	0.00	0.00
Sc	0.00	0.00	0.00	0.00	0.00	0.00	0.00	0.00	0.00	0.00	0.00
V	0.00	0.00	0.00	0.00	0.01	0.01	0.00	0.00	0.00	0.00	0.00
Fe3+	1.99	1.99	1.95	1.98	1.97	1.98	1.98	1.99	1.98	1.97	1.83
Fe2+	0.99	0.99	0.99	1.00	1.00	0.99	1.00	1.00	0.99	1.00	1.00
Mg	0.00	0.00	0.00	0.00	0.00	0.00	0.00	0.00	0.00	0.01	0.00
Mn	0.00	0.00	0.00	0.00	0.00	0.00	0.00	0.00	0.00	0.00	0.00
Co	0.00	0.00	0.00	0.00	0.00	0.00	0.00	0.00	0.00	0.00	0.00
Ca	0.00	0.00	0.00	0.00	0.00	0.00	0.00	0.00	0.00	0.00	0.00
Na	0.00	0.00	0.00	0.00	0.00	0.01	0.00	0.00	0.00	0.00	0.00
K	0.00	0.00	0.00	0.00	0.00	0.00	0.00	0.00	0.00	0.00	0.00

Rock code: FSV = Felsic subvolcanic; GRN = Granitic rocks; Bt-Chl = Biotite-chlorite alteration rocks; Amp = Amphibole-biotite alteration rocks; Mag = Magnetite-apatite-quartz alteration rocks; Mag RS = Magnetitite rock sample; Arqueada = Serra Arqueada iron deposit.

Disseminated hydrothermal magnetites were analysed in two samples in biotite-chlorite alteration rocks from drill core DH132. Magnetite occurs in medium-size (up to 1-2 mm) euhedral crystals. Magnetite has low (< 0.18 wt.%; Fig. 19A) and scattered TiO_2 that, together with NiO contents (< 0.19 wt.%) are comparable with results obtained for those in magnetite-apatite-quartz-rich rocks from DH132. However, V_2O_3 contents (0.11-0.42 wt.%; Fig. 19A) are distinctively higher in one sample (sample MFO-27).

Magnetite was analysed in three samples from outcrops in the southern portion of the Jaguar deposit. These samples were collected in boulders of a massive magnetitite (samples MFO102A and MFO102B) and a magnetite-garnet-amphibole-quartz rock (sample MFO101). These rocks, which occur within a domain of felsic subvolcanic rocks, are interpreted as hydrothermal alteration zones. Magnetite in these

three samples has TiO_2 (< 0.35 wt.%), V_2O_3 (< 0.19 wt.%) and NiO (< 0.21 wt.%) contents comparable with or lower than those obtained for magnetite-apatite-quartz-rich rocks from DH132 (Fig. 19B).

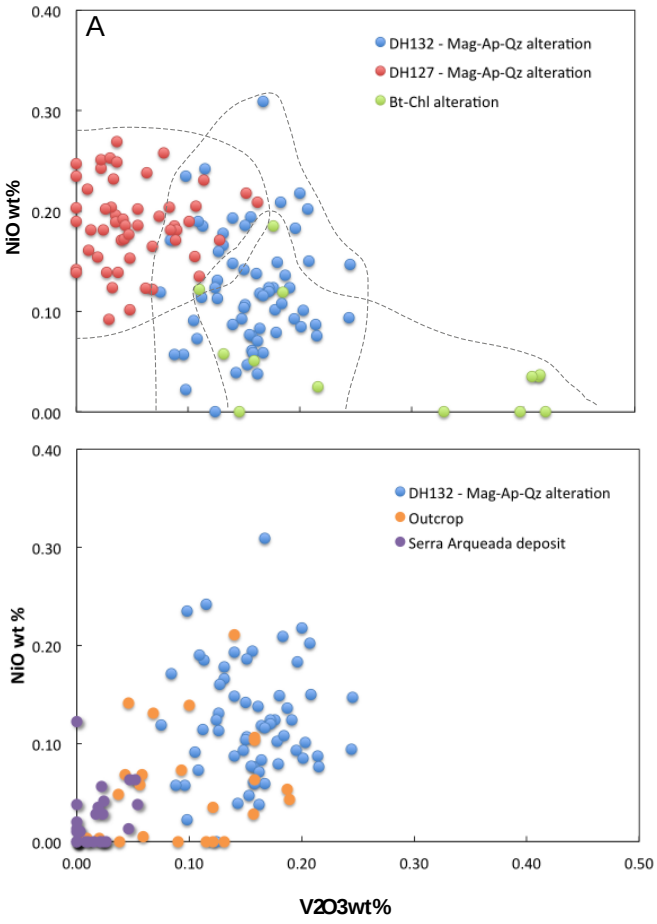

Fig. 19. Plot of V_2O_3 (wt.%) vs NiO (wt.%) for magnetite. A) Magnetite from hydrothermal alteration rocks from drill core samples from the northern (DH127) and southern (DH132) portions of the Jaguar deposit. B) Magnetite from hydrothermal alteration rocks from outcrops of the southern portion of the Jaguar deposit and from banded iron formation of the Serra Arqueada iron ore deposit. Results for magnetite from magnetite-apatite-quartz-rich rocks from the southern portion are also indicated for comparison. Dashed lines separate different groups of samples indicated in the figure.

Magnetite was also analysed in three samples of banded iron formation from a drill core of the Serra Arqueada iron deposit. Magnetite from both laminated and massive samples of the iron formation have similar compositions characterized by low TiO_2 (< 0.22 wt.%), NiO (< 0.12 wt.%) and V_2O_3 (< 0.05 wt.%) contents. V_2O_3 and

NiO contents of magnetite from the Serra Arqueada banded iron formation are distinctively lower than those obtained for hydrothermal magnetite from the Jaguar deposit (Fig. 19B).

Apatite

Representative compositions of apatite from the Jaguar deposit are shown in Table 4. The composition of apatite was systematically analysed in different rock types from drill core DH132. Apatite was analysed in samples including subvolcanic rocks with minor alteration veins (2 samples) and rocks from different alteration zones (1 sample from amphibolite-biotite zone; 6 samples from biotite-chlorite zones; 4 samples from magnetite-apatite-quartz zones). Apatite is less abundant in the northern portion of the Jaguar deposit, and less analyses were carried on in samples from drill core DH127: one granitic rock with minor alteration veins and three samples from magnetite-apatite-quartz alteration zone. The modal proportion of apatite is highly variable in all samples investigated, from an accessory mineral in discrete alteration veins in host rocks, to an abundant mineral (up to 25 vol. %) in one rock from the amphibolite-biotite alteration zone (sample MFO-15) and several ore samples from magnetite-apatite-quartz alteration zones. Apatite occurs in fine- to medium-grained euhedral to subhedral crystals, commonly rounded when hosted in sulfide aggregates.

The analysed apatite crystals from all samples investigated are fluorapatite with close compositions to the ideal composition. Except for analyses from amphibole-biotite alteration zone (sample MFO-15), contents of CaO (50.52-57.24 wt.%) and P_2O_5 (40.84-44.42 wt.%) from all samples largely overlap (Fig. 20A) and indicate values close to the ideal composition $Ca_5(PO_4)_3(OH,F,Cl)$. This feature is consistent with very low contents for all analysed elements that commonly replace Ca (e.g., Fe^{+2}, Mn^{+2}, Sr, Al, REE) or P (e.g., V, C, Si) in apatite from different rock types of the Jaguar deposit. Except for FeO (up to 0.9 wt.%, but mainly < 0.4 wt.%), contents for all elements that may replace Ca or P are close to or below detection limits of routine EMP analyses.

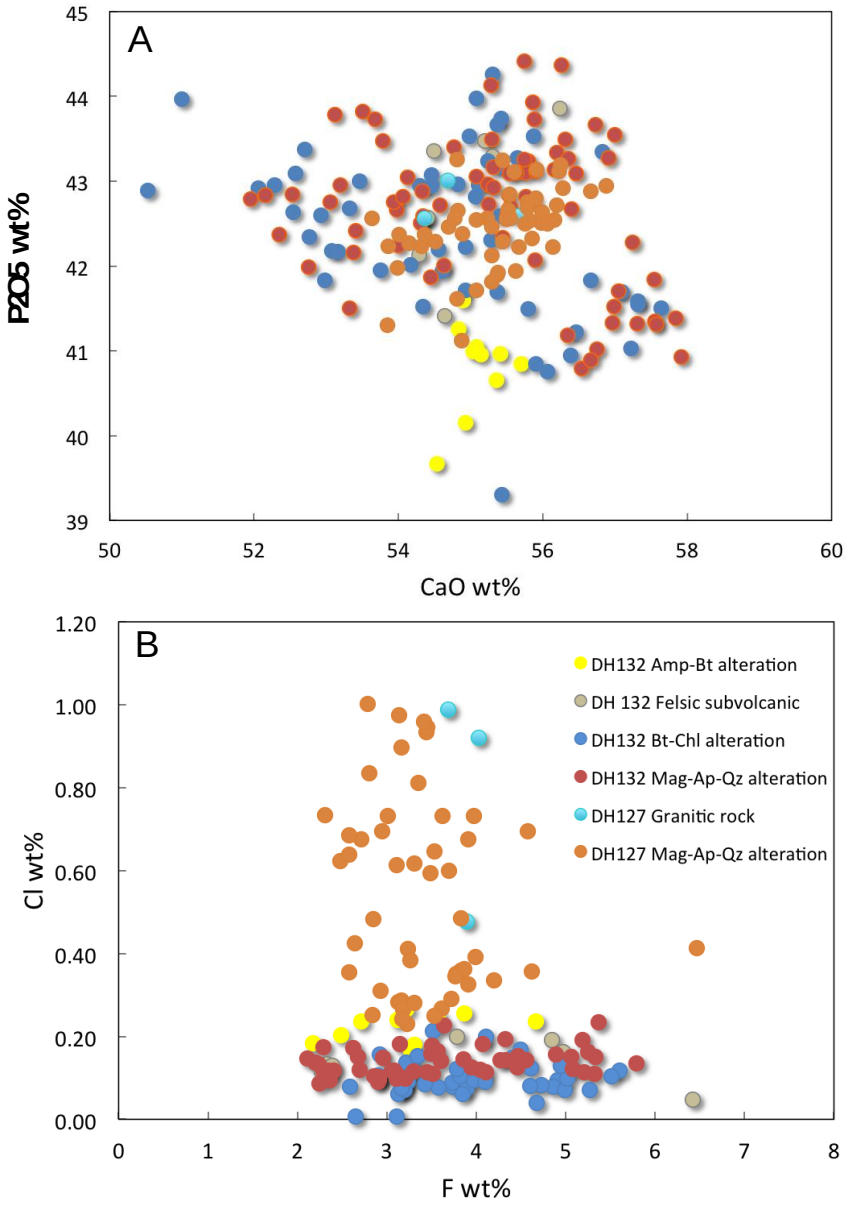

Fig. 20. A) Plot of CaO (wt.%) vs P_2O_5 (wt.%) for apatite samples from the northern (DH127) and southern portions (DH132) of the Jaguar deposit. B) Plot of F (wt.%) vs Cl (wt.%) for apatite samples from the northern (DH127) and southern portions (DH132) of the Jaguar deposit.

Sample MFO-15, an apatite-rich rock from an amphibole-biotite alteration zone, has P_2O_5 contents (39.67-41.59 wt.%) distinctively lower than the other samples. Because the contents of analysed elements that commonly replace P in apatite are also very low for sample MFO-15, it is likely that P replacement consist of a complex process involving SO_4 and/or CO_3OH. The plot of F vs Cl (Fig. 20B) indicates that all analysed samples from the southern portion of the deposit (drill core DH132) have high F contents (2.11-6.42 wt.%) and low Cl contents (< 0.27 wt.%).

Table 4. Representative microprobe analyses of apatite.

Rock Type	Amp	FSV	Bt-Chl	Bt-Chl	Bt-Chl	Bt-Chl	Mag	Mag	Mag	Mag	GRN
Sample	MFO15	MFO08	MFO03	MFO05	MFO17	MFO16	MFO13	MFO14	MFO09	MFO28	MFO20
Analysis (wt%)	C3_Ap_1.7	C1_Ap_1	C1_Ap_1	C4_Ap_1	C3_Ap_1	C3_Ap_1.4	C1_Ap_9	C1_Ap_3	C2_Ap_2	C2_Ap_1	C2_Ap_3
SiO2	0.13	0.02	0.02	0.09	0.11	0.10	0.05	0.04	0.04	0.03	0.10
TiO2	0.08	0.08	0.00	0.12	0.00	0.25	0.10	0.09	0.00	0.04	0.05
Al2O3	0.00	0.00	0.00	0.03	0.00	0.00	0.00	0.00	0.00	0.02	0.04
Cr2O3	0.00	0.05	0.04	0.00	0.09	0.14	0.04	0.00	0.00	0.00	0.04
FeO	0.05	0.18	0.01	0.42	0.09	0.11	0.10	0.10	0.27	0.17	0.07
MnO	0.00	0.00	0.00	0.00	0.00	0.02	0.02	0.00	0.00	0.00	0.04
MgO	0.00	0.00	0.00	0.01	0.00	0.02	0.00	0.02	0.03	0.01	0.03
P2O5	40.99	42.13	42.95	43.08	41.95	42.20	42.61	43.09	42.25	42.56	42.56
CaO	55.03	54.29	55.11	54.46	53.75	54.56	55.51	55.54	54.00	53.64	54.36
Na2O	0.00	0.05	0.01	0.01	0.05	0.02	0.00	0.03	0.01	0.02	0.10
K2O	0.00	0.03	0.01	0.02	0.00	0.00	0.02	0.00	0.01	0.00	0.03
SrO	0.00	0.03	0.12	0.05	0.02	0.00	0.06	0.02	0.07	0.00	0.08
NiO	0.05	0.00	0.02	0.00	0.04	0.00	0.03	0.02	0.23	0.03	0.04
V2O3	0.00	0.00	0.04	0.00	0.00	0.00	0.06	0.00	0.03	0.01	0.00
BaO	0.00	0.10	0.00	0.00	0.03	0.05	0.04	0.00	0.00	0.00	0.02
F	2.17	4.84	3.74	3.58	3.52	4.10	3.86	2.29	5.08	4.20	4.03
Cl	0.18	0.19	0.08	0.08	0.21	0.20	0.14	0.17	0.12	0.73	0.92
Total	97.74	99.90	100.55	100.41	98.32	99.98	100.98	100.39	99.96	99.52	100.60

Rock code: FSV = Felsic subvolcanic; GRN = Granitic rocks; Bt-Chl = Biotite-chlorite alteration rocks; Amp = Amphibole-biotite alteration rocks; Mag = Magnetite-apatite-quartz alteration rocks.

Results for F and Cl are scattered for individual samples from the southern portion and they largely overlap for apatites from different alteration zones. The F contents of apatites from the northern portion (drill core DH127) are similar to those described for samples from the south, but Cl contents are distinctively higher (0.23-1.00 wt.%; Fig. 20B). Although compositions of apatite were not investigated in detail for samples from the northern portion, higher Cl contents and Cl/F ratios in the investigated samples (one from host granite with alteration veins and three from a magnetite-apatite-quartz alteration zone) suggest that variable compositions of apatite may occur in different portions of the Jaguar deposit.

Biotite

Representative compositions of biotite from the Jaguar deposit are shown in Table 5. Structural formulae of biotite were recalculated in the basis of 11 anions (O, OH, F, Cl). The composition of biotite was analysed in rocks from different alteration zones from drill core DH132 (biotite-chlorite and magnetite-apatite-quartz alteration) and DH127 (biotite-chlorite alteration). Biotite is the most common hydrothermal mineral in alteration zones of the Jaguar deposit, being particularly abundant in biotite-chlorite alteration zones. Biotite occurs in fine-grained brown to greenish brown lamellae and can be classified as ferrous-flogopite (Deer et al., 1992). The #Mg

(Mg/Mg+Fe^{+2}) ranges from moderate to high (0.54-0.75) and largely overlap for samples from drill core DH132 and DH127, as well as for samples from biotite-chlorite and magnetite-apatite-quartz alteration zones from drill core DH132 (Fig. 21). TiO_2 contents in biotite also largely overlap for the analysed samples (Fig. 22A), but samples from drill core DH127 (1.14-1.96 wt.%) have higher contents than those from DH132 (0.66-1.39 wt.%). Biotite from rocks from different alteration zones have variable but usually much higher F (up 1.30 wt.%) than Cl (up to 0.63 wt.%) contents (Fig. 21C and 21D). However, Cl contents are still unusually high. Weak correlations for F and Cl contents with Mg# do not support that their incorporation in biotite are mainly controlled by Fe-F and Mg-Cl avoidance mechanism, respectively.

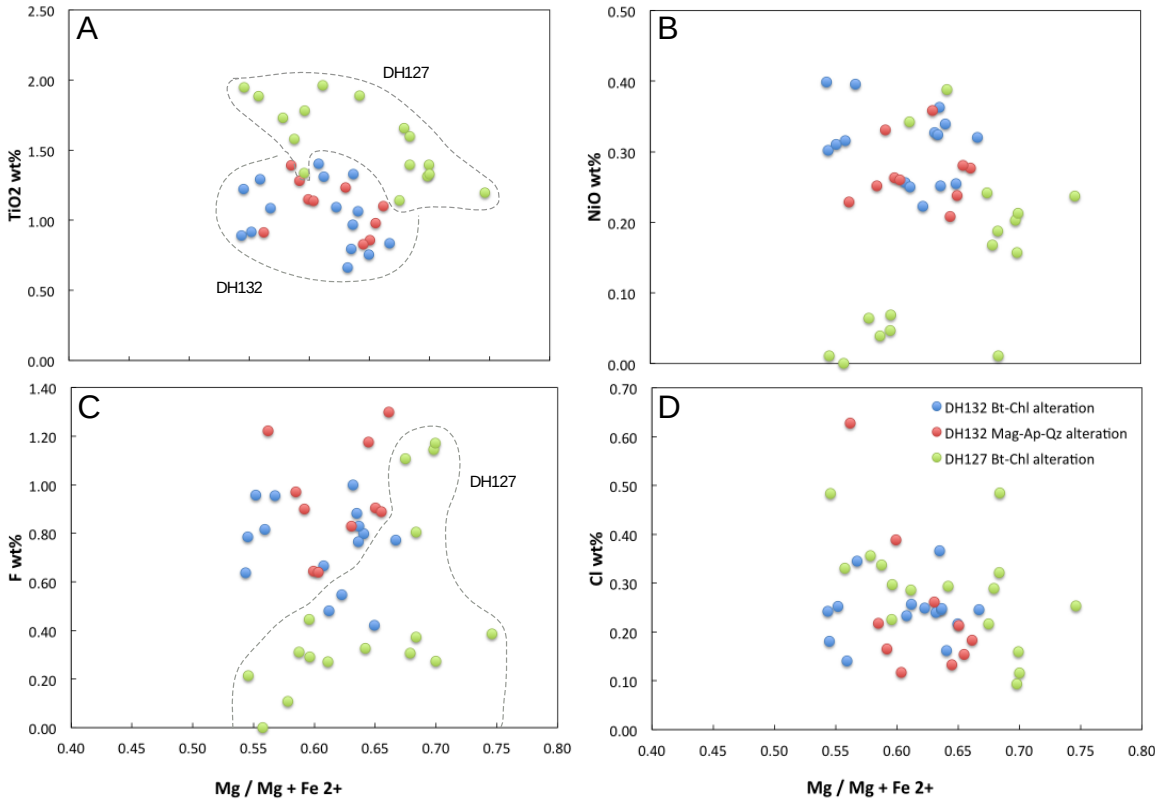

Fig. 21. Plot of #Mg = Mg/(Mg+Fe^{2+}) of biotite samples from DH127 and DH132 vs A) TiO_2 (wt.%), B) NiO (wt.%), C) F (wt.%) and D) Cl (wt.%). Dashed lines separate different drill cores.

Table 5. Representative microprobe analyses of biotite. Rock code: FSV = Felsic subvolcanic; GRN = Granitic rocks; Bt-Chl = Biotite-chlorite alteration rocks; Amp = Amphibole-biotite alteration rocks; Mag = Magnetite-apatite-quartz alteration rocks.

Rock Type	Mag	Mag	Mag	Bt-Chl	Bt-Chl	Bt-Chl	Bt-Chl	Bt-Chl	Bt-Chl	Bt-Chl
Sample	MFO13	MFO09	MFO10	MFO05	MFO17	MFO11	MFO18	MFO27	MFO31	MFO23
Analysis (wt%)	C1 Bt 3	C4 Bt 3	C4 Bt 2	C2 Bt 3	C4 Bt 1	C2 Bt 2	C2 Bt 5	C3 Bt 2	C3 Bt 3	C3 Bt 1.1
SiO2	38.33	38.75	35.97	36.82	39.48	38.46	36.57	38.10	37.10	38.06
TiO2	0.83	1.10	1.28	1.22	0.66	1.33	1.95	1.60	1.96	1.31
Al2O3	13.10	13.08	14.14	14.90	13.66	12.42	16.61	14.34	15.42	14.84
FeO	16.35	16.97	22.43	19.49	16.68	18.23	18.11	15.33	16.34	14.04
MnO	0.01	0.04	0.12	0.10	0.00	0.00	0.00	0.05	0.04	0.09
MgO	15.64	16.09	13.24	12.54	15.72	15.23	12.10	16.22	13.85	16.48
CaO	0.08	0.00	0.01	0.04	0.02	0.00	0.00	0.00	0.05	0.00
Na2O	0.05	0.09	0.04	0.05	0.11	0.06	0.17	0.15	0.13	0.06
K2O	9.12	9.04	7.80	9.43	9.32	8.80	9.50	9.41	9.63	9.40
BaO	0.06	0.12	0.04	0.17	0.04	0.13	0.12	0.00	0.31	0.05
Cr2O3	0.00	0.00	0.07	0.06	0.00	0.07	0.02	0.00	0.07	0.00
V2O3	0.06	0.08	0.04	0.08	0.06	0.10	0.13	0.05	0.07	0.04
NiO	0.21	0.28	0.33	0.30	0.33	0.25	0.01	0.01	0.34	0.20
SrO	0.05	0.00	0.03	0.07	0.00	0.01	0.09	0.09	0.05	0.11
P2O5	0.00	0.00	0.00	0.01	0.04	0.00	0.02	0.00	0.00	0.00
F	1.18	1.30	0.90	0.79	1.00	0.83	0.21	0.81	0.27	1.15
Cl	0.13	0.18	0.17	0.18	0.24	0.25	0.48	0.49	0.29	0.09
Total	94.66	96.53	96.18	95.88	96.89	95.77	95.90	96.19	95.76	95.41
Number of cations per 11 oxygens										
Si	2.92	2.91	2.77	2.82	2.94	2.92	2.77	2.85	2.80	2.85
Al (IV)	1.08	1.09	1.23	1.18	1.06	1.08	1.23	1.15	1.20	1.15
Al (VI)	0.10	0.06	0.05	0.17	0.13	0.03	0.26	0.11	0.17	0.16
Ti	0.05	0.06	0.07	0.07	0.04	0.08	0.11	0.09	0.11	0.07
Cr	0.00	0.00	0.00	0.00	0.00	0.00	0.00	0.00	0.00	0.00
Fe^{3+}	0.06	0.14	0.40	0.05	0.02	0.17	0.01	0.12	0.04	0.08
Fe^{2+}	0.98	0.92	1.05	1.20	1.02	0.98	1.14	0.84	0.99	0.80
Mn	0.00	0.00	0.01	0.01	0.00	0.00	0.00	0.00	0.00	0.01
Mg	1.78	1.80	1.52	1.43	1.74	1.72	1.37	1.81	1.56	1.84
Ca	0.01	0.00	0.00	0.00	0.00	0.00	0.00	0.00	0.00	0.00
Na	0.01	0.01	0.01	0.01	0.02	0.01	0.02	0.02	0.02	0.01
K	0.89	0.86	0.77	0.92	0.88	0.85	0.92	0.90	0.93	0.90
Ba	0.00	0.00	0.00	0.01	0.00	0.00	0.00	0.00	0.01	0.00
V	0.00	0.00	0.00	0.00	0.00	0.01	0.01	0.00	0.00	0.00
Ni	0.01	0.02	0.02	0.02	0.02	0.02	0.00	0.00	0.02	0.01
Zr	0.00	0.00	0.00	0.00	0.00	0.00	0.00	0.00	0.00	0.00
Sc	0.00	0.00	0.00	0.00	0.00	0.00	0.00	0.00	0.00	0.00
Co	0.00	0.00	0.00	0.00	0.00	0.00	0.00	0.00	0.00	0.00
Rb	0.00	0.00	0.00	0.00	0.00	0.00	0.00	0.00	0.00	0.00
Cs	0.00	0.00	0.00	0.00	0.00	0.00	0.00	0.00	0.00	0.00
Cations	7.89	7.89	7.90	7.89	7.88	7.88	7.84	7.89	7.87	7.88
F	0.28	0.31	0.22	0.19	0.24	0.20	0.05	0.19	0.06	0.27
Cl	0.02	0.02	0.02	0.02	0.03	0.03	0.06	0.06	0.04	0.01
OH	1.70	1.67	1.76	1.79	1.73	1.77	1.89	1.75	1.90	1.72

Chlorite

Representative compositions of chlorite from the Jaguar deposit are shown in Table 6. The composition of chlorite was analysed in different rocks from th northern and southern portions of the deposit, including rocks from weakly altered host rocks, as well as rocks from biotite-chlorite, amphibole-biotite and magnetite-apatite-quartz alteration zones. Chlorite is a common hydrothermal mineral throughout the Jaguar deposit. It is a particularly abundant mineral in rocks from biotite-chlorite alteration zones, where it occurs mainly as fine-grained greenish pleochroic lamellae closely associated with biotite. Chlorite has highly variable habit, modal proportion and color (from light green to green) in rocks from weakly altered host rocks and in rocks from magnetite-apatite-quartz and amphibole-biotite alteration zones. The #Mg

(Mg/Mg+Fe^{+2}) ranges from moderate to high (0.47-0.78). The plot of #Mg ratio vs Al^{IV} (Fig. 22A) indicates variable compositions.

Chlorite in the granitic host rocks was analysed in two samples: MFO-20, a chlorite-rich unaltered rock and MFO-22, an altered rock, associated with abundant feldspar. Compositional differences are probably due to temperature variations associated to the hydrothermal alteration progress. In general, compositional ranges of chlorite in biotite-chlorite alteration rocks of the northern portion (DH127) largely overlap and have composition between chlorite from the unaltered granitic rock and the highly altered rock (Fig. 22A). On the other hand, chlorite associated to the magnetite-apatite-quartz alteration from the same portion of the deposit has highly variable compositions, even within the same sample. Different chlorite generations are found in theses samples. Chlorite associated to sulfides shows higher Al^{IV} contents than a late-stage chlorite that crosscuts the sulfide assemblage.

Chlorite from the subvolcanic rock (southern portion; DH132) has higher Al^{IV} contents when compared to the hydrothermal alteration superimposed to this host rock (Fig. 22A). Chlorite from both magnetite-apatite-quartz and biotite-chlorite alteration zones has similar composition.

The most significant compositional feature of chlorite from the Jaguar deposit is the consistently high NiO contents (up to 1.0 wt.%). Except for the weakly altered host rocks (NiO < 0.2 wt.%), high NiO contents (> 0.2 wt.%) characterize chlorite from rocks from different alteration zones (Fig. 23B). NiO contents in chlorite may also be highly variable for each rock type and even for a single sample. The highest Ni contents occur when chlorite is associated to sulfides. Chlorite from rocks from different alteration zones has low F (up to 0.19 wt.%; but mainly < 0.06 wt.%) and Cl (up to 0.11 wt.%; but mainly < 0.05 wt.%) contents, and highly variable F/Cl ratio.

Table 6. Representative microprobe analyses of chlorite.

Rock Type	Amp	Bt-Chl	Bt-Chl	Bt-Chl	Mag	Mag	Mag	FSV	GRN	Bt-Chl	Bt-Chl
Sample	MFO15	MFO03	MFO12	MFO16	MFO10	MFO13	MFO29	MFO08	MFO20	MFO27	MFO04
Analysis (wt%)	C1 chl 1	C2 chl 9	C2 chl 3	C1 chl 1.2	C1 chl 1	C3 chl 2	C2 chl 1.2	C2 chl 3	C1 chl 2.3	C2 chl 4	C2 chl 2
SiO2	26.97	26.14	27.24	26.91	27.24	27.99	31.78	22.35	24.03	26.34	26.81
TiO2	0.00	0.10	0.00	0.00	0.21	0.00	0.25	0.09	0.00	0.12	0.05
Al2O3	19.36	19.36	19.21	19.31	19.26	18.06	11.03	20.60	21.78	20.29	15.79
Cr2O3	0.02	0.00	0.02	0.01	0.00	0.00	0.00	0.00	0.00	0.03	0.03
FeO	20.25	22.07	19.70	21.09	22.82	18.31	23.51	27.76	17.81	17.35	25.91
MnO	0.01	0.09	0.07	0.12	0.07	0.00	0.05	0.15	0.08	0.10	0.12
MgO	20.24	18.15	20.66	18.71	17.49	21.02	19.70	13.68	21.90	21.05	13.54
BaO	0.02	0.06	0.03	0.08	0.08	0.07	0.00	0.00	0.00	0.00	0.00
CaO	0.02	0.03	0.04	0.04	0.02	0.01	0.13	0.01	0.00	0.02	0.05
Na2O	0.02	0.03	0.02	0.04	0.03	0.00	0.00	0.00	0.03	0.01	0.01
K2O	0.06	0.06	0.02	0.10	0.03	0.04	0.03	0.04	0.01	0.06	0.01
V2O3	0.01	0.03	0.00	0.06	0.01	0.05	0.02	0.01	0.00	0.06	0.07
NiO	0.39	0.47	0.29	0.34	0.38	0.49	0.35	0.16	0.05	0.09	1.01
F	0.00	0.00	0.00	0.00	0.06	0.03	0.08	0.00	0.00	0.04	0.00
Cl	0.05	0.01	0.04	0.05	0.04	0.02	0.02	0.07	0.04	0.07	0.01
Total	87.43	86.60	87.35	86.86	87.75	86.08	86.97	84.93	85.74	85.62	83.42
	Number of cations per 28 oxygens										
Si	5.57	5.51	5.60	5.62	5.68	5.81	6.70	5.00	5.01	5.47	6.03
Al (IV)	2.43	2.49	2.40	2.38	2.32	2.19	1.30	3.00	2.99	2.53	1.97
Al (VI)	2.27	2.32	2.26	2.37	2.41	2.22	1.44	2.44	2.37	2.44	2.21
Ti	0.00	0.02	0.00	0.00	0.03	0.00	0.04	0.02	0.00	0.02	0.01
Cr	0.00	0.00	0.00	0.00	0.00	0.00	0.00	0.00	0.00	0.00	0.01
Fe	3.49	3.89	3.39	3.68	3.98	3.18	4.14	5.20	3.11	3.01	4.87
Mn	0.00	0.02	0.01	0.02	0.01	0.00	0.01	0.03	0.01	0.02	0.02
Mg	6.23	5.71	6.34	5.82	5.43	6.50	6.19	4.56	6.81	6.52	4.54
Zn	0.00	0.00	0.00	0.00	0.00	0.00	0.00	0.00	0.00	0.00	0.00
Ca	0.00	0.01	0.01	0.01	0.00	0.00	0.03	0.00	0.00	0.00	0.01
Na	0.01	0.01	0.01	0.02	0.01	0.00	0.00	0.00	0.01	0.00	0.00
K	0.02	0.02	0.01	0.03	0.01	0.01	0.01	0.01	0.00	0.02	0.00
Ba	0.00	0.00	0.00	0.01	0.01	0.01	0.00	0.00	0.00	0.00	0.00
V	0.00	0.01	0.00	0.01	0.00	0.01	0.00	0.00	0.00	0.01	0.01
Ni	0.07	0.08	0.05	0.06	0.06	0.08	0.06	0.03	0.01	0.01	0.18
F	0.00	0.00	0.00	0.00	0.04	0.02	0.06	0.00	0.00	0.02	0.00
Cl	0.02	0.00	0.01	0.02	0.01	0.01	0.01	0.03	0.01	0.02	0.00
OH	15.98	16.00	15.99	15.98	15.94	15.97	15.94	15.97	15.99	15.95	16.00
Cations	20.12	20.08	20.09	20.05	20.02	20.03	19.99	20.31	20.34	20.11	19.88

Rock code: FSV = Felsic subvolcanic; GRN = Granitic rocks; Bt-Chl = Biotite-chlorite alteration rocks; Amp = Amphibole-biotite alteration rocks; Mag = Magnetite-apatite-quartz alteration rocks.

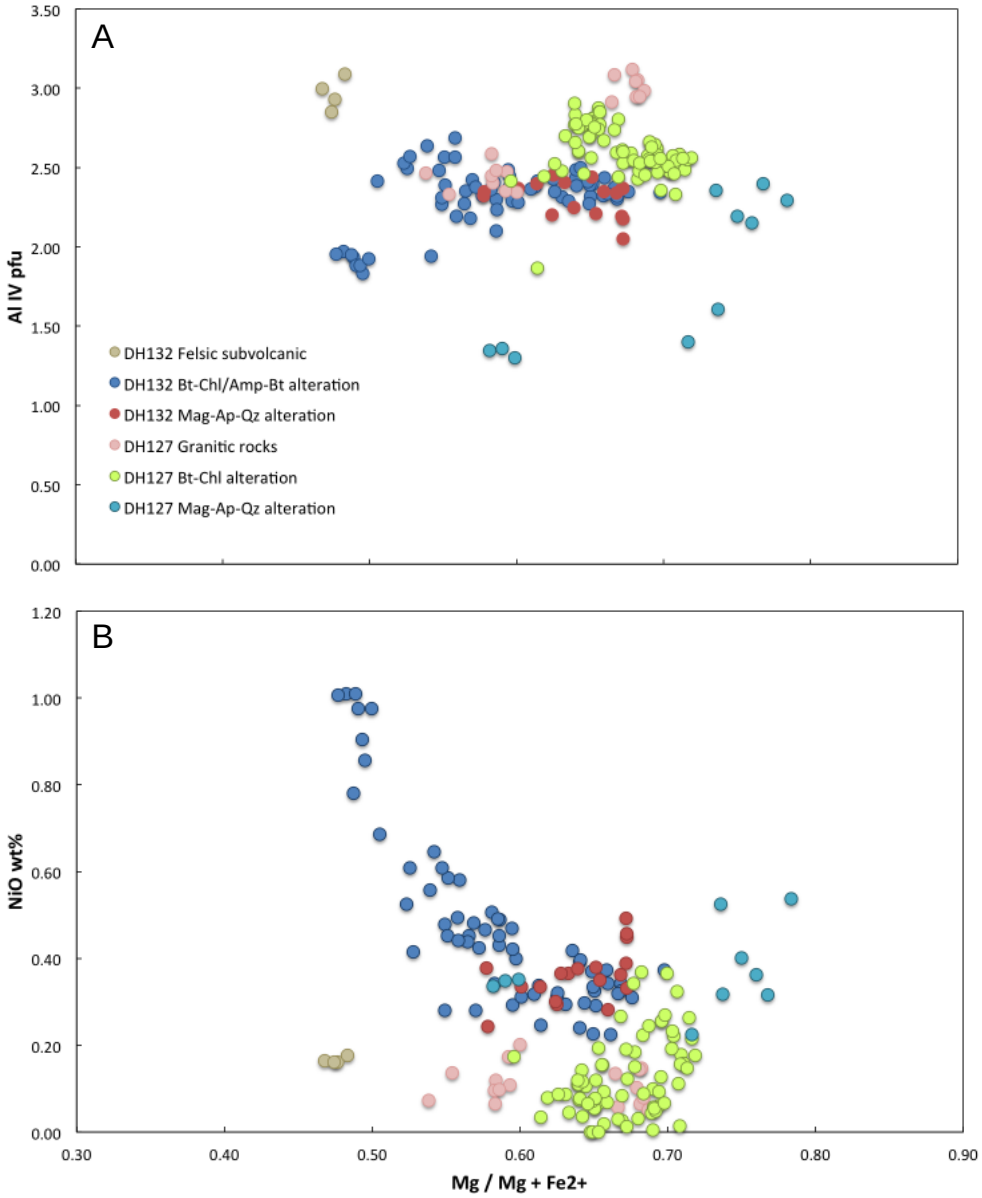

Fig. 22. Plot of #Mg = Mg/(Mg+Fe^{2+}) of chlorite samples from DH127 and DH132 vs A) Al^{IV} (pfu) and B) NiO (wt.%).

Pyrite

The composition of pyrite was analysed in different rocks from drill core DH132 and DH127, including rocks from biotite-chlorite and magnetite-apatite-quartz alteration zones. Pyrite is the most abundant sulfide in the Jaguar deposit. It occurs in all alteration types and in host rocks in minor amount. In barren or weakly mineralized rocks, pyrite may occur in minor amounts as subhedral fine grains randomly distributed in the very fine-grained foliated biotite-chlorite-rich rocks or associated with magnetite in rocks from the magnetite-apatite-quartz alteration zones. In mineralized rocks, pyrite

generally forms subhedral coarser crystals, surrounded by an intergranular mass of fine-grained, anhedral sulfides (pentlandite, millerite, etc).

The plot of Ni vs S (Fig. 23) shows that pyrite has variable Ni contents (0-7830 ppm), even for a single sample, and the highest values are generally found associated to magnetite-apatite-quartz alteration in granitic host rocks (DH127). Cu contents are also variable (0-1110 ppm) and, in contrast, the highest values are associated to biotite-chlorite alteration of subvolcanic host rocks (DH132). Pb (up to 2780 ppm) and Mo (up to 1770 ppm) can reach high values. In most cases, the concentration of Zn in pyrite is around 240 ppm but a few high values (>1000 ppm) have been found in pyrite with direct contact with sphalerite. Co shows high contents (up to 2.39 wt.%) and the highest values are associated to hydrothermally altered granitic rocks (DH127).

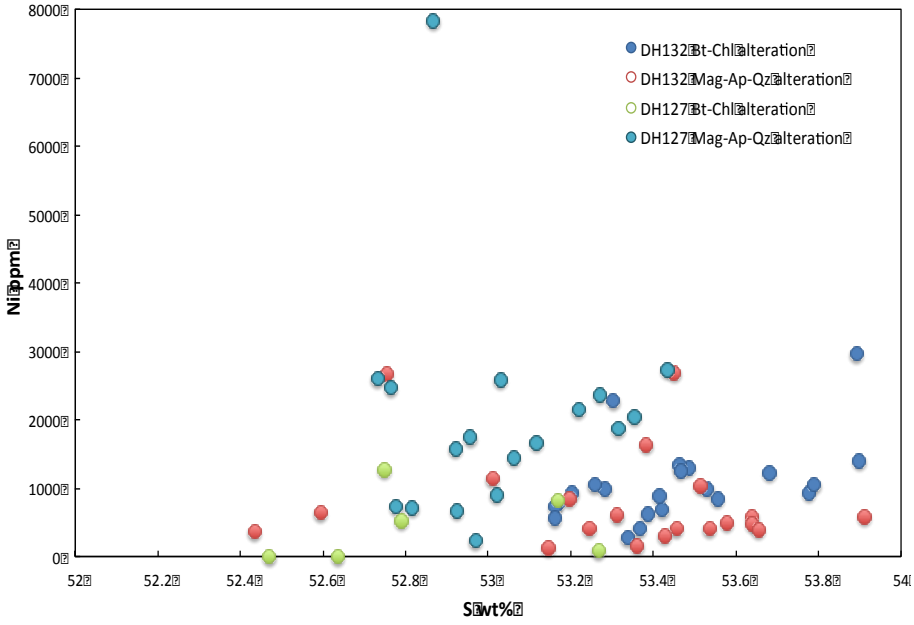

Fig. 23. Plot of NiO (wt.%) vs S (wt.%) for pyrites from drill cores DH127 and DH132.

Sphalerite

The composition of sphalerite was analysed in samples from drill core DH127 and included rocks from magnetite-apatite-quartz alteration zones. Sphalerite forms subhedral, coarser crystals when compared to pentlandite, chalcopyrite and millerite, mostly associated to pyrite. Even though sphalerite may also occur in DH132, as well as in other rock types, it is fairly less abundant and occurs as thin veins, crosscutting alteration zones. The abundance of sphalerite in DH127, where granitic host rocks occur, is consistent with the higher Zn contents observed in lihtogeochemical results

(Fig. 12A). Sphalerite has composition close to the ideal composition (Zn, Fe)S. Cu content is variable (0-2800 ppm), whereby a constant low level of Cu in homogeneous sphalerite crystals is readily distinguishable from the higher level of Cu in the presence of microscopic chalcopyrite exsolution inclusions (Fig. 10F), explaining the heterogeneous distribution pattern of Cu in a few samples. The Cd contents in sphalerite are high (up to 2530 ppm), and as occurs in pyrite, Pb, Co, Ni and Mo contents are also high (up to 1890, 1070, 2940 and 2440 ppm respectively).

Chalcopyrite

The composition of chalcopyrite from the Jaguar deposit was analysed in samples from drill hole DH132, including rocks from both biotite-chlorite alteration (1 sample) and magnetite-apatite-quartz alteration (3 samples), and DH127 (2 samples – magnetite-apatite-quartz alteration). Chalcopyrite is fairly more abundant in DH132 and is mostly associated to magnetite-apatite-quartz alteration. This feature is evidenced by the higher Cu grades in lithogeochemical results shown in DH132 (Fig. 12B). Chalcopyrite from the Jaguar deposit has composition close to the ideal composition ($CuFeS_2$) and occurs as fine-grained, anhedral crystals associated to other sulfides surrounding coarser pyrite and magnetite. As occurs in all the other sulfides in the deposit, chalcopyrite is enriched in Pb (up to 2400 ppm). One chalcopyrite sample (MFO-10) displays high Ni contents (up to 1.03 wt.%).

Pentlandite

The composition of pentlandite was analysed in samples from drill holes DH132 (3 samples) and DH127 (4 samples), only in rocks from magnetite-apatite-quartz alteration, where it is fairly more abundant. Pentlandite from the Jaguar deposit has compositional range close to the ideal composition $(Fe,Ni)_9S_8$. Pentlandite is a common sulfide and forms anhedral to subhedral grains, mostly associated to millerite, pyrhotite and pyrite. Pentlandite has variable Co contents (0-6780 ppm) and shows negative correlation with Ni (-0.61). The high Co values are restricted (except for sample MFO13) to mineralized zones associated to magnetite-apatite-quartz alteration in granitic host rocks (DH127) whereas Ni contents are lower in the same samples. Pb contents are variable but can achieve high values (up to 2200 ppm).

Millerite

The composition of millerite was analysed in samples from drill holes DH132,

in both biotite-chlorite and magnetite-apatite-quartz alteration rocks. Millerite occurs more commonly in the southern portion of the Jaguar deposit and is the main Ni sulfide. The high Ni contents are responsible for the high-grade mineralization. It occurs associated to pentlandite, pyrrotite, and minor chalcopyrite and sphalerite in a fine-grained intergranular network around pyrite and magnetite coarser grains. Fe contents in millerite range from 0.33 to 1.20 wt.%. High Co (up to 2370 ppm) and Pb (up to 2160 ppm) are also observed.

Discussion

The Hydrothermal System of the Jaguar Deposit

The following section will discuss the main characteristics of the hydrothermal system of the Jaguar deposit. A schematic model illustrates the evolution of the hydrothermal alteration and the related Ni mineralization (Fig. 24). Based on geological, mineralogical and geochemical data, a complex evolution of the hydrothermal alteration and associated mineralization is described, involving gneissic rocks (Xingu Complex), granitic intrusions (Plaquê Suite) and felsic subvolcanics of a volcanic-sedimentary sequence along a regional W-NW fault system. Mineralized zones are mainly confined to the contact between the northern granitic-gneissic rocks and the southern felsic subvolcanic rocks (Fig. 24). The Canaan fault system and the intersection with regional structures provided the conditions for high fluid/rock interaction and formation of hydrothermal mineral assemblages.

Unaltered to poorly altered host rocks grade to pervasively altered bodies with increasing hydrothermal alteration towards the mineralized zones, where partial to total obliteration of primary igneous textures and minerals occurs. A complex hydrothermal system characterized by overlapping stages begins with pervasive biotite-chlorite alteration followed by local amphibole-biotite alteration (Stage 1), magnetite-apatite-quartz formation (Stage 2), Ni sulfide mineralization (Stage 3) and minor late carbonate, fluorite, quartz veins infillings.

Biotite + chlorite + quartz ± amphibole assemblage represents an early alteration stage. This alteration type is the most widespread and occurs under ductile conditions. It grades from partially modified rocks to the complete replacement of the original

characteristics of the host rocks, resulting in hydrothermal rocks with mylonitic foliation. Significant FeO and MgO enrichment, matched with mild K_2O enrichment and decrease in Na_2O, occur in this stage, consistent with abundant biotite and chlorite.

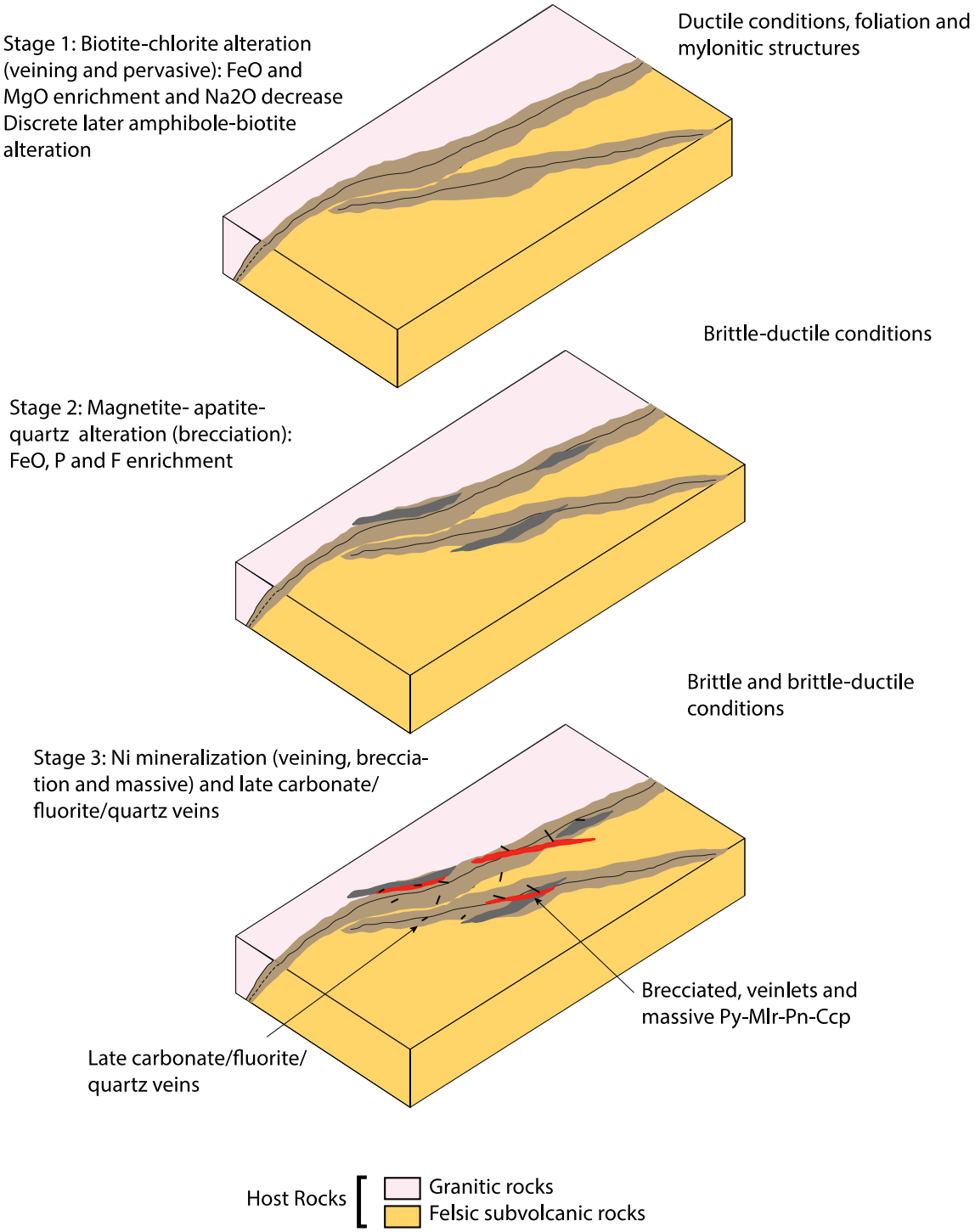

Fig. 24. Schematic model illustrating the evolution of the hydrothermal alteration in the Jaguar deposit. Note that only the main stages are represented.

Chloritization can locally form chlorite-rich bands, mostly in the northern part of

the deposit, where it is associated to granitic host rocks. The early alteration assemblage is commonly associated with quartz and minor, magnetite, apatite, allanite, titanite, fluorite, zircon, tourmaline and epidote, sparsely distributed. The early alteration is associated with deformational processes that initially took place in a ductile regime. Amphibole-biotite alteration locally overprints early alteration zones. This alteration type is restricted and occurs mainly associated to the mineralized zones. CaO contents increase in this stage.

The onset of iron oxide precipitation within the Jaguar deposit alteration sequence is represented by magnetite formation during magnetite-apatite-quartz alteration. This alteration stage is characterized by strong FeO enrichment, resulting from abundant Fe-bearing minerals (e.g., magnetite and biotite), P_2O_5 and F enrichment, resulting from widespread apatite formation. Brecciation takes place in a brittle regime and was probably related to overpressured fluids that caused the hydraulic disaggregation of the host rocks forming crackle breccias infilled with magnetite, apatite, amphibole and minor quartz, biotite and chlorite followed by the Ni sulfide mineralization, comprising the breccia matrix.

The late-stage mineralizing event is concentrated in steeply dipping bodies. Sulfide-rich rocks, including rocks from both magnetite-apatite-quartz and biotite-chlorite alteration zones, are highly enriched in FeO and P_2O_5. Pyrite is the main sulfide, followed by millerite, pentlandite and minor chalcopyrite, pyrrhotite and sphalerite. Millerite and pentlandite are commonly altered to violarite. Vein and disseminated mineralization style are more common and host lower Ni grades whereas subordinate breccia and massive mineralization style hosts the highest Ni grades. Minor carbonates can occur, particularly in association with sulfides that tend to be paragenetically late and post-date the high-temperature alteration. Post-mineralization alteration is represented by late veins of fluorite, carbonate, quartz and minor chlorite that crosscut the mineralized bodies.

Trace element contents of host rocks are altered by fluid-rock interactions and is more expressive in pervasively altered rocks. The hydrothermal alteration products have comparatively higher La/Sm ratios than their host rocks, suggesting LREE enrichment as well as higher total REE contents. This difference is more significant in the subvolcanic rocks domain (337-497 ppm in subvolcanic host rocks, 337-1,578 ppm in

unmineralized alteration rocks and 629-2,658 ppm in mineralized rocks of drill hole DH132). This can be explained by the higher modal content of apatite, allanite and titanite. Regarding the LILE contents, in general, highly altered and mineralized rocks have higher Pb contents. On the other hand, they are strongly depleted in Ba and Sr when compared to the precursor rocks. Zr and Ti contents are also lower in more altered rocks. All hydrothermal rocks are anomaly enriched in U.

The mineralogical and geochemical characteristics described in this study provide compelling evidence for fluids involvement in the mineralization processes in the Jaguar deposit. The variable REE patterns (Fig. 16) indicate that the fluid transport process was complex and the fluids may have interacted with other rock types *en route* to the Jaguar deposit, and in the process either gained or deposited elements.

Gieré (1996) proposes that high amounts of REE (>100 ppm) can only be transported by magmatic fluids of high temperatures and salinity. According to Banks et al. (1994), in ancient hydrothermal systems the largest amounts of REE have been found in very saline magmatic solutions, showing that saline solutions of high temperature are very effective for carrying large proportions of REE. The REE enrichment in the Jaguar deposit is interpreted to be related to intense hydrothermal activity, carried out by high temperatures and salinity ore forming fluids.

The Jaguar Deposit Compared with IOCG deposits

The Jaguar deposit shares a number of similarities with IOCG deposits elsewhere in the world, and particularly with those from the CMP. A connection between hydrothermal Ni and IOCG deposits in the CMP was also suggested for the GT-34 deposit (Siepierski, 2008). However, critical differences in mineralization deposition and fluid composition must be considered to fit the Jaguar deposit in the context of widespread hydrothermal system in the province. The similar characteristics and differences are indicated in the following topics. Table 7 summarizes the main features of the IOCG deposits in the CMP and the Jaguar deposit.

1. Geological and Structural Controls

The spatial relation with shear zones is an important feature in the IOCG deposits in the CMP. They are structurally controlled by regional-scale faults and

brittle-ductile shear zones (e.g., Alvo 118, Sossego, Cristalino, Salobo). The host rocks are variable but involve the metavolcanic-sedimentary units of the Itacaiúnas Supergroup and basement rocks. Similarly, the Jaguar deposit is confined to a regional W-NW fault system – the Canaan fault. The Jaguar deposit is hosted by subvolcanic rocks of the Itacaiúnas Supergroup and basement granitoids, similarly to many IOCG deposits of the CMP.

2. Magmatic – Hydrothermal system

In general, IOCG deposits in the world are associated with granitic rocks that range from diorites to granites (Williams et al., 2005). The establishment of magmatic-hydrothermal as responsible for the iron oxide Cu-Au mineralization systems in the CMP has been reinforced by important Archean and Paleoproterozoic granitic magmatism (Grainger et al., 2008). However, geological and chronological relationship between intrusions and IOCG ore bodies are not clearly defined in the CMP. In the Jaguar deposit, no evident relation with closely associated magmatism was found.

3. Hydrothermal alteration

The hydrothermal alteration in IOCG deposits in Carajás commonly displays an early sodic-calcic alteration controlled by ductile structures and mylonitic fabrics. Following this early stage, potassic alteration is generally present and is subsequently overprinted by chlorite, carbonate-epidote, or sericite-hematite alteration and Cu-Au mineralization, all controlled by brittle structures (e.g., Sossego and Alvo 118). Hydrothermal alteration defined as potassic alteration is generally constituted by variable amounts of actinolite, biotite, quartz, potassic feldspar and pyroxene. Sodic-calcic alteration comprises variable amounts of albite, actinolite, and epidote.

When compared to the Jaguar deposit, the hydrothermal alteration has a similar structure. Typical early alteration stage in the Jaguar deposit is also controlled by ductile structures and mylonitic fabrics. A later alteration stage is developed, controlled by brittle structures, partially overprinting and crosscutting the early stages. Differences in alteration styles between the Jaguar deposit and IOCG deposits of the CMP rely mainly on the alteration mineral assemblage. In the Jaguar deposit, there is no evidence of sodic alteration. Although Na-minerals are present, this metasomatism type is not effectively discriminated by different bulk compositions of hydrothermal rocks and

their protoliths. The early biotite-chlorite alteration in the Jaguar deposit is followed by discrete amphibole-biotite alteration and magnetite-apatite-quartz alteration.

Table 7. Comparative table of IOCG deposits from the CMP and the Jaguar deposit.

Deposit	Host Rocks	Hydrothermal Alteration	Sulfide Ore	Reported Resource	References
Jaguar	Granitic and felsic sub-volcanic rocks	Biotite-chlorite alteration (weak to pervasive), followed by amphibole-biotite (poorly developed) and later magnetite-apatite-quartz alteration (pervasive)	Py, Mlr, Pn, Ccp and Sp associated to Mag, Ap and Amp.	92 Mt @ 0.65% Ni	This issue
Salobo	Salobo Group (Itacaiunas Supergroup)	Bt-Grt-Qtz−rich rock (hydrothermally altered dacite), Hs-Pl−bearing rock (hydrothernally altered tholeiitic basalt), Mag-rich rock (Fa, Gru, Mn Alm, Fe Bt, Cl-Hs, schorlitic Tur, Aln, and Qtz)	Disseminations and seams of Bn, Cc, and Ccp associated with Cv, Mo, cobaltite, safflorite, Gr, native Au, and Ag	789 Mt @ 0.96% Cu, 0.52 g/t Au, and 55 g/t Ag	Vieira et al., 1988; Souza and Vieira, 2000; Lindenmayer, 2003
Igarapé-Bahia/Alemão	Chl-altered basalt, associated hyaloclastite, banded iron formation (BIF), and chert in the footwall and a dominantly coarse- to fine- grained metasedimentary sequence in the hanging wall (Igarapé Bahia Group, Itacaiunas Supergroup)	Chl in weakly mineralized zones, abundant Fe-K alteration minerals (Mag, Bt, Sd, Fe Act, Stp) in strongly mineralized zones	Disseminated to locally massive, Ccp, Bn, associated Mag, Au, U, and LREE minerals, cobaltite, Py, and Mo. Late mineralized veins are composed of variable amounts of Ccp, Py, Qtz, Cal, Chl, and Fl	219 Mt @ 1.4 % Cu, 0.86 g/t Au (Ig. Bahia) and 170 Mt @ 1.5% Cu and 0.8 g/t Au (Alemão)	Tazava, 1999; Tazava and Oliveira, 2000; Tallarico et al., 2005; Lindenmayer et al., 1998; Cordeiro, 1999; Santos, 2002; Dreher et al., 2008
Cristalino	Mafic to felsic metavolcanic rocks, intercalated with BIF of the Grão Pará Group	Siliceous, sodic (Ab and Scp) and potassic (Bt and Mc) alteration, substituted by Am (Hs, Act, and Gru) and Mag and subsequently overprinted by Chl, Ep, Ap, Aln, and Tur	Ccp, Py, Mag, Mrc, bravoite, cobaltite, Mlr, vaesite, and Au, with subordinate Hem, Bn, Cv, Cc, Mo, and Sp	500 Mt @ 1.0 % Cu, 0.3 g/t Au	Huhn et al., 1999
Sossego	Tonalitic rocks (Mesoarchean basement), Sossego granophyric granite, gabbro intrusions and felsic volcanic rocks with minor lenses of meta-ultramafic rocks.	Sequeirinho: sodic and Act-rich sodic-calcic alteration, spatially restricted zones of potassic (Bt and K-Fsp) alteration and Chl-rich zones. Sossego: Ab, sodic-calcic alteration (poorly developed), potassic alteration, Chl zone and late hydrolytic (Ser-Hem-Qtz) assemblages crosscut by calcite veins	Ccp, Py, Au, siegenite, Mlr, Pd melonite, hessite, Cst, Sp, Gn, Mo, thorianite, and Mnz.	245 Mt @ 1.1 % Cu, 0.28 g/t Au	Lancaster Oliveira et al., 2000; Morais and Alkmim, 2005; Monteiro et al., 2008; Carvalho, 2009; Domingos, 2009
Alvo 118	Mafic and intermediate-composition metavolcanic rocks attributed to the Grão Pará Group (Itacaiúnas Supergroup), together with granite and gabbro intrusions and porphyry dikes	Sodic alteration (poorly developed - Ab and Scp), pervasive potassic alteration (K-Fsp and Bt) accompanied by Mag, Chl alteration (widespread) and later Qtz-Ser alteration	Ccp, Bn, Hem, Mag and minor to trace amounts of native Au, Cc, Gn, Sp, Cst, and Bi-Te-Au-Ag minerals	170 Mt @ 1.0 % Cu, 0.3 g/t Au	Rigon et al., 2000; Tallarico, 2003; Xavier et al., 2008; Torresi et al., 2011

The deposits share common geochemical characteristics such as LREE, Fe, U, F, Cl, P, Pb and relative Co and Ni enrichment and are depleted in Zr and Ti (e.g., Alemão, Ronzê 2000; Salobo, Réquia and Fontboté, 2000; Igarapé Bahia deposit; Tazava, 1999). However, most IOCG deposits in the CMP have higher Ba, Ag and Pd contents than in the Jaguar deposit. F is fairly more abundant than Cl in the Jaguar deposit, in contrast to many IOCG deposits in the CMP, where Cl predominates.

4. Mineral chemistry

The composition of amphiboles of the Jaguar deposit are compared to hydrothermal amphiboles from IOCG deposits in the CMP (Fig. 25), such as Gameleira and Salobo (Gomes and Lindenmeyer, 2003), Sossego (Monteiro et al., 2008b) and Igarapé Bahia (Dreher, 2004; Gomes and Lindenmayer, 2003). Compositional clusters and trends indicate the presence of at least two co-existing amphibole types in each deposit. Fe/(Fe+Mg) ratios in the Jaguar deposit are variable (0.13-0.34), and considerably lower than most deposits, overlapping only with compositions of the actinolites from the Sequeirinho ore body from the Sossego deposit (Fig. 25). The overall Cl and K contents of the amphiboles (actinolite and hornblende) from the Jaguar deposit are generally lower than in other deposits, except for actinolites from Gameleira, Sequeirinho, Sossego and Igarapé Bahia that have similar values (Fig. 25). The Jaguar deposit only has amphiboles with $(Na+K)_A$ contents lower than 0.5, in contrast to the other deposits in the CMP that show the common presence of both amphiboles with $(Na+K)_A$ higher and lower than 0.5. #Mg ($Mg/(Mg + Fe^{2+})$ is higher (Fig. 25), also overlapping with the actinolites from Sequeirinho.

Ti incorporation increases with temperature (Sato et al., 1997), thus, high Ti contents in amphiboles indicate high temperature formation. The low contents in the Jaguar deposit (up to 0.07 pfu) are similar to those found in IOCG deposits in the CMP (e.g., Gameleira = 0.07 pfu and Igarapé Bahia = 0.02 pfu), except for the Salobo deposit (0.13 pfu), witch has a higher temperature mineral assemblage indicated by the amphibole garnet equilibrium temperatures (Lindenmayer and Teixeira, 1998).

Low-Ti magnetite is commonly considered characteristic in IOCG deposits (Dupuis and Beaudoin, 2011). The overall Ti contents in alteration rocks from the Jaguar deposit (av. 0.05 wt.%) are very similar to those reported in the Sequeirinho ore

body in the Sossego deposit (av. 0.05 wt.%; Monteiro et al., 2008b) and other IOCG deposits elsewhere (av. 0.04 wt.%; Dupuis and Beaudoin, 2011). As expected, Ni contents are higher in magnetites in alteration rocks from the Jaguar deposit (av. 0.10 wt.%) when compared to other IOCG deposits (Dupuis and Beaudoin, 2011; av. 0.025 wt.%). Unfortunately, NiO contents of magnetite compositions are not reported for the IOCG deposits in the CMP. V contents (av. 0.08 wt.%) are generally lower than in the Sossego deposit (av. 0.35 wt.% in Sequeirinho and 0.11 wt.% in Sossego) and higher than in other IOCG deposits (av. 0.04 wt.%).

A significant compositional feature from biotites from the Jaguar deposit is the high F content (up to 1.30 wt.%), much higher than those reported for biotites from the Sossego deposit (up to 0.24 wt.%; Monteiro et al., 2008b). In contrast, Cl contents are lower in the Jaguar deposit (up to 0.63 wt.%) when compared to the Sossego deposit (up to 3.06 wt.%; Monteiro et al., 2008b).

The abundance of F in hydrothermal minerals in the Jaguar deposit (e.g., fluorite, apatite and biotite) and minor Cl may reflect an eminent role of volatiles (H_2O, Cl, CO_2, F, PO_4) in metal transport. Fluorine and chlorine are ubiquitous constituents of hydrothermal fluids in the Earth's crust (Zhu and Sverjensky, 1991). Their importance in metal transport through the formation of aqueous metal halide complexes (Helgeson, 1964, 1969; Barnes, 1979) and in metasomatism through ionization of the acids HF and HCl (Meyer and Hemley, 1967) has led to considerable effort to establish the fluoride and chloride contents of hydrothermal fluids associated with magmatic, metamorphic, and ore-forming processes. Fluoride and chloride concentrations of former aqueous phases can be predicted from the F and Cl composition in minerals (Zhu and Sverjensky, 1991). The fluid responsible for metal transport in the Jaguar deposit was uncommonly enriched in F, when compared to some IOCG deposits in the CMP (e.g. Igarapé Bahia and Sossego), where Cl is more abundant and has an important role as a ligand in Cu/Au transport. Fluid inclusions and active geothermal systems reveal that Cl and HS are the most important ligands for a wide range of metals. In the Jaguar deposit, the precise role of the anomalous F content in Ni transport deposit is still unknown, and may represent a key for understanding the Ni mineralization.

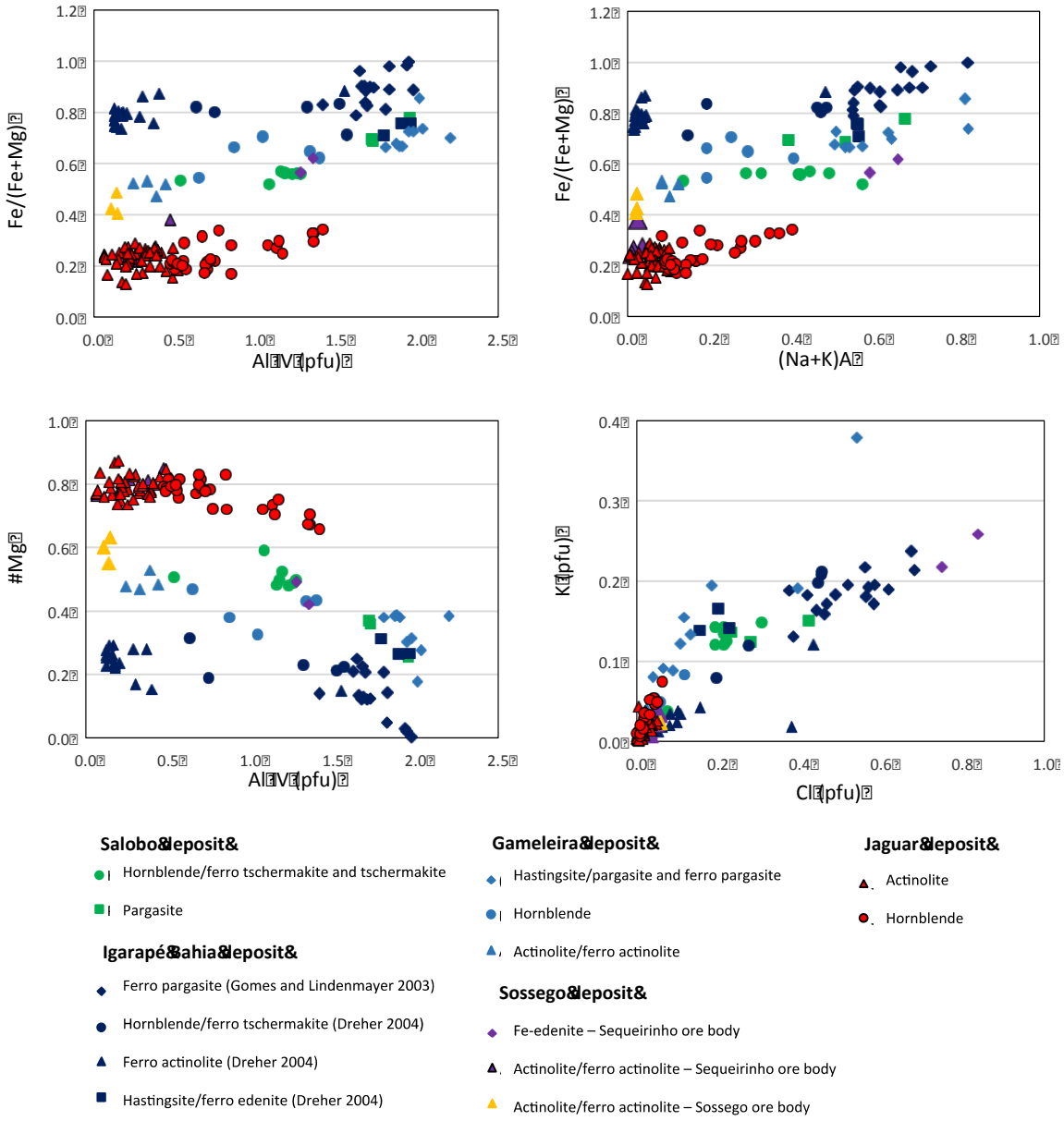

Fig. 25. Diagrams showing amphiboles compositions from IOCG deposits from the CMP and the Jaguar deposit. A) Fe/(Fe+Mg) vs Al^{IV} (pfu); B) Fe/(Fe+Mg) vs $(Na+K)_A$; C) #Mg = $Mg/(Mg+Fe^{2+})$ vs Al^{IV} (pfu) and D) K (pfu) vs Cl (pfu). Data sources: Jaguar deposit (this work); Gameleira and Salobo deposits (Gomes and Lindenmayer 2003); Sossego deposit (Monteiro et al., 2008); Igarapé Bahia deposit (Dreher 2004; Gomes and Lindenmayer 2003).

5. Ore bodies

In the Jaguar deposit, Ni mineralization forms steeply dipping, both lens-shaped bodies and breccia bodies. Copper-gold mineralization in the IOCG deposits in the CMP formed in shallower systems comprise breccia bodies more commonly (e.g. Sossego) in contrast to those formed at deeper systems (e.g Salobo), that form lens shaped and massive replacement bodies parallel to foliation. Ore mineral assemblages

were invariably introduced during the late stages of all IOCG deposits in the CMP as well as in the Jaguar deposit. This is also the case in other IOCG systems elsewhere (e.g., Candelária; Marschik and Fontboté 2001 and Ernest Henry; Mark et al., 2006), where Cu–Au mineralization postdates the main iron oxide stage.

6. Sulfide mineralogy

Chalcopyrite is the most common sulfide in IOCG deposits in the CMP, followed by bornite, chalcocite, pyrite and covellite. In the Jaguar deposit pyrite is the dominant sulfide followed by millerite, pentlandite and minor chalcopyrite, pyrrotite and sphalerite. In the CMP, millerite was also reported in Cristalino (Huhn et al., 2000) and Sossego deposits (Monteiro et al., 2008). The ore mineral assemblage in IOCG deposits is variable and dependent on the sulfidation state of the source fluids. It can provide insights on redox conditions of the hydrothermal system. For example, the mineral assemblage chalcopyrite + bornite in the Salobo deposit (Lindenmayer, 1990; Réquia et al., 1995) indicates more oxidizing conditions than the assemblage chalcopyrite + pyrite, found in the Sossego deposit (Xavier et al., 2012) as indicated by phase relations in the Fe-Cu-S system. In terms of phase relationships, in the system Fe-Ni-S-O (Craig and Kullerund, 1969; Craig, 1973; Frost, 1985) oxidizing conditions drive assemblages towards the oxygen apex of the Fe-Ni-S-O tetrahedron, giving rise to the assemblage: magnetite + millerite + pyrite. In the Jaguar deposit, the presence of millerite can be indicative of oxidizing conditions of the hydrothermal system. The mineral assemblage of the Jaguar deposit thus indicates higher oxidizing conditions compared with pyrrhotite + pentlandite assemblage of the GT-34 deposit (Siepierski, 2008).

The Co content in pyrite in the Jaguar deposit (up to 2.39 wt.%) is comparable to IOCG deposits in the CMP (up to 2.28 wt.% in Sossego deposit; Monteiro et al., 2008b). Investigations have tried to relate the Co/Ni ratio of pyrite to environments of ore genesis (e.g., Brill, 1989 and Raymond, 1996). Carstens (1941) proposed that hydrothermal pyrite generally contains >400 ppm Co and Co/Ni ratio >1. Co/Ni ratios in pyrite from the Jaguar deposit display a wide variation (0.19 to 80.67). However, in most cases the ratios are around 11 and ratios over 20 or less than 1 are rare. This evidences that pyrite is enriched in Co relative to Ni.

How the Jaguar deposit fits into hydrothermal nickel deposits

Hydrothermal Ni deposits are relatively rare. Since the discovery of the Avebury deposit in 1997 in Tasmania (Keays et al., 2009), more attention has been focused on this deposit type, contributing to additional Ni resources being identified as hydrothermal type, notably the Enterprise deposit in Zambia (Capistrant et al., 2015) and Doriri Creek in Papua New Guinea (González-Álvarez et al., 2013). The main deposits described in literature and their geological features are resumed in González-Álvarez et al. (2013). Hydrothermal Ni deposits occur in variable geologic time and tectonic settings, making it difficult to understand what controls Ni solubility in different environments and with diverse potential ligands, differing from Cu and Co.

The Jaguar deposit shows critical differences from other hydrothermal Ni deposits elsewhere:

i. In general, hydrothermal Ni deposits are directly associated to remobilization of Ni in magmatic deposits in mafic-ultramafic rocks or in poly-metallic (Ni-Mo-PGE-Au-Cu-Zn) deposits in black-shales (González-Álvarez et al., 2013). The Jaguar deposit has no association with black shales and is hosted by granitic and felsic subvolcanic rocks;

ii. Except for the Talvivaara deposit in Finland (1550 Mt @ 0.22% Ni; Loukola-Ruskeeniemi and Lahtinen, 2013), hydrothermal Ni deposits have low tonnage (up to 29.3 Mt in Avebury deposit) but can eventually have high Ni grades (2.42 % in Doriri Creek deposit in Papua New Guinea; Lindley and Kirakar, 2007). The Jaguar deposit has considerably larger tonnage (92 Mt @ 0.65% Ni - potential for world class);

iii. Alteration assemblage in hydrothermal Ni deposits is highly variable and the most common minerals are talc, carbonates and amphiboles. The most common alteration minerals in the Jaguar deposit are biotite, magnetite, chlorite and apatite. Iron oxides are rare or absent in most deposits while in the Jaguar deposit iron oxides are abundant (magnetite).

A common feature in the Jaguar deposit and other hydrothermal Ni deposits worldwide is the presence of millerite. It is the most important Ni sulfide in the Jaguar deposit and a common mineral in hydrothermal Ni deposits, notably the Epoch deposit in Zimbabwe (Keays et al., 2009) and the deposits in the Yangtze Platform, south China

(Xu et al., 2011). Laboratory experiments indicate that it may form under hydrothermal conditions at temperatures above 300°C (Kullerud and Yund, 1962). Millerite can also be an important secondary mineral in hydrothermally altered magmatic Ni deposits (e.g., Grguric et al., 2006; Barnes et al., 2009).

A conceptual model for the Jaguar deposit formation is shown in Fig. 26. The Jaguar deposit formation starts with intense Ni mobilization by hydrothermal fluids that are transported in regional scale faults systems. Fluid transport process was complex and the fluids may have interacted with other rock types *en route* to the Jaguar deposit. The fluid was enriched in Ni, Cu, Zn, S, Fe, Mg, P, F, REE and U and was responsible for creating, biotite, chlorite, magnetite, apatite and amphibole-rich alteration zones that extend for several km away from the mineralized bodies. Mineralization represents the last stage of the hydrothermal event. Mineralized bodies overprint and crosscut the alteration zones. Mineralization in the Jaguar deposit is not directly connected to the Ni source. Two possible sources for the Ni mobilized by the hydrothermal fluids may be considered for the Jaguar deposit:

i. Ni for the Jaguar deposit may have been sourced from magmatic Ni-Cu-(PGE) sulfides already present in mafic-ultramafic rocks somewhere within the plumbing system of the hydrothermal fluids. Magmatic Ni–Cu sulfide deposits contain appreciable to very high PGE levels (Naldrett, 1989).

ii. Mafic-ultramafic magmatism is very common in the southern portion of the Carajás Domain. In the Jaguar deposit, Ni may also have been sourced from PGE-poor mafic-ultramafic rocks at depth below the deposit, being liberated from mafic minerals (olivine and orthopyroxene) by fluids of an unknown source. These rocks would have had very low PGE contents, similar to those found in the Jaguar deposit.

In terms of element solubility in hydrothermal fluids, Cu and paladium-group PGEs (Pt, Pd and Rh) behave differently than Ni, Co, and iridium-group PGEs (Ru, Ir and Os). Although the behavior of the different metals varies with fluid composition, temperature, pressure, fO_2, and fS_2, according to Lesher and Keays (2002), the general order of solubility in hydrothermal fluids appears to be Fe>Cu~Au>Pt~Pd>Ni>Co>> Ru ~ Ir. Alteration of sulfides is a far more effective means of mobilizing base and precious metals than alteration of silicates, as has been demonstrated in a variety of

hydrothermal systems (e.g. Jowitt et al., 2012). However, considering the high PGE levels in sulfides and their partitioning into hydrothermal fluids, Ni remobilized from Ni–Cu–(PGE) sulfides would probably have PGE levels elevated above those of its original host rocks. In contrast, Pt-Pd contents in the Jaguar deposit are very low, normally below the detection limits. It is highly unlikely that Ni and Cu mobilization by the fluids was not matched by Pt-Pd removal. Ni originated in a model that involves mobilization of Ni and Cu from mafic-ultramafic rocks seems more suitable for the Jaguar deposit.

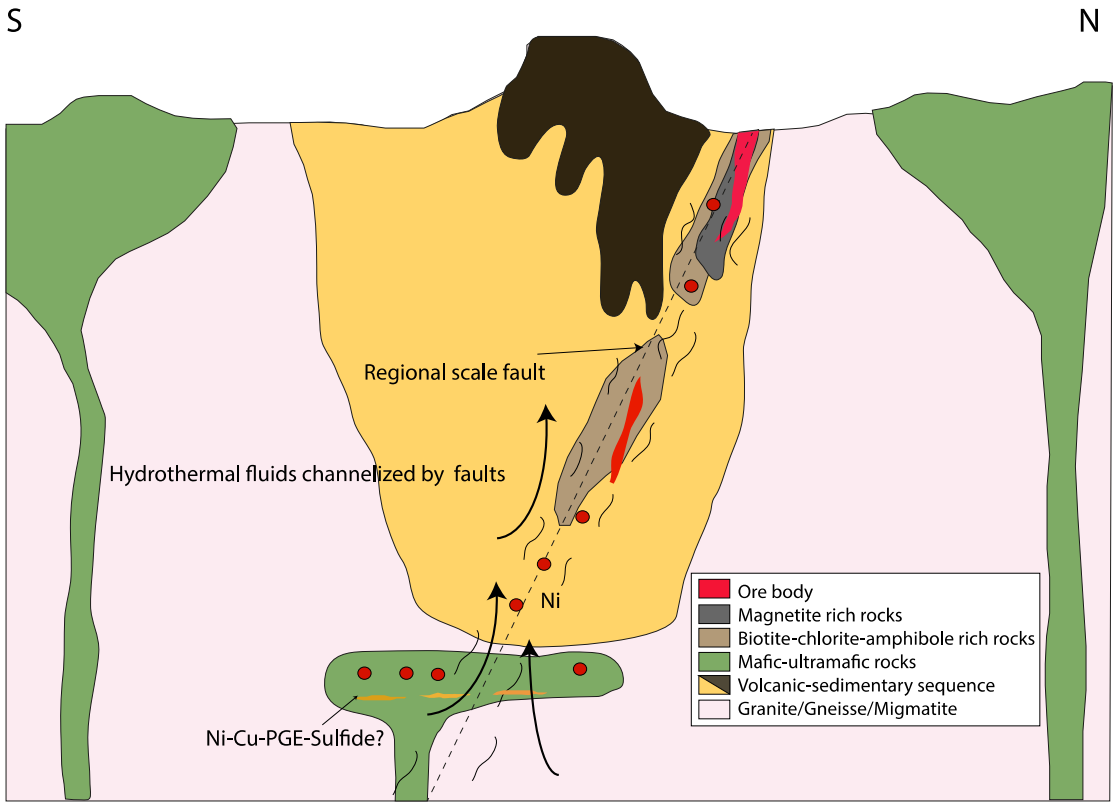

Fig. 26. Conceptual model for the Ni sulfide mineralization formation of the Jaguar deposit. Elements are not in scale.

Implications for exploration for nickel deposits

Ni is currently mined in magmatic sulfide deposits or in lateritic deposits. Both types are associated to mafic-ultramafic rocks. Hydrothermal Ni deposits have smaller economic significance (Fig. 27) and are mostly hosted by mafic-ultramafic rocks.

Exploration for Ni deposits is currently restricted to regions where theses rocks occur. The most notable difference in the Jaguar deposit when compared to the majority of Ni deposits (magmatic, lateritic and hydrothermal) in the world is the lack of direct association with mafic-ultramafic rocks. The similarities of the Jaguar deposit with IOCG deposits from the CMP are also an important aspect to be considered for mineral exploration.

At global scale, the tectonic environments of IOCG deposits involve significant to voluminous igneous activity, structural control (high to low angle faults, generally splays of major, crustal-scale faults), replacement of host rocks by hydrothermal alteration zones and abundance of iron oxide minerals (Hitzman, 2000). Similar features have been observed in the Jaguar deposit and may open possibilities for Ni exploration in geological environments normally considered unprospective for this commodity.

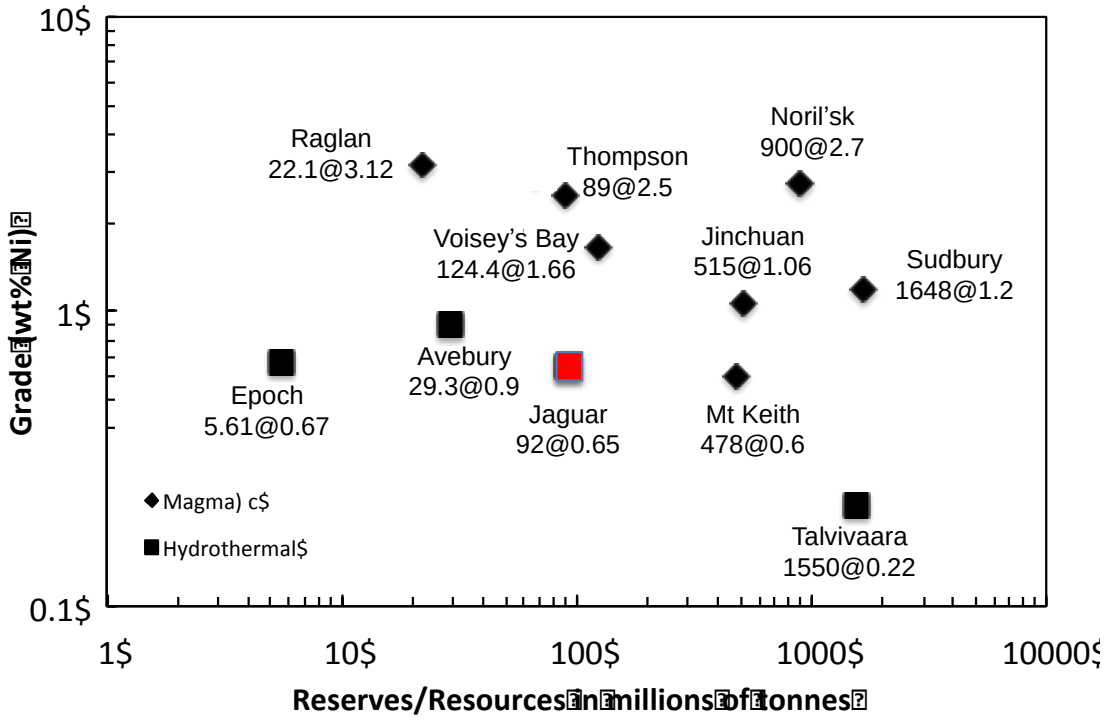

Fig. 27. Plot of Ni grade in wt.% vs resources and reserves in millions of tonnes for major Ni sulfide deposits in the world. Data source for magmatic deposits – Naldrett (1999) and for hydrothermal deposits – González-Álvarez (2013).

A possible source for Ni are mafic-ultramafic rocks. Many deposits are located in regions with occurrence of mafic rocks (e.g. Conclurry District, Australia). The association between relative Ni enrichment and mafic rocks in IOCG deposits has been documented in the Cloncurry district (Eloise and Mt. Elliot deposits; Baker, 1998 and

Wang and Williams, 2001) as well as in Central Andean IOCG deposits (e.g. Candelária and Punta del Cobre; Sillitoe, 2003). The ore signature in the Olympic Dam IOCG deposit is not derived only from the host granite, but can be the result of mafic-ultramafic dikes that occur in the area, as indicated by Sm-Nd isotopic studies (Johnson and McCulloch, 1995). The association of Ni with IOCG districts worldwide and the presence of mafic-ultramafic rocks is not yet recognized as a key for exploration but can represent a new guideline.

When considering the IOCG deposits of the CMP, they also share a considerable number of similarities with the Jaguar deposit, as exposed above. The large scale structures in the southern portion of the Carajás Domain and the abundance of mafic-ultramafic rocks in that region can represent an exploration guideline for Ni mineralization in IOCG districts. In the Sossego deposit, the relative enrichment in Co, Ni, Pd and Se showed in EMP studies, may reflect the chemistry of the gabbro bodies leached by hydrothermal fluids, which have close spatial association with mineralized zones and can represent a possible source for Co and Ni (Monteiro et al., 2008b). The results presented in this study show that this Ni mineralization type and IOCG deposits in the CMP have common characteristics. This opens an exploratory window for Ni deposits in the CMP and elsewhere. Additionally, it is not known what fraction of the Ni and Cu was leached by the ore-forming fluids. It is possible that a magmatic Ni–Cu sulfide residue contains appreciable Ni and Cu.

Conclusion

The Jaguar deposit represents a unique example of hydrothermal Ni deposit of large tonnage and significant ore grade located in the CMP. The deposit lies along a regional, WNW-ESE striking structure. The hydrothermal system was dominantly developed in felsic subvolcanic rocks and subordinately in granitic-gneissic rocks. Hydrothermal alteration forms steeply dipping to vertical structures that envelop the mineralized bodies. Host rocks display the following alteration sequence: i) early pervasive biotite-chlorite alteration with local chlorite-rich bands; ii) restricted amphibole-biotite alteration; iii) late magnetite-apatite-quartz alteration partially overprinting and crosscutting earlier stages. Typical early alteration stage is controlled by ductile structures and mylonitic fabrics. The later alteration stage is controlled by

brittle structures.

Mineralization is the last significant event in the hydrothermal system, overprinting or crosscutting all alteration stages. Two main types of Ni mineralization occur: i) veins and veinlets to stringer sulfides in biotite-chlorite alteration zones comprise the low-grade ore and ii) magnetite-, apatite- and sulfide-rich breccia bodies associated with the magnetite-apatite-quartz alteration, which is less abundant but has the highest ore grades. Disseminated and massive sulfide can also occur. The main sulfide assemblage is pyrite >> millerite > pentlandite > chalcopyrite> pyrrhotite > sphalerite. Hydrothermal alteration zones are characterized by FeO, P_2O_5 and F enrichment. The sulfide mineral assemblage is always associated to abundant magnetite, suggesting oxidizing conditions of the hydrothermal system. Biotite-chlorite alteration zones have mild to distinctive increase in K_2O matched with decrease in Na_2O and increase in MgO. CaO contents are highly variable in the alteration zones and can show local enrichment. The hydrothermal alteration products show LREE enrichment as well as higher total REE contents. Highly altered and mineralized rocks have generally higher Pb and U contents, lower Ba, Sr, Zr and Ti when compared to the precursor rocks.

The Jaguar deposit shares a number of similarities with IOCG deposits of the CMP: structural control along major fault systems and shear zones, spatial association between hydrothermal alteration zones and ore bodies, similar alteration patterns, LREE, Fe, U, F, Cl, P, Pb, Ni and Co enrichment, depletion in Zr and Ti, steeply dipping ore bodies, alteration controlled by both ductile structures and mylonitic fabrics and by brittle structures, abundant iron oxides and hosted by rocks from the Itacaiúnas Supergroup and Xingu Complex.

A possible source of Ni for the Jaguar deposit is the Ni present in mafic-ultramafic rocks, fairly abundant in the southern portion of the Carajás Domain. Pt-Pd contents in the Jaguar deposit are very low, normally below the detection limits. If these mafic-ultramafic rocks are PGE-poor, it seems suitable that Ni mineralization from the Jaguar deposit was originated in a model that involves mobilization of Ni and Cu from mafic-ultramafic rocks.

The abundance of F in hydrothermal minerals (e.g., fluorite, apatite, biotite and

some amphiboles) and REE may reflect the eminent role of volatiles in metal transport and the saline nature of hydrothermal fluids responsible for Ni mineralization. When compared to IOCG deposits from the CMP, F contents from the Jaguar deposit are significantly higher. In contrast, Cl contents are much lower than in IOCG deposits from the same province. The precise role of F in Ni mobilization is unknown but the unusual contents may represent a distinctive feature for Ni transport in hydrothermal fluids.

The different nature of the host rocks of the Jaguar deposit defined specific chemical characteristics in hydrothermal minerals indicating the dependency of mineral compositions on fluid/rock interactions. Differences in chemical compositions within different crystals of the same sample (e.g. compositional variations in amphiboles) may reflect temperature variation during hydrothermal alteration and/or episodic hydrothermal fluid pulses.

The jaguar deposit is an important hydrothermal Ni discovery. It has a higher Ni content compared to the deposits of the same type that have been reported. The Jaguar deposit is not hosted by mafic-ultramafic rocks, unlike most hydrothermal Ni deposits described in literature and unlike all magmatic Ni deposits. This feature represents an important prospective highlight for Ni exploration. The similarities between the Jaguar deposit and the IOCG deposits from the CMP drives the attention for Ni exploration to this unconventional geological environment for Ni mineralization. The abundance of mafic-ultramafic rocks in the southern portion of the Carajás Domain and the presence of a widespread hydrothermal system can indicate possibilities of Ni leaching by hydrothermal fluids and mineralization.

Finally, considering that Ni can be mobilized in a large variety of environments, in different temperatures and by diverse ligands, there is still the potential for discovery of new classes of hydrothermal Ni deposits. It is therefore important to develop a good understanding of the geological processes involved in Ni-mineralization, at different scale of space and time. This is critical not only for efficient mineral exploration, but for understanding metal mobility (Hronsky and Groves, 2008 and Pirajno, 2009). Studies combining the use of tracers (e.g., S isotopes) and laboratory experiments (i.e., with different F and Cl conditions) may be useful to acquire better knowledge on this unusual mineralization type. In the economic point of view, it is necessary to develop a

new empirical model in order to achieve deeper insight into these systems.

Acknowledgments

This study was supported by CNPq (Conselho Nacional de Desenvolvimento Científico e Tecnológico) and Vale S.A. Analytical facilities of the Instituto de Geociências of the University of Brasília (UnB) provided additional support for this research. The authors acknowledge Vale S.A., particularly Fernando Greco (Exploration Manager in Brazil) and Fernando Matos (Geology Specialist), for providing access to the company's private data and for supporting field activities. This study is part of the first author's (Mariana Mota Ferraz de Oliveira) M.Sc. dissertation developed at the University of Brasília. Mariana thanks CAPES-MEC (Coordenação de Aperfeiçoamento de Pessoal de Nível Superior - Ministério da Educação) for the M.Sc scholarship.

References

Araújo, O.J.B., and Maia, R.G.N., 1991, Serra dos Carajás, folha SB.22-ZA, Estado do Pará: Programa Levantamentos Geológicos Básicos do Brasil, Companhia de Pesquisa de Recursos Minerais, 136 p.

Araújo, O.J.B., Maia, R.G.N., Jorge-João, X.S., and Costa, J.B.S., 1988, A megaestruturação da folha Serra dos Carajás: Congresso Latino Americano de Geologia, 7th, Brazil, Proceedings, p. 324–333.

Baker, T., 1998, Alteration, mineralization, and fluid evolution at the Eloise Cu–Au deposit, Cloncurry district, northwest Queensland, Australia: Economic Geology, v.93, p.1213–1236.

Banks, D.A., Yardley, B.W.D., Campbell, A.R., and Jarvis, K.E., 1994, REE composition of an aqueous magmatic fluid: a fluid inclusion study from the Capitan Pluton, New Mexico: Chemical Geology, v.113, p.259-272.

Barnes, H.L., 1979, Geochemistry of Hydrothermal Ore Deposits, 2nd ed. 798 p.

Barnes, S.J., Wells, M.A., and Verrall, M.R., 2009, Effects of Magmatic Processes, Serpentinization, and Talc-Carbonate Alteration on Sulfide Mineralogy and Ore Textures in the Black Swan Disseminated Nickel Sulfide Deposit, Yilgarn Craton: Economic Geology, v.104, p. 539-562.

Brill, B.A., 1989, Trace-element contents and partitioning of elements in ore minerals from the CSA Cu-Pb-Zn deposit, Australia: Canadian Mineralogist, v.27, p.263-274.

Capistrant, P.L., Hitzman, M.W., Wood, D., Kelly, N.M., Williams, G., Zimba, M.,

Kuiper, Y., Jack, D., and Stein, H., 2015, Geology of the Enterprise Hydrothermal Nickel Deposit, North-Western Province, Zambia: Economic Geology, v.110, p.19-38.

Carstens, C.W., 1941, Om geokjemisk undersokelser av maimer: Norsk Geol Tids, v.21, p.213-221.

Carvalho, E.R., 2009, Caracterização geológica e gênese das mineralizações de óxido de Fe-Cu-Au e metais associados na Província Mineral de Carajás: estudo de caso do depósito de Sossego: Unpublished Ph.D. thesis, Universidade Estadual de Campinas, 141 p.

Costa, M.L., Choque, O.J., and Requelme, M.E.R., 2005, O depósito de manganês do Azul, Carajás: estratigrafia, geoquímica e evolução geológica, in Marini, O.J., Queiroz, E.T., and Ramos, B.W., ed., Caracterização de depósitos minerais em Distritos Mineiros da Amazônia: DNPM-CT-Mineral- FINEP-ADIMB, p. 227−333.

Craig, J.R., 1973, Pyrite-pentlandite assemblages and other low-temperature phase relations in the Fe-Ni-S system: American Journal of Science, v. 273A, p. 496-510.

Craig, J.R., and Kullerud, G., 1969, Phase relations in the Cu-Fe-Ni-S system and their application to magmatic ore deposits: Economic Geology, v.4, p. 344-358.

Dall'Agnol, R., Oliveira, M.A., Almeida, J.A.C., Althoff, F.J., Leite, A.A.S., Oliveira, D.C., and Barros, C.E.M., 2006, Archean and paleoproterozoic granitoids of the Carajás Metallogenic Province, eastern Amazonian craton: Symposium on magmatism, crustal evolution and metallogenesis of the Amazonian Craton, Belém, Excursion Guide, p. 99–150.

Dardenne, M.A., Ferreira Filho, C.F., and Meirelles, M.R., 1988, The role of shoshonitic and calc-alkaline suites in the tectonic evolution of the Carajás District, Brazil: Journal of South American Earth Sciences, v.1, p. 363-372.

Domingos, F., 2009, The structural setting of the Canaã dos Carajás region and Sossego-Sequeirinho deposits, Carajás, Brazil: Unpublished Ph.D. thesis, Durham University, 483 p. (available at Durham E-Theses Online: http://etheses.dur.ac.uk/144/).

Donaldson, M.J., 1981, Redistribution ore elements during serpentinization and talc–carbonate alteration of some Archaean dunites, Western Australia: Economic Geology, v. 76, p. 1698–1715.

DOCEGEO, 1988, Revisão litoestratigráfica da Província Mineral de Carajás-Litoestratigrafia e principais depósitos minerais: Congresso Brasileiro de Geologia, 35th, Belém, Sociedade Brasileira de Geologia, Proceedings, p. 11−54.

Dreher, A.M., 2004, O depósito primário de Cu-Au de Igarapé Bahia, Carajás: Rochas fragmentárias, fluidos mineralizantes e modelo metalogenético: Unpublished Ph.D. thesis, Universidade Estadual de Campinas, 221 p.

Dreher, A.M., Xavier, R.P., Taylor, B.E., and Martini, S., 2008, New geologic, fluid inclusion and stable isotope studies on the controversial Igarapé Bahia Cu-Au deposit, Carajás province, Brazil: Mineralium Deposita, v. 43, p. 161−184.

Dupuis, C., Beaudoin, G., 2011, Discriminant diagrams for iron oxide trace element fingerprinting of mineral deposit types: Mineralium Deposita, v.46, p.319-335.

Feio, G.R.L., 2011, Magmatismo granitóide arqueano da área de Canaã dos Carajás: implicações para a evolução crustal da Província Carajás. Unpublished Ph.D. thesis, Universidade Federal do Pará, 190 p.

Feio, G.R.L., Dall'Agnol, R., Dantas, E.L., Macambira, M.J.B., Gomes, A.C.B., Sardinha, A.S., Oliveira, D.C., Santos, R.D., and Santos, P.A., 2012, Geochemistry, geochronology, and origin of the Neoarchean Planalto Granite suite, Carajás, Amazonian craton: A-type or hydrated charnockitic granites?: Lithos, v. 151, p. 57–73.

Feio, G.R.L., Dall'Agnol, R., Dantas, E.L., Macambira, M.J.B., Santos, J.O.S., Althoff F.J., and Soares, J.E.B., 2013, Archean granitoid magmatism in the Canaã dos Carajás area: Implications for crustal evolution of the Carajás province, Amazonian craton, Brazil: Precambrian Research, v. 227, p. 157–185.

Ferreira Filho, C.F., Cançado, F., Correa, C., Macambira, E.M.B., Siepierski, L., and Brod, T.C.J., 2007, Mineralizações estratiformes de EGP-Ni associadas a complexos acamadados em Carajás: os exemplos de Luanga e Serra da Onça, in Contribuições à Geologia da Amazônia, Publitec Gráfica & Editora, v. 5, p. 01-14.

Frost, B.R., 1985, On the stability of sulfides, oxides and native metals in serpentinite: Journal of Petrology, v. 26, p. 31–63.

Gieré, R., 1996, Formation of rare earth minerals in hydrothermal systems, in Jones, A.P., Wall, F., Williams, C.T., ed., Rare earth minerals: chemistry, origin and ore deposits, London, p.105-150.

Gibbs, A.K., Wirth, K.R., 1990, Geologic setting of the Serra dos Carajás iron deposits, Brazil, in Chauvel, J.J., ed., Ancient Banded Iron Formations (Regional Presentations): Theophrastus, Athens, p. 83–102.

Gibbs, A.K., Wirth, K.R., Hirata, W.K., and Olszewski, W.J., Jr., 1986, Age and composition of the Grão Pará Group volcanics, Serra dos Carajás: Revista Brasileira de Geociências, v. 16, p. 201–211.

Gomes, C.H., Lindenmayer, Z.G., 2003, Anfibólios cálcicos dos depósitos de Cu–Au de Gameleira, Salobo e Bahia, Província Mineral de Carajás, Pará: minerais metamórficos ou hidrotermais?, in Ronchi, L.H., Althoff, F.J., ed., Caracterização e modelamento de depósitos minerais, 1st ed.: São Leopoldo, Rio Grande do Sul, v. 1, p. 119–145.

González-Álvarez, I., Pirajno, F., and Kerrich, R., 2013, Hydrothermal nickel deposits: Secular variation and diversity: Ore Geology Reviews, v. 52, p. 1–3.

Grainger, C.J., Groves, D.I., Tallarico, F.H.B, and Fletcher, I.R., 2008, Metallogenesis of the Carajás mineral province, Southern Amazon craton, Brazil: Varying styles of Archean through Paleoproterozoic to Neoproterozoic base- and precious-metal mineralization: Ore Geology Reviews, v. 33, p. 451–489.

Grguric, B.A., Rosengren, N.M., Fletcher, C.M., and Hronsky, J.M.A., 2006, Type 2 deposits: Geology, mineralogy and processing of the Mount Keith and Yakabindie

orebodies, Western Australia: Society of Economic Geologists Special Publication, v. 13, p. 119–138.

Hawthorne, F.C., Oberti, R., Harlow, G.E., Maresch, W.V., Martin, R.F., Shumacher, J.C. and Welch, M.D., 2012, Nomenclature of the amphibole supergroup: American Mineralogist, v. 97, p. 2031–2048.

Helgeson, H. C., 1964, Complexing and Hydrothermal ore deposits: New York, Pergamon Press, 128 p.

Helgeson, H. C., 1969, Thermodynamics of hydrothermal systems at elevated temperatures and pressures. American Journal of Sciences, v. 267, p. 729- 894.

Hirata, W.K., Rigon J.C., Kadekaru K., Cordeiro A.A.C., and Meireles E.A., 1982, Geologia Regional da Província Mineral de Carajás: Simpósio de Geologia da Amazônia, 1st, Belém, Brasil, Sociedade Brasileira de Geologia- Núcleo Norte (SBG/NO), p. 100–110.

Hitzman, M.W., 2000, Iron oxide–Cu–Au deposits: what, where, when, and why, in: Porter, T.M., ed., Hydrothermal Iron Oxide Cooper–Gold and Related Deposits: a Global Perspective. Australian Mineral Foundation, vol.1. Adelaide, p. 9–25.

Hronsky, J.M.A., Groves, D.I., 2008. Science of targeting: definition, strategies, targeting and performance measurement. Australian Journal of Earth Sciences, v. 55, p. 3–12.

Huhn, S.R.B., Souza, C.I.J., Albuquerque, M.C., Leal, E.D., and Brustolin, V., 1999a, Descoberta do depósito Cu-(Au) Cristalino: Geologia e mineralização associada região da Serra do Rabo, Carajás, PA: Simpósio de Geologia da Amazônia, 6th, Belém, Sociedade Brasileira de Geologia, Proceedings, p. 140−143.

Huhn, S.R.B., Macambira, M.J.B., and Dall'Agnol, R., 1999b, Geologia e geocronologia Pb-Pb do Granito Alcalino Planalto, Região da Serra do Rabo, Carajás-PA: Simpósio de Geologia da Amazônia, 6th, Sociedade Brasileira de Geologia-Núcleo Norte (SBG/NO), p. 463–466.

Huhn, S.R.B., Soares, A.D.V., Souza, C.I.J., Albuquerque, M.A.C., Leal, E.D., Vieira, E.A.P., Masotti, F.S., Brustolin, V., 2000. The Cristalino copper–gold deposit, Serra dos Carajás, Pará. International Geological Congress, 31st, Rio de Janeiro, International Union of Geological Sciences, [CD-ROM].

Johnson, J.P., McCulloch, M.T., 1995, Sources of mineralizing fluids for the Olympic Dam deposit (South Australia): Sm–Nd isotopic constraints: Chemical Geology, v.121, p.177–199.

Jowitt, S.M., Jenkin, G.R.T., Coogan, L.A., and Naden, J., 2012, Quantifying the release of base metals from source rocks for volcanogenic massive sulfide deposits: effects of protolith composition and alteration mineralogy: Journal of Geochemical Exploration, v. 118, p. 47–59.

Keays, R.R., 1987, Principles of mobilisation (dissolution) of metals in mafic and ultra-mafic rocks: the role of immiscible magmatic sulphides in the generation of

hydrothermal gold and volcanogenic massive sulphide deposits: Ore Geology Reviews, v. 2, p. 47–63.

Keays, R.R., Jowitt, S.M., and Callaghan, T., 2009, The Avebury Ni deposit, Tasmania: a case study of an unconventional Ni deposit, in Williams, P.J., ed., Smart Science for Exploration and Mining: Proceedings of the Tenth Biennial SGA Meeting, Economic Geology Research Unit, Townsville, p. 173–175.

Kullerud, G., 1969, Sulfide phase relations: Mineralogical Society of America, Special paper 3, p. 199-210.

Kullerud, G., and Yund, R. A., 1962, The Ni-S system and related minerals: Journal of Petrology, v. 8, p. l26-175.

Lancaster Oliveira, J., Fanton, J., Almeida, A.J., Leveille, R.A., and Vieira, S., 2000, Discovery and geology of the Sossego copper-gold deposit, Carajás district, Pará State, Brazil: International Geology Congress, 31st, Rio de Janeiro, 6−17 August, Proceedings [CD-ROM].

Leite, A.A.S., 2001, Geoquímica, petrogênese e evolução estrutural dos granitóides arqueanos da região de Xinguara, SE do Cráton Amazônico**,** Unpublished PhD thesis, Brazil, Universidade Federal do Pará, Belém, 330p.

Lesher, C.M., and Keays R.R., 2002, Discrimination between magmatic and hydrothermal Ni–Cu–PGE and PGE mineralization [ext. abs.]: International Platinum Symposium, 9th, Stillwater, United States, 2002, Extended Abstracts

Lindenmayer, Z.G., 1990, Salobo sequence, Carajás, Brasil: Geology, geochemistry and metamorphism: Unpublished Ph.D. thesis, Canada, University of Western Ontario, 407 p.

Lindenmayer, Z.G., 2003, Depósito de Cu–Au do Salobo, Serra dos Carajás: Uma revisão, in Ronchi, L.H., Althoff, F.J., ed, Caracterização e modelamento de depósitos minerais, São Leopoldo, p. 69–98.

Lindenmayer, Z.G., and Teixeira, J.B.G., 1999, Ore genesis at the Salobo copper deposit, Serra dos Carajás, in Silva, M.G., and Misi, A., ed., Base metal deposits of Brazil: MME/CPRM/DNPM, p. 33−43.

Lindley, I.D., Kirakar, J.K., 2007, Hydrothermal alteration patterns in the Doriri Creek Pd–Pt–Ni Prospect, EL 1424 Mt Suckling, Northern Province, Papuan Precious Metals Internal Report, 24 p.

Liu, W., Migdisov, A., and Williams-Jones, A., 2012, The stability of aqueous nickel (II) chloride complexes in hydrothermal solutions: results of UV–visible spectroscopic experiments: Geochimica et Cosmochimica Acta, v. 94, p. 276–290.

Lobato, L.M., Rosière, C.A., Silva, R.C.F., Zucchetti, M., Baars, F.J., Seoane, J.C.S., Rios, F.J., Pimentel, M., Mendes, G.E., and Monteiro, A.M., 2005, A mineralização hidrotermal de ferro da Província Mineral de Carajás, controle estrutural e contexto na evolução metalogenética da Província, in Marini, J.O., Queiróz, E.T., and Ramos, W.B., ed., Caracterização de Distritos Mineiros da Amazônia, DNPM-CT-Mineral-ADIMB, p. 25−92.

Loukola-Ruskeeniemi, K., Lahtinen, H., 2013, Multiphase evolution in the black-shale-hosted Ni–Cu–Zn–Co deposit at Talvivaara, Finland: Ore Geology Reviews, v.52, p.85–99.

Macambira, E.M.B., and Ferreira Filho, C.F., 2002, Fracionamento Magmático dos Corpos Máfico-Ultramáficos da Suíte Intrusiva Cateté – Sul do Pará, in Klein, E.L., Vasquez, M.L., and Rosa Costa, L.T., ed., Contribuições à Geologia da Amazônia, SBG-Núcleo Norte, v. 3, p. 105-114.

Macambira, M.J.B., and Lancelot, J., 1996, Time constraints of Archean Rio Maria crust, Southeastern Amazonian Craton, Brazil: International Geology Review, v. 38, p. 1134–1142.

Machado, N., Lindenmayer, D.H., Krough, T.E., and Lindenmayer, Z.G., 1991, U-Pb geochronology of Archean magmatism and basement reactivation in the Carajás area, Amazon Shield, Brazil: Precambrian Research, v. 49, p. 1−26.

Mansur, E.T., Ferreira Filho, C.F., 2016, Magmatic structure and geochemistry of the Luanga Mafic-Ultramafic Complex: Further constraints for the PGE-mineralized magmatism in Carajás, Brazil: Lithos, v.266, p.28-43.

Mark, G., Oliver, N.H., and, Williams, P.J., 2006, Mineralogical and chemical evolution of the Ernest Henry Fe oxide–Cu–Au ore system, Cloncurry district, northwest Queensland, Australia: Mineralium Deposita, v.40, p.769–801.

Marschik, R., and Fontboté, L., 2001, The Candelaria-Punta del Cobre Iron Oxide Cu–Au (Zn–Ag) deposits, Chile: Economic Geology, v.96, p.1799–1826.

Meyer, C., and Hemley, J. J., 1967, Wall rock alteration, in Barnes, H.L., ed., Geochemistry of Hydrothermal Ore Deposits, Holt Rinehart and Winston, New York, p.166-235.

Monteiro, L.V.S., Xavier, R.P., Carvalho, E.R., Hitzman, M.W., Johnson, C.A., Souza Filho, C.R., and Torresi, I., 2008a, Spatial and temporal zoning of hydrothermal alteration and mineralization in the Sossego iron oxide-copper-gold deposit, Carajás mineral province, Brazil: Parageneses and stable isotope constraints: Mineralium Deposita, v. 43, p. 129−159.

Monteiro, L.V.S., Xavier, R.P., Hitzman, M.W., Juliani, C., Souza Filho, C.R., and Carvalho, E.R., 2008b, Mineral chemistry of ore and hydrothermal alteration at the Sossego iron oxide-copper-gold deposit, Carajás mineral province, Brazil: Ore Geology Reviews, v. 34, p. 317−336.

Morais, R.P.S., and Alkmim, F.F., 2005, O controle litoestrutural da mineralização de cobre do Depósito Sequeirinho, Canaã dos Carajás, PA: Simpósio Brasileiro de Metalogenia, I, Gramado, Sociedade Brasileira de Geologia, Proceedings [CD-ROM].

Moreto, C.P.N., Monteiro, L.V.S., Xavier, R.P., Amaral, W.S., Santos, T.J.S., Juliani, C., and Souza Filho, C.R., 2011, Mesoarchean (3.0 and 2.86 Ga) host rocks of the iron oxide-Cu-Au Bacaba deposit, Carajás Mineral province: U-Pb geochronology and metallogenetic implications: Mineralium Deposita, v. 46, p. 789–811.

Moreto, C.P.N., Monteiro, L.V.S., Xavier, R.P., Creaser, R.A., DuFrane, A., Melo, G.H.C., Silva, M.A.D., Tassinari, C.C.G., and Sato, K., 2015a, Timing of multiple hydrothermal events in the iron oxide-copper-gold deposits of the Southern copper belt, Carajás province, Brazil: Mineralium Deposita, v. 50, p. 517-546.

Moreto, C.P.N., Monteiro, L.V.S., Xavier, R.P., Creaser, R.A., DuFrane, S.A., Tassinari, C.C.G., Sato, K., Kemp, A.I.S., and Amaral, W.S., 2015b, Neoarchean and Paleoproterozoic Iron Oxide-Copper-Gold Events at the Sossego Deposit, Carajás Province, Brazil: Re-Os and U-Pb Geochronological Evidence: Economic Geology, v. 110, p. 809–835.

Moroni, M., Girardi, V.A.V., and Ferrario, A., 2001, The Serra Pelada Au–PGE deposit, Serra dos Carajás (Pará State, Brazil): geological and geochemical indications for a composite mineralising process: Mineralium Deposita, v. 36, p. 768–785.

Naldrett, A.J., 1989, Magmatic Sulfide Deposits: Wotton-under-Edge, Clarendon Press, 186 p.

Naldrett, A.J., 1998, World-class Ni-Cu-PGE deposits: key factors in their genesis: Mineralium Deposita, v.34, p.227-240.

Nogueira, A.C.R., 1985, Análise faciológica e aspectos estruturais da Formação Águas Claras, região central da Serra dos Carajás: Unpublished M.Sc. thesis, Belém, Brazil, Universidade Federal do Pará, 104 p.

Pidgeon, R.T., Macambira, M.J.B., and Lafon, J.M., 2000, Th-U-Pb isotopic systems and internal structures of complex zircons from an enderbite from the Pium Complex, Carajás province, Brazil: Evidence for the ages of granulite facies metamorphism and the protolith of the enderbite: Chemical Geology, v. 166, p. 157−171.

Pirajno, F., 2009, Hydrothermal Processes and Mineral Systems: Berlin, Germany, Springer, 1250 p.

Raymond, O.L., 1996, Pyrite composition and ore genesis in the Prince Lyell copper deposit, Mt Lyell mineral field, western Tasmania, Australia: Ore Geology Reviews, v.10, p.231-250.

Réquia, K., Stein, H., Fontboté, 2002, The Salobo iron oxide copper-gold deposit, Carajás, northern Brazil, in Porter, T.M., ed., Hydrothermal Iron Oxide Copper-Gold and Related Deposits: A Global Perspective, v. 1, Adelaide, p. 225-236.

Réquia, K., Stein, H., Fontboté, L., and Chiaradia, M., 2003, Re-Os and Pb-Pb geochronology of the Archean Salobo iron oxide copper–gold deposit, Carajás mineral province, northern Brazil: Mineralium Deposita, v. 38, p. 727–738.

Réquia, K., Xavier, R.P., and Figueiredo, B., 1995, Evolucão paragenética, textural e das fases fluidas no depósito polimetálico de Salobo, Província Mineral de Carajás, Pará: Boletim do Museo Paraense Emilio Goeldi, Série Ciências da Terra, v. 7, p. 27–39.

Rigon, J.C., Munaro, P., Santos, L.A., Nascimento, J.A.S., and Barreira, C.F., 2000, Alvo 118 copper-gold deposit: Geology and mineralization, Serra dos Carajás, Pará, Brazil [abs.]: International Geological Congress, 31st, Rio de Janeiro, Sociedade

Brasileira de Geologia, International Union of Geological Sciences, Abstract Volume [CD-ROM].

Rollinson, H.R., 1993, Using Geochemical Data: Evaluation, Presentation, Interpretation: Harlow, England, Pearson Education Limited, 384 p.

Ronzê, P.C., Soares, A.D.V., Santos, M.G.S., Barreira, C.F., 2000, Alemão copper-gold-(U-REE) deposit, Carajás, Brazil, in Porter, T.M., ed., Hydrothermal Iron Oxide Copper-Gold and Related Deposits: A Global Perspective, v. 1, Adelaide, p. 191-202.

Rosa, W.D., 2014, Complexos acamadados da Serra da Onça e Serra do Puma: geologia e petrologia de duas intrusões máfico-ultramáficas com sequência de cristalização distinta na Província Arqueana de Carajás, Brasil: Unpublished M.Sc. thesis, Brasilia, Brazil, Universidade de Brasilia, 65 p.

Sato, H., Yamaguchi, Y., Makino, K., 1997, Cl incorporation into successfully zoned amphiboles from the Ramnes Caouldron, Norway: American Mineralogist, v.82, p.316-324.

Siepierski, L., Geologia e petrologia do prospecto gt-34: evidência de metassomatismo de alta temperatura e baixa fo_2, Província Mineral Carajás, Brasil, Unpublished M.Sc. thesis, Brasilia, Brazil, Universidade de Brasília, 72 p.

Sillitoe, R.H., 2003, Iron oxide–copper–gold deposits: an Andean view: Mineralium Deposita, v.38, p.787–812.

Silva, C.M.C., and Villas, R.N., 1998, The Águas Claras Cu-sulfide ± Au deposit, Carajás region, Pará, Brazil: geological setting, wall-rock alteration and mineralizing fluids: Revista Brasileira Geociências, v. 28(3), p. 315– 326.

Silva, M.G., Teixeira, J.B.G., Pimentel, M.M., Vasconcelos, P.M., Arielo, A., and Rocha, W.J.S.F., 2005, Geologia e mineralizações de Fe–Cu–Au do Alvo GT46 (Igarapé Cinzento, Carajás) in Marini, O.J., Queiroz, E.T., and Ramos, B.W., ed., Caracterização de Depósitos Minerais em Distritos Mineiros da Amazônia, DNPM-CT/Mineral-ADIMB, Brasília, Brazil, p. 94–151.

Souza, S.R.B., Macambira, M.J.B., and Sheller, T., 1996, Novos dados geocronológicos para os granitos deformados do Rio Itacaiúnas (Serra dos Carajás, PA); implicações estratigráficas: Simpósio de Geologia da Amazônia, Belém, Brazil, 1996, Proceedings, p. 380–383.

Souza, Z.S., Potrel, H., Lafon, J.M., Althoff, F.J., Pimentel, M.M., Dall'Agnol, R., and Oliveira, C.G., 2001, Nd, Pb and Sr isotopes of the identidade belt, an archaean greenstone belt of the Rio Maria region (Carajás Province, Brazil): implications for the archaean geodynamic evolution of the Amazonian craton: Precambrian Research, v. 109, p. 293–315.

Souza, L.H., and Vieira, E.A.P., 2000, Salobo 3 Alpha deposit: Geology and mineralization, in Porter, T.M., ed., Hydrothermal iron-oxide copper-gold and related deposits: A global perspective: Adelaide, PGC Publishing, v. 1, p. 213−224.

Sun, S. S., and McDonough, W.F., 1989, Chemical and isotopic systematics of oceanic basalts; implications for mantle composition and processes. In: Magmatism in the ocean

basin, in: Saunders, A.D. and Norry, M.J., ed, Geological Society of London, London, v.42, p.313-345.

Tallarico, F.H.B., 2003, O cinturão cupro-aurífero de Carajás, Brasil. Unpublished Ph. D. thesis, Campinas, Brazil, Universidade Estadual de Campinas, 229 p.

Tallarico, F.H.B., Figueiredo, B.R., Groves, D.I., Kositcin, N., McNaughton, N.J., Fletcher I.R., and Rego J.L., 2005, Geology and SHRIMP U-Pb geochronology of the Igarapé Bahia deposit, Carajás copper-gold belt, Brazil: An Archean (2.57 Ga) example of iron-oxide Cu-Au-(U-REE) mineralization: Economic Geology, v. 100, p. 7−28.

Tallarico, F.H.B., Oliveira, C.G., and Figueiredo, B.R., 2000, The Igarapé Bahia Cu–Au mineralization, Carajás Province: Revista Brasileira de Geociências, v. 30, p. 230–233.

Tallarico, F.H.B., McNaughton, N.J., Groves, D.I., Fletcher, I.R., Figueiredo, B.R., Carvalho, J.B., Rego, J.L., and Nunes, A.R., 2004, SHRIMP II U–Pb constraints on the age of the Breves Cu–Au– (W–Bi–Sn) mineralization: evidence of Paleoproterozoic (1.88 Ga) metallogeny in the Carajás Copper–Gold Belt, Brazil: Mineralium Deposita v.39, p.68–86.

Tazava, E., 1999, Mineralização de Au-Cu-(ETR-U) associada às brechas hidrotermais do depósito de Igarapé Bahia, província Mineral de Carajás, PA: Unpublished M.Sc. dissertation, Universidade Federal de Ouro Preto, 81p.

Tazava, E., Oliveira, C.G., and Gomes, N.S., 1999, Ocorrência de ferrospirosmalita nas brechas mineralizadas do depósito de Au-Cu-(+ETR-U) de Igarapé Bahia, Província Mineral de Carajás: Revista Brasileira de Geociências, v. 29, p. 345−348.

Teixiera, A.S., Ferreira Filho, C.F., Della Giustina, M.E.S., Araújo, S.M., Silva, H.H.A.B., 2015, Geology, petrology and geochronology of the Lago Grande layered complex: Evidence for a PGE-mineralized magmatic suite in the Carajás Mineral Province, Brazil: Journal of South American Earth Sciences, v.64, p.116-138.

Tolbert, G.E., Tremaine, J.W., Melcher, G.C., and Gomes, C.B., 1971, The recently discovered Serra dos Carajás iron deposit, northern Brazil: Economic Geology, v. 66, p. 985–994.

Torresi, I., Xavier, R.P., Bortholoto, D.F.A., and Monteiro, L.V.S., 2011, Hydrothermal alteration, fluid inclusions and stable isotope systematics of the Alvo 118 iron oxide-copper-gold deposit, Carajás mineral province (Brazil): Implications for ore genesis: Mineralium Deposita, v. 47, p. 299−323.

Vasquez, L.V., Rosa-Costa, L.R., Silva, C.G., Ricci, P.F., Barbosa, J.O., Klein, E.L., Lopes, E.S., Macambira, E.B., Chaves, C.L., Carvalho, J.M., Oliveira, G., Anjos, G.C., and Silva, H.R., 2008a, Geologia e Recursos Minerais do Estado do Pará: Sistema de Informações Geográficas-SIG: Texto explicativo dos Mapas Geológico e Tectônico e de Recursos Minerais do Estado do Pará, 1:1.000.000:Companhia de Pesquisa de Recursos Minerais-Serviço Geológico do Brasil, Superintendência Regional de Belém.

Vasquez, M.L., Sousa, C.S., and Carvalho, J.M.A., 2008b, Mapa Geológico e de Recursos Minerais do Estado do Pará, escala 1:1.000.000, Programa Geologia do Brasil (PGB), Integração, Atualização e Difusão de Dados da Geologia do Brasil, Mapas

Geológicos Estaduais: Companhia de Pesquisa de Recursos Minerais-Serviço Geológico do Brasil, Superintendência Regional de Belém.

Vieira, E.A.P., Saueressig, R., Siqueira, J.B., Silva, E.R.P., Rego, J.L., and Castro, F.D.C., 1988, Caracterização geológica da jazida polimetálica do Salobo 3a, reavaliação: Congresso Brasileiro de Geologia, 35th, Belém, Sociedade Brasileira de Geologia, Proceedings, p. 97-111.

Wang, S., and, Williams, P.J., 2001, Geochemistry and origin of Proterozoic skarns at the Mount Elliot Cu–Au–(–Co–Ni) deposit, Cloncurry district, NW Queensland, Australia: Mineralium Deposita, v.36, p.109–124.

Williams, P.J., Barton, M.D., Johnson, D.A, Fontboté, L., de Haller, A., Mark, G., Oliver, N.H.S., and Marschik, R., 2005, Iron oxide-copper-gold deposits: Geology, space-time distribution, and possible modes of origin: Economic Geology 100th Anniversary Volume, p. 371−405.

Wirth, K.R., Gibbs, A.K., and Olszewski, W.J., Jr., 1986, U-Pb ages of zircons from the Grão Pará Group and Serra dos Carajás granite, Pará, Brasil: Revista Brasileira de Geociências, v. 16, p. 195−200.

Whitney, D.L., Evans, B.W., 2010, Abbreviations for names of rock-forming minerals: American Mineralogist, v. 95, p.185-187.

Xavier, R.P., Monteiro, L.V.S., Moreto, C.P.N., Pestilho, A.L.S., Melo, G.H.C., Silva, M.A.D., Aires, B., Ribeiro, C., and Silva, F.H.F., 2012, The iron oxide copper-gold systems of the Carajás mineral province, Brazil: Society of Economic Geologists, Special Publication no. 16, p. 433–454.

Xavier, R.P., Monteiro, L.V.S., Souza Filho, C.R., Torresi, I., Carvalho, E.R., Dreher, A.M., Wiedenbeck, M., Trumbull, R.B., Pestilho, A.L.S., and Moreto, C.P.N., 2010, The iron oxide copper–gold deposits of the Carajás Mineral Province, Brazil: an updated and critical review, in Porter, T.M., ed., Hydrothermal iron oxide copper-gold & related deposits: a global perspective: Adelaide, Australian Miner, p. 285–306.

Xu, L.G., Lehmanna, B., Mao, J.W., Qu, W.J., and Du, A.D., 2011, Re–Os age of polymetallic Ni– Mo–PGE–Au mineralization in Early Cambrian black shales of South China - a reassessment: Economic Geology, v. 106, p. 511–522.

Zhu, C. and Sverjensky, D.A., 1991, Partitioning of F-Cl-OH between minerals and hydrothermal fluids: Geochimica et Cosmochimica Acta, v.55, p. 1837-1858.

Zucchetti, M., 2007, Rochas máficas do grupo Grão Pará e sua relação com a mineralização de ferro dos depósitos N4 E N5, Carajás, PA: Unpublished Ph.D. thesis, Belo Horizonte, Brazil, Universidade Federal de Minas Gerais, 165 p.

CONCLUSÕES

O depósito Jaguar representa um exemplo único de mineralização de Ni de origem hidrotermal de grande volume e teor, localizado na Província Mineral de Carajás (PMC). O depósito se encontra encaixado ao longo de estruturas regionais de direção WNW-ESE. O sistema hidrotermal foi predominantemente desenvolvido em rochas subvulcânicas félsicas e, subordinadamente, em rochas granito-gnáissicas. A alteração hidrotermal forma estruturas subverticais a verticais que englobam corpos mineralizados e possui os seguintes estágios de alteração: i) alteração pervasiva inicial a biotita-clorita, contendo localmente bandas de enriquecimento em clorita; ii) alteração a anfibólio-biotita, de ocorrência restrita; iii) alteração tardia a magnetita-apatita-quartzo sobreposta ou cortando parcialmente as alterações iniciais. A alteração hidrotermal inicial é controlada por estruturas com caráter dúctil e texturas miloníticas. A alteração tardia é controlada principalmente por estruturas de caráter rúptil.

A mineralização constitui o estágio final do sistema hidrotermal e ocorre sobrepondo ou cortando as zonas de alteração. Dois tipos principais de mineralização de Ni podem ocorrer: i) veios, vênulas e stringers em zonas de alteração a biotita-clorita, compondo a mineralização de baixo teor e ii) corpos brechados ricos em magnetita, apatita e sulfetos, associados a alteração a magnetita-apatita-quartzo. Este tipo de mineralização possui ocorrência mais restrita que a primeira, embora contenha os teores mais altos de Ni. Sulfetos maciços e disseminados também podem ocorrer. A assembleia de sulfetos principal é constituída por: pirita>>milerita>pentlandita>calcopirita>pirrotita>esfalerita. Esta assembleia mineral está invariavelmente associada a abundante magnetita sugerindo condição oxidantes para o sistema hidrotermal. Zonas de alteração hidrotermal são caracterizadas por enriquecimento em FeO, P2O5 e F. A alteração hidrotermal a biotita-clorita é enriquecida em MgO e pode ter enriquecimento em K2O leve a distintivo, combinado com redução de Na2O. Os valores de CaO são variáveis nas zonas de alteração podendo mostrar enriquecimento local. Os produtos de alteração hidrotermal são enriquecidos em ETRL, assim como no valores totais de ETR. Rochas muitos alteradas e mineralizadas, possuem em geral conteúdo elevado de Pb e U e conteúdo reduzido de Ba, Sr, Zr e Ti, quando comparadas com as rochas hospedeiras.

O deposito Jaguar possui várias similaridades com os depósitos IOCG da PMC:

forte controle estrutural ao longo de sistemas de falhamentos regionais e zonas de cisalhamento, associação espacial entre a alteração hidrotermal e os corpos de minério, padrões de alteração similares, enriquecimento em ETRL, Fe, U, F, P, Pb, Ni e Co, são depletados em Zr e Ti, corpos mineralizados subverticais a verticais, alteração controlada tanto por estruturas dúcteis quanto rúpteis, abundância em óxidos de ferro e hospedeiras pertencentes ao Supergrupo Itacaiúnas e Complexo Xingu.

Umas das possibilidades apresentadas neste trabalho para a fonte do Ni são as rochas máfico-ultramáficas, de ampla ocorrência principalmente na porção sul do Domínio Carajás. Os teores de Pt-Pd do depósito Jaguar são baixos, em geral abaixo do limite de detecção. Se estas rochas máfico-ultramáficas forem pobres em PGE, é razoável dizer que o depósito Jaguar teve origem em um modelo que envolve mobilização de Ni e Cu por fluidos hidrotermais de rochas máfica-ultramáficas em profundidade abaixo do depósito.

A abundancia de F em minerais hidrotermais (e.g., fluorita, apatita, biotita e alguns anfibólios) e ETR associada à mineralização, pode refletir um papel importante dos voláteis no transporte de metais e a natureza altamente salina dos fluidos responsáveis pela mineralização de Ni. Quando comparados com os depósitos IOCG de Carajás, o conteúdo de F do depósito Jaguar é significativamente mais alto. Em contrapartida , o Cl é mais baixo. O papel preciso do F na mobilização de Ni é ainda desconhecido, mas o conteúdo incomum pode representar uma feição distintiva para o transporte de Ni em fluidos hidrotermais.

A natureza diferente das encaixantes do depósito Jaguar definem características químicas específicas em minerais hidrotermais, o que indica a dependência da composição dos minerais nas interações fluido/rocha. As diferenças composicionais em cristais diferentes dentro da mesma amostra (e.g., variação composicional em anfibólios) pode refletir variações de temperatura durante a alteração hidrotermal e/ou pulsos episódicos de fluidos hidrotermais.

O depósito Jaguar não está hospedado em rochas máfica-ultramáficas, ao contrário do que ocorre na maioria dos depósitos de Ni de origem hidrotermal e em todos os depósitos de Ni de origem magmática. Isto representa um destaque prospectivo importante para exploração de Ni. As semelhanças entre o depósito jaguar e os

depósitos IOCG da PMC chama atenção para a exploração de Ni em ambientes geológicos não convencionais para este metal. A abundância de rochas máfica-ultramáficas na porção sul do Domínio Carajás somados a presença de um sistema hidrotermal eficiente na província pode indicar possibilidades de mobilização de Ni por fluidos hidrotermais e posterior mineralização.

Finalmente, considerando-se que o Ni pode ser mobilizado em uma variedade grande de ambientes geológicos, em diferentes temperaturas e por complexantes diversos, existe ainda potencial para novas descobertas de depósitos de Ni de origem hidrotermal. Para este propósito, faz-se imprescindível desenvolver um bom conhecimento do processo geológico envolvido na mineralização de Ni, em diferentes escalas de espaço e tempo. Isto é crítico não apenas para exploração mineral eficiente mas para o entendimento de mobilidade de metais (Hronsky and Groves, 2008; Pirajno 2009). Estudos que combinem o uso de traçadores (e.g., isótopos de S) e experimentos em laboratório (i.e., com diferentes condições de F e Cl) podem ser úteis no desenvolvimento do conhecimento deste tipo raro de mineralização. Do ponto de vista econômico, é necessário desenvolver um novo modelo empírico, de forma a atingir maior compreensão destes sistemas.

ANEXOS

Tabela 1A. Resultados analíticos de microssonda em anfibólio.

Tabela 2A. Resultados analíticos de microssonda em magnetita.

Tabela 3A. Resultados analíticos de microssonda em feldspato.

Tabela 4A. Resultados analíticos de microssonda em apatita.

Tabela 5A. Resultados analíticos de microssonda em biotita.

Tabela 6A. Resultados analíticos de microssonda em clorita.

Tabela 1A. Resultados analíticos de microssonda em anfibólio.

Rock Type	Amp	Bt-Chl	Bt-Chl	Bt-Chl	Bt-Chl	Bt-Chl	Bt-Chl	Bt-Chl	Bt-Chl	Bt-Chl	Bt-Chl	Bt-Chl	Bt-Chl	Bt-Chl	Bt-Chl	Bt-Chl	Bt-Chl	Bt-Chl
Sample	MFO15	MFO15	MFO15	MFO15	MFO15	MFO15	MFO15	MFO15	MFO15	MFO15	MFO15	MFO15	MFO15	MFO12	MFO12	MFO12	MFO12	MFO12
Analysis (wt%)	C1 anf 1	C1 anf 2	C1 anf 3	C1 anf 4	C2 anf 1	C2 anf 2	C2 anf 3	C2 anf 4	C2 anf 5	C3 anf 2	C3 anf 3	C3 anf 4	C3 anf 5	C4 anf 1	C4 anf 2	C4 anf 3	C4 anf 6	C4 anf 7
SiO2	54.50	55.24	55.83	56.41	54.51	53.25	54.02	51.52	53.48	55.76	54.08	54.46	52.57	55.45	56.31	56.11	56.79	55.10
TiO2	0.17	0.00	0.00	0.25	0.15	0.02	0.11	0.17	0.02	0.00	0.07	0.03	0.27	0.09	0.18	0.00	0.11	0.21
Al2O3	1.57	1.47	1.20	1.17	2.30	3.46	3.02	4.96	3.11	1.88	1.58	3.27	4.28	1.85	1.77	1.17	0.69	1.90
Cr2O3	0.00	0.01	0.05	0.00	0.00	0.05	0.00	0.06	0.00	0.00	0.00	0.03	0.06	0.01	0.00	0.00	0.00	0.02
FeO	10.46	9.82	10.80	9.67	11.08	11.38	10.73	12.83	10.75	11.93	11.43	11.03	11.91	10.02	9.42	8.93	10.19	10.31
MnO	0.09	0.16	0.03	0.06	0.04	0.03	0.14	0.16	0.10	0.14	0.08	0.14	0.12	0.14	0.07	0.01	0.12	0.06
MgO	17.93	18.76	18.04	18.81	17.45	17.34	17.86	15.63	17.25	17.90	17.08	17.47	16.36	18.34	19.05	19.04	18.33	18.06
CaO	12.13	12.16	12.31	12.23	12.19	12.14	11.91	11.65	11.97	11.19	11.54	12.03	12.01	11.86	12.06	12.31	12.44	11.82
Na2O	0.29	0.32	0.18	0.24	0.45	0.49	0.54	0.84	0.51	0.40	0.22	0.57	0.78	0.36	0.39	0.29	0.15	0.42
K2O	0.06	0.05	0.02	0.02	0.05	0.05	0.07	0.04	0.05	0.04	0.24	0.08	0.09	0.14	0.07	0.02	0.01	0.10
NiO	0.28	0.09	0.18	0.29	0.31	0.14	0.19	0.18	0.23	0.17	0.23	0.17	0.16	0.06	0.28	0.19	0.17	0.05
V2O3	0.03	0.05	0.01	0.01	0.01	0.00	0.00	0.01	0.00	0.01	0.00	0.06	0.03	0.05	0.00	0.03	0.00	0.02
P2O5	0.04	0.04	0.00	0.01	0.04	0.03	0.00	0.01	0.01	0.00	0.02	0.01	0.05	0.05	0.00	0.00	0.00	0.06
SrO	0.05	0.00	0.07	0.00	0.14	0.01	0.13	0.00	0.04	0.09	0.00	0.00	0.00	0.00	0.00	0.00	0.00	0.09
F	0.00	0.02	0.00	0.00	0.06	0.09	0.00	0.06	0.00	0.00	0.00	0.00	0.09	0.06	0.12	0.07	0.00	0.03
Cl	0.06	0.03	0.00	0.01	0.06	0.01	0.05	0.05	0.03	0.04	0.02	0.04	0.06	0.14	0.02	0.02	0.01	0.15
Total	97.65	98.20	98.71	99.16	98.80	98.45	98.75	98.11	97.54	99.53	96.58	99.37	98.79	98.56	99.69	98.15	99.01	98.34
Number of ions on the basis of 23 oxygens																		
TSi	7.74	7.76	7.84	7.85	7.68	7.51	7.58	7.33	7.60	7.79	7.81	7.61	7.43	7.78	7.79	7.86	7.94	7.76
TAl (IV)	0.26	0.24	0.16	0.15	0.32	0.49	0.42	0.67	0.39	0.21	0.19	0.39	0.56	0.21	0.22	0.14	0.07	0.23
TP	0.01	0.00		0.00	0.01	0.00		0.00	0.00		0.00	0.00	0.01	0.01				0.01
CAl (VI)	0.01	0.01	0.04	0.04	0.06	0.09	0.08	0.16	0.13	0.10	0.08	0.15	0.15	0.10	0.07	0.06	0.05	0.08
CCr		0.00	0.01			0.01		0.01				0.00	0.01	0.00				0.00
CFe3+	0.19	0.21	0.11	0.07	0.21	0.38	0.30	0.53	0.25	0.13	0.07	0.23	0.29	0.09	0.12	0.09	0.02	0.11
CTi	0.02			0.03	0.02	0.00	0.01	0.02	0.00		0.01	0.00	0.03	0.01	0.02		0.01	0.02
CMg	3.80	3.93	3.78	3.90	3.66	3.65	3.74	3.31	3.66	3.73	3.68	3.64	3.45	3.84	3.93	3.98	3.82	3.79
CFe2+	0.95	0.84	1.05	0.93	1.01	0.87	0.85	0.94	0.94	1.03	1.14	0.96	1.05	0.95	0.83	0.85	1.08	0.98
CNi	0.03	0.01	0.02	0.03	0.04	0.02	0.02	0.02	0.03	0.02	0.03	0.02	0.02	0.01	0.03	0.02	0.02	0.01
CV	0.00	0.01	0.00	0.00	0.00			0.00		0.00		0.01	0.00	0.01		0.00		0.00
BCa	1.85	1.83	1.85	1.82	1.84	1.83	1.79	1.78	1.82	1.68	1.78	1.80	1.82	1.78	1.79	1.85	1.86	1.78
BNa	0.04	0.04	0.02	0.04	0.06	0.07	0.07	0.15	0.07	0.07	0.04	0.08	0.10	0.07	0.07	0.05	0.04	0.08
BFe2+	0.10	0.11	0.11	0.13	0.08	0.10	0.11	0.05	0.09	0.24	0.17	0.10	0.07	0.13	0.14	0.10	0.09	0.13
BMn2+	0.01	0.02	0.00	0.01	0.00	0.00	0.02	0.02	0.01	0.02	0.01	0.02	0.02	0.02	0.01	0.00	0.02	0.01
BSr	0.00		0.01		0.01		0.01		0.00	0.01								0.01
ANa	0.04	0.04	0.02	0.02	0.06	0.07	0.07	0.08	0.07	0.04	0.02	0.07	0.12	0.03	0.04	0.03	0.01	0.04
AK	0.01	0.01	0.00	0.00	0.01	0.01	0.01	0.01	0.01	0.01	0.04	0.01	0.02	0.03	0.01	0.00	0.00	0.02
Cations	15.05	15.05	15.03	15.03	15.07	15.08	15.09	15.08	15.08	15.05	15.07	15.09	15.13	15.06	15.05	15.04	15.01	15.06
WF		0.01			0.03	0.04		0.03					0.04	0.03	0.05	0.03		0.01
WCl	0.02	0.01		0.00	0.02	0.00	0.01	0.01	0.01	0.01	0.00	0.01	0.01	0.03	0.00	0.01	0.00	0.04
WOH	1.99	1.98	2.00	2.00	1.96	1.96	1.99	1.96	1.99	1.99	2.00	1.99	1.95	1.94	1.94	1.97	2.00	1.95

Tabela 1A. (Cont.). Resultados analíticos de microssonda em anfibólio.

Rock Type	Bt-Chl	Bt-Chl	Bt-Chl	Bt-Chl	Bt-Chl	Bt-Chl	Bt-Chl	Bt-Chl	Bt-Chl	Bt-Chl	Bt-Chl	Bt-Chl	Bt-Chl	Bt-Chl	Bt-Chl	Bt-Chl	Mag	Mag
Sample	MFO12	MFO12	MFO16	MFO16	MFO16	MFO16	MFO16	MFO16	MFO16	MFO16	MFO16	MFO16	MFO16	MFO16	MFO11	MFO11	MFO26	MFO26
Analysis (wt%)	C4 anf 8	C4 anf 10	C1 anf 1	C2 anf 1	C2 anf 2	C2 anf 3	C2 anf 4	C2 anf 5	C2 anf 6	C3 anf 1	C3 anf 3	C3 anf 4	C4 anf 1	C4 anf 2	C4 anf 1.1	C4 anf 1.2	C1 anf 1	C1 anf 2
SiO2	55.35	56.70	54.26	54.44	54.52	55.93	54.55	54.07	54.45	50.30	54.17	54.43	55.34	55.66	55.58	54.93	52.18	51.23
TiO2	0.00	0.00	0.00	0.14	0.00	0.02	0.05	0.08	0.00	0.16	0.00	0.05	0.00	0.04	0.20	0.36	0.15	0.00
Al2O3	1.75	0.51	2.09	2.36	2.41	0.71	2.21	2.89	2.42	6.35	2.21	1.74	2.04	1.54	1.78	1.38	5.64	5.66
Cr2O3	0.09	0.06	0.00	0.00	0.04	0.00	0.00	0.04	0.00	0.11	0.00	0.05	0.00	0.00	0.00	0.02	0.01	0.00
FeO	9.91	10.09	11.89	11.35	11.04	9.58	10.69	11.36	10.23	13.29	10.82	9.55	10.43	10.04	8.89	8.38	11.23	11.28
MnO	0.14	0.05	0.05	0.08	0.19	0.11	0.17	0.12	0.16	0.09	0.31	0.12	0.14	0.12	0.03	0.04	0.07	0.15
MgO	18.57	18.55	16.68	17.28	17.98	18.42	18.06	17.40	18.15	14.68	17.95	18.92	17.73	17.56	19.02	18.89	16.71	16.22
CaO	11.77	12.46	11.98	11.85	11.62	12.26	11.94	11.65	11.85	11.30	11.93	11.90	12.02	12.23	11.87	11.97	11.57	11.65
Na2O	0.39	0.13	0.36	0.34	0.54	0.15	0.42	0.61	0.53	1.09	0.41	0.33	0.39	0.23	0.38	0.43	1.02	0.95
K2O	0.11	0.09	0.05	0.09	0.12	0.02	0.13	0.14	0.09	0.12	0.07	0.12	0.05	0.02	0.21	0.14	0.08	0.08
NiO	0.07	0.14	0.23	0.08	0.13	0.20	0.16	0.11	0.07	0.17	0.11	0.07	0.14	0.14	0.13	0.19	0.16	0.34
V2O3	0.03	0.04	0.10	0.04	0.03	0.00	0.02	0.05	0.02	0.03	0.01	0.05	0.00	0.03	0.03	0.00	0.00	0.01
P2O5	0.00	0.02	0.02	0.05	0.03	0.00	0.03	0.01	0.01	0.04	0.00	0.01	0.00	0.00	0.00	0.13	0.02	0.00
SrO	0.00	0.00	0.00	0.13	0.00	0.00	0.02	0.00	0.00	0.00	0.00	0.00	0.03	0.00	0.00	0.17	0.00	0.10
F	0.00	0.06	0.00	0.00	0.09	0.00	0.02	0.11	0.00	0.00	0.09	0.00	0.00	0.04	0.09	0.17	0.13	0.00
Cl	0.11	0.03	0.03	0.10	0.20	0.04	0.12	0.21	0.14	0.06	0.15	0.15	0.06	0.05	0.09	0.07	0.03	0.05
Total	98.27	98.88	97.74	98.31	98.86	97.40	98.54	98.75	98.09	97.77	98.17	97.46	98.36	97.65	98.24	97.17	98.94	97.71
Number of ions on the basis of 23 oxygens																		
TSi	7.78	7.94	7.75	7.71	7.66	7.93	7.68	7.63	7.68	7.23	7.66	7.70	7.79	7.89	7.79	7.79	7.30	7.30
TAl (IV)	0.22	0.06	0.25	0.28	0.33	0.07	0.32	0.37	0.32	0.77	0.34	0.29	0.21	0.11	0.21	0.20	0.70	0.70
TP		0.00	0.00	0.01	0.00		0.00	0.00	0.00	0.01		0.00				0.02	0.00	
CAl (VI)	0.07	0.02	0.10	0.11	0.07	0.05	0.05	0.11	0.08	0.31	0.03		0.13	0.15	0.08	0.03	0.23	0.25
CCr	0.01	0.01			0.00			0.00		0.01		0.01				0.00	0.00	
CFe3+	0.13	0.03	0.14	0.13	0.23	0.04	0.23	0.23	0.22	0.38	0.30	0.26	0.11	0.01	0.09	0.10	0.52	0.40
CTi				0.01		0.00	0.01	0.01		0.02				0.00	0.02	0.04	0.02	
CMg	3.89	3.87	3.55	3.65	3.77	3.89	3.79	3.66	3.82	3.14	3.78	3.99	3.72	3.71	3.97	3.99	3.49	3.45
CFe2+	0.88	1.05	1.17	1.09	0.91	1.00	0.90	0.98	0.87	1.12	0.88	0.73	1.03	1.11	0.82	0.82	0.73	0.87
CNi	0.01	0.02	0.03	0.01	0.02	0.02	0.02	0.01	0.01	0.02	0.01	0.01	0.02	0.02	0.01	0.02	0.02	0.04
CV	0.00	0.00	0.01	0.01	0.00		0.00	0.01	0.00	0.00	0.00	0.01		0.00	0.00			0.00
BCa	1.77	1.87	1.83	1.80	1.75	1.86	1.80	1.76	1.79	1.74	1.81	1.80	1.81	1.86	1.78	1.82	1.73	1.78
BNa	0.06	0.03	0.05	0.05	0.07	0.03	0.06	0.09	0.07	0.15	0.06	0.04	0.07	0.06	0.08	0.09	0.19	0.11
BFe2+	0.15	0.10	0.11	0.13	0.15	0.10	0.12	0.14	0.12	0.10	0.10	0.14	0.10	0.07	0.14	0.08	0.07	0.08
BMn2+	0.02	0.01	0.01	0.01	0.02	0.01	0.02	0.01	0.02	0.01	0.04	0.01	0.02	0.01	0.00	0.01	0.01	0.02
BSr				0.01			0.00						0.00			0.01		0.01
ANa	0.04	0.01	0.05	0.04	0.07	0.01	0.06	0.08	0.07	0.15	0.06	0.05	0.04	0.00	0.03	0.03	0.09	0.15
AK	0.02	0.02	0.01	0.02	0.02	0.00	0.02	0.03	0.02	0.02	0.01	0.02	0.01	0.00	0.04	0.03	0.01	0.01
Cations	15.06	15.03	15.05	15.06	15.10	15.02	15.08	15.10	15.09	15.18	15.07	15.07	15.05	15.01	15.07	15.06	15.10	15.16
WF		0.03			0.04		0.01	0.05			0.04			0.02	0.04	0.08	0.06	
WCl	0.03	0.01	0.01	0.02	0.05	0.01	0.03	0.05	0.03	0.01	0.04	0.04	0.02	0.01	0.02	0.02	0.01	0.01
WOH	1.98	1.97	1.99	1.98	1.91	1.99	1.96	1.90	1.97	1.99	1.92	1.96	1.99	1.97	1.94	1.91	1.93	1.99

Tabela 1A. (Cont.). Resultados analíticos de microssonda em anfibólio.

Rock Type	Mag	Mag	Mag	Mag	Mag	Mag	Mag	Mag	Mag	Mag	Mag	Mag	Mag	Mag	Mag	Mag	Mag	Bt-Chl
Sample	MFO26	MFO26	MFO26	MFO26	MFO26	MFO26	MFO25	MFO25	MFO25	MFO25	MFO28	MFO28	MFO28	MFO28	MFO28	MFO28	MFO28	MFO31
Analysis (wt%)	C1 anf 3	C2 anf 1	C2 anf 2	C3 anf 1	C3 anf 2	C3 anf 3	C1 anf 1	C1 anf 2	C1 anf 3	C1 anf 4	C1 anf 1	C1 anf 2	C2 anf 1	C3 anf 1	C3 anf 2	C3 anf 3	C3 anf 4	C1 anf 1.1
SiO2	50.29	53.89	50.17	51.26	51.30	56.97	52.65	53.10	56.19	56.17	54.76	52.78	52.53	52.78	53.69	52.93	45.09	45.55
TiO2	0.00	0.07	0.00	0.00	0.17	0.00	0.00	0.02	0.00	0.00	0.09	0.00	0.02	0.05	0.05	0.00	0.00	0.31
Al2O3	6.34	3.54	6.14	6.08	5.44	1.30	4.21	4.44	1.61	1.59	2.92	4.43	4.54	4.38	4.15	4.95	8.00	11.23
Cr2O3	0.01	0.00	0.07	0.00	0.01	0.00	0.00	0.02	0.00	0.06	0.00	0.01	0.01	0.00	0.00	0.02	0.07	0.02
FeO	10.96	9.41	11.87	11.49	10.93	7.03	9.62	10.08	6.47	6.42	9.75	10.33	10.49	10.65	10.89	10.98	17.34	14.21
MnO	0.14	0.07	0.26	0.14	0.19	0.05	0.00	0.14	0.03	0.06	0.12	0.11	0.15	0.12	0.08	0.02	0.19	0.15
MgO	15.89	18.18	15.91	16.00	16.62	19.62	17.54	17.07	20.22	20.39	18.15	16.86	17.15	16.74	16.97	16.94	15.11	12.39
CaO	11.42	12.04	11.22	11.39	11.42	12.56	11.71	11.51	12.60	12.73	11.98	11.62	11.30	11.39	10.77	11.47	7.76	11.79
Na2O	0.99	0.71	1.03	1.06	0.94	0.27	0.80	0.82	0.37	0.34	0.58	0.72	0.79	0.78	0.71	0.83	0.79	1.41
K2O	0.08	0.06	0.13	0.04	0.06	0.00	0.07	0.06	0.04	0.03	0.03	0.05	0.03	0.07	0.02	0.05	0.08	0.29
NiO	0.19	0.27	0.55	0.49	0.12	0.32	0.13	0.16	0.14	0.15	0.30	0.14	0.11	0.23	0.21	0.14	0.26	0.10
V2O3	0.03	0.03	0.03	0.01	0.05	0.03	0.00	0.00	0.00	0.00	0.02	0.02	0.06	0.03	0.01	0.02	0.05	0.09
P2O5	0.02	0.00	0.01	0.08	0.03	0.00	0.02	0.03	0.03	0.05	0.00	0.00	0.00	0.01	0.03	0.01	0.04	0.02
SrO	0.04	0.00	0.14	0.06	0.10	0.06	0.00	0.00	0.03	0.00	0.00	0.12	0.12	0.03	0.00	0.00	0.00	0.00
F	0.10	0.11	0.09	0.08	0.07	0.08	0.20	0.19	0.26	0.18	0.05	0.05	0.04	0.00	0.07	0.14	0.00	0.00
Cl	0.03	0.06	0.07	0.04	0.02	0.02	0.02	0.00	0.01	0.01	0.00	0.04	0.03	0.05	0.00	0.03	0.01	0.16
Total	96.48	98.37	97.63	98.17	97.42	98.27	96.87	97.57	97.86	98.09	98.72	97.24	97.34	97.31	97.60	98.48	94.79	97.68
Number of ions on the basis of 23 oxygens																		
TSi	7.25	7.56	7.15	7.27	7.31	7.92	7.50	7.52	7.82	7.80	7.65	7.52	7.47	7.52	7.61	7.45	6.69	6.64
TAl (IV)	0.75	0.45	0.85	0.72	0.69	0.08	0.50	0.47	0.18	0.20	0.35	0.49	0.53	0.48	0.39	0.55	1.31	1.36
TP	0.00		0.00	0.01	0.00		0.00	0.00	0.00	0.01				0.00	0.00	0.00	0.01	0.00
CAl (VI)	0.33	0.14	0.18	0.30	0.23	0.13	0.21	0.27	0.09	0.06	0.14	0.26	0.23	0.25	0.31	0.27	0.09	0.57
CCr	0.00		0.01		0.00			0.00		0.01		0.00	0.00			0.00	0.01	0.00
CFe3+	0.37	0.28	0.72	0.41	0.40	0.01	0.30	0.25	0.11	0.13	0.21	0.25	0.31	0.25	0.16	0.30	1.18	0.42
CTi		0.01			0.02			0.00			0.01		0.00	0.01	0.01			0.03
CMg	3.41	3.80	3.38	3.38	3.53	4.07	3.72	3.61	4.20	4.22	3.78	3.58	3.64	3.55	3.59	3.55	3.34	2.69
CFe2+	0.86	0.74	0.64	0.86	0.81	0.75	0.75	0.86	0.60	0.57	0.83	0.89	0.81	0.91	0.92	0.86	0.34	1.26
CNi	0.02	0.03	0.06	0.06	0.01	0.04	0.02	0.02	0.02	0.02	0.03	0.02	0.01	0.03	0.02	0.02	0.03	0.01
CV	0.00	0.00	0.00	0.00	0.01	0.00					0.00	0.00	0.01	0.00	0.00	0.00	0.01	0.01
BCa	1.76	1.81	1.71	1.73	1.74	1.87	1.79	1.75	1.88	1.89	1.80	1.77	1.72	1.74	1.64	1.73	1.23	1.84
BNa	0.13	0.10	0.19	0.15	0.13	0.07	0.12	0.15	0.06	0.05	0.09	0.12	0.12	0.13	0.14	0.13	0.11	0.08
BFe2+	0.09	0.08	0.05	0.10	0.10	0.05	0.09	0.09	0.05	0.05	0.10	0.09	0.13	0.11	0.21	0.14	0.63	0.06
BMn2+	0.02	0.01	0.03	0.02	0.02	0.01		0.02	0.00	0.01	0.01	0.01	0.02	0.01	0.01	0.00	0.02	0.02
BSr	0.00		0.01	0.01	0.01	0.01			0.00			0.01	0.01	0.00				
ANa	0.15	0.09	0.10	0.14	0.13	0.00	0.10	0.08	0.04	0.04	0.07	0.08	0.10	0.08	0.05	0.10	0.11	0.31
AK	0.01	0.01	0.02	0.01	0.01		0.01	0.01	0.01	0.01	0.01	0.01	0.01	0.01	0.00	0.01	0.02	0.05
Cations	15.17	15.10	15.12	15.15	15.14	15.01	15.11	15.09	15.04	15.05	15.07	15.09	15.11	15.10	15.05	15.11	15.13	15.37
WF	0.04	0.05	0.04	0.04	0.03	0.03	0.09	0.09	0.11	0.08	0.02	0.02	0.02		0.03	0.06		
WCl	0.01	0.01	0.02	0.01	0.00	0.00	0.00		0.00	0.00		0.01	0.01	0.01		0.01	0.00	0.04
WOH	1.95	1.94	1.94	1.95	1.97	1.96	1.91	1.91	1.89	1.92	1.98	1.97	1.98	1.99	1.97	1.93	2.00	1.96

Tabela 1A .(Cont.). Resultados analíticos de microssonda em anfibólio.

Rock Type	Bt-Chl	Bt-Chl	Bt-Chl	Bt-Chl	Bt-Chl	Bt-Chl	Bt-Chl	Bt-Chl	Bt-Chl	Bt-Chl	Bt-Chl	Bt-Chl	Bt-Chl	Bt-Chl	Bt-Chl	Bt-Chl	Bt-Chl	Bt-Chl
Sample	MFO31	MFO31	MFO31	MFO31	MFO31	MFO31	MFO31	MFO31	MFO31	MFO30	MFO30	MFO30	MFO30	MFO30	MFO30	MFO30	MFO30	MFO30
Analysis (wt%)	C1 anf 1.2	C1 anf 2.1	C1 anf 2.2	C1 anf 3.1	C1 anf 3.2	C1 anf 4.2	C4 anf 1.1	C4 anf 1.2	C4 anf 1.3	C1 anf 1	C3 anf 1	C3 anf 2	C3 anf 3	C4 anf 1	C4 anf 2	C4 anf 3	C4 anf 4	C4 anf 5
SiO2	44.65	48.44	45.99	49.29	47.33	45.69	47.14	47.17	55.43	51.27	52.49	54.83	53.31	53.49	50.65	52.83	52.71	52.62
TiO2	0.26	0.51	0.08	0.34	0.32	0.22	0.39	0.38	0.02	0.64	0.17	0.15	0.02	0.62	0.49	0.30	0.05	0.33
Al2O3	11.33	8.84	11.38	7.20	8.94	10.87	9.29	9.33	2.00	4.23	4.06	1.85	3.19	2.94	5.32	3.74	4.41	4.48
Cr2O3	0.05	0.06	0.00	0.00	0.07	0.05	0.00	0.00	0.07	0.00	0.04	0.00	0.15	0.04	0.00	0.11	0.04	0.12
FeO	14.84	13.27	14.74	12.84	12.93	14.34	12.60	13.58	9.25	9.94	10.48	8.32	9.87	9.04	11.46	9.62	10.28	9.98
MnO	0.11	0.34	0.08	0.21	0.18	0.07	0.12	0.15	0.11	0.18	0.10	0.09	0.18	0.19	0.01	0.09	0.18	0.19
MgO	11.88	14.04	12.41	14.30	14.00	12.86	14.24	13.49	19.10	17.50	17.11	19.15	17.85	18.84	16.26	17.83	17.53	17.31
CaO	11.74	11.68	11.76	11.17	11.81	11.57	11.46	11.56	12.63	12.44	11.63	12.28	11.51	12.35	11.54	12.18	11.84	11.70
Na2O	1.41	1.07	1.39	1.21	1.17	1.29	1.22	1.17	0.16	0.57	0.77	0.25	0.60	0.38	0.90	0.53	0.70	0.71
K2O	0.39	0.17	0.26	0.14	0.16	0.25	0.19	0.28	0.00	0.18	0.10	0.07	0.04	0.09	0.27	0.12	0.09	0.11
NiO	0.15	0.00	0.08	0.07	0.08	0.03	0.12	0.00	0.15	0.11	0.08	0.22	0.15	0.10	0.08	0.07	0.10	0.01
V2O3	0.08	0.05	0.06	0.03	0.00	0.10	0.02	0.07	0.00	0.00	0.09	0.04	0.09	0.00	0.00	0.03	0.02	0.04
P2O5	0.01	0.08	0.00	0.03	0.01	0.00	0.00	0.04	0.00	0.00	0.00	0.04	0.00	0.06	0.00	0.02	0.01	0.04
SrO	0.00	0.04	0.00	0.00	0.04	0.08	0.00	0.00	0.00	0.07	0.00	0.00	0.00	0.00	0.01	0.00	0.13	0.01
F	0.05	0.00	0.07	0.00	0.03	0.00	0.00	0.00	0.00	0.02	0.05	0.00	0.03	0.11	0.04	0.00	0.04	0.00
Cl	0.25	0.10	0.17	0.10	0.07	0.17	0.07	0.13	0.02	0.13	0.06	0.04	0.07	0.10	0.21	0.13	0.06	0.03
Total	97.11	98.67	98.40	96.88	97.11	97.54	96.83	97.31	98.94	97.23	97.18	97.33	97.03	98.28	97.17	97.56	98.15	97.65
Number of ions on the basis of 23 oxygens																		
TSi	6.58	6.92	6.65	7.15	6.87	6.64	6.84	6.85	7.70	7.32	7.49	7.73	7.59	7.50	7.28	7.48	7.43	7.45
TAl (IV)	1.42	1.07	1.35	0.85	1.13	1.36	1.16	1.14	0.30	0.68	0.51	0.26	0.41	0.49	0.72	0.52	0.57	0.54
TP	0.00	0.01		0.00	0.00			0.01				0.01		0.01		0.00	0.00	0.01
CAl (VI)	0.55	0.42	0.59	0.38	0.40	0.51	0.42	0.45	0.03	0.03	0.17	0.05	0.13		0.18	0.11	0.17	0.20
CCr	0.01	0.01			0.01	0.01			0.01		0.00		0.02	0.00		0.01	0.00	0.01
CFe3+	0.47	0.42	0.49	0.35	0.46	0.58	0.51	0.42	0.26	0.42	0.30	0.16	0.25	0.34	0.37	0.30	0.37	0.26
CTi	0.03	0.06	0.01	0.04	0.04	0.02	0.04	0.04	0.00	0.07	0.02	0.02	0.00	0.06	0.05	0.03	0.01	0.04
CMg	2.61	2.99	2.68	3.09	3.03	2.79	3.08	2.92	3.96	3.72	3.64	4.03	3.79	3.94	3.48	3.77	3.68	3.65
CFe2+	1.31	1.11	1.22	1.13	1.06	1.09	0.93	1.15	0.73	0.74	0.86	0.72	0.79	0.65	0.90	0.77	0.76	0.84
CNi	0.02		0.01	0.01	0.01	0.00	0.01		0.02	0.01	0.01	0.03	0.02	0.01	0.01	0.01	0.01	0.00
CV	0.01	0.01	0.01	0.00		0.01	0.00	0.01			0.01	0.01	0.01			0.00	0.00	0.01
BCa	1.85	1.79	1.82	1.74	1.84	1.80	1.78	1.80	1.88	1.90	1.78	1.86	1.76	1.86	1.78	1.85	1.79	1.77
BNa	0.08	0.11	0.10	0.16	0.09	0.10	0.12	0.11	0.02	0.05	0.11	0.03	0.09	0.05	0.12	0.07	0.10	0.11
BFe2+	0.06	0.06	0.07	0.08	0.05	0.08	0.09	0.08	0.09	0.02	0.10	0.10	0.14	0.07	0.10	0.07	0.08	0.09
BMn2+	0.01	0.04	0.01	0.03	0.02	0.01	0.02	0.02	0.01	0.02	0.01	0.01	0.02	0.02	0.00	0.01	0.02	0.02
BSr		0.00			0.00	0.01				0.01					0.00		0.01	0.00
ANa	0.33	0.19	0.30	0.18	0.24	0.26	0.23	0.22	0.02	0.11	0.10	0.04	0.08	0.05	0.13	0.07	0.10	0.08
AK	0.07	0.03	0.05	0.03	0.03	0.05	0.04	0.05	0.00	0.03	0.02	0.01	0.01	0.02	0.05	0.02	0.02	0.02
Cations	15.40	15.22	15.34	15.20	15.27	15.31	15.26	15.28	15.02	15.14	15.12	15.05	15.09	15.07	15.18	15.10	15.11	15.10
WF	0.02		0.03		0.01					0.01	0.02		0.02	0.05	0.02		0.02	
WCl	0.06	0.02	0.04	0.02	0.02	0.04	0.02	0.03	0.01	0.03	0.02	0.01	0.02	0.02	0.05	0.03	0.02	0.01
WOH	1.92	1.98	1.93	1.98	1.97	1.96	1.98	1.97	2.00	1.96	1.96	1.99	1.97	1.93	1.93	1.97	1.97	1.99

Tabela 2A. Resultados analíticos de microssonda em magnetita.

Rock Type	Mag	Mag	Mag	Mag	Mag	Mag	Mag	Mag	Mag	Mag	Mag	Mag	Mag	Mag	Mag	Mag	Mag	Mag	Mag	Mag
Sample	MFO09	MFO09	MFO09	MFO09	MFO09	MFO09	MFO09	MFO09	MFO09	MFO09	MFO09	MFO09	MFO09	MFO09	MFO09	MFO09	MFO10	MFO10	MFO10	MFO10
Analysis (wt%	C1 Mag 1	C1 Mag 2	C1 Mag 3	C1 Mag 4	C2 Mag 1.1	C2 Mag 1.2	C2 Mag 1.3	C2 Mag 1.4	C2 Mag 1.5	C3 Mag 1	C3 Mag 2	C3 Mag 4	C3 Mag 5	C4 Mag 1	C4 Mag 2	C4 Mag 3	C1 Mag 1	C1 Mag 2	C3 Mag 1	C3 Mag 2
SiO2	0.65	0.17	0.03	0.45	0.04	1.51	0.06	0.01	1.72	1.83	0.06	0.35	0.00	0.03	0.09	0.10	0.05	0.08	0.07	0.03
TiO2	0.11	0.06	0.00	0.09	0.04	0.27	0.15	0.09	0.11	0.28	0.00	0.07	0.00	0.03	0.00	0.01	0.00	0.00	0.06	0.15
Al2O3	0.06	0.04	0.02	0.20	0.05	0.13	0.05	0.04	0.56	0.44	0.05	0.03	0.05	0.00	0.03	0.05	0.01	0.02	0.05	0.07
Fe2O3	67.38	67.63	68.11	67.02	67.45	62.53	67.56	67.40	62.60	62.54	68.55	67.61	68.16	67.82	67.36	66.83	68.84	68.29	67.61	69.07
FeO	31.37	30.73	30.66	31.09	30.36	30.87	30.71	30.50	31.39	31.94	30.68	31.14	30.17	30.42	30.42	30.00	30.95	30.83	30.59	31.15
MnO	0.04	0.08	0.05	0.08	0.01	0.00	0.00	0.10	0.03	0.01	0.01	0.04	0.03	0.00	0.00	0.04	0.00	0.05	0.00	0.00
MgO	0.24	0.02	0.00	0.21	0.00	0.72	0.00	0.00	0.36	0.40	0.00	0.13	0.00	0.00	0.01	0.06	0.00	0.00	0.04	0.02
CaO	0.12	0.03	0.00	0.00	0.00	0.00	0.00	0.00	0.27	0.37	0.00	0.00	0.02	0.05	0.00	0.01	0.04	0.00	0.02	0.03
Na2O	0.00	0.01	0.01	0.00	0.00	0.01	0.00	0.00	0.06	0.03	0.05	0.00	0.07	0.03	0.00	0.00	0.01	0.00	0.00	0.03
Cr2O3	0.00	0.00	0.06	0.00	0.02	0.00	0.00	0.08	0.00	0.02	0.03	0.00	0.00	0.02	0.01	0.00	0.00	0.00	0.04	0.03
V2O3	0.20	0.18	0.24	0.16	0.12	0.21	0.11	0.15	0.08	0.18	0.18	0.20	0.20	0.10	0.13	0.10	0.14	0.11	0.13	0.08
NiO	0.22	0.10	0.09	0.06	0.24	0.20	0.19	0.05	0.17	0.11	0.15	0.09	0.18	0.06	0.17	0.24	0.09	0.09	0.13	0.12
Total	100.38	99.04	99.27	99.34	98.33	96.44	98.82	98.41	97.35	98.16	99.76	99.65	98.87	98.56	98.21	97.43	100.13	99.47	98.73	100.75
Number of cations per 4 oxygens																				
Ni	0.01	0.00	0.00	0.00	0.01	0.01	0.01	0.00	0.01	0.00	0.00	0.00	0.01	0.00	0.01	0.01	0.00	0.00	0.00	0.00
Si	0.02	0.01	0.00	0.02	0.00	0.06	0.00	0.00	0.07	0.07	0.00	0.01	0.00	0.00	0.00	0.00	0.00	0.00	0.00	0.00
Ti	0.00	0.00	0.00	0.00	0.00	0.01	0.00	0.00	0.00	0.01	0.00	0.00	0.00	0.00	0.00	0.00	0.00	0.00	0.00	0.00
Cr	0.00	0.00	0.00	0.00	0.00	0.00	0.00	0.00	0.00	0.00	0.00	0.00	0.00	0.00	0.00	0.00	0.00	0.00	0.00	0.00
Sc	0.00	0.00	0.00	0.00	0.00	0.00	0.00	0.00	0.00	0.00	0.00	0.00	0.00	0.00	0.00	0.00	0.00	0.00	0.00	0.00
V	0.01	0.01	0.01	0.00	0.00	0.01	0.00	0.00	0.00	0.01	0.01	0.01	0.01	0.00	0.00	0.00	0.00	0.00	0.00	0.00
Al	0.00	0.00	0.00	0.01	0.00	0.01	0.00	0.00	0.03	0.02	0.00	0.00	0.00	0.00	0.00	0.00	0.00	0.00	0.00	0.00
Fe3+	1.94	1.98	1.99	1.95	1.98	1.85	1.98	1.98	1.84	1.82	1.98	1.96	1.99	1.99	1.99	1.98	1.99	1.99	1.98	1.98
Mg	0.01	0.00	0.00	0.01	0.00	0.04	0.00	0.00	0.02	0.02	0.00	0.01	0.00	0.00	0.00	0.00	0.00	0.00	0.00	0.00
Fe2+	0.99	1.00	0.99	1.00	0.99	1.00	1.00	1.00	0.98	0.98	0.99	1.00	0.98	0.99	1.00	0.99	1.00	1.00	1.00	1.00
Mn	0.00	0.00	0.00	0.00	0.00	0.00	0.00	0.00	0.00	0.00	0.00	0.00	0.00	0.00	0.00	0.00	0.00	0.00	0.00	0.00
Co	0.00	0.00	0.00	0.00	0.00	0.00	0.00	0.00	0.00	0.00	0.00	0.00	0.00	0.00	0.00	0.00	0.00	0.00	0.00	0.00
Ca	0.00	0.00	0.00	0.00	0.00	0.00	0.00	0.00	0.01	0.02	0.00	0.00	0.00	0.00	0.00	0.00	0.00	0.00	0.00	0.00
Na	0.00	0.00	0.00	0.00	0.00	0.00	0.00	0.00	0.00	0.00	0.00	0.00	0.01	0.00	0.00	0.00	0.00	0.00	0.00	0.00
K	0.00	0.00	0.00	0.00	0.00	0.00	0.00	0.00	0.00	0.00	0.00	0.00	0.00	0.00	0.00	0.00	0.00	0.00	0.00	0.00

Tabela 2A. (Cont.). Resultados analíticos de microssonda em magnetita.

Rock Type	Mag	Mag	Mag	Mag	Mag	Mag	Mag	Mag	Mag	Mag	Mag	Mag	Mag	Mag	Mag	Mag	Mag	Mag	Mag	Mag	Mag
Sample	MFO10	MFO10	MFO10	MFO10	MFO10	MFO10	MFO10	MFO13	MFO13	MFO13	MFO13	MFO13	MFO13	MFO13	MFO13	MFO13	MFO13	MFO13	MFO13	MFO13	MFO13
Analysis (wt%)	C3 Mag 3	C3 Mag 4	C4 Mag 1	C4 Mag 2	C4 Mag 3	C4 Mag 5	C4 Mag 6	C2 Mag 1	C2 Mag 2	C2 Mag 3	C2 Mag 4	C2 Mag 5	C3 Mag 1	C3 Mag 2	C3 Mag 3	C3 Mag 4	C3 Mag 5	C4 Mag 1	C4 Mag 2	C4 Mag 3	C4 Mag 4
SiO2	0.06	0.05	0.00	0.08	0.01	0.57	0.11	0.04	0.08	1.34	2.07	1.30	0.09	0.05	0.08	0.04	1.43	0.05	0.17	0.06	0.06
TiO2	0.16	0.07	0.16	0.17	0.21	0.27	0.00	0.00	0.00	0.00	0.23	0.10	0.09	0.00	0.00	0.00	0.00	0.02	0.04	0.14	0.00
Al2O3	0.00	0.05	0.04	0.06	0.01	0.16	0.05	0.01	0.03	0.50	0.42	0.39	0.03	0.02	0.03	0.01	0.30	0.05	0.00	0.01	0.03
Fe2O3	67.54	68.72	68.13	67.28	68.14	66.74	68.08	68.62	68.07	64.73	63.12	64.35	67.15	68.25	67.62	67.87	65.01	68.05	67.91	68.03	68.64
FeO	30.80	31.10	30.81	30.67	30.88	31.47	30.88	30.76	30.74	31.45	31.79	31.59	30.30	30.62	30.46	30.59	31.66	30.53	30.69	30.75	30.57
MnO	0.03	0.00	0.10	0.00	0.00	0.03	0.03	0.00	0.00	0.03	0.05	0.00	0.08	0.12	0.00	0.00	0.03	0.00	0.14	0.04	0.04
MgO	0.02	0.01	0.03	0.00	0.00	0.10	0.00	0.02	0.04	0.20	1.09	0.34	0.00	0.00	0.00	0.00	0.34	0.00	0.04	0.00	0.00
CaO	0.01	0.07	0.02	0.06	0.03	0.10	0.02	0.00	0.03	0.27	0.07	0.07	0.01	0.00	0.00	0.01	0.19	0.01	0.02	0.00	0.00
Na2O	0.00	0.00	0.01	0.00	0.02	0.03	0.00	0.02	0.00	0.07	0.03	0.00	0.04	0.00	0.04	0.00	0.05	0.02	0.02	0.04	0.07
Cr2O3	0.01	0.04	0.03	0.06	0.00	0.02	0.00	0.00	0.00	0.00	0.05	0.00	0.06	0.04	0.10	0.01	0.00	0.00	0.00	0.02	0.05
V2O3	0.16	0.11	0.10	0.13	0.16	0.16	0.17	0.17	0.20	0.16	0.17	0.17	0.09	0.16	0.21	0.15	0.11	0.13	0.14	0.20	0.12
NiO	0.04	0.07	0.02	0.16	0.08	0.08	0.06	0.12	0.09	0.14	0.12	0.31	0.06	0.19	0.09	0.11	0.11	0.18	0.04	0.10	0.12
Total	98.82	100.28	99.43	98.67	99.55	99.72	99.39	99.76	99.29	98.90	99.21	98.62	97.99	99.46	98.62	98.79	99.23	99.04	99.21	99.39	99.70
									Number of cations per 4 oxygens												
Ni	0.00	0.00	0.00	0.01	0.00	0.00	0.00	0.00	0.00	0.00	0.00	0.01	0.00	0.01	0.00	0.00	0.00	0.01	0.00	0.00	0.00
Si	0.00	0.00	0.00	0.00	0.00	0.02	0.00	0.00	0.00	0.05	0.08	0.05	0.00	0.00	0.00	0.00	0.05	0.00	0.01	0.00	0.00
Ti	0.00	0.00	0.00	0.01	0.01	0.01	0.00	0.00	0.00	0.00	0.01	0.00	0.00	0.00	0.00	0.00	0.00	0.00	0.00	0.00	0.00
Cr	0.00	0.00	0.00	0.00	0.00	0.00	0.00	0.00	0.00	0.00	0.00	0.00	0.00	0.00	0.00	0.00	0.00	0.00	0.00	0.00	0.00
Sc	0.00	0.00	0.00	0.00	0.00	0.00	0.00	0.00	0.00	0.00	0.00	0.00	0.00	0.00	0.00	0.00	0.00	0.00	0.00	0.00	0.00
V	0.01	0.00	0.00	0.00	0.01	0.00	0.01	0.01	0.01	0.00	0.01	0.01	0.00	0.00	0.01	0.00	0.00	0.00	0.00	0.01	0.00
Al	0.00	0.00	0.00	0.00	0.00	0.01	0.00	0.00	0.00	0.02	0.02	0.02	0.00	0.00	0.00	0.00	0.01	0.00	0.00	0.00	0.00
Fe3+	1.98	1.99	1.99	1.98	1.98	1.93	1.98	1.99	1.99	1.87	1.81	1.87	1.98	1.99	1.98	1.99	1.88	1.99	1.98	1.98	1.99
Mg	0.00	0.00	0.00	0.00	0.00	0.01	0.00	0.00	0.00	0.01	0.06	0.02	0.00	0.00	0.00	0.00	0.02	0.00	0.00	0.00	0.00
Fe2+	1.00	1.00	1.00	1.00	1.00	0.99	1.00	0.99	1.00	0.98	0.99	1.00	0.99	0.99	0.99	1.00	0.99	0.99	0.99	1.00	0.99
Mn	0.00	0.00	0.00	0.00	0.00	0.00	0.00	0.00	0.00	0.00	0.00	0.00	0.00	0.00	0.00	0.00	0.00	0.00	0.00	0.00	0.00
Co	0.00	0.00	0.00	0.00	0.00	0.00	0.00	0.00	0.00	0.00	0.00	0.00	0.00	0.00	0.00	0.00	0.00	0.00	0.00	0.00	0.00
Ca	0.00	0.00	0.00	0.00	0.00	0.00	0.00	0.00	0.00	0.01	0.00	0.00	0.00	0.00	0.00	0.00	0.01	0.00	0.00	0.00	0.00
Na	0.00	0.00	0.00	0.00	0.00	0.00	0.00	0.00	0.00	0.01	0.00	0.00	0.00	0.00	0.00	0.00	0.00	0.00	0.00	0.00	0.01
K	0.00	0.00	0.00	0.00	0.00	0.00	0.00	0.00	0.00	0.00	0.00	0.00	0.00	0.00	0.00	0.00	0.00	0.00	0.00	0.00	0.00

Tabela 2A. (Cont.). Resultados analíticos de microssonda em magnetita.

Rock Type	Mag	Mag	Mag	Mag	Mag	Mag	Mag	Mag	Mag	Mag	Mag	Mag	Mag	Mag	Mag	Mag	Mag	Mag	Mag	Mag	Mag
Sample	MFO14	MFO14	MFO14	MFO14	MFO14	MFO14	MFO14	MFO14	MFO14	MFO14	MFO14	MFO29	MFO29	MFO29	MFO29	MFO29	MFO29	MFO29	MFO29	MFO29	MFO29
Analysis (wt%	C1 Mag 1	C1 Mag 2	C1 Mag 3	C1 Mag 4	C2 Mag 1	C2 Mag 2	C2 Mag 3	C2 Mag 4	C3 Mag 1	C3 Mag 2	C3 Mag 3	C1 Mag 1.1	C1 Mag 1.2	C1 Mag 1.3	C1 Mag 2.1	C1 Mag 2.2	C1 Mag 3.1	C1 Mag 3.2	C2 Mag 1	C2 Mag 2	C3 Mag 1
SiO2	1.23	0.29	0.06	0.21	0.30	0.30	0.21	0.60	0.01	0.04	0.04	0.08	0.16	0.06	0.07	0.13	0.05	0.19	0.05	0.09	0.08
TiO2	0.12	0.00	0.01	0.00	0.15	0.09	0.07	0.04	0.00	0.00	0.07	0.17	0.15	0.04	0.09	0.00	0.09	0.24	0.14	0.15	0.12
Al2O3	0.21	0.05	0.04	0.03	0.05	0.01	0.03	0.07	0.00	0.03	0.03	0.01	0.11	0.06	0.01	0.02	0.00	0.08	0.00	0.02	0.09
Fe2O3	65.04	67.81	69.29	67.27	68.04	67.01	68.13	67.14	68.11	68.46	68.53	69.06	67.14	67.85	68.08	67.16	68.00	65.29	68.24	67.77	68.46
FeO	31.49	31.01	31.10	30.44	31.32	30.66	31.03	30.79	30.40	30.60	30.99	31.09	30.01	30.55	30.73	30.23	30.72	29.76	30.70	30.50	31.01
MnO	0.00	0.00	0.00	0.03	0.00	0.09	0.05	0.00	0.00	0.00	0.00	0.07	0.10	0.00	0.00	0.00	0.00	0.00	0.04	0.00	0.10
MgO	0.34	0.09	0.00	0.02	0.15	0.06	0.06	0.23	0.03	0.02	0.01	0.00	0.11	0.00	0.00	0.10	0.00	0.07	0.03	0.00	0.02
CaO	0.21	0.00	0.01	0.09	0.02	0.03	0.00	0.16	0.06	0.02	0.04	0.03	0.02	0.00	0.00	0.00	0.00	0.06	0.14	0.29	0.01
Na2O	0.04	0.01	0.03	0.03	0.00	0.02	0.00	0.08	0.03	0.05	0.00	0.04	0.07	0.03	0.00	0.00	0.00	0.04	0.00	0.01	0.00
Cr2O3	0.08	0.06	0.03	0.00	0.07	0.04	0.00	0.04	0.04	0.02	0.03	0.05	0.00	0.02	0.00	0.00	0.02	0.06	0.04	0.00	0.05
V2O3	0.16	0.17	0.14	0.18	0.19	0.13	0.15	0.12	0.16	0.15	0.21	0.01	0.00	0.05	0.00	0.00	0.08	0.06	0.04	0.03	0.10
NiO	0.12	0.12	0.15	0.08	0.14	0.11	0.19	0.00	0.06	0.09	0.15	0.18	0.25	0.10	0.24	0.14	0.20	0.20	0.14	0.09	0.19
Total	99.03	99.60	100.86	98.38	100.43	98.54	99.93	99.27	98.91	99.48	100.09	100.78	98.10	98.74	99.22	97.77	99.16	96.04	99.55	98.94	100.23
										Number of cations per 4 oxygens											
Ni	0.00	0.00	0.00	0.00	0.00	0.00	0.01	0.00	0.00	0.00	0.00	0.01	0.01	0.00	0.01	0.00	0.01	0.01	0.00	0.00	0.01
Si	0.05	0.01	0.00	0.01	0.01	0.01	0.01	0.02	0.00	0.00	0.00	0.00	0.01	0.00	0.00	0.00	0.00	0.01	0.00	0.00	0.00
Ti	0.00	0.00	0.00	0.00	0.00	0.00	0.00	0.00	0.00	0.00	0.00	0.00	0.00	0.00	0.00	0.00	0.00	0.01	0.00	0.00	0.00
Cr	0.00	0.00	0.00	0.00	0.00	0.00	0.00	0.00	0.00	0.00	0.00	0.00	0.00	0.00	0.00	0.00	0.00	0.00	0.00	0.00	0.00
Sc	0.00	0.00	0.00	0.00	0.00	0.00	0.00	0.00	0.00	0.00	0.00	0.00	0.00	0.00	0.00	0.00	0.00	0.00	0.00	0.00	0.00
V	0.01	0.01	0.00	0.01	0.01	0.00	0.00	0.00	0.00	0.00	0.01	0.00	0.00	0.00	0.00	0.00	0.00	0.00	0.00	0.00	0.00
Al	0.01	0.00	0.00	0.00	0.00	0.00	0.00	0.00	0.00	0.00	0.00	0.00	0.00	0.00	0.00	0.00	0.00	0.00	0.00	0.00	0.00
Fe3+	1.88	1.97	1.99	1.98	1.96	1.97	1.97	1.95	1.99	1.99	1.98	1.98	1.98	1.99	1.99	1.99	1.99	1.97	1.99	1.98	1.98
Mg	0.02	0.01	0.00	0.00	0.01	0.00	0.00	0.01	0.00	0.00	0.00	0.00	0.00	0.00	0.00	0.00	0.00	0.00	0.00	0.00	0.00
Fe2+	0.99	1.00	0.99	0.99	1.00	0.99	1.00	0.99	0.99	0.99	1.00	0.99	0.98	1.00	1.00	0.99	1.00	0.99	0.99	0.99	1.00
Mn	0.00	0.00	0.00	0.00	0.00	0.00	0.00	0.00	0.00	0.00	0.00	0.00	0.00	0.00	0.00	0.00	0.00	0.00	0.00	0.00	0.00
Co	0.00	0.00	0.00	0.00	0.00	0.00	0.00	0.00	0.00	0.00	0.00	0.00	0.00	0.00	0.00	0.00	0.00	0.00	0.00	0.00	0.00
Ca	0.01	0.00	0.00	0.00	0.00	0.00	0.00	0.01	0.00	0.00	0.00	0.00	0.00	0.00	0.00	0.00	0.00	0.00	0.01	0.01	0.00
Na	0.00	0.00	0.00	0.00	0.00	0.00	0.00	0.01	0.00	0.00	0.00	0.00	0.01	0.00	0.00	0.00	0.00	0.00	0.00	0.00	0.00
K	0.00	0.00	0.00	0.00	0.00	0.00	0.00	0.00	0.00	0.00	0.00	0.00	0.00	0.00	0.00	0.00	0.00	0.00	0.00	0.00	0.00

Tabela 2A. (Cont.). Resultados analíticos de microssonda em magnetita.

Rock Type	Mag	Mag	Mag	Mag	Mag	Mag	Mag	Mag	Mag	Mag	Mag	Mag	Mag	Mag	Mag	Mag	Mag	Mag	Mag	Mag
Sample	MFO29	MFO29	MFO29	MFO29	MFO29	MFO26	MFO26	MFO26	MFO26	MFO26	MFO26	MFO26	MFO26	MFO26	MFO26	MFO26	MFO25	MFO25	MFO25	MFO25	MFO25
Analysis (wt%)	C3 Mag 2	C3 Mag 3	C3 Mag 4	C3 Mag 5	C3 Mag 6	C1 Mag 1.1	C1 Mag 1.2	C1 Mag 1.3	C1 Mag 1.4	C2 Mag 1.1	C2 Mag 1.2	C2 Mag 1.3	C3 Mag 1	C3 Mag 2	C3 Mag 3	C3 Mag 4	C1 Mag 1.2	C1 Mag 2.1	C1 Mag 2.2	C2 Mag 1	C2 Mag 2
SiO2	2.48	0.08	0.11	0.05	0.03	1.31	0.27	1.95	0.28	0.01	0.06	0.03	0.04	0.40	0.04	0.04	1.94	0.04	2.09	0.07	0.11
TiO2	0.00	0.00	0.00	0.07	0.00	0.00	0.00	0.12	0.16	0.00	0.07	0.11	0.02	0.25	0.24	0.00	0.13	0.19	0.09	0.00	0.00
Al2O3	0.04	0.04	0.00	0.08	0.05	0.49	0.08	0.38	0.10	0.05	0.04	0.04	0.03	0.16	0.05	0.03	0.24	0.07	0.23	0.07	0.01
Fe2O3	63.10	67.33	68.02	67.18	67.34	64.55	67.66	63.50	66.30	67.90	67.35	67.41	67.93	66.94	67.89	67.72	63.13	67.39	63.20	67.50	67.35
FeO	31.91	30.15	30.24	30.30	30.12	31.42	30.87	32.40	29.53	30.35	30.38	30.29	30.52	30.94	30.51	30.44	31.71	30.62	32.03	30.22	30.35
MnO	0.00	0.04	0.02	0.02	0.07	0.06	0.00	0.00	0.01	0.03	0.04	0.11	0.00	0.09	0.06	0.00	0.00	0.05	0.00	0.00	0.05
MgO	1.07	0.06	0.01	0.00	0.00	0.43	0.04	0.58	0.07	0.02	0.01	0.00	0.00	0.07	0.00	0.00	0.76	0.00	0.74	0.06	0.03
CaO	0.00	0.01	0.00	0.02	0.01	0.09	0.04	0.10	0.05	0.03	0.01	0.03	0.00	0.07	0.00	0.00	0.11	0.00	0.22	0.03	0.01
Na2O	0.07	0.00	0.08	0.00	0.00	0.01	0.00	0.00	0.17	0.00	0.00	0.01	0.02	0.05	0.07	0.00	0.00	0.00	0.00	0.00	0.00
Cr2O3	0.00	0.04	0.05	0.00	0.00	0.00	0.04	0.00	0.06	0.00	0.04	0.00	0.00	0.04	0.01	0.07	0.04	0.00	0.05	0.00	0.13
V2O3	0.06	0.02	0.01	0.11	0.06	0.13	0.04	0.00	0.04	0.02	0.04	0.09	0.07	0.05	0.07	0.03	0.02	0.02	0.04	0.01	0.04
NiO	0.19	0.24	0.16	0.23	0.24	0.17	0.20	0.14	0.19	0.18	0.19	0.18	0.12	0.15	0.17	0.20	0.25	0.15	0.17	0.22	0.19
Total	98.91	98.01	98.70	98.07	97.92	98.66	99.24	99.16	96.96	98.59	98.22	98.28	98.75	99.19	99.10	98.53	98.33	98.53	98.87	98.16	98.27
Number of cations per 4 oxygens																					
Ni	0.01	0.01	0.01	0.01	0.01	0.01	0.01	0.00	0.01	0.01	0.01	0.01	0.00	0.00	0.01	0.01	0.01	0.00	0.01	0.01	0.01
Si	0.09	0.00	0.00	0.00	0.00	0.05	0.01	0.07	0.01	0.00	0.00	0.00	0.00	0.02	0.00	0.00	0.07	0.00	0.08	0.00	0.00
Ti	0.00	0.00	0.00	0.00	0.00	0.00	0.00	0.00	0.00	0.00	0.00	0.00	0.00	0.01	0.01	0.00	0.00	0.01	0.00	0.00	0.00
Cr	0.00	0.00	0.00	0.00	0.00	0.00	0.00	0.00	0.00	0.00	0.00	0.00	0.00	0.00	0.00	0.00	0.00	0.00	0.00	0.00	0.00
Sc	0.00	0.00	0.00	0.00	0.00	0.00	0.00	0.00	0.00	0.00	0.00	0.00	0.00	0.00	0.00	0.00	0.00	0.00	0.00	0.00	0.00
V	0.00	0.00	0.00	0.00	0.00	0.00	0.00	0.00	0.00	0.00	0.00	0.00	0.00	0.00	0.00	0.00	0.00	0.00	0.00	0.00	0.00
Al	0.00	0.00	0.00	0.00	0.00	0.02	0.00	0.02	0.00	0.00	0.00	0.00	0.00	0.01	0.00	0.00	0.01	0.00	0.01	0.00	0.00
Fe3+	1.81	1.99	1.99	1.98	1.99	1.87	1.97	1.83	1.97	1.99	1.99	1.99	1.99	1.95	1.98	1.99	1.83	1.98	1.82	1.99	1.98
Mg	0.06	0.00	0.00	0.00	0.00	0.02	0.00	0.03	0.00	0.00	0.00	0.00	0.00	0.00	0.00	0.00	0.04	0.00	0.04	0.00	0.00
Fe2+	1.00	0.99	0.99	0.99	0.99	0.99	1.00	1.00	0.98	0.99	1.00	0.99	1.00	0.99	0.99	1.00	1.00	1.00	0.99	0.99	0.99
Mn	0.00	0.00	0.00	0.00	0.00	0.00	0.00	0.00	0.00	0.00	0.00	0.00	0.00	0.00	0.00	0.00	0.00	0.00	0.00	0.00	0.00
Co	0.00	0.00	0.00	0.00	0.00	0.00	0.00	0.00	0.00	0.00	0.00	0.00	0.00	0.00	0.00	0.00	0.00	0.00	0.00	0.00	0.00
Ca	0.00	0.00	0.00	0.00	0.00	0.00	0.00	0.00	0.00	0.00	0.00	0.00	0.00	0.00	0.00	0.00	0.00	0.00	0.01	0.00	0.00
Na	0.00	0.00	0.01	0.00	0.00	0.00	0.00	0.00	0.01	0.00	0.00	0.00	0.00	0.00	0.01	0.00	0.00	0.00	0.00	0.00	0.00
K	0.00	0.00	0.00	0.00	0.00	0.00	0.00	0.00	0.00	0.00	0.00	0.00	0.00	0.00	0.00	0.00	0.00	0.00	0.00	0.00	0.00

Tabela 2A. (Cont.). Resultados analíticos de microssonda em magnetita.

Rock Type	Mag	Mag	Mag	Mag	Mag	Mag	Mag	Mag	Mag	Mag	Mag	Mag	Mag	Mag	Mag	Mag	Mag	Mag	Mag	Mag	Mag
Sample	MFO25	MFO25	MFO25	MFO25	MFO25	MFO28	MFO28	MFO28	MFO28	MFO28	MFO28	MFO28	MFO10	MFO13	MFO13	MFO13	MFO13	MFO13	MFO13	MFO13	MFO13
Analysis (wt%)	C2 Mag 3	C2 Mag 4	C3 Mag 1	C3 Mag 2	C3 Mag 4	C1 Mag 1	C1 Mag 2	C1 Mag 3	C1 Mag 4	C2 Mag 1	C3 Mag 1	C3 Mag 2	C1 Mag 2	C1 Mag 1	C1 Mag 2	C1 Mag 3	C1 Mag 4	C2 Mag 1	C2 Mag 2	C3 Mag 1	C3 Mag 2
SiO2	2.76	1.87	1.95	2.02	1.98	2.20	0.94	0.13	0.04	0.00	3.13	0.96	0.05	0.94	0.73	0.04	2.14	0.03	0.03	0.34	0.15
TiO2	0.03	0.14	0.00	0.00	0.11	0.14	0.20	0.12	0.23	0.06	0.05	0.09	0.00	0.13	0.28	0.24	0.04	0.07	0.00	0.00	0.00
Al2O3	0.27	0.30	0.33	0.40	0.39	0.16	0.23	0.05	0.02	0.05	0.32	0.27	0.06	0.14	0.21	0.00	0.26	0.00	0.05	0.01	0.02
Fe2O3	62.10	63.32	63.09	63.09	63.47	63.37	65.91	67.30	68.70	67.85	60.55	66.61	70.85	68.35	69.17	71.06	64.58	70.26	71.50	69.29	69.80
FeO	32.09	31.71	31.54	31.79	31.84	32.17	31.74	30.74	31.23	30.18	32.31	32.08	31.60	32.08	32.56	32.51	32.63	31.77	31.69	31.53	31.71
MnO	0.09	0.01	0.00	0.01	0.00	0.00	0.00	0.00	0.04	0.09	0.00	0.04	0.05	0.00	0.00	0.00	0.00	0.00	0.00	0.00	0.01
MgO	0.92	0.66	0.60	0.66	0.79	0.73	0.29	0.01	0.02	0.02	1.30	0.18	0.00	0.31	0.15	0.02	1.00	0.00	0.00	0.14	0.00
CaO	0.32	0.27	0.20	0.23	0.09	0.20	0.04	0.00	0.00	0.00	0.14	0.07	0.01	0.16	0.05	0.00	0.02	0.01	0.05	0.00	0.00
Na2O	0.07	0.00	0.05	0.00	0.04	0.05	0.00	0.00	0.00	0.03	0.02	0.00	0.06	0.08	0.09	0.00	0.00	0.00	0.07	0.04	0.00
Cr2O3	0.03	0.00	0.12	0.04	0.10	0.05	0.04	0.03	0.00	0.00	0.03	0.00	0.00	0.00	0.00	0.03	0.11	0.01	0.03	0.00	0.00
V2O3	0.03	0.00	0.04	0.03	0.04	0.03	0.05	0.06	0.09	0.03	0.11	0.11	0.16	0.15	0.11	0.22	0.19	0.25	0.14	0.16	0.15
NiO	0.20	0.19	0.17	0.25	0.25	0.14	0.18	0.12	0.17	0.23	0.21	0.14	0.08	0.10	0.19	0.08	0.12	0.15	0.19	0.07	0.14
Total	98.90	98.48	98.10	98.53	99.08	99.23	99.62	98.56	100.54	98.54	98.16	100.55	102.91	102.44	103.54	104.20	101.09	102.54	103.75	101.59	101.98
Number of cations per 4 oxygens																					
Ni	0.01	0.01	0.01	0.01	0.01	0.00	0.01	0.00	0.01	0.01	0.01	0.00	0.00	0.00	0.01	0.00	0.00	0.00	0.01	0.00	0.00
Si	0.11	0.07	0.08	0.08	0.08	0.08	0.04	0.00	0.00	0.00	0.12	0.04	0.00	0.03	0.03	0.00	0.08	0.00	0.00	0.01	0.01
Ti	0.00	0.00	0.00	0.00	0.00	0.00	0.01	0.00	0.01	0.00	0.00	0.00	0.00	0.00	0.01	0.01	0.00	0.00	0.00	0.00	0.00
Cr	0.00	0.00	0.00	0.00	0.00	0.00	0.00	0.00	0.00	0.00	0.00	0.00	0.00	0.00	0.00	0.00	0.00	0.00	0.00	0.00	0.00
Sc	0.00	0.00	0.00	0.00	0.00	0.00	0.00	0.00	0.00	0.00	0.00	0.00	0.00	0.00	0.00	0.00	0.00	0.00	0.00	0.00	0.00
V	0.00	0.00	0.00	0.00	0.00	0.00	0.00	0.00	0.00	0.00	0.00	0.00	0.00	0.00	0.00	0.01	0.01	0.01	0.00	0.00	0.00
Al	0.01	0.01	0.02	0.02	0.02	0.01	0.01	0.00	0.00	0.00	0.01	0.01	0.00	0.01	0.01	0.00	0.01	0.00	0.00	0.00	0.00
Fe3+	1.78	1.83	1.83	1.82	1.82	1.82	1.90	1.98	1.98	1.99	1.74	1.91	1.99	1.92	1.92	1.98	1.82	1.98	1.99	1.97	1.98
Mg	0.05	0.04	0.03	0.04	0.04	0.04	0.02	0.00	0.00	0.00	0.07	0.01	0.00	0.02	0.01	0.00	0.06	0.00	0.00	0.01	0.00
Fe2+	0.98	0.99	0.99	0.99	0.99	0.99	1.00	1.00	1.00	0.99	0.99	1.00	0.99	0.99	0.99	1.00	1.00	1.00	0.98	1.00	1.00
Mn	0.00	0.00	0.00	0.00	0.00	0.00	0.00	0.00	0.00	0.00	0.00	0.00	0.00	0.00	0.00	0.00	0.00	0.00	0.00	0.00	0.00
Co	0.00	0.00	0.00	0.00	0.00	0.00	0.00	0.00	0.00	0.00	0.00	0.00	0.00	0.00	0.00	0.00	0.00	0.00	0.00	0.00	0.00
Ca	0.01	0.01	0.01	0.01	0.00	0.01	0.00	0.00	0.00	0.00	0.01	0.00	0.00	0.01	0.00	0.00	0.00	0.00	0.00	0.00	0.00
Na	0.01	0.00	0.00	0.00	0.00	0.00	0.00	0.00	0.00	0.00	0.00	0.00	0.00	0.01	0.01	0.00	0.00	0.00	0.01	0.00	0.00
K	0.00	0.00	0.00	0.00	0.00	0.00	0.00	0.00	0.00	0.00	0.00	0.00	0.00	0.00	0.00	0.00	0.00	0.00	0.00	0.00	0.00

Tabela 2A. (Cont.). Resultados analíticos de microssonda em magnetita.

Rock Type	Mag	Mag	Mag	Mag	Mag	Mag	Mag	Mag	Mag	Mag	Mag	Mag	Arqueada	Arqueada	Arqueada	Arqueada	Arqueada	Arqueada	Arqueada	Arqueada	Arqueada
Sample	MFO28	MFO28	MFO28	MFO29	MFO29	MFO09	MFO09	MFO26	MFO26	MFO26	MFO26	MFO26	MFO50	MFO50	MFO50	MFO50	MFO50	MFO50	MFO50	MFO50	MFO50
Analysis (wt%	C1 Mag 1	C1 Mag 2	C3 Mag 1	C2 Mag 1	C2 Mag 2	C1 Mag 2	C3 Mag 1	C1 Mag 1	C1 Mag 2	C1 Mag 3	C2 Mag 1	C2 Mag 2	C1 Mag 1	C1 Mag 2	C1 Mag 3	C1 Mag 4	C1 Mag 5	C2 Mag 1	C2 Mag 2	C2 Mag 3	C2 Mag 4
SiO2	0.07	0.14	1.88	0.03	0.01	1.00	0.09	0.93	0.05	0.03	0.37	0.77	2.29	2.12	2.17	2.06	2.24	2.15	1.96	3.13	1.83
TiO2	0.00	0.00	0.11	0.07	0.09	0.07	0.00	0.25	0.18	0.02	0.08	0.13	0.01	0.01	0.08	0.10	0.02	0.13	0.00	0.02	0.00
Al2O3	0.07	0.04	0.32	0.02	0.03	0.25	0.05	0.21	0.07	0.04	0.07	0.19	0.00	0.00	0.01	0.00	0.01	0.01	0.00	0.04	0.00
Fe2O3	70.15	69.68	66.02	69.07	69.29	66.81	69.31	66.32	69.47	70.08	69.65	68.24	64.20	65.31	64.43	65.42	65.95	64.52	66.27	63.32	66.13
FeO	31.57	31.61	33.05	30.92	31.07	31.43	31.31	31.82	31.60	31.30	31.81	32.20	34.15	34.28	33.85	34.20	34.88	34.37	34.49	35.94	34.11
MnO	0.07	0.00	0.09	0.08	0.00	0.00	0.01	0.00	0.00	0.10	0.05	0.11	0.04	0.00	0.13	0.03	0.07	0.00	0.00	0.02	0.03
MgO	0.00	0.03	0.52	0.02	0.06	0.49	0.00	0.24	0.00	0.00	0.19	0.22	0.02	0.01	0.10	0.01	0.00	0.01	0.00	0.03	0.00
CaO	0.03	0.01	0.32	0.03	0.00	0.17	0.02	0.15	0.00	0.02	0.06	0.06	0.01	0.04	0.01	0.00	0.03	0.05	0.02	0.01	0.00
Na2O	0.00	0.00	0.00	0.00	0.00	0.04	0.00	0.00	0.00	0.02	0.00	0.00	0.03	0.00	0.02	0.05	0.01	0.00	0.00	0.00	0.00
Cr2O3	0.07	0.12	0.01	0.09	0.05	0.06	0.02	0.00	0.01	0.00	0.00	0.00	0.05	0.02	0.00	0.01	0.00	0.08	0.01	0.00	0.04
V2O3	0.08	0.11	0.16	0.04	0.00	0.18	0.18	0.08	0.15	0.03	0.07	0.09	0.00	0.00	0.05	0.00	0.00	0.00	0.02	0.00	0.02
NiO	0.18	0.16	0.21	0.27	0.20	0.12	0.21	0.26	0.22	0.12	0.20	0.19	0.00	0.12	0.06	0.00	0.01	0.01	0.00	0.00	0.03
Total	102.30	101.89	102.69	100.62	100.80	100.61	101.20	100.23	101.75	101.76	102.54	102.19	100.79	101.90	100.92	101.87	103.22	101.33	102.77	102.51	102.18
Number of cations per 4 oxygens																					
Ni	0.01	0.00	0.01	0.01	0.01	0.00	0.01	0.01	0.01	0.00	0.01	0.01	0.00	0.00	0.00	0.00	0.00	0.00	0.00	0.00	0.00
Si	0.00	0.01	0.07	0.00	0.00	0.04	0.00	0.04	0.00	0.00	0.01	0.03	0.09	0.08	0.08	0.08	0.08	0.08	0.07	0.12	0.07
Ti	0.00	0.00	0.00	0.00	0.00	0.00	0.00	0.01	0.01	0.00	0.00	0.00	0.00	0.00	0.00	0.00	0.00	0.00	0.00	0.00	0.00
Cr	0.00	0.00	0.00	0.00	0.00	0.00	0.00	0.00	0.00	0.00	0.00	0.00	0.00	0.00	0.00	0.00	0.00	0.00	0.00	0.00	0.00
Sc	0.00	0.00	0.00	0.00	0.00	0.00	0.00	0.00	0.00	0.00	0.00	0.00	0.00	0.00	0.00	0.00	0.00	0.00	0.00	0.00	0.00
V	0.00	0.00	0.00	0.00	0.00	0.01	0.01	0.00	0.00	0.00	0.00	0.00	0.00	0.00	0.00	0.00	0.00	0.00	0.00	0.00	0.00
Al	0.00	0.00	0.01	0.00	0.00	0.01	0.00	0.01	0.00	0.00	0.00	0.01	0.00	0.00	0.00	0.00	0.00	0.00	0.00	0.00	0.00
Fe3+	1.98	1.98	1.84	1.98	1.99	1.90	1.98	1.90	1.98	1.99	1.96	1.92	1.83	1.84	1.83	1.84	1.83	1.83	1.85	1.77	1.86
Mg	0.00	0.00	0.03	0.00	0.00	0.03	0.00	0.01	0.00	0.00	0.01	0.01	0.00	0.00	0.01	0.00	0.00	0.00	0.00	0.00	0.00
Fe2+	0.99	1.00	0.98	0.99	0.99	0.99	1.00	0.99	1.00	0.99	1.00	0.99	1.00	1.00	0.99	1.00	1.00	1.00	1.00	1.00	1.00
Mn	0.00	0.00	0.00	0.00	0.00	0.00	0.00	0.00	0.00	0.00	0.00	0.00	0.00	0.00	0.00	0.00	0.00	0.00	0.00	0.00	0.00
Co	0.00	0.00	0.00	0.00	0.00	0.00	0.00	0.00	0.00	0.00	0.00	0.00	0.00	0.00	0.00	0.00	0.00	0.00	0.00	0.00	0.00
Ca	0.00	0.00	0.01	0.00	0.00	0.01	0.00	0.01	0.00	0.00	0.00	0.00	0.00	0.00	0.00	0.00	0.00	0.00	0.00	0.00	0.00
Na	0.00	0.00	0.00	0.00	0.00	0.00	0.00	0.00	0.00	0.00	0.00	0.00	0.00	0.00	0.00	0.00	0.00	0.00	0.00	0.00	0.00
K	0.00	0.00	0.00	0.00	0.00	0.00	0.00	0.00	0.00	0.00	0.00	0.00	0.00	0.00	0.00	0.00	0.00	0.00	0.00	0.00	0.00

Tabela 2A. (Cont.). Resultados analíticos de microssonda em magnetita.

Rock Type	Arqueada	Arqueada	Arqueada	Arqueada	Arqueada	Arqueada	Arqueada	Arqueada	Arqueada	Arqueada	Arqueada	Arqueada	Arqueada	Arqueada	Arqueada	Arqueada	Arqueada	Arqueada	Arqueada	Mag RS	Mag RS
Sample	MFO50	MFO51	MFO51	MFO51	MFO51	MFO51	MFO51	MFO51	MFO51	MFO51	MFO52	MFO52	MFO52	MFO52	MFO52	MFO52	MFO52	MFO52	MFO52	MFO101	MFO101
Analysis (wt%	C2 Mag 5	C1 Mag 1	C1 Mag 2	C1 Mag 3	C1 Mag 4	C1 Mag 5	C2 Mag 2	C2 Mag 3	C2 Mag 4	C2 Mag 5	C1 Mag 1	C1 Mag 2	C1 Mag 3	C1 Mag 4	C2 Mag 1	C2 Mag 2	C2 Mag 3	C2 Mag 4	C2 Mag 5	C1 Mag 1	C1 Mag 2
SiO2	2.07	0.49	0.37	0.39	0.25	0.24	0.06	0.26	0.34	0.21	0.30	0.06	0.11	0.12	0.17	0.23	0.19	0.23	0.44	0.28	0.34
TiO2	0.03	0.16	0.14	0.03	0.23	0.00	0.00	0.00	0.00	0.11	0.00	0.00	0.00	0.07	0.10	0.01	0.06	0.16	0.00	0.27	0.21
Al2O3	0.01	0.09	0.04	0.01	0.02	0.00	0.00	0.01	0.00	0.05	0.06	0.08	0.03	0.04	0.04	0.04	0.02	0.02	0.04	0.21	0.22
Fe2O3	66.05	64.67	69.87	68.31	69.77	66.16	69.73	69.67	69.20	65.30	68.01	70.72	69.68	70.36	70.26	70.36	70.00	69.78	68.74	65.29	65.07
FeO	34.51	28.96	32.33	31.57	32.00	30.12	31.11	31.84	31.95	29.78	31.17	31.95	31.51	32.03	32.18	32.22	31.76	32.11	31.99	30.33	30.49
MnO	0.10	0.01	0.00	0.04	0.03	0.00	0.00	0.05	0.02	0.08	0.00	0.00	0.12	0.00	0.09	0.00	0.01	0.03	0.00	0.00	0.06
MgO	0.06	0.21	0.03	0.00	0.02	0.05	0.00	0.04	0.00	0.04	0.06	0.00	0.00	0.00	0.00	0.00	0.02	0.04	0.01	0.00	0.01
CaO	0.00	0.47	0.05	0.02	0.00	0.07	0.01	0.00	0.00	0.00	0.03	0.05	0.01	0.03	0.00	0.02	0.04	0.02	0.00	0.02	0.04
Na2O	0.00	0.12	0.02	0.01	0.06	0.01	0.06	0.00	0.00	0.03	0.01	0.00	0.00	0.00	0.00	0.00	0.04	0.00	0.00	0.06	0.00
Cr2O3	0.00	0.03	0.00	0.05	0.00	0.05	0.00	0.04	0.03	0.01	0.00	0.02	0.01	0.04	0.06	0.00	0.00	0.04	0.00	0.00	0.00
V2O3	0.00	0.00	0.00	0.05	0.01	0.02	0.00	0.02	0.02	0.01	0.05	0.02	0.03	0.02	0.02	0.05	0.00	0.02	0.00	0.09	0.16
NiO	0.00	0.02	0.00	0.06	0.00	0.00	0.04	0.04	0.00	0.00	0.01	0.04	0.00	0.06	0.00	0.04	0.01	0.03	0.00	0.00	0.06
Total	102.84	95.21	102.84	100.54	102.39	96.71	101.02	101.96	101.56	95.61	99.70	102.92	101.48	102.76	102.93	102.97	102.14	102.48	101.22	96.54	96.67
Number of cations per 4 oxygens																					
Ni	0.00	0.00	0.00	0.00	0.00	0.00	0.00	0.00	0.00	0.00	0.00	0.00	0.00	0.00	0.00	0.00	0.00	0.00	0.00	0.00	0.00
Si	0.08	0.02	0.01	0.01	0.01	0.01	0.00	0.01	0.01	0.01	0.01	0.00	0.00	0.00	0.01	0.01	0.01	0.01	0.02	0.01	0.01
Ti	0.00	0.00	0.00	0.00	0.01	0.00	0.00	0.00	0.00	0.00	0.00	0.00	0.00	0.00	0.00	0.00	0.00	0.00	0.00	0.01	0.01
Cr	0.00	0.00	0.00	0.00	0.00	0.00	0.00	0.00	0.00	0.00	0.00	0.00	0.00	0.00	0.00	0.00	0.00	0.00	0.00	0.00	0.00
Sc	0.00	0.00	0.00	0.00	0.00	0.00	0.00	0.00	0.00	0.00	0.00	0.00	0.00	0.00	0.00	0.00	0.00	0.00	0.00	0.00	0.00
V	0.00	0.00	0.00	0.00	0.00	0.00	0.00	0.00	0.00	0.00	0.00	0.00	0.00	0.00	0.00	0.00	0.00	0.00	0.00	0.00	0.01
Al	0.00	0.00	0.00	0.00	0.00	0.00	0.00	0.00	0.00	0.00	0.00	0.00	0.00	0.00	0.00	0.00	0.00	0.00	0.00	0.01	0.01
Fe3+	1.84	1.96	1.97	1.97	1.97	1.98	2.00	1.98	1.97	1.98	1.97	1.99	1.99	1.98	1.98	1.98	1.98	1.97	1.96	1.95	1.95
Mg	0.00	0.01	0.00	0.00	0.00	0.00	0.00	0.00	0.00	0.00	0.00	0.00	0.00	0.00	0.00	0.00	0.00	0.00	0.00	0.00	0.00
Fe2+	1.00	0.97	1.00	1.00	0.99	1.00	0.99	1.00	1.00	0.99	1.00	1.00	1.00	1.00	1.00	1.00	1.00	1.00	1.00	0.99	1.00
Mn	0.00	0.00	0.00	0.00	0.00	0.00	0.00	0.00	0.00	0.00	0.00	0.00	0.00	0.00	0.00	0.00	0.00	0.00	0.00	0.00	0.00
Co	0.00	0.00	0.00	0.00	0.00	0.00	0.00	0.00	0.00	0.00	0.00	0.00	0.00	0.00	0.00	0.00	0.00	0.00	0.00	0.00	0.00
Ca	0.00	0.02	0.00	0.00	0.00	0.00	0.00	0.00	0.00	0.00	0.00	0.00	0.00	0.00	0.00	0.00	0.00	0.00	0.00	0.00	0.00
Na	0.00	0.01	0.00	0.00	0.00	0.00	0.00	0.00	0.00	0.00	0.00	0.00	0.00	0.00	0.00	0.00	0.00	0.00	0.00	0.00	0.00
K	0.00	0.00	0.00	0.00	0.00	0.00	0.00	0.00	0.00	0.00	0.00	0.00	0.00	0.00	0.00	0.00	0.00	0.00	0.00	0.00	0.00

Tabela 2A. (Cont.). Resultados analíticos de microssonda em magnetita.

Rock Type	Mag RS	Mag RS	Mag RS	Mag RS	Mag RS	Mag RS	Mag RS	Mag RS	Bt-Chl	Bt-Chl	Bt-Chl	Bt-Chl	Bt-Chl	Bt-Chl	Bt-Chl	Bt-Chl	Bt-Chl	Bt-Chl	Bt-Chl	Bt-Chl
Sample	MFO101	MFO101	MFO101	MFO101	MFO101	MFO101	MFO101	MFO101	MFO23	MFO23	MFO23	MFO23	MFO23	MFO23	MFO23	MFO27	MFO27	MFO27	MFO27	MFO27	MFO27
Analysis (wt%)	C1 Mag 3	C1 Mag 4	C1 Mag 5	C2 Mag 1	C2 Mag 2	C2 Mag 3	C2 Mag 4	C2 Mag 5	C1 Mag 1	C1 Mag 2	C1 Mag 3	C2 Mag 1	C2 Mag 2	C2 Mag 3	C3 Mag 1	C1 Mag 4.1	C1 Mag 4.2	C1 Mag 4.3	C3 Mag 1.1	C3 Mag 1.2	C3 Mag 1.3
SiO2	0.15	0.09	0.14	0.29	0.18	0.16	0.14	0.14	0.25	0.12	0.22	0.17	0.15	0.34	0.07	0.07	0.01	0.05	0.08	0.03	0.08
TiO2	0.10	0.12	0.16	0.00	0.09	0.16	0.35	0.06	0.11	0.18	0.00	0.00	0.09	0.10	0.11	0.16	0.00	0.00	0.00	0.13	0.13
Al2O3	0.16	0.29	0.17	0.24	0.31	0.30	0.36	0.21	0.08	0.03	0.05	0.04	0.08	0.10	0.09	0.06	0.04	0.07	0.11	0.04	0.02
Fe2O3	66.42	67.39	66.11	65.70	66.59	66.44	66.39	65.88	66.75	67.95	68.27	67.91	68.43	60.26	67.93	68.20	68.48	68.20	69.20	68.62	68.56
FeO	30.44	30.73	30.14	30.37	30.27	30.73	30.57	30.22	30.47	30.99	31.03	30.96	31.18	27.64	31.01	31.34	31.07	31.08	31.10	31.28	31.20
MnO	0.07	0.00	0.11	0.01	0.14	0.06	0.07	0.04	0.08	0.11	0.04	0.04	0.00	0.00	0.00	0.00	0.02	0.04	0.06	0.01	0.00
MgO	0.00	0.05	0.04	0.04	0.03	0.00	0.02	0.00	0.02	0.00	0.07	0.00	0.05	0.08	0.04	0.00	0.00	0.00	0.01	0.01	0.04
CaO	0.03	0.00	0.05	0.02	0.00	0.03	0.03	0.00	0.01	0.01	0.00	0.00	0.00	0.11	0.00	0.00	0.00	0.00	0.01	0.00	0.03
Na2O	0.00	0.03	0.01	0.00	0.06	0.00	0.07	0.00	0.03	0.00	0.01	0.00	0.04	0.07	0.00	0.00	0.00	0.00	0.07	0.01	0.04
Cr2O3	0.00	0.00	0.00	0.03	0.04	0.00	0.00	0.01	0.00	0.00	0.04	0.00	0.08	0.25	0.08	0.05	0.08	0.13	0.10	0.02	0.17
V2O3	0.06	0.12	0.04	0.12	0.16	0.13	0.19	0.12	0.11	0.18	0.19	0.13	0.22	0.16	0.15	0.33	0.40	0.42	0.41	0.42	0.41
NiO	0.01	0.00	0.05	0.00	0.03	0.00	0.05	0.04	0.12	0.19	0.12	0.06	0.03	0.05	0.00	0.00	0.00	0.00	0.04	0.04	0.04
Total	97.43	98.81	97.00	96.82	97.91	98.00	98.24	96.71	98.04	99.75	100.04	99.32	100.33	89.16	99.46	100.21	100.09	99.99	101.18	100.61	100.71
									Number of cations per 4 oxygens												
Ni	0.00	0.00	0.00	0.00	0.00	0.00	0.00	0.00	0.00	0.01	0.00	0.00	0.00	0.00	0.00	0.00	0.00	0.00	0.00	0.00	0.00
Si	0.01	0.00	0.01	0.01	0.01	0.01	0.01	0.01	0.01	0.00	0.01	0.01	0.01	0.01	0.00	0.00	0.00	0.00	0.00	0.00	0.00
Ti	0.00	0.00	0.00	0.00	0.00	0.00	0.01	0.00	0.00	0.01	0.00	0.00	0.00	0.00	0.00	0.00	0.00	0.00	0.00	0.00	0.00
Cr	0.00	0.00	0.00	0.00	0.00	0.00	0.00	0.00	0.00	0.00	0.00	0.00	0.00	0.01	0.00	0.00	0.00	0.00	0.00	0.00	0.01
Sc	0.00	0.00	0.00	0.00	0.00	0.00	0.00	0.00	0.00	0.00	0.00	0.00	0.00	0.00	0.00	0.00	0.00	0.00	0.00	0.00	0.00
V	0.00	0.00	0.00	0.00	0.00	0.00	0.01	0.00	0.00	0.01	0.01	0.00	0.01	0.01	0.00	0.01	0.01	0.01	0.01	0.01	0.01
Al	0.01	0.01	0.01	0.01	0.01	0.01	0.02	0.01	0.00	0.00	0.00	0.00	0.00	0.01	0.00	0.00	0.00	0.00	0.00	0.00	0.00
Fe3+	1.97	1.97	1.97	1.96	1.96	1.96	1.95	1.97	1.97	1.97	1.97	1.98	1.97	1.95	1.98	1.97	1.98	1.98	1.98	1.98	1.97
Mg	0.00	0.00	0.00	0.00	0.00	0.00	0.00	0.00	0.00	0.00	0.00	0.00	0.00	0.01	0.00	0.00	0.00	0.00	0.00	0.00	0.00
Fe2+	1.00	1.00	0.99	1.00	0.99	1.00	0.99	1.00	0.99	1.00	1.00	1.00	1.00	0.99	1.00	1.00	1.00	1.00	0.99	1.00	1.00
Mn	0.00	0.00	0.00	0.00	0.00	0.00	0.00	0.00	0.00	0.00	0.00	0.00	0.00	0.00	0.00	0.00	0.00	0.00	0.00	0.00	0.00
Co	0.00	0.00	0.00	0.00	0.00	0.00	0.00	0.00	0.00	0.00	0.00	0.00	0.00	0.00	0.00	0.00	0.00	0.00	0.00	0.00	0.00
Ca	0.00	0.00	0.00	0.00	0.00	0.00	0.00	0.00	0.00	0.00	0.00	0.00	0.00	0.00	0.00	0.00	0.00	0.00	0.00	0.00	0.00
Na	0.00	0.00	0.00	0.00	0.00	0.00	0.01	0.00	0.00	0.00	0.00	0.00	0.00	0.01	0.00	0.00	0.00	0.00	0.01	0.00	0.00
K	0.00	0.00	0.00	0.00	0.00	0.00	0.00	0.00	0.00	0.00	0.00	0.00	0.00	0.00	0.00	0.00	0.00	0.00	0.00	0.00	0.00

Tabela 2A. (Cont.). Resultados analíticos de microssonda em magnetita.

Rock Type	Mag RS	Mag RS	Mag RS	Mag RS	Mag RS	Mag RS	Mag RS	Mag RS	Mag RS	Mag RS	Mag RS	Mag RS	Mag RS	Mag RS
Sample	MFO102AB	MFO102AB	MFO102AB	MFO102AB	MFO102AB	MFO102AB	MFO102AB	MFO102B	MFO102B	MFO102B	MFO102B	MFO102B	MFO102B	MFO102B
Analysis (wt%	C1 Mag 1	C1 Mag 2	C1 Mag 3	C1 Mag 4	C2 Mag 1	C2 Mag 2	C2 Mag 3	C1 Mag 1	C1 Mag 2	C1 Mag 3	C2 Mag 1	C2 Mag 2	C2 Mag 3	C3 Mag 1
SiO2	0.05	0.06	0.08	0.07	0.16	0.04	0.13	0.05	0.06	0.13	0.05	0.05	0.33	0.20
TiO2	0.06	0.09	0.04	0.10	0.19	0.02	0.30	0.19	0.28	0.07	0.12	0.00	0.00	0.04
Al2O3	0.18	0.06	0.00	0.09	0.08	0.08	0.04	0.10	0.11	0.14	0.06	0.01	0.10	0.10
Fe2O3	67.92	68.53	66.33	68.40	68.31	68.20	63.68	65.19	64.18	63.71	65.66	64.44	63.95	62.07
FeO	30.66	30.71	29.87	30.60	31.04	30.57	29.23	29.13	29.26	28.60	29.76	29.01	29.49	28.35
MnO	0.00	0.00	0.05	0.00	0.13	0.00	0.00	0.11	0.00	0.10	0.00	0.02	0.00	0.00
MgO	0.11	0.13	0.11	0.21	0.13	0.08	0.10	0.12	0.11	0.15	0.07	0.09	0.05	0.10
CaO	0.01	0.00	0.00	0.01	0.02	0.01	0.02	0.00	0.00	0.01	0.01	0.00	0.01	0.00
Na2O	0.01	0.03	0.00	0.03	0.00	0.03	0.03	0.07	0.01	0.05	0.00	0.00	0.00	0.00
Cr2O3	0.00	0.10	0.07	0.00	0.00	0.06	0.18	0.06	0.07	0.30	0.00	0.03	0.02	0.07
V2O3	0.02	0.05	0.01	0.06	0.07	0.16	0.04	0.16	0.14	0.10	0.06	0.19	0.09	0.04
NiO	0.00	0.14	0.00	0.07	0.13	0.11	0.00	0.10	0.21	0.14	0.06	0.04	0.07	0.07
Total	99.02	99.89	96.55	99.63	100.26	99.34	93.75	95.28	94.43	93.49	95.85	93.88	94.10	91.04
Number of cations per 4 oxygens														
Ni	0.00	0.00	0.00	0.00	0.00	0.00	0.00	0.00	0.01	0.00	0.00	0.00	0.00	0.00
Si	0.00	0.00	0.00	0.00	0.01	0.00	0.01	0.00	0.00	0.01	0.00	0.00	0.01	0.01
Ti	0.00	0.00	0.00	0.00	0.01	0.00	0.01	0.01	0.01	0.00	0.00	0.00	0.00	0.00
Cr	0.00	0.00	0.00	0.00	0.00	0.00	0.01	0.00	0.00	0.01	0.00	0.00	0.00	0.00
Sc	0.00	0.00	0.00	0.00	0.00	0.00	0.00	0.00	0.00	0.00	0.00	0.00	0.00	0.00
V	0.00	0.00	0.00	0.00	0.00	0.00	0.00	0.01	0.00	0.00	0.00	0.01	0.00	0.00
Al	0.01	0.00	0.00	0.00	0.00	0.00	0.00	0.00	0.01	0.01	0.00	0.00	0.00	0.00
Fe3+	1.98	1.98	1.99	1.99	1.97	1.98	1.96	1.98	1.97	1.97	1.98	1.99	1.97	1.97
Mg	0.00	0.00	0.00	0.00	0.01	0.00	0.01	0.00	0.00	0.00	0.00	0.00	0.00	0.01
Fe2+	1.00	0.99	1.00	0.99	1.00	0.99	1.00	0.98	1.00	0.98	1.00	0.99	1.00	1.00
Mn	0.00	0.00	0.00	0.00	0.00	0.00	0.00	0.00	0.00	0.00	0.00	0.00	0.00	0.00
Co	0.00	0.00	0.00	0.00	0.00	0.00	0.00	0.00	0.00	0.00	0.00	0.00	0.00	0.00
Ca	0.00	0.00	0.00	0.00	0.00	0.00	0.00	0.00	0.00	0.00	0.00	0.00	0.00	0.00
Na	0.00	0.00	0.00	0.00	0.00	0.00	0.00	0.01	0.00	0.00	0.00	0.00	0.00	0.00
K	0.00	0.00	0.00	0.00	0.00	0.00	0.00	0.00	0.00	0.00	0.00	0.00	0.00	0.00

Tabela 3A. Resultados analíticos de microssonda em feldspato.

Rock Type	GRN	GRN	GRN	GRN	GRN	GRN	GRN	GRN	GRN	GRN	GRN	GRN	GRN
Sample	MFO 22	MFO 22	MFO 22	MFO 22	MFO 22	MFO 22	MFO 22	MFO 22	MFO 22	MFO 22	MFO 22	MFO 22	MFO 22
Analysis (wt%)	C1 Kfs 1	C1 Kfs 2	C1 Kfs 3	C1 Kfs 4	C1 Kfs 5	C2 Kfs 1	C2 Kfs 2	C2 Kfs 4	C2 Kfs 5	C3 Kfs 1	C3 Kfs 2	C3 Kfs 3	C3 Kfs 4
SiO2	58.07	59.85	61.81	61.35	61.07	63.10	61.90	61.37	60.37	60.11	61.04	60.93	60.52
TiO2	0.18	0.10	0.00	0.05	0.04	0.05	0.00	0.00	0.00	0.01	0.00	0.20	0.00
Al2O3	18.17	18.11	17.99	18.54	18.57	18.44	19.47	17.97	18.03	17.86	18.05	17.83	17.74
Cr2O3	0.00	0.00	0.05	0.00	0.00	0.00	0.01	0.00	0.05	0.05	0.00	0.03	0.00
FeO	0.77	0.64	0.65	0.54	0.15	0.41	0.81	0.73	0.33	0.11	0.02	0.05	0.08
MnO	0.01	0.03	0.07	0.00	0.06	0.00	0.01	0.00	0.00	0.00	0.00	0.00	0.04
MgO	0.21	0.06	0.02	0.10	0.03	0.00	0.15	0.00	0.04	0.03	0.01	0.02	0.00
CaO	0.07	0.02	0.01	0.03	0.04	0.03	0.06	0.04	0.00	0.00	0.02	0.00	0.05
Na2O	0.76	0.30	0.54	0.32	0.17	0.99	1.20	0.11	0.63	0.09	0.18	0.09	0.10
K2O	14.05	14.80	14.64	15.46	14.98	15.07	14.03	16.04	15.30	16.23	16.01	16.39	16.08
BaO	0.37	0.24	0.02	0.31	0.16	0.47	0.37	0.08	0.20	0.07	0.07	0.13	0.00
V2O3	0.03	0.00	0.00	0.02	0.00	0.02	0.02	0.00	0.00	0.00	0.00	0.00	0.00
SrO	0.04	0.00	0.00	0.12	0.13	0.17	0.13	0.15	0.00	0.05	0.00	0.02	0.07
Total	92.72	94.15	95.84	96.89	95.38	98.75	98.16	96.51	94.96	94.60	95.42	95.69	94.68
Number of cations per 8 oxygens													
Si	2.90	2.95	2.99	2.94	2.97	2.96	2.91	2.95	2.94	2.94	2.96	2.95	2.96
Al	1.07	1.05	1.02	1.05	1.06	1.02	1.08	1.02	1.03	1.03	1.03	1.02	1.02
Cr	0.00	0.00	0.00	0.00	0.00	0.00	0.00	0.00	0.00	0.00	0.00	0.00	0.00
Ti	0.01	0.00	0.00	0.00	0.00	0.00	0.00	0.00	0.00	0.00	0.00	0.01	0.00
Fe3+	0.03	0.00	0.00	0.02	0.00	0.02	0.03	0.03	0.01	0.00	0.00	0.00	0.00
Fe2+	0.00	0.02	0.03	0.00	0.01	0.00	0.00	0.00	0.00	0.00	0.00	0.00	0.00
Mn	0.00	0.00	0.00	0.00	0.00	0.00	0.00	0.00	0.00	0.00	0.00	0.00	0.00
Mg	0.02	0.00	0.00	0.01	0.00	0.00	0.01	0.00	0.00	0.00	0.00	0.00	0.00
Ba	0.01	0.00	0.00	0.01	0.00	0.01	0.01	0.00	0.00	0.00	0.00	0.00	0.00
Zn	0.00	0.00	0.00	0.00	0.00	0.00	0.00	0.00	0.00	0.00	0.00	0.00	0.00
Ca	0.00	0.00	0.00	0.00	0.00	0.00	0.00	0.00	0.00	0.00	0.00	0.00	0.00
Na	0.07	0.03	0.05	0.03	0.02	0.09	0.11	0.01	0.06	0.01	0.02	0.01	0.01
K	0.89	0.93	0.90	0.94	0.93	0.90	0.84	0.98	0.95	1.01	0.99	1.01	1.00
Sc	0.00	0.00	0.00	0.00	0.00	0.00	0.00	0.00	0.00	0.00	0.00	0.00	0.00
V	0.00	0.00	0.00	0.00	0.00	0.00	0.00	0.00	0.00	0.00	0.00	0.00	0.00
Pb	0.00	0.00	0.00	0.00	0.00	0.00	0.00	0.00	0.00	0.00	0.00	0.00	0.00
Eu	0.00	0.00	0.00	0.00	0.00	0.00	0.00	0.00	0.00	0.00	0.00	0.00	0.00
Sr	0.00	0.00	0.00	0.00	0.00	0.00	0.00	0.00	0.00	0.00	0.00	0.00	0.00
Rb	0.00	0.00	0.00	0.00	0.00	0.00	0.00	0.00	0.00	0.00	0.00	0.00	0.00
Cs	0.00	0.00	0.00	0.00	0.00	0.00	0.00	0.00	0.00	0.00	0.00	0.00	0.00
% An	0.36	0.08	0.03	0.17	0.22	0.14	0.30	0.20	0.02	0.00	0.11	0.00	0.24
% Ab	7.52	3.01	5.32	3.05	1.64	9.01	11.36	1.03	5.86	0.86	1.69	0.82	0.91
% Or	91.39	96.42	94.62	96.19	97.82	89.98	87.62	98.62	93.76	99.02	98.07	98.95	98.85
% Cel	0.74	0.49	0.03	0.59	0.32	0.86	0.72	0.16	0.37	0.12	0.13	0.24	0.00

Tabela 3A. (Cont.). Resultados analíticos de microssonda em feldspato.

Rock Type	FSV	FSV	FSV	FSV	FSV	FSV	FSV	FSV	Bt-Chl	Bt-Chl	Bt-Chl	Bt-Chl	Bt-Chl
Sample	MFO 02	MFO 02	MFO 02	MFO 02	MFO 02	MFO 08	MFO 08	MFO 08	MFO 30	MFO 30	MFO 30	MFO 30	MFO 30
Analysis (wt%)	C1 Pl 1	C1 Pl 2	C1 Pl 3	C2 Pl 1.1	C3 Pl 1	C3 Pl 1	C3 Pl 2	C3 Pl 3	C1 Pl 1	C1 Pl 2	C2 Pl 1	C2 Pl 2	C2 Pl 4
SiO2	54.47	55.97	54.79	54.70	59.92	61.96	62.62	63.03	64.46	66.12	58.71	63.38	66.15
TiO2	0.07	0.00	0.00	0.06	0.04	0.10	0.11	0.00	0.00	0.08	0.00	0.12	0.00
Al2O3	17.32	17.49	17.50	17.28	18.20	19.19	19.33	18.86	21.39	19.87	24.36	22.79	20.01
Cr2O3	0.06	0.02	0.07	0.05	0.00	0.10	0.00	0.00	0.00	0.07	0.00	0.00	0.00
FeO	0.12	0.16	0.09	0.07	0.12	0.17	0.17	0.22	0.33	0.12	0.17	0.14	0.13
MnO	0.00	0.06	0.00	0.00	0.00	0.02	0.00	0.02	0.02	0.00	0.04	0.00	0.02
MgO	0.01	0.01	0.02	0.00	0.04	0.03	0.00	0.01	0.32	0.03	0.02	0.05	0.00
CaO	0.20	0.16	0.35	0.09	0.17	0.30	0.31	0.39	2.21	1.12	5.38	4.09	1.43
Na2O	9.59	9.48	10.89	10.34	11.39	11.48	11.38	11.77	9.60	10.47	5.79	9.02	10.53
K2O	1.60	1.50	0.10	0.63	0.20	0.07	0.10	0.08	0.17	0.08	2.46	0.08	0.06
BaO	0.01	0.01	0.00	0.06	0.00	0.01	0.00	0.00	0.00	0.08	0.26	0.00	0.00
V2O3	0.00	0.07	0.00	0.00	0.04	0.00	0.03	0.01	0.00	0.00	0.00	0.00	0.00
SrO													
Total	83.46	84.91	83.84	83.27	90.16	93.42	94.04	94.39	98.50	98.03	97.24	99.66	98.40
Number of cations per 8 oxygens													
Si	2.84	2.88	2.82	2.84	2.88	2.88	2.89	2.90	2.89	2.97	2.72	2.82	2.95
Al	1.06	1.06	1.06	1.06	1.03	1.05	1.05	1.02	1.13	1.05	1.33	1.19	1.05
Cr	0.00	0.00	0.00	0.00	0.00	0.00	0.00	0.00	0.00	0.00	0.00	0.00	0.00
Ti	0.00	0.00	0.00	0.00	0.00	0.00	0.00	0.00	0.00	0.00	0.00	0.00	0.00
Fe3+	0.01	0.01	0.00	0.00	0.00	0.01	0.01	0.01	0.00	0.00	0.00	0.00	0.00
Fe2+	0.00	0.00	0.00	0.00	0.00	0.00	0.00	0.00	0.01	0.00	0.01	0.01	0.00
Mn	0.00	0.00	0.00	0.00	0.00	0.00	0.00	0.00	0.00	0.00	0.00	0.00	0.00
Mg	0.00	0.00	0.00	0.00	0.00	0.00	0.00	0.00	0.02	0.00	0.00	0.00	0.00
Ba	0.00	0.00	0.00	0.00	0.00	0.00	0.00	0.00	0.00	0.00	0.00	0.00	0.00
Zn	0.00	0.00	0.00	0.00	0.00	0.00	0.00	0.00	0.00	0.00	0.00	0.00	0.00
Ca	0.01	0.01	0.02	0.00	0.01	0.01	0.02	0.02	0.11	0.05	0.27	0.19	0.07
Na	0.97	0.94	1.09	1.04	1.06	1.03	1.02	1.05	0.83	0.91	0.52	0.78	0.91
K	0.11	0.10	0.01	0.04	0.01	0.00	0.01	0.00	0.01	0.00	0.15	0.00	0.00
Sc	0.00	0.00	0.00	0.00	0.00	0.00	0.00	0.00	0.00	0.00	0.00	0.00	0.00
V	0.00	0.00	0.00	0.00	0.00	0.00	0.00	0.00	0.00	0.00	0.00	0.00	0.00
Pb	0.00	0.00	0.00	0.00	0.00	0.00	0.00	0.00	0.00	0.00	0.00	0.00	0.00
Eu	0.00	0.00	0.00	0.00	0.00	0.00	0.00	0.00	0.00	0.00	0.00	0.00	0.00
Sr	0.00	0.00	0.00	0.00	0.00	0.00	0.00	0.00	0.00	0.00	0.00	0.00	0.00
Rb	0.00	0.00	0.00	0.00	0.00	0.00	0.00	0.00	0.00	0.00	0.00	0.00	0.00
Cs	0.00	0.00	0.00	0.00	0.00	0.00	0.00	0.00	0.00	0.00	0.00	0.00	0.00
% An	1.01	0.81	1.72	0.43	0.80	1.39	1.48	1.80	11.18	5.54	28.50	19.95	6.97
% Ab	89.18	89.82	97.71	95.60	98.07	98.18	97.97	97.75	87.79	93.87	55.49	79.59	92.68
% Or	9.79	9.34	0.57	3.86	1.12	0.41	0.55	0.45	1.03	0.45	15.51	0.46	0.35
% Cel	0.02	0.03	0.00	0.11	0.01	0.02	0.00	0.00	0.00	0.14	0.51	0.00	0.00

Tabela 4A. Resultados analíticos de microssonda em apatita.

Rock Type	Amp	Amp	Amp	Amp	Amp	Amp	Amp	Amp	Amp	Amp	FSV	FSV	FSV	FSV	FSV	FSV	FSV	Bt-Chl	Bt-Chl	Bt-Chl	GRN	GRN	GRN
Sample	MFO15	MFO15	MFO15	MFO15	MFO15	MFO15	MFO15	MFO15	MFO15	MFO15	MFO02	MFO02	MFO08	MFO08	MFO08	MFO08	MFO08	MFO03	MFO03	MFO03	MFO20	MFO20	MFO20
Analysis (wt%)	C1_Ap1.1	C1_Ap1.2	C1_Ap1.3	C3_Ap1.1	C3_Ap1.2	C3_Ap1.3	C3_Ap1.4	C3_Ap1.5	C3_Ap1.6	C3_Ap1.7	C3_Ap1	C3_Ap2	C1_Ap1	C1_Ap2	C1_Ap3	C3_Ap1	C3_Ap2	C1_Ap1	C1_Ap2	C1_Ap3	C2_Ap1	C2_Ap2	C2_Ap3
SiO2	0.01	0.14	0.09	0.09	0.12	0.14	0.11	0.07	0.25	0.13	0.09	0.07	0.02	0.03	0.02	0.03	0.05	0.02	0.07	0.05	0.03	0.05	0.10
TiO2	0.00	0.00	0.17	0.03	0.00	0.00	0.00	0.00	0.02	0.08	0.00	0.00	0.08	0.06	0.00	0.03	0.07	0.00	0.13	0.00	0.00	0.00	0.05
Al2O3	0.00	0.00	0.01	0.00	0.00	0.00	0.03	0.00	0.02	0.00	0.01	0.02	0.00	0.00	0.00	0.00	0.00	0.00	0.01	0.00	0.00	0.00	0.04
Cr2O3	0.08	0.03	0.00	0.10	0.02	0.00	0.02	0.14	0.01	0.00	0.03	0.00	0.05	0.00	0.11	0.09	0.15	0.04	0.00	0.00	0.05	0.11	0.04
FeO	0.09	0.02	0.08	0.08	0.03	0.13	0.02	0.01	0.13	0.05	0.13	0.14	0.18	0.07	0.24	0.11	0.17	0.01	0.12	0.04	0.07	0.06	0.07
MnO	0.04	0.00	0.06	0.00	0.07	0.00	0.06	0.00	0.00	0.00	0.11	0.11	0.00	0.08	0.07	0.00	0.07	0.00	0.05	0.05	0.00	0.00	0.04
MgO	0.04	0.00	0.00	0.03	0.00	0.04	0.05	0.00	0.07	0.00	0.02	0.04	0.00	0.01	0.00	0.00	0.03	0.00	0.00	0.00	0.00	0.00	0.03
P2O5	40.95	39.67	40.85	40.96	40.66	41.59	41.05	41.26	40.15	40.99	43.30	43.47	42.13	42.57	41.42	43.35	43.85	42.95	42.01	41.52	43.01	42.59	42.56
CaO	55.14	54.53	55.70	55.41	55.36	54.89	55.08	54.84	54.94	55.03	55.30	55.20	54.29	54.41	54.65	54.49	56.23	55.11	54.17	54.34	54.68	55.65	54.36
Na2O	0.00	0.02	0.08	0.03	0.01	0.02	0.02	0.00	0.06	0.00	0.03	0.05	0.05	0.02	0.04	0.03	0.03	0.01	0.02	0.02	0.05	0.04	0.10
K2O	0.02	0.01	0.01	0.00	0.02	0.00	0.00	0.03	0.02	0.00	0.01	0.01	0.03	0.00	0.05	0.03	0.00	0.01	0.00	0.00	0.02	0.00	0.03
SrO	0.05	0.03	0.00	0.07	0.08	0.02	0.00	0.06	0.00	0.00	0.07	0.05	0.03	0.02	0.00	0.00	0.00	0.12	0.02	0.07	0.06	0.07	0.08
NiO	0.00	0.01	0.05	0.03	0.00	0.08	0.00	0.08	0.00	0.05	0.06	0.00	0.00	0.08	0.02	0.04	0.00	0.02	0.04	0.00	0.00	0.07	0.04
V2O3	0.00	0.00	0.00	0.00	0.00	0.04	0.02	0.03	0.00	0.00	0.04	0.01	0.00	0.02	0.00	0.01	0.00	0.04	0.03	0.03	0.05	0.00	0.00
BaO	0.00	0.15	0.00	0.00	0.05	0.08	0.07	0.00	0.00	0.00	0.00	0.00	0.10	0.00	0.02	0.00	0.00	0.00	0.00	0.11	0.05	0.00	0.02
F	2.72	4.67	2.49	3.86	3.57	3.31	3.11	3.22	3.27	2.17	2.27	2.32	4.84	4.97	6.42	3.78	2.39	3.74	4.91	4.86	3.69	3.89	4.03
Cl	0.24	0.24	0.20	0.26	0.25	0.18	0.24	0.27	0.17	0.18	0.11	0.13	0.19	0.16	0.05	0.20	0.13	0.08	0.09	0.08	0.99	0.48	0.92
Total	98.18	97.49	98.69	99.25	98.68	99.08	98.53	98.57	97.67	97.74	100.59	100.61	99.90	100.38	100.38	100.55	102.14	100.55	99.59	99.11	100.96	101.25	100.60

Rock Type	Mag	Mag	Mag	Mag	Mag	Mag	Mag	Mag	Mag	Mag	Mag	Mag	Mag	Mag	Mag	Mag	Mag	Mag	Mag	Mag	Mag	GRN	GRN	GRN
Sample	MFO14	MFO14	MFO14	MFO14	MFO14	MFO14	MFO14	MFO14	MFO14	MFO10	MFO10	MFO10	MFO10	MFO10	MFO10	MFO10	MFO10	MFO10	MFO10	MFO10	MFO10	MFO20	MFO20	MFO20
Analysis (wt%)	C1_Ap2	C1_Ap3	C1_Ap4	C3_Ap1	C3_Ap2	C4_Ap1	C4_Ap2	C4_Ap3	C4_Ap4	C1_Ap1	C1_Ap2	C1_Ap3	C1_Ap4	C2_Ap3	C2_Ap4	C3_Ap1	C3_Ap2	C3_Ap3	C3_Ap4	C3_Ap5	C2_Ap1	C2_Ap2	C2_Ap3
SiO2	0.05	0.04	0.07	0.03	0.18	0.01	0.01	0.04	0.05	0.01	0.04	0.04	0.02	0.03	0.03	0.05	0.05	0.03	0.06	0.04	0.03	0.05	0.10
TiO2	0.00	0.09	0.10	0.00	0.00	0.00	0.00	0.00	0.00	0.00	0.08	0.00	0.00	0.07	0.11	0.00	0.04	0.00	0.00	0.00	0.00	0.00	0.05
Al2O3	0.00	0.00	0.00	0.00	0.05	0.01	0.00	0.00	0.01	0.00	0.00	0.01	0.00	0.03	0.01	0.00	0.02	0.01	0.03	0.01	0.00	0.00	0.04
Cr2O3	0.01	0.00	0.00	0.10	0.04	0.02	0.01	0.00	0.00												0.05	0.11	0.04
FeO	0.14	0.10	0.10	0.14	0.44	0.09	0.16	0.18	0.24	0.07	0.08	0.10	0.26	0.20	0.15	0.00	0.05	0.03	0.10	0.04	0.07	0.06	0.07
MnO	0.01	0.00	0.18	0.08	0.03	0.07	0.05	0.05	0.08	0.04	0.00	0.00	0.00	0.09	0.00	0.07	0.00	0.13	0.00	0.02	0.00	0.00	0.04
MgO	0.01	0.02	0.02	0.00	0.00	0.00	0.00	0.01	0.02												0.00	0.00	0.03
P2O5	42.73	43.09	42.82	43.66	41.87	43.12	43.55	42.92	43.09	42.96	41.98	43.41	43.78	42.79	43.05	43.26	43.28	42.84	43.82	42.85	43.01	42.59	42.56
CaO	55.25	55.54	55.77	56.73	54.45	55.90	57.00	55.32	56.46	53.19	52.76	54.77	53.12	51.95	54.13	56.35	56.91	52.15	53.50	52.53	54.68	55.65	54.36
Na2O	0.04	0.03	0.03	0.04	0.04	0.00	0.00	0.08	0.01	0.00	0.00	0.00	0.01	0.02	0.01	0.02	0.03	0.00	0.01	0.03	0.05	0.04	0.10
K2O	0.00	0.00	0.00	0.00	0.06	0.00	0.00	0.00	0.03	0.00	0.00	0.03	0.00	0.01	0.00	0.00	0.00	0.01	0.26	0.00	0.02	0.00	0.03
SrO	0.13	0.02	0.02	0.00	0.05	0.00	0.00	0.00	0.05	1.97	0.02	0.05	0.02	0.02	0.02	0.00	0.01	0.01	0.00	0.00	0.06	0.07	0.08
NiO	0.12	0.02	0.00	0.01	0.47	0.01	0.00	0.02	0.01												0.00	0.07	0.04
V2O3	0.03	0.00	0.01	0.04	0.05	0.01	0.00	0.00	0.00												0.05	0.00	0.00
BaO	0.00	0.00	0.03	0.01	0.00	0.00	0.00	0.07	0.12												0.05	0.00	0.02
F	3.95	2.29	2.29	2.24	4.33	3.15	2.24	4.47	2.11	3.75	3.46	3.77	4.02	4.03	4.07	3.49	3.21	3.26	3.86	3.51	3.69	3.89	4.03
Cl	0.13	0.17	0.12	0.09	0.14	0.18	0.13	0.15	0.15												0.99	0.48	0.92
Total	100.90	100.39	100.56	102.21	100.34	101.19	102.17	101.39	101.50												100.96	101.25	100.60

Tabela 4A. (Cont.). Resultados analíticos de microssonda em apatita.

Rock Type	Bt-Chl	Bt-Chl	Bt-Chl	Bt-Chl	Bt-Chl	Bt-Chl	Bt-Chl	Bt-Chl	Bt-Chl	Bt-Chl	Bt-Chl	Bt-Chl	Bt-Chl	Bt-Chl	Bt-Chl	Bt-Chl	Bt-Chl	Bt-Chl	Bt-Chl	Mag
Sample	MFO05	MFO05	MFO05	MFO05	MFO17	MFO16	MFO16	MFO16	MFO16	MFO11	MFO11	MFO11	MFO11	MFO11	MFO11	MFO11	MFO11	MFO11	MFO11	MFO10
Analysis (wt%)	C1_Ap1	C1_Ap2	C1_Ap3	C1_Ap4	C3_Ap1	C3_Ap1.1	C3_Ap1.2	C3_Ap1.3	C3_Ap1.4	C2_Ap1	C2_Ap2	C2_Ap3	C2_Ap4	C2_Ap5	C2_Ap6	C2_Ap7	C2_Ap8	C2_Ap9	C2_Ap10	C1_Ap1
SiO2	0.04	0.00	0.03	0.04	0.11	0.02	0.03	0.06	0.10	0.06	0.11	0.01	0.00	0.11	0.04	0.04	0.11	0.04	0.07	0.04
TiO2	0.15	0.00	0.04	0.00	0.00	0.06	0.19	0.00	0.25	0.00	0.07	0.07	0.17	0.13	0.00	0.04	0.13	0.07	0.02	0.04
Al2O3	0.01	0.00	0.00	0.00	0.00	0.00	0.00	0.00	0.00	0.03	0.01	0.02	0.00	0.03	0.05	0.03	0.01	0.01	0.01	0.00
Cr2O3					0.09	0.00	0.05	0.03	0.14	0.00	0.00	0.00	0.00	0.00	0.00	0.14	0.00	0.02	0.13	0.00
FeO	0.00	0.00	0.03	0.12	0.09	0.00	0.09	0.18	0.11	0.27	0.37	0.22	0.17	0.13	0.30	0.35	0.34	0.31	0.37	0.24
MnO	0.02	0.00	0.03	0.04	0.00	0.05	0.02	0.03	0.02	0.03	0.00	0.00	0.13	0.14	0.02	0.05	0.04	0.04	0.00	0.05
MgO					0.00	0.00	0.00	0.01	0.02	0.03	0.03	0.02	0.01	0.02	0.02	0.00	0.02	0.03	0.02	0.00
P2O5	42.18	42.64	42.60	42.68	41.95	43.28	42.94	43.97	42.20	43.67	43.53	43.74	43.16	42.59	42.81	42.94	43.23	43.53	44.26	43.49
CaO	53.08	52.54	52.92	53.33	53.75	55.65	54.46	55.08	54.56	55.36	55.87	55.42	55.43	55.41	55.07	54.30	55.24	54.99	55.30	55.30
Na2O	0.09	0.00	0.00	0.01	0.05	0.04	0.03	0.02	0.02	0.01	0.05	0.00	0.01	0.03	0.01	0.01	0.00	0.01	0.02	0.02
K2O	0.01	0.00	0.00	0.00	0.00	0.02	0.00	0.03	0.00	0.03	0.00	0.00	0.00	0.00	0.04	0.06	0.07	0.01	0.02	0.00
SrO	0.04	0.07	0.06	0.02	0.02	0.00	0.03	0.00	0.00	0.06	0.00	0.00	0.05	0.06	0.15	0.02	0.09	0.03	0.00	0.00
NiO					0.04	0.00	0.01	0.02	0.00	0.00	0.07	0.00	0.00	0.00	0.07	0.05	0.06	0.01	0.00	0.00
V2O3					0.00	0.00	0.00	0.00	0.00	0.00	0.04	0.00	0.02	0.00	0.00	0.01	0.00	0.00	0.01	0.00
BaO					0.03	0.00	0.00	0.05	0.05	0.08	0.00	0.06	0.00	0.13	0.00	0.12	0.00	0.00	0.07	0.00
F	3.93	4.29	3.80	4.16	3.52	2.92	4.49	3.28	4.10	3.82	2.59	4.41	2.90	3.22	3.79	5.02	3.19	3.34	3.23	5.33
Cl					0.21	0.16	0.17	0.13	0.20	0.10	0.08	0.15	0.11	0.14	0.12	0.10	0.09	0.15	0.09	0.11
Total					98.32	100.93	100.59	101.47	99.98	101.92	101.71	102.22	100.92	100.76	100.85	101.14	101.28	101.16	102.23	102.33

Rock Type	Bt-Chl	Bt-Chl	Bt-Chl	Bt-Chl	Bt-Chl	Bt-Chl	Bt-Chl	Bt-Chl	Bt-Chl	Bt-Chl	Bt-Chl	Bt-Chl	Bt-Chl	Bt-Chl	Bt-Chl	Bt-Chl	Bt-Chl	Bt-Chl	Bt-Chl	Bt-Chl
Sample	MFO03	MFO03	MFO03	MFO03	MFO03	MFO03	MFO03	MFO04	MFO04	MFO04	MFO04	MFO04	MFO04	MFO04	MFO04	MFO04	MFO04	MFO04	MFO04	MFO05
Analysis (wt%)	C1_Ap4	C1_Ap5	C1_Ap6	C1_Ap7	C1_Ap8	C1_Ap9	C1_Ap10	C1_Ap1	C1_Ap2	C1_Ap3	C1_Ap4	C2_Ap1	C2_Ap3	C2_Ap4	C3_Ap1	C3_Ap2	C3_Ap3	C3_Ap4	C3_Ap5	C4_Ap1
SiO2	0.07	0.08	0.04	0.08	0.04	0.07	0.05	0.03	0.03	0.05	0.00	0.04	0.06	0.04	0.03	0.03	0.04	0.04	0.09	0.09
TiO2	0.06	0.00	0.01	0.04	0.12	0.12	0.18	0.00	0.06	0.05	0.03	0.00	0.28	0.10	0.00	0.08	0.00	0.11	0.09	0.12
Al2O3	0.03	0.04	0.00	0.00	0.03	0.01	0.01	0.01	0.01	0.01	0.00	0.00	0.00	0.04	0.00	0.00	0.00	0.00	0.00	0.03
Cr2O3	0.05	0.03	0.00	0.00	0.01	0.00	0.04	0.03	0.01	0.00	0.00									0.00
FeO	0.00	0.14	0.06	0.04	0.06	0.08	0.07	0.40	0.32	0.26	0.16	0.49	0.35	0.85	0.02	0.12	0.05	0.07	0.13	0.42
MnO	0.00	0.00	0.01	0.00	0.00	0.09	0.12	0.04	0.00	0.00	0.00	0.06	0.04	0.03	0.00	0.00	0.06	0.00	0.03	0.00
MgO	0.03	0.01	0.02	0.03	0.03	0.00	0.00	0.00	0.00	0.00	0.02									0.01
P2O5	41.70	41.94	42.23	42.31	40.84	41.49	41.71	43.00	42.17	42.34	41.84	43.96	42.92	42.89	43.35	42.96	43.09	43.38	42.96	43.08
CaO	55.37	54.60	54.93	55.28	55.90	55.80	54.93	53.46	53.16	52.77	52.98	51.00	52.06	50.52	56.82	52.28	52.57	52.71	54.83	54.46
Na2O	0.04	0.00	0.03	0.03	0.00	0.04	0.08	0.00	0.02	0.00	0.04	0.01	0.00	0.03	0.00	0.00	0.00	0.00	0.00	0.01
K2O	0.02	0.00	0.02	0.00	0.00	0.00	0.00	0.00	0.00	0.00	0.02	0.00	0.00	0.00	0.00	0.00	0.00	0.00	0.00	0.02
SrO	0.18	0.00	0.11	0.03	0.07	0.00	0.06	0.01	0.04	0.00	0.07	0.07	0.03	0.03	0.00	0.00	0.02	0.05	0.07	0.05
NiO	0.00	0.04	0.06	0.13	0.02	0.24	0.20	0.00	0.02	0.00	0.01									0.00
V2O3	0.00	0.00	0.05	0.00	0.00	0.00	0.00	0.06	0.02	0.01	0.00									0.00
BaO	0.03	0.00	0.00	0.00	0.01	0.08	0.00	0.00	0.03	0.00	0.00									0.00
F	4.67	4.73	3.89	3.85	3.11	2.65	4.99	3.15	5.60	5.51	3.73	3.78	3.34	3.90	4.09	4.37	4.98	4.53	3.84	3.58
Cl	0.04	0.08	0.08	0.06	0.01	0.01	0.07	0.07	0.12	0.10	0.09									0.08
Total	100.32	99.69	99.87	100.24	98.94	99.57	100.39	98.93	99.23	98.76	97.38									100.41

Tabela 4A. (Cont.). Resultados analíticos de microssonda em apatita.

Rock Type	Mag	Mag	Mag	Mag	Mag	Mag	Mag	Mag	Mag	Mag	Mag	Mag	Mag	Mag	Mag	Mag	Mag	Mag	Mag	Mag	Mag
Sample	MFO10	MFO10	MFO10	MFO10	MFO10	MFO10	MFO10	MFO10	MFO10	MFO10	MFO13	MFO13	MFO13	MFO13	MFO13	MFO13	MFO13	MFO13	MFO13	MFO14	MFO09
Analysis (wt%)	C1_Ap2	C1_Ap3	C2_Ap2	C3_Ap1	C3_Ap2	C3_Ap3	C3_Ap4	C3_Ap5	C4_Ap1	C4_Ap2	C1_Ap1	C1_Ap2	C1_Ap3	C1_Ap5	C1_Ap6	C1_Ap7	C1_Ap8	C1_Ap9	C1_Ap10	C1_Ap11	C2_Ap1
SiO2	0.00	0.03	0.05	0.08	0.03	0.04	0.06	0.01	0.03	0.07	0.06	0.05	0.05	0.05	0.08	0.04	0.07	0.05	0.03	0.05	0.05
TiO2	0.05	0.12	0.01	0.00	0.03	0.05	0.00	0.00	0.15	0.00	0.14	0.07	0.16	0.00	0.00	0.00	0.02	0.10	0.00	0.08	0.01
Al2O3	0.00	0.00	0.00	0.02	0.00	0.01	0.00	0.00	0.00	0.01	0.02	0.01	0.00	0.00	0.01	0.00	0.00	0.00	0.00	0.03	0.02
Cr2O3	0.06	0.00	0.10	0.10	0.00	0.01	0.00	0.06	0.03	0.01	0.00	0.00	0.14	0.00	0.04	0.00	0.01	0.04	0.07	0.00	0.01
FeO	0.23	0.37	0.29	0.21	0.08	0.21	0.22	0.17	0.18	0.28	0.15	0.18	0.15	0.07	0.13	0.09	0.06	0.10	0.21	0.10	0.18
MnO	0.00	0.10	0.00	0.00	0.06	0.00	0.00	0.00	0.07	0.00	0.00	0.00	0.01	0.05	0.03	0.02	0.02	0.02	0.00	0.04	0.06
MgO	0.01	0.00	0.02	0.05	0.01	0.00	0.02	0.01	0.04	0.03	0.02	0.04	0.00	0.02	0.03	0.04	0.04	0.00	0.00	0.01	0.04
P2O5	43.06	42.51	44.13	44.42	43.34	43.24	43.10	42.34	42.01	43.16	42.78	43.73	42.84	42.70	43.14	44.37	42.96	42.61	42.07	43.49	42.67
CaO	55.08	54.31	55.29	55.74	56.20	55.80	55.77	55.44	54.63	55.32	55.88	55.88	55.53	55.55	56.17	56.25	55.24	55.51	55.90	56.32	53.98
Na2O	0.05	0.01	0.01	0.06	0.03	0.01	0.02	0.08	0.04	0.01	0.01	0.00	0.01	0.01	0.03	0.04	0.03	0.00	0.03	0.04	0.04
K2O	0.01	0.01	0.00	0.02	0.00	0.00	0.00	0.02	0.00	0.00	0.01	0.00	0.03	0.00	0.00	0.00	0.00	0.02	0.00	0.02	0.02
SrO	0.00	0.00	0.15	0.10	0.04	0.06	0.00	0.04	0.08	0.00	0.06	0.00	0.10	0.09	0.15	0.00	0.04	0.06	0.01	0.01	0.00
NiO	0.02	0.00	0.04	0.13	0.02	0.06	0.09	0.06	0.00	0.08	0.00	0.09	0.03	0.02	0.00	0.05	0.04	0.03	0.02	0.00	0.08
V2O3	0.00	0.03	0.00	0.01	0.00	0.04	0.00	0.00	0.00	0.01	0.03	0.00	0.00	0.00	0.00	0.00	0.02	0.06	0.00	0.02	0.01
BaO	0.00	0.07	0.09	0.00	0.00	0.02	0.06	0.00	0.02	0.00	0.00	0.09	0.08	0.00	0.11	0.02	0.00	0.04	0.02	0.04	0.06
F	5.19	5.33	3.64	2.35	2.41	5.79	3.57	5.37	5.25	3.49	3.50	3.06	4.46	4.89	3.08	2.20	2.96	3.86	4.33	2.36	2.86
Cl	0.19	0.15	0.23	0.12	0.12	0.14	0.17	0.24	0.16	0.16	0.18	0.12	0.13	0.16	0.12	0.14	0.15	0.14	0.19	0.09	0.10
Total	101.73	100.76	102.45	102.37	101.32	103.01	101.53	101.53	100.44	101.13	101.32	102.00	101.81	101.51	101.78	102.31	100.37	100.98	101.02	101.67	98.95

Rock Type	Mag	Mag	Mag	Mag	Mag	Mag	Mag	Mag	Mag	Mag	Mag	Mag	Mag	Mag	Mag	Mag	Mag	Mag	Mag	Mag	Mag
Sample	MFO09	MFO09	MFO09	MFO09	MFO09	MFO09	MFO09	MFO09	MFO09	MFO09	MFO09	MFO09	MFO09	MFO09	MFO09	MFO09	MFO09	MFO09	MFO28	MFO28	MFO28
Analysis (wt%)	C2_Ap2	C2_Ap3	C4_Ap1	C4_Ap2	C4_Ap3	C4_Ap4	C4_Ap5	C4_Ap6	C1_Ap1	C1_Ap2	C1_Ap3	C1_Ap4	C1_Ap5	C2_Ap1	C2_Ap2	C2_Ap3	C2_Ap4	C3_Ap1	C2_Ap1	C2_Ap2	C2_Ap3
SiO2	0.04	0.04	0.29	0.05	0.04	0.06	0.06	0.05	0.04	0.05	0.03	0.03	0.08	0.03	0.05	0.05	0.02	0.01	0.03	0.05	0.02
TiO2	0.00	0.01	0.00	0.00	0.13	0.00	0.06	0.07	0.00	0.00	0.00	0.00	0.00	0.03	0.00	0.00	0.00	0.00	0.04	0.00	0.04
Al2O3	0.00	0.00	0.08	0.02	0.01	0.01	0.03	0.00	0.00	0.01	0.02	0.02	0.01	0.00	0.01	0.02	0.00	0.01	0.02	0.00	0.00
Cr2O3	0.00	0.00	0.00	0.00	0.00	0.09	0.00	0.04											0.00	0.00	0.00
FeO	0.27	0.27	0.29	0.11	0.08	0.16	0.20	0.15	0.16	0.16	0.18	0.08	0.25	0.05	0.18	0.16	0.08	0.07	0.17	0.20	0.07
MnO	0.00	0.03	0.12	0.00	0.07	0.06	0.04	0.03	0.02	0.05	0.00	0.00	0.05	0.02	0.01	0.02	0.07	0.00	0.00	0.09	0.00
MgO	0.03	0.06	0.12	0.00	0.00	0.00	0.02	0.00											0.01	0.04	0.03
P2O5	42.25	42.59	42.41	42.88	42.75	43.48	43.73	42.76	43.25	43.10	42.28	42.82	42.67	42.37	41.50	43.93	42.72	42.16	42.56	42.23	42.37
CaO	54.00	54.34	53.40	54.34	53.05	53.79	53.68	53.94	55.75	55.63	57.24	54.06	56.40	52.35	53.33	55.87	54.57	53.38	53.64	53.86	54.01
Na2O	0.01	0.01	0.01	0.00	0.03	0.00	0.01	0.07	0.00	0.00	0.02	0.00	0.00	0.00	0.00	0.00	0.00	0.00	0.02	0.00	0.02
K2O	0.01	0.00	0.01	0.00	0.00	0.00	0.01	0.00	0.00	0.00	0.00	0.00	0.00	0.00	0.00	0.00	0.01	0.00	0.00	0.00	0.03
SrO	0.07	0.00	0.01	0.09	0.11	0.03	0.00	0.00	0.07	0.08	0.03	0.00	0.06	0.02	0.04	0.07	0.02	0.00	0.00	0.00	0.02
NiO	0.23	0.04	0.02	0.03	0.09	0.05	0.02	0.02											0.03	0.04	0.00
V2O3	0.03	0.03	0.00	0.00	0.00	0.00	0.01	0.00											0.01	0.02	0.00
BaO	0.00	0.00	0.10	0.17	0.08	0.05	0.14	0.01											0.00	0.00	0.00
F	5.08	3.14	3.21	4.11	5.20	2.62	4.05	3.60	3.75	3.95	1.97	3.91	4.30	3.59	4.32	3.60	4.13	4.04	4.20	6.47	3.83
Cl	0.12	0.10	0.10	0.11	0.11	0.17	0.12	0.14											0.73	0.48	0.69
Total	99.96	99.32	98.80	100.16	99.54	99.42	100.42	99.32											99.52	100.65	99.36

Tabela 5A. Resultados analíticos de microssonda em biotita.

Rock Type	Bt-Chl	Bt-Chl	Bt-Chl	Bt-Chl	Bt-Chl	Bt-Chl	Bt-Chl	Bt-Chl	Bt-Chl	Bt-Chl	Bt-Chl	Bt-Chl	Bt-Chl	Bt-Chl	Bt-Chl	Bt-Chl	Bt-Chl	Bt-Chl	Bt-Chl	Bt-Chl
Sample	MFO05	MFO05	MFO12	MFO12	MFO17	MFO17	MFO16	MFO16	MFO16	MFO11	MFO11	MFO11	MFO18	MFO18	MFO18	MFO21	MFO21	MFO21	MFO03	MFO03
Analysis (wt%)	C2 Bt 3	C3 Bt 1	C1 Bt 5	C3 Bt 1	C4 Bt 1	C4 Bt 2	C1 Bt 3	C1 Bt 4	C1 Bt 5	C2 Bt 1	C2 Bt 2	C2 Bt 4	C2 Bt 4	C2 Bt 5	C3 Bt 1	C2 Bt 4	C2 Bt 5	C3 Bt 2	C2 Bt 3	C2 Bt 4
SiO2	36.82	37.05	38.21	38.64	39.48	37.86	38.55	39.50	39.26	38.39	38.46	37.95	36.04	36.57	35.61	37.07	37.17	36.81	36.18	36.98
TiO2	1.22	0.89	0.84	1.06	0.66	0.97	1.40	1.09	1.31	0.76	1.33	0.80	1.89	1.95	1.73	1.34	1.58	1.78	0.92	1.29
Al2O3	14.90	14.93	12.87	13.14	13.66	12.87	13.34	13.14	12.62	13.09	12.42	12.11	16.09	16.61	15.80	16.59	16.57	16.80	14.11	14.25
FeO	19.49	19.58	17.47	17.11	16.68	16.72	19.43	17.40	17.99	16.43	18.23	18.62	18.16	18.11	17.79	16.39	16.67	15.97	20.59	19.05
MnO	0.10	0.09	0.05	0.05	0.00	0.00	0.18	0.12	0.11	0.00	0.00	0.03	0.05	0.00	0.04	0.06	0.00	0.03	0.00	0.01
MgO	12.54	12.67	16.02	15.39	15.72	15.15	14.40	15.15	14.56	15.77	15.23	15.28	12.12	12.10	12.55	13.52	13.31	13.23	12.56	13.01
CaO	0.04	0.01	0.05	0.04	0.02	0.01	0.09	0.02	0.06	0.02	0.00	0.11	0.01	0.00	0.02	0.01	0.02	0.02	0.04	0.01
Na2O	0.05	0.03	0.11	0.03	0.11	0.09	0.08	0.06	0.09	0.01	0.06	0.03	0.09	0.17	0.11	0.16	0.18	0.12	0.03	0.03
K2O	9.43	9.42	8.34	8.93	9.32	9.14	8.52	8.89	8.39	9.16	8.80	8.51	9.01	9.50	8.87	9.15	9.54	9.47	8.48	9.68
BaO	0.17	0.19	0.04	0.11	0.04	0.03	0.16	0.19	0.07	0.00	0.13	0.06	0.12	0.12	0.15	0.15	0.23	0.11	0.23	0.18
Cr2O3	0.06	0.05	0.08	0.00	0.00	0.08	0.04	0.00	0.01	0.00	0.07	0.04	0.00	0.02	0.02	0.03	0.08	0.09	0.00	0.00
V2O3	0.08	0.02	0.00	0.02	0.06	0.06	0.09	0.07	0.03	0.01	0.10	0.04	0.14	0.13	0.07	0.09	0.04	0.05	0.10	0.04
NiO	0.30	0.40	0.32	0.34	0.33	0.36	0.26	0.22	0.25	0.26	0.25	0.32	0.00	0.01	0.06	0.05	0.04	0.07	0.31	0.32
SrO	0.07	0.04	0.08	0.00	0.00	0.04	0.08	0.00	0.00	0.04	0.01	0.11	0.03	0.09	0.04	0.00	0.06	0.00	0.04	0.09
P2O5	0.01	0.00	0.03	0.01	0.04	0.00	0.00	0.00	0.04	0.00	0.00	0.05	0.02	0.02	0.00	0.00	0.00	0.01	0.00	0.00
F	0.79	0.64	0.77	0.80	1.00	0.77	0.67	0.55	0.48	0.42	0.83	0.88	0.00	0.21	0.11	0.45	0.31	0.29	0.96	0.82
Cl	0.18	0.24	0.25	0.16	0.24	0.25	0.23	0.25	0.26	0.22	0.25	0.37	0.33	0.48	0.36	0.23	0.34	0.30	0.25	0.14
Total	95.88	95.91	95.12	95.46	96.89	94.02	97.19	96.35	95.25	94.34	95.77	94.83	94.03	95.90	93.21	95.03	95.91	94.94	94.33	95.52
Number of cations per 11 oxygens																				
Si	2.82	2.84	2.90	2.92	2.94	2.91	2.89	2.95	2.97	2.92	2.92	2.92	2.78	2.77	2.77	2.80	2.79	2.78	2.83	2.84
Al (IV)	1.18	1.16	1.10	1.08	1.06	1.09	1.11	1.05	1.03	1.08	1.08	1.08	1.22	1.23	1.23	1.20	1.21	1.22	1.17	1.16
Al (VI)	0.17	0.18	0.06	0.09	0.13	0.08	0.07	0.11	0.09	0.10	0.03	0.02	0.24	0.26	0.22	0.28	0.26	0.28	0.13	0.14
Ti	0.07	0.05	0.05	0.06	0.04	0.06	0.08	0.06	0.07	0.04	0.08	0.05	0.11	0.11	0.10	0.08	0.09	0.10	0.05	0.07
Cr	0.00	0.00	0.00	0.00	0.00	0.01	0.00	0.00	0.00	0.00	0.00	0.00	0.00	0.00	0.00	0.00	0.00	0.01	0.00	0.00
Fe^{3+}	0.05	0.04	0.20	0.11	0.02	0.08	0.18	0.06	0.10	0.08	0.17	0.19	0.07	0.01	0.10	0.00	0.00	0.00	0.16	0.05
Fe^{2+}	1.20	1.21	0.91	0.97	1.02	1.00	1.04	1.02	1.04	0.97	0.98	1.01	1.10	1.14	1.06	1.03	1.05	1.01	1.19	1.18
Mn	0.01	0.01	0.00	0.00	0.00	0.00	0.01	0.01	0.01	0.00	0.00	0.00	0.00	0.00	0.00	0.00	0.00	0.00	0.00	0.00
Mg	1.43	1.45	1.81	1.73	1.74	1.74	1.61	1.69	1.64	1.79	1.72	1.75	1.39	1.37	1.46	1.52	1.49	1.49	1.47	1.49
Ca	0.00	0.00	0.00	0.00	0.00	0.00	0.01	0.00	0.00	0.00	0.00	0.01	0.00	0.00	0.00	0.00	0.00	0.00	0.00	0.00
Na	0.01	0.00	0.02	0.00	0.02	0.01	0.01	0.01	0.01	0.00	0.01	0.00	0.01	0.02	0.02	0.02	0.03	0.02	0.01	0.00
K	0.92	0.92	0.81	0.86	0.88	0.90	0.82	0.85	0.81	0.89	0.85	0.84	0.89	0.92	0.88	0.88	0.91	0.91	0.85	0.95
Ba	0.01	0.01	0.00	0.00	0.00	0.00	0.00	0.01	0.00	0.00	0.00	0.00	0.00	0.00	0.00	0.00	0.01	0.00	0.01	0.01
V	0.00	0.00	0.00	0.00	0.00	0.00	0.01	0.00	0.00	0.00	0.01	0.00	0.01	0.01	0.00	0.01	0.00	0.00	0.01	0.00
Ni	0.02	0.02	0.02	0.02	0.02	0.02	0.02	0.01	0.02	0.02	0.02	0.02	0.00	0.00	0.00	0.00	0.00	0.00	0.02	0.02
Zr	0.00	0.00	0.00	0.00	0.00	0.00	0.00	0.00	0.00	0.00	0.00	0.00	0.00	0.00	0.00	0.00	0.00	0.00	0.00	0.00
Sc	0.00	0.00	0.00	0.00	0.00	0.00	0.00	0.00	0.00	0.00	0.00	0.00	0.00	0.00	0.00	0.00	0.00	0.00	0.00	0.00
Co	0.00	0.00	0.00	0.00	0.00	0.00	0.00	0.00	0.00	0.00	0.00	0.00	0.00	0.00	0.00	0.00	0.00	0.00	0.00	0.00
Rb	0.00	0.00	0.00	0.00	0.00	0.00	0.00	0.00	0.00	0.00	0.00	0.00	0.00	0.00	0.00	0.00	0.00	0.00	0.00	0.00
Cs	0.00	0.00	0.00	0.00	0.00	0.00	0.00	0.00	0.00	0.00	0.00	0.00	0.00	0.00	0.00	0.00	0.00	0.00	0.00	0.00
Cations	7.89	7.90	7.88	7.86	7.88	7.90	7.85	7.83	7.80	7.89	7.88	7.90	7.83	7.84	7.85	7.83	7.85	7.83	7.89	7.91
F	0.19	0.15	0.19	0.19	0.24	0.19	0.16	0.13	0.11	0.10	0.20	0.21	0.00	0.05	0.03	0.11	0.07	0.07	0.24	0.20
Cl	0.02	0.03	0.03	0.02	0.03	0.03	0.03	0.03	0.03	0.03	0.03	0.05	0.04	0.06	0.05	0.03	0.04	0.04	0.03	0.02
OH	1.79	1.81	1.78	1.79	1.73	1.78	1.81	1.84	1.85	1.87	1.77	1.74	1.96	1.89	1.93	1.86	1.88	1.89	1.73	1.78

Tabela 5A. (Cont). Resultados analíticos de microssonda em biotita.

Rock Type	Bt-Chl	Bt-Chl	Bt-Chl	Bt-Chl	Bt-Chl	Bt-Chl	Bt-Chl	Bt-Chl	Bt-Chl	Bt-Chl	Bt-Chl	Mag	Mag	Mag	Mag	Mag	Mag	Mag	Mag	Mag	Mag
Sample	MFO03	MFO27	MFO31	MFO31	MFO23	MFO23	MFO23	MFO30	MFO30	MFO30	MFO30	MFO09	MFO10	MFO10	MFO10	MFO13	MFO13	MFO13	MFO14	MFO14	MFO14
Analysis (wt%)	C2 Bt 5	C3 Bt 2	C3 Bt 1	C3 Bt 3	C3 Bt 1.1	C3 Bt 1.2	C3 Bt 1.3	C2 Bt 1	C2 Bt 2	C2 Bt 3	C2 Bt 4	C4 Bt 3	C4 Bt 2	C4 Bt 3	C4 Bt 4	C1 Bt 1	C1 Bt 2	C1 Bt 3	C3 Bt 4	C4 Bt 1	C4 Bt 2
SiO2	37.48	38.10	36.57	37.10	38.06	37.91	37.72	38.06	35.98	36.38	37.37	38.75	35.97	36.44	37.11	38.74	38.78	38.33	38.02	37.79	38.85
TiO2	1.09	1.60	1.89	1.96	1.31	1.39	1.14	1.66	1.20	1.40	1.33	1.10	1.28	1.39	0.91	0.86	0.98	0.83	1.15	1.14	1.24
Al2O3	13.62	14.34	15.33	15.42	14.84	14.11	14.64	14.99	15.62	14.60	15.43	13.08	14.14	13.68	12.66	12.74	13.09	13.10	13.48	13.90	13.24
FeO	19.65	15.33	16.50	16.34	14.04	13.84	14.25	14.16	14.78	14.82	13.61	16.97	22.43	20.38	21.31	16.20	15.87	16.35	19.13	17.63	17.51
MnO	0.00	0.05	0.07	0.04	0.09	0.05	0.09	0.04	0.04	0.04	0.03	0.04	0.12	0.01	0.12	0.06	0.06	0.01	0.11	0.03	0.00
MgO	13.29	16.22	14.14	13.85	16.48	16.47	16.07	15.79	16.71	15.63	16.20	16.09	13.24	13.48	13.16	15.73	15.77	15.64	14.34	14.25	15.29
CaO	0.00	0.00	0.00	0.05	0.00	0.00	0.00	0.04	0.01	0.08	0.06	0.00	0.01	0.07	0.00	0.04	0.04	0.08	0.00	0.02	0.00
Na2O	0.00	0.15	0.16	0.13	0.06	0.17	0.34	0.13	0.19	0.15	0.13	0.09	0.04	0.06	0.08	0.05	0.10	0.05	0.06	0.01	0.05
K2O	9.16	9.41	8.68	9.63	9.40	9.24	9.53	9.32	7.95	9.09	9.08	9.04	7.80	8.90	8.46	8.89	8.90	9.12	9.21	9.33	9.36
BaO	0.08	0.00	0.23	0.31	0.05	0.07	0.00	0.09	0.10	0.14	0.14	0.12	0.04	0.23	0.13	0.00	0.00	0.06	0.23	0.16	0.17
Cr2O3	0.03	0.00	0.00	0.07	0.00	0.05	0.01	0.00	0.00	0.00	0.00	0.00	0.07	0.00	0.06	0.07	0.00	0.00	0.00	0.00	0.00
V2O3	0.01	0.05	0.00	0.07	0.04	0.04	0.00	0.05	0.09	0.06	0.02	0.08	0.04	0.08	0.05	0.02	0.01	0.06	0.10	0.05	0.05
NiO	0.40	0.01	0.39	0.34	0.20	0.16	0.24	0.17	0.24	0.19	0.21	0.28	0.33	0.25	0.23	0.24	0.28	0.21	0.26	0.26	0.36
SrO	0.02	0.09	0.14	0.05	0.11	0.00	0.00	0.01	0.01	0.00	0.00	0.00	0.03	0.03	0.00	0.01	0.07	0.05	0.02	0.00	0.01
P2O5	0.00	0.00	0.00	0.00	0.00	0.02	0.00	0.00	0.00	0.02	0.00	0.00	0.00	0.00	0.05	0.07	0.01	0.00	0.00	0.00	0.00
F	0.95	0.81	0.33	0.27	1.15	1.17	1.11	0.31	0.39	0.37	0.27	1.30	0.90	0.97	1.22	0.91	0.89	1.18	0.64	0.64	0.83
Cl	0.35	0.49	0.29	0.29	0.09	0.16	0.22	0.29	0.25	0.32	0.12	0.18	0.17	0.22	0.63	0.21	0.15	0.13	0.39	0.12	0.26
Total	95.65	96.19	94.50	95.76	95.41	94.30	94.86	94.90	93.35	93.06	93.86	96.53	96.18	95.73	95.51	94.39	94.58	94.66	96.77	95.03	96.78
Number of cations per 11 oxygens																					
Si	2.88	2.85	2.79	2.80	2.85	2.87	2.85	2.85	2.74	2.80	2.82	2.91	2.77	2.81	2.89	2.95	2.94	2.92	2.88	2.88	2.91
Al (IV)	1.12	1.15	1.21	1.20	1.15	1.13	1.15	1.15	1.26	1.20	1.18	1.09	1.23	1.19	1.11	1.05	1.06	1.08	1.12	1.12	1.09
Al (VI)	0.11	0.11	0.17	0.17	0.16	0.13	0.15	0.17	0.15	0.13	0.19	0.06	0.05	0.06	0.05	0.10	0.11	0.10	0.08	0.13	0.08
Ti	0.06	0.09	0.11	0.11	0.07	0.08	0.06	0.09	0.07	0.08	0.08	0.06	0.07	0.08	0.05	0.05	0.06	0.05	0.07	0.07	0.07
Cr	0.00	0.00	0.00	0.00	0.00	0.00	0.00	0.00	0.00	0.00	0.00	0.00	0.00	0.00	0.00	0.00	0.00	0.00	0.00	0.00	0.00
Fe^{3+}	0.10	0.12	0.16	0.04	0.08	0.08	0.03	0.05	0.30	0.12	0.08	0.14	0.40	0.21	0.20	0.07	0.07	0.06	0.13	0.06	0.10
Fe^{2+}	1.16	0.84	0.90	0.99	0.80	0.80	0.87	0.83	0.65	0.83	0.78	0.92	1.05	1.10	1.19	0.96	0.94	0.98	1.08	1.07	1.00
Mn	0.00	0.00	0.00	0.00	0.01	0.00	0.01	0.00	0.00	0.00	0.00	0.00	0.01	0.00	0.01	0.00	0.00	0.00	0.01	0.00	0.00
Mg	1.52	1.81	1.61	1.56	1.84	1.86	1.81	1.76	1.90	1.80	1.82	1.80	1.52	1.55	1.53	1.79	1.78	1.78	1.62	1.62	1.71
Ca	0.00	0.00	0.00	0.00	0.00	0.00	0.00	0.00	0.00	0.01	0.00	0.00	0.00	0.01	0.00	0.00	0.00	0.01	0.00	0.00	0.00
Na	0.00	0.02	0.02	0.02	0.01	0.02	0.05	0.02	0.03	0.02	0.02	0.01	0.01	0.01	0.01	0.01	0.01	0.01	0.01	0.00	0.01
K	0.90	0.90	0.84	0.93	0.90	0.89	0.92	0.89	0.77	0.89	0.87	0.86	0.77	0.88	0.84	0.86	0.86	0.89	0.89	0.91	0.89
Ba	0.00	0.00	0.01	0.01	0.00	0.00	0.00	0.00	0.00	0.00	0.00	0.00	0.00	0.01	0.00	0.00	0.00	0.00	0.01	0.00	0.00
V	0.00	0.00	0.00	0.00	0.00	0.00	0.00	0.00	0.01	0.00	0.00	0.00	0.00	0.00	0.00	0.00	0.00	0.00	0.01	0.00	0.00
Ni	0.02	0.00	0.02	0.02	0.01	0.01	0.01	0.01	0.01	0.01	0.01	0.02	0.02	0.02	0.01	0.01	0.02	0.01	0.02	0.02	0.02
Zr	0.00	0.00	0.00	0.00	0.00	0.00	0.00	0.00	0.00	0.00	0.00	0.00	0.00	0.00	0.00	0.00	0.00	0.00	0.00	0.00	0.00
Sc	0.00	0.00	0.00	0.00	0.00	0.00	0.00	0.00	0.00	0.00	0.00	0.00	0.00	0.00	0.00	0.00	0.00	0.00	0.00	0.00	0.00
Co	0.00	0.00	0.00	0.00	0.00	0.00	0.00	0.00	0.00	0.00	0.00	0.00	0.00	0.00	0.00	0.00	0.00	0.00	0.00	0.00	0.00
Rb	0.00	0.00	0.00	0.00	0.00	0.00	0.00	0.00	0.00	0.00	0.00	0.00	0.00	0.00	0.00	0.00	0.00	0.00	0.00	0.00	0.00
Cs	0.00	0.00	0.00	0.00	0.00	0.00	0.00	0.00	0.00	0.00	0.00	0.00	0.00	0.00	0.00	0.00	0.00	0.00	0.00	0.00	0.00
Cations	7.89	7.89	7.84	7.87	7.88	7.88	7.92	7.85	7.88	7.91	7.86	7.89	7.90	7.92	7.90	7.86	7.86	7.89	7.90	7.88	7.88
F	0.23	0.19	0.08	0.06	0.27	0.28	0.26	0.07	0.09	0.09	0.07	0.31	0.22	0.24	0.30	0.22	0.21	0.28	0.15	0.15	0.20
Cl	0.04	0.06	0.04	0.04	0.01	0.02	0.03	0.04	0.03	0.04	0.01	0.02	0.02	0.03	0.08	0.03	0.02	0.02	0.05	0.02	0.03
OH	1.72	1.75	1.88	1.90	1.72	1.70	1.71	1.89	1.87	1.87	1.92	1.67	1.76	1.73	1.62	1.75	1.77	1.70	1.80	1.83	1.77

Tabela 6A. Resultados analíticos de microssonda em clorita.

Rock Type	Amp	Amp	Amp	Amp	Bt-Chl	Bt-Chl	Bt-Chl	Bt-Chl	Bt-Chl	Bt-Chl	Bt-Chl	Bt-Chl	Bt-Chl	Bt-Chl	Bt-Chl	Bt-Chl	Bt-Chl	Bt-Chl	Bt-Chl	Bt-Chl
Sample	MFO15	MFO15	MFO15	MFO15	MFO03	MFO04	MFO04	MFO04	MFO04	MFO04	MFO04	MFO04	MFO04	MFO04	MFO04	MFO04	MFO04	MFO04	MFO04	MFO04
Analysis (wt%)	C1_chl1	C1_chl2	C1_chl3	C1_chl4	C2_chl9	C1_chl1	C1_chl2	C1_chl3	C1_chl4	C1_chl5	C1_chl6	C1_chl7	C1_chl9	C1_chl10	C2_chl1	C2_chl2	C2_chl3	C2_chl4	C2_chl5	C2_chl6	C2_chl7
SiO2	26.97	27.66	27.49	26.80	26.14	25.95	25.96	26.05	27.04	26.09	26.18	26.14	26.66	26.40	26.00	26.81	27.63	26.89	27.33	28.01	26.41
TiO2	0.00	0.00	0.00	0.16	0.10	0.01	0.00	0.02	0.00	0.14	0.20	0.21	0.08	0.00	0.18	0.05	0.14	0.00	0.08	0.24	0.05
Al2O3	19.36	19.11	18.92	19.73	19.36	18.51	18.05	17.90	17.92	18.37	16.39	18.09	17.67	18.13	17.86	15.79	16.08	15.73	15.95	15.42	17.17
Cr2O3	0.02	0.05	0.03	0.05	0.00	0.03	0.03	0.02	0.06	0.00	0.01	0.00	0.01	0.04	0.00	0.03	0.03	0.00	0.02	0.00	0.00
FeO	20.25	20.57	19.54	20.22	22.07	22.68	22.11	23.11	22.56	22.07	20.92	21.47	21.95	21.25	22.25	25.91	26.11	26.38	26.25	25.83	22.94
MnO	0.01	0.10	0.05	0.11	0.09	0.00	0.10	0.01	0.12	0.09	0.13	0.16	0.03	0.06	0.07	0.12	0.06	0.14	0.11	0.12	0.09
MgO	20.24	19.72	20.40	20.20	18.15	16.55	16.08	15.79	16.69	17.17	16.61	17.06	17.47	17.67	16.99	13.54	14.01	13.50	14.01	14.22	16.32
BaO	0.02	0.00	0.00	0.00	0.06	0.00	0.08	0.00	0.00	0.00	0.00	0.02	0.07	0.00	0.00	0.00	0.00	0.00	0.06	0.03	0.00
CaO	0.02	0.00	0.02	0.00	0.03	0.03	0.08	0.07	0.07	0.02	0.00	0.01	0.03	0.00	0.02	0.05	0.03	0.03	0.05	0.03	0.04
Na2O	0.02	0.07	0.00	0.00	0.03	0.03	0.02	0.00	0.03	0.03	0.00	0.01	0.00	0.04	0.00	0.01	0.00	0.00	0.00	0.00	0.02
K2O	0.06	0.06	0.03	0.02	0.06	0.03	0.05	0.16	0.06	0.06	0.07	0.04	0.03	0.00	0.05	0.01	0.05	0.04	0.01	0.24	0.10
V2O3	0.01	0.06	0.00	0.03	0.03	0.00	0.02	0.05	0.03	0.08	0.03	0.00	0.04	0.05	0.03	0.07	0.01	0.03	0.01	0.04	0.06
NiO	0.39	0.29	0.33	0.24	0.47	0.45	0.44	0.48	0.48	0.51	0.43	0.45	0.49	0.40	0.47	1.01	1.01	1.01	0.78	0.86	0.58
F	0.00	0.00	0.05	0.00	0.00	0.03	0.01	0.03	0.09	0.08	0.09	0.07	0.04	0.00	0.00	0.00	0.04	0.15	0.11	0.16	0.09
Cl	0.05	0.03	0.01	0.04	0.01	0.04	0.05	0.03	0.02	0.04	0.02	0.04	0.06	0.04	0.03	0.01	0.01	0.03	0.01	0.03	0.05
Total	87.43	87.72	86.86	87.60	86.60	84.35	83.07	83.72	85.17	84.74	81.08	83.77	84.62	84.07	83.93	83.42	85.21	83.93	84.79	85.23	83.93
Number of cations per 28 oxygens																					
Si	5.57	5.68	5.68	5.51	5.51	5.65	5.73	5.73	5.82	5.64	5.90	5.70	5.76	5.71	5.68	6.03	6.07	6.05	6.05	6.17	5.81
Al (IV)	2.43	2.32	2.32	2.49	2.49	2.35	2.27	2.27	2.18	2.36	2.10	2.30	2.24	2.29	2.32	1.97	1.93	1.95	1.95	1.83	2.19
Al (VI)	2.27	2.31	2.29	2.30	2.32	2.39	2.42	2.38	2.37	2.33	2.25	2.35	2.26	2.33	2.27	2.21	2.23	2.21	2.21	2.17	2.26
Ti	0.00	0.00	0.00	0.02	0.02	0.00	0.00	0.00	0.00	0.02	0.03	0.03	0.01	0.00	0.03	0.01	0.02	0.00	0.01	0.04	0.01
Cr	0.00	0.01	0.00	0.01	0.00	0.01	0.01	0.00	0.01	0.00	0.00	0.00	0.00	0.01	0.00	0.01	0.01	0.00	0.00	0.00	0.00
Fe	3.49	3.54	3.38	3.48	3.89	4.13	4.08	4.25	4.06	3.99	3.94	3.92	3.97	3.84	4.06	4.87	4.79	4.96	4.86	4.75	4.22
Mn	0.00	0.02	0.01	0.02	0.02	0.00	0.02	0.00	0.02	0.02	0.02	0.03	0.01	0.01	0.01	0.02	0.01	0.03	0.02	0.02	0.02
Mg	6.23	6.04	6.29	6.20	5.71	5.37	5.29	5.18	5.36	5.54	5.58	5.55	5.63	5.70	5.53	4.54	4.59	4.52	4.62	4.67	5.35
Zn	0.00	0.00	0.00	0.00	0.00	0.00	0.00	0.00	0.00	0.00	0.00	0.00	0.00	0.00	0.00	0.00	0.00	0.00	0.00	0.00	0.00
Ca	0.00	0.00	0.00	0.00	0.01	0.01	0.02	0.02	0.02	0.00	0.00	0.00	0.01	0.00	0.00	0.01	0.01	0.01	0.01	0.01	0.01
Na	0.01	0.03	0.00	0.00	0.01	0.01	0.01	0.00	0.01	0.01	0.00	0.00	0.00	0.02	0.00	0.00	0.00	0.00	0.00	0.00	0.01
K	0.02	0.02	0.01	0.01	0.02	0.01	0.01	0.04	0.02	0.02	0.02	0.01	0.01	0.00	0.01	0.00	0.01	0.01	0.00	0.07	0.03
Ba	0.00	0.00	0.00	0.00	0.00	0.00	0.01	0.00	0.00	0.00	0.00	0.00	0.01	0.00	0.00	0.00	0.00	0.00	0.01	0.00	0.00
V	0.00	0.01	0.00	0.01	0.01	0.00	0.00	0.01	0.01	0.01	0.00	0.00	0.01	0.01	0.00	0.01	0.00	0.01	0.00	0.01	0.01
Ni	0.07	0.05	0.05	0.04	0.08	0.08	0.08	0.08	0.08	0.09	0.08	0.08	0.09	0.07	0.08	0.18	0.18	0.18	0.14	0.15	0.10
F	0.00	0.00	0.03	0.00	0.00	0.02	0.00	0.02	0.06	0.05	0.06	0.05	0.02	0.00	0.00	0.00	0.03	0.11	0.07	0.11	0.06
Cl	0.02	0.01	0.00	0.02	0.00	0.02	0.02	0.01	0.01	0.01	0.01	0.01	0.02	0.01	0.01	0.00	0.00	0.01	0.00	0.01	0.02
OH	15.98	15.99	15.97	15.98	16.00	15.96	15.98	15.97	15.93	15.93	15.93	15.94	15.95	15.99	15.99	16.00	15.97	15.88	15.92	15.88	15.92
Cations	20.12	20.03	20.07	20.09	20.08	20.04	19.96	20.01	20.01	20.10	20.01	20.04	20.04	20.00	20.02	19.88	19.88	20.05	19.97	20.01	20.09

Tabela 6A. (Cont). Resultados analíticos de microssonda em clorita.

Rock Type	Bt-Chl	Bt-Chl	Bt-Chl	Mag	Mag	Mag	Mag	Bt-Chl	Bt-Chl	Bt-Chl	Bt-Chl	Bt-Chl	Bt-Chl	Bt-Chl	Bt-Chl	Bt-Chl	Bt-Chl	Bt-Chl	Bt-Chl	Bt-Chl	Bt-Chl
Sample	MFO04	MFO04	MFO04	MFO09	MFO09	MFO09	MFO09	MFO05	MFO05	MFO05	MFO05	MFO05	MFO05	MFO05	MFO05	MFO05	MFO05	MFO12	MFO12	MFO12	MFO12
Analysis (wt%)	C2 chl 8	C2 chl 9	C2 chl 10	C3 chl 1	C3 chl 2	C3 chl 3	C3 chl 4	C1 chl 1	C1 chl 2	C1 chl 3	C3 chl 1	C3 chl 2	C3 chl 3	C3 chl 4	C3 chl 5	C4 chl 3	C4 chl 5	C2 chl 1	C2 chl 2	C2 chl 3	C2 chl 4
SiO2	27.37	27.57	27.25	26.82	28.47	29.65	27.14	25.83	25.58	25.34	25.93	26.21	26.49	25.74	25.36	24.73	26.11	27.50	27.84	27.24	27.61
TiO2	0.22	0.21	0.13	0.00	0.06	0.09	0.11	0.07	0.03	0.00	0.28	0.12	0.10	0.00	0.20	0.07	0.16	0.00	0.07	0.00	0.12
Al2O3	15.35	15.65	15.17	19.36	18.32	18.21	18.43	19.69	20.42	20.73	19.91	19.06	18.71	20.51	20.85	19.29	20.95	18.84	18.77	19.21	18.74
Cr2O3	0.01	0.00	0.08	0.00	0.08	0.01	0.00	0.05	0.00	0.10	0.00	0.00	0.05	0.03	0.02	0.00	0.06	0.00	0.00	0.02	0.01
FeO	25.77	25.54	25.78	19.60	19.74	18.65	19.18	24.93	23.72	24.39	25.35	26.28	24.36	25.07	23.87	22.25	23.58	19.13	18.84	19.70	18.77
MnO	0.03	0.11	0.10	0.00	0.11	0.10	0.07	0.16	0.00	0.15	0.09	0.09	0.08	0.11	0.04	0.16	0.00	0.03	0.03	0.07	0.00
MgO	13.93	13.95	14.43	20.53	20.94	21.46	20.84	15.49	16.32	16.02	15.62	15.06	16.79	15.71	16.90	15.10	16.71	20.71	21.28	20.66	21.24
BaO	0.04	0.06	0.02	0.00	0.00	0.02	0.02	0.00	0.00	0.03	0.00	0.00	0.00	0.00	0.00	0.00	0.00	0.00	0.03	0.03	0.01
CaO	0.02	0.00	0.01	0.01	0.01	0.00	0.00	0.14	0.01	0.03	0.16	0.02	0.02	0.01	0.03	0.06	0.00	0.01	0.02	0.04	0.03
Na2O	0.03	0.03	0.02	0.03	0.00	0.00	0.00	0.00	0.01	0.04	0.05	0.00	0.03	0.02	0.01	0.02	0.00	0.04	0.02	0.02	0.05
K2O	0.07	0.12	0.04	0.00	0.00	0.00	0.00	0.14	0.04	0.02	0.09	0.09	0.02	0.15	0.05	0.08	0.05	0.13	0.04	0.02	0.05
V2O3	0.02	0.06	0.06	0.02	0.08	0.00	0.10	0.04	0.01	0.02	0.01	0.04	0.00	0.06	0.05	0.01	0.00	0.00	0.04	0.00	0.03
NiO	0.98	0.91	0.98	0.38	0.35	0.45	0.28	0.61	0.45	0.56	0.53	0.69	0.59	0.42	0.49	0.61	0.44	0.37	0.34	0.29	0.33
F	0.11	0.05	0.03	0.07	0.02	0.08	0.06	0.06	0.00	0.05	0.00	0.01	0.01	0.02	0.00	0.01	0.00	0.00	0.00	0.00	0.10
Cl	0.02	0.00	0.04	0.03	0.03	0.05	0.02	0.04	0.03	0.03	0.05	0.05	0.02	0.02	0.01	0.04	0.02	0.04	0.04	0.04	0.05
Total	83.97	84.26	84.13	86.84	88.20	88.77	86.25	87.24	86.62	87.50	88.07	87.71	87.26	87.87	87.89	82.43	88.08	86.79	87.35	87.35	87.14
Number of cations per 28 oxygens																					
Si	6.12	6.12	6.07	5.56	5.79	5.95	5.65	5.51	5.43	5.36	5.47	5.58	5.61	5.43	5.31	5.52	5.43	5.68	5.70	5.60	5.68
Al (IV)	1.88	1.88	1.93	2.44	2.21	2.05	2.35	2.49	2.57	2.64	2.53	2.42	2.39	2.57	2.69	2.48	2.57	2.32	2.30	2.40	2.32
Al (VI)	2.16	2.21	2.06	2.29	2.18	2.26	2.18	2.45	2.54	2.53	2.42	2.37	2.28	2.53	2.46	2.59	2.57	2.26	2.22	2.26	2.22
Ti	0.04	0.04	0.02	0.00	0.01	0.01	0.02	0.01	0.00	0.00	0.04	0.02	0.02	0.00	0.03	0.01	0.03	0.00	0.01	0.00	0.02
Cr	0.00	0.00	0.01	0.00	0.01	0.00	0.00	0.01	0.00	0.02	0.00	0.00	0.01	0.01	0.00	0.00	0.01	0.00	0.00	0.00	0.00
Fe	4.82	4.74	4.81	3.40	3.36	3.13	3.34	4.44	4.21	4.32	4.47	4.68	4.31	4.42	4.18	4.15	4.10	3.30	3.22	3.39	3.23
Mn	0.01	0.02	0.02	0.00	0.02	0.02	0.01	0.03	0.00	0.03	0.02	0.02	0.01	0.02	0.01	0.03	0.00	0.01	0.01	0.01	0.00
Mg	4.64	4.61	4.80	6.34	6.35	6.42	6.47	4.92	5.17	5.05	4.91	4.78	5.30	4.94	5.28	5.02	5.18	6.38	6.49	6.34	6.51
Zn	0.00	0.00	0.00	0.00	0.00	0.00	0.00	0.00	0.00	0.00	0.00	0.00	0.00	0.00	0.00	0.00	0.00	0.00	0.00	0.00	0.00
Ca	0.00	0.00	0.00	0.00	0.00	0.00	0.00	0.03	0.00	0.01	0.04	0.00	0.00	0.00	0.01	0.01	0.00	0.00	0.00	0.01	0.01
Na	0.01	0.01	0.01	0.01	0.00	0.00	0.00	0.00	0.00	0.02	0.02	0.00	0.01	0.01	0.00	0.01	0.00	0.02	0.01	0.01	0.02
K	0.02	0.04	0.01	0.00	0.00	0.00	0.00	0.04	0.01	0.00	0.02	0.02	0.01	0.04	0.01	0.02	0.01	0.03	0.01	0.01	0.01
Ba	0.00	0.00	0.00	0.00	0.00	0.00	0.00	0.00	0.00	0.00	0.00	0.00	0.00	0.00	0.00	0.00	0.00	0.00	0.00	0.00	0.00
V	0.00	0.01	0.01	0.00	0.01	0.00	0.02	0.01	0.00	0.00	0.00	0.01	0.00	0.01	0.01	0.00	0.00	0.00	0.01	0.00	0.00
Ni	0.18	0.16	0.18	0.06	0.06	0.07	0.05	0.10	0.08	0.09	0.09	0.12	0.10	0.07	0.08	0.11	0.07	0.06	0.06	0.05	0.05
F	0.08	0.04	0.02	0.04	0.01	0.05	0.04	0.04	0.00	0.03	0.00	0.01	0.01	0.01	0.00	0.01	0.00	0.00	0.00	0.00	0.07
Cl	0.01	0.00	0.02	0.01	0.01	0.02	0.01	0.01	0.01	0.01	0.02	0.02	0.01	0.01	0.00	0.02	0.01	0.01	0.01	0.01	0.02
OH	15.91	15.96	15.97	15.95	15.98	15.93	15.95	15.95	15.99	15.96	15.98	15.97	15.99	15.98	16.00	15.98	15.99	15.99	15.99	15.99	15.92
Cations	19.97	19.88	19.96	20.16	20.02	19.98	20.13	20.10	20.03	20.11	20.06	20.05	20.07	20.07	20.09	19.99	19.99	20.07	20.05	20.09	20.17

Tabela 6A. (Cont). Resultados analíticos de microssonda em clorita.

Rock Type	Bt-Chl	Bt-Chl	Bt-Chl	Bt-Chl	Bt-Chl	Bt-Chl	Bt-Chl	Bt-Chl	Bt-Chl	Bt-Chl	Bt-Chl	Bt-Chl	Bt-Chl	Bt-Chl	Bt-Chl	Bt-Chl	Bt-Chl	Bt-Chl	Bt-Chl	Bt-Chl	Bt-Chl
Sample	MFO12	MFO12	MFO12	MFO12	MFO12	MFO16	MFO16	MFO16	MFO16	MFO16	MFO16	MFO16	MFO16	MFO16	MFO16	MFO16	MFO16	MFO16	MFO11	MFO11	MFO11
Analysis (wt%)	C2 chl 5	C2 chl 6	C2 chl 8	C2 chl 9	C2 chl 10	C1 chl 1.1	C1 chl 1.2	C1 chl 1.3	C4 chl 1	C4 chl 2	C4 chl 3	C4 chl 4	C4 chl 5	C4 chl 6	C4 chl 7	C4 chl 8	C4 chl 9	C4 chl 10	C1 chl 1	C1 chl 2	C1 chl 3
SiO2	26.98	27.85	27.75	27.13	27.54	26.23	26.91	28.36	26.89	26.43	26.74	27.19	26.75	26.81	27.29	26.64	26.99	26.68	27.39	27.01	27.13
TiO2	0.04	0.00	0.10	0.04	0.00	0.14	0.00	0.20	0.01	0.00	0.00	0.19	0.00	0.26	0.05	0.00	0.02	0.03	0.07	0.24	0.00
Al2O3	19.24	19.38	19.22	19.68	19.16	19.19	19.31	16.28	19.62	19.24	18.95	19.05	18.56	20.20	19.56	18.99	19.24	19.14	19.62	19.30	18.97
Cr2O3	0.00	0.00	0.00	0.00	0.00	0.03	0.01	0.00	0.02	0.11	0.00	0.00	0.00	0.01	0.07	0.01	0.00	0.02	0.09	0.00	0.05
FeO	21.22	18.53	19.18	19.19	19.04	21.83	21.09	24.26	21.21	23.35	22.13	21.16	24.05	19.79	21.44	23.15	22.65	22.79	19.47	19.49	20.71
MnO	0.00	0.08	0.14	0.08	0.00	0.12	0.12	0.05	0.00	0.00	0.07	0.00	0.16	0.08	0.11	0.05	0.03	0.00	0.10	0.12	0.03
MgO	19.83	21.67	21.50	20.86	20.86	17.99	18.71	16.10	18.94	17.37	18.23	17.89	16.44	20.06	18.79	17.38	17.74	18.02	20.25	20.19	19.42
BaO	0.02	0.03	0.00	0.03	0.00	0.00	0.08	0.00	0.00	0.01	0.05	0.00	0.00	0.00	0.00	0.08	0.00	0.03	0.03	0.01	0.10
CaO	0.00	0.02	0.06	0.00	0.02	0.03	0.04	0.09	0.07	0.03	0.06	0.03	0.00	0.00	0.00	0.02	0.03	0.02	0.01	0.00	0.00
Na2O	0.01	0.00	0.00	0.02	0.00	0.04	0.04	0.02	0.01	0.00	0.00	0.01	0.00	0.02	0.05	0.04	0.19	0.01	0.03	0.03	0.04
K2O	0.01	0.06	0.02	0.10	0.04	0.00	0.10	0.73	0.08	0.16	0.21	0.22	0.71	0.03	0.05	0.08	0.43	0.02	0.19	0.08	0.07
V2O3	0.00	0.00	0.00	0.00	0.01	0.01	0.06	0.00	0.01	0.01	0.00	0.00	0.00	0.00	0.00	0.01	0.07	0.01	0.06	0.00	0.04
NiO	0.31	0.31	0.32	0.34	0.22	0.42	0.34	0.65	0.25	0.28	0.29	0.31	0.28	0.30	0.32	0.43	0.34	0.49	0.33	0.37	0.32
F	0.00	0.07	0.02	0.09	0.05	0.00	0.00	0.04	0.00	0.04	0.00	0.00	0.00	0.00	0.00	0.00	0.13	0.06	0.00	0.00	0.06
Cl	0.03	0.01	0.04	0.03	0.05	0.04	0.05	0.09	0.05	0.02	0.08	0.04	0.11	0.02	0.06	0.03	0.11	0.02	0.02	0.02	0.06
Total	87.70	88.01	88.34	87.60	86.99	86.08	86.86	86.86	87.16	87.05	86.81	86.09	87.06	87.58	87.78	86.90	87.97	87.34	87.66	86.86	87.01
Number of cations per 28 oxygens																					
Si	5.57	5.65	5.63	5.56	5.67	5.56	5.62	6.06	5.59	5.58	5.62	5.72	5.69	5.50	5.63	5.62	5.64	5.59	5.61	5.59	5.65
Al (IV)	2.43	2.35	2.37	2.44	2.33	2.44	2.38	1.94	2.41	2.42	2.38	2.28	2.31	2.50	2.37	2.38	2.36	2.41	2.39	2.41	2.35
Al (VI)	2.25	2.28	2.22	2.32	2.31	2.34	2.37	2.16	2.39	2.36	2.32	2.44	2.34	2.38	2.39	2.35	2.38	2.32	2.34	2.29	2.31
Ti	0.01	0.00	0.02	0.01	0.00	0.02	0.00	0.03	0.00	0.00	0.00	0.03	0.00	0.04	0.01	0.00	0.00	0.00	0.01	0.04	0.00
Cr	0.00	0.00	0.00	0.00	0.00	0.01	0.00	0.00	0.00	0.02	0.00	0.00	0.00	0.00	0.01	0.00	0.00	0.00	0.01	0.00	0.01
Fe	3.66	3.14	3.25	3.29	3.28	3.87	3.68	4.33	3.69	4.12	3.89	3.72	4.28	3.39	3.70	4.09	3.96	4.00	3.33	3.37	3.61
Mn	0.00	0.01	0.02	0.01	0.00	0.02	0.02	0.01	0.00	0.00	0.01	0.00	0.03	0.01	0.02	0.01	0.01	0.00	0.02	0.02	0.01
Mg	6.10	6.55	6.50	6.38	6.40	5.68	5.82	5.13	5.87	5.46	5.72	5.61	5.21	6.13	5.78	5.47	5.53	5.63	6.18	6.23	6.03
Zn	0.00	0.00	0.00	0.00	0.00	0.00	0.00	0.00	0.00	0.00	0.00	0.00	0.00	0.00	0.00	0.00	0.00	0.00	0.00	0.00	0.00
Ca	0.00	0.00	0.01	0.00	0.00	0.01	0.01	0.02	0.02	0.01	0.01	0.01	0.00	0.00	0.00	0.00	0.01	0.00	0.00	0.00	0.00
Na	0.00	0.00	0.00	0.01	0.00	0.02	0.02	0.01	0.00	0.00	0.00	0.00	0.00	0.01	0.02	0.02	0.08	0.00	0.01	0.01	0.02
K	0.00	0.01	0.00	0.03	0.01	0.00	0.03	0.20	0.02	0.04	0.06	0.06	0.19	0.01	0.01	0.02	0.11	0.01	0.05	0.02	0.02
Ba	0.00	0.00	0.00	0.00	0.00	0.00	0.01	0.00	0.00	0.00	0.00	0.00	0.00	0.00	0.00	0.01	0.00	0.00	0.00	0.00	0.01
V	0.00	0.00	0.00	0.00	0.00	0.00	0.01	0.00	0.00	0.00	0.00	0.00	0.00	0.00	0.00	0.00	0.01	0.00	0.01	0.00	0.01
Ni	0.05	0.05	0.05	0.06	0.04	0.07	0.06	0.11	0.04	0.05	0.05	0.05	0.05	0.05	0.05	0.07	0.06	0.08	0.06	0.06	0.05
F	0.00	0.04	0.01	0.06	0.03	0.00	0.00	0.02	0.00	0.03	0.00	0.00	0.00	0.00	0.00	0.00	0.09	0.04	0.00	0.00	0.04
Cl	0.01	0.00	0.01	0.01	0.02	0.01	0.02	0.03	0.02	0.01	0.03	0.01	0.04	0.01	0.02	0.01	0.04	0.01	0.01	0.01	0.02
OH	15.99	15.95	15.98	15.93	15.95	15.99	15.98	15.94	15.98	15.96	15.97	15.99	15.96	15.99	15.98	15.99	15.88	15.95	15.99	15.99	15.94
Cations	20.10	20.11	20.10	20.17	20.09	20.05	20.05	20.05	20.05	20.10	20.10	19.94	20.14	20.04	20.02	20.05	20.26	20.11	20.04	20.05	20.12

Tabela 6A. (Cont). Resultados analíticos de microssonda em clorita.

Rock Type	Bt-Chl	Bt-Chl	Bt-Chl	Bt-Chl	Mag	Mag	Mag	Mag	Mag	Mag	Mag	Mag	Mag	Mag	Mag	Mag	Mag	Mag	Mag	Mag	Mag
Sample	MFO11	MFO11	MFO11	MFO11	MFO10	MFO10	MFO10	MFO10	MFO10	MFO10	MFO10	MFO13	MFO13	MFO13	MFO14	MFO14	MFO14	MFO14	MFO29	MFO29	MFO29
Analysis (wt%)	C1 chl4	C1 chl5	C2 chl1.1	C2 chl1.2	C1 chl1	C1 chl3	C2 chl1	C2 chl2	C2 chl3	C2 chl4	C2 chl5	C3 chl1	C3 chl2	C3 chl3	C1 chl1	C1 chl2	C1 chl3	C1 chl4	C2 chl1.1	C2 chl1.2	C2 chl1.3
SiO2	26.67	27.55	28.00	26.88	27.24	26.84	26.67	27.03	26.75	26.97	26.31	27.77	27.99	28.06	27.34	27.52	27.79	27.58	31.26	31.78	31.48
TiO2	0.00	0.13	0.16	0.00	0.21	0.18	0.02	0.00	0.11	0.00	0.11	0.12	0.00	0.00	0.23	0.00	0.24	0.10	0.00	0.25	0.00
Al2O3	18.55	18.43	18.96	18.71	19.26	18.87	18.91	19.62	19.45	19.95	20.12	17.93	18.06	17.76	19.01	19.54	18.02	19.44	11.16	11.03	11.75
Cr2O3	0.04	0.04	0.02	0.00	0.00	0.02	0.04	0.00	0.00	0.00	0.00	0.10	0.00	0.00	0.00	0.00	0.00	0.00	0.16	0.00	0.08
FeO	16.46	20.43	19.56	20.16	22.82	22.99	21.67	20.28	20.95	20.90	19.88	20.80	18.31	18.48	18.47	18.36	20.36	18.46	24.38	23.51	23.75
MnO	0.02	0.09	0.12	0.09	0.07	0.04	0.04	0.13	0.10	0.10	0.11	0.06	0.00	0.07	0.01	0.01	0.03	0.02	0.08	0.05	0.08
MgO	21.30	19.97	20.34	20.17	17.49	17.68	18.32	19.61	18.68	19.53	18.81	19.36	21.02	21.28	20.85	21.14	20.23	21.18	19.03	19.70	19.18
BaO	0.00	0.00	0.00	0.00	0.08	0.00	0.00	0.00	0.00	0.00	0.00	0.04	0.07	0.07	0.05	0.00	0.01	0.04	0.00	0.00	0.13
CaO	0.00	0.00	0.04	0.00	0.02	0.00	0.01	0.03	0.02	0.00	0.03	0.03	0.01	0.03	0.01	0.00	0.00	0.00	0.13	0.13	0.10
Na2O	0.00	0.00	0.01	0.00	0.03	0.03	0.04	0.00	0.00	0.00	0.03	0.00	0.00	0.02	0.01	0.00	0.00	0.01	0.00	0.00	0.01
K2O	0.03	0.09	0.04	0.00	0.03	0.02	0.05	0.01	0.01	0.00	0.03	0.04	0.04	0.04	0.00	0.02	0.02	0.00	0.03	0.03	0.04
V2O3	0.01	0.00	0.07	0.08	0.01	0.07	0.01	0.04	0.07	0.00	0.01	0.01	0.05	0.02	0.00	0.06	0.10	0.04	0.03	0.02	0.01
NiO	0.37	0.42	0.23	0.40	0.38	0.24	0.34	0.37	0.34	0.29	0.37	0.30	0.49	0.33	0.36	0.46	0.38	0.39	0.34	0.35	0.35
F	0.02	0.08	0.02	0.10	0.06	0.14	0.00	0.03	0.08	0.00	0.00	0.00	0.03	0.13	0.11	0.02	0.07	0.00	0.08	0.08	0.08
Cl	0.03	0.02	0.02	0.04	0.04	0.04	0.04	0.04	0.02	0.03	0.03	0.05	0.02	0.00	0.04	0.03	0.05	0.04	0.01	0.02	0.02
Total	83.50	87.25	87.59	86.63	87.75	87.16	86.16	87.19	86.57	87.77	85.83	86.62	86.08	86.29	86.50	87.15	87.31	87.30	86.68	86.97	87.06
Number of cations per 28 oxygens																					
Si	5.66	5.71	5.73	5.61	5.68	5.65	5.63	5.59	5.60	5.55	5.52	5.80	5.81	5.82	5.66	5.63	5.75	5.63	6.65	6.70	6.64
Al (IV)	2.34	2.29	2.27	2.39	2.32	2.35	2.37	2.41	2.40	2.45	2.48	2.20	2.19	2.18	2.34	2.37	2.25	2.37	1.35	1.30	1.36
Al (VI)	2.30	2.21	2.30	2.22	2.41	2.33	2.33	2.37	2.40	2.39	2.49	2.21	2.22	2.17	2.30	2.34	2.15	2.31	1.45	1.44	1.56
Ti	0.00	0.02	0.02	0.00	0.03	0.03	0.00	0.00	0.02	0.00	0.02	0.02	0.00	0.00	0.04	0.00	0.04	0.02	0.00	0.04	0.00
Cr	0.01	0.01	0.00	0.00	0.00	0.00	0.01	0.00	0.00	0.00	0.00	0.02	0.00	0.00	0.00	0.00	0.00	0.00	0.03	0.00	0.01
Fe	2.92	3.54	3.35	3.52	3.98	4.05	3.83	3.51	3.67	3.60	3.49	3.63	3.18	3.21	3.20	3.14	3.52	3.15	4.34	4.14	4.19
Mn	0.00	0.02	0.02	0.02	0.01	0.01	0.01	0.02	0.02	0.02	0.02	0.01	0.00	0.01	0.00	0.00	0.01	0.00	0.01	0.01	0.01
Mg	6.74	6.17	6.20	6.28	5.43	5.55	5.77	6.05	5.83	5.99	5.88	6.03	6.50	6.58	6.43	6.45	6.24	6.45	6.04	6.19	6.03
Zn	0.00	0.00	0.00	0.00	0.00	0.00	0.00	0.00	0.00	0.00	0.00	0.00	0.00	0.00	0.00	0.00	0.00	0.00	0.00	0.00	0.00
Ca	0.00	0.00	0.01	0.00	0.00	0.00	0.00	0.01	0.00	0.00	0.01	0.01	0.00	0.01	0.00	0.00	0.00	0.00	0.03	0.03	0.02
Na	0.00	0.00	0.00	0.00	0.01	0.01	0.02	0.00	0.00	0.00	0.01	0.00	0.00	0.01	0.00	0.00	0.00	0.00	0.00	0.00	0.00
K	0.01	0.02	0.01	0.00	0.01	0.00	0.01	0.00	0.00	0.00	0.01	0.01	0.01	0.01	0.00	0.00	0.01	0.00	0.01	0.01	0.01
Ba	0.00	0.00	0.00	0.00	0.01	0.00	0.00	0.00	0.00	0.00	0.00	0.00	0.01	0.01	0.00	0.00	0.00	0.00	0.00	0.00	0.01
V	0.00	0.00	0.01	0.01	0.00	0.01	0.00	0.01	0.01	0.00	0.00	0.00	0.01	0.00	0.00	0.01	0.02	0.01	0.00	0.00	0.00
Ni	0.06	0.07	0.04	0.07	0.06	0.04	0.06	0.06	0.06	0.05	0.06	0.05	0.08	0.06	0.06	0.08	0.06	0.06	0.06	0.06	0.06
F	0.01	0.05	0.01	0.07	0.04	0.09	0.00	0.02	0.05	0.00	0.00	0.00	0.02	0.09	0.07	0.01	0.05	0.00	0.05	0.06	0.05
Cl	0.01	0.01	0.01	0.01	0.01	0.01	0.02	0.02	0.01	0.01	0.01	0.02	0.01	0.00	0.02	0.01	0.02	0.01	0.00	0.01	0.01
OH	15.98	15.94	15.98	15.92	15.94	15.89	15.98	15.97	15.94	15.99	15.99	15.98	15.97	15.91	15.91	15.98	15.93	15.99	15.94	15.94	15.94
Cations	20.06	20.12	19.99	20.20	20.02	20.14	20.05	20.06	20.07	20.05	20.00	20.00	20.03	20.15	20.12	20.05	20.11	20.03	20.02	19.99	19.98

Tabela 6A. (Cont). Resultados analíticos de microssonda em clorita.

Rock Type	Mag	Mag	Mag	Mag	Mag	Mag	FSV	FSV	FSV	FSV	GRN	GRN	GRN	GRN	GRN	GRN	GRN	GRN	GRN	GRN	GRN	Mag
Sample	MFO29	MFO29	MFO29	MFO29	MFO29	MFO26	MFO08	MFO08	MFO08	MFO08	MFO20	MFO20	MFO20	MFO20	MFO20	MFO20	MFO20	MFO20	MFO22	MFO22	MFO22	MFO25
Analysis (wt%)	C2 chl2	C2 chl3	C2 chl4	C2 chl5	C2 chl6	C2 chl2	C2 chl2	C2 chl3	C2 chl4	C2 chl5	C1 chl1.1	C1 chl1.3	C1 chl2.1	C1 chl2.2	C1 chl2.3	C1 chl3.1	C1 chl3.2	C1 chl3.3	C1 chl1	C1 chl2	C1 chl3	C2 anf1
SiO2	32.34	28.78	28.09	29.01	31.24	27.85	22.49	22.35	21.49	22.92	23.55	23.01	23.45	23.49	24.03	23.57	23.64	23.42	25.97	25.71	25.20	28.38
TiO2	0.10	0.04	0.14	0.02	0.17	0.20	0.25	0.09	0.06	0.47	0.21	0.00	0.00	0.12	0.00	0.00	0.03	0.00	0.11	0.07	0.30	0.00
Al2O3	12.46	18.39	20.30	17.94	13.96	19.56	19.81	20.60	19.84	19.36	20.82	21.99	20.37	22.13	21.78	21.02	22.11	22.22	17.01	16.78	17.43	19.52
Cr2O3	0.02	0.08	0.00	0.03	0.12	0.00	0.03	0.00	0.00	0.15	0.02	0.00	0.02	0.00	0.00	0.00	0.00	0.00	0.28	0.29	0.24	0.00
FeO	16.99	14.33	13.29	13.91	15.28	14.89	27.25	27.76	27.30	26.87	17.55	18.03	18.43	18.90	17.81	17.43	17.88	17.52	23.50	24.00	25.09	12.27
MnO	0.03	0.06	0.07	0.00	0.18	0.04	0.08	0.15	0.05	0.03	0.03	0.04	0.08	0.07	0.08	0.05	0.07	0.04	0.01	0.00	0.07	0.06
MgO	24.09	24.14	24.63	24.69	24.03	23.26	13.91	13.68	14.32	13.59	21.06	21.39	20.48	21.19	21.90	21.13	21.56	20.98	18.50	18.82	16.40	24.95
BaO	0.00	0.00	0.00	0.00	0.03	0.01	0.00	0.00	0.00	0.14	0.00	0.00	0.00	0.00	0.00	0.00	0.00	0.00	0.02	0.03	0.00	0.00
CaO	0.14	0.09	0.00	0.18	0.22	0.02	0.00	0.01	0.00	0.01	0.06	0.02	0.06	0.00	0.00	0.07	0.03	0.01	0.04	0.02	0.09	0.04
Na2O	0.02	0.03	0.00	0.03	0.04	0.03	0.06	0.00	0.01	0.03	0.06	0.00	0.06	0.01	0.03	0.05	0.03	0.04	0.00	0.01	0.00	0.04
K2O	0.03	0.02	0.01	0.02	0.03	0.00	0.27	0.04	0.07	1.07	0.06	0.01	0.02	0.06	0.01	0.02	0.01	0.05	0.18	0.07	0.20	0.00
V2O3	0.03	0.07	0.03	0.07	0.04	0.00	0.03	0.01	0.00	0.09	0.00	0.03	0.00	0.03	0.00	0.04	0.02	0.07	0.04	0.04	0.00	0.04
NiO	0.22	0.40	0.32	0.36	0.32	0.53	0.16	0.16	0.18	0.16	0.07	0.10	0.14	0.06	0.05	0.08	0.15	0.14	0.12	0.10	0.07	0.54
F	0.11	0.01	0.00	0.00	0.08	0.01	0.10	0.00	0.00	0.00	0.00	0.02	0.02	0.00	0.00	0.00	0.00	0.00	0.11	0.14	0.11	0.06
Cl	0.00	0.00	0.04	0.01	0.00	0.03	0.04	0.07	0.05	0.07	0.06	0.03	0.06	0.01	0.04	0.05	0.03	0.04	0.01	0.02	0.01	0.03
Total	86.59	86.44	86.91	86.27	85.74	86.42	84.47	84.93	83.37	84.95	83.54	84.68	83.18	86.07	85.74	83.50	85.55	84.53	85.90	86.09	85.21	85.93
Number of cations per 28 oxygens																						
Si	6.60	5.81	5.60	5.85	6.39	5.64	5.07	5.00	4.91	5.15	5.05	4.88	5.09	4.91	5.01	5.05	4.95	4.96	5.60	5.55	5.53	5.71
Al (IV)	1.40	2.19	2.40	2.15	1.61	2.36	2.93	3.00	3.09	2.85	2.95	3.12	2.91	3.09	2.99	2.95	3.05	3.04	2.40	2.45	2.47	2.29
Al (VI)	1.59	2.18	2.37	2.11	1.76	2.31	2.33	2.44	2.25	2.27	2.32	2.38	2.29	2.37	2.37	2.36	2.40	2.50	1.92	1.82	2.04	2.33
Ti	0.02	0.01	0.02	0.00	0.03	0.03	0.04	0.02	0.01	0.08	0.03	0.00	0.00	0.02	0.00	0.00	0.00	0.00	0.02	0.01	0.05	0.00
Cr	0.00	0.01	0.00	0.01	0.02	0.00	0.01	0.00	0.00	0.03	0.00	0.00	0.00	0.00	0.00	0.00	0.00	0.00	0.05	0.05	0.04	0.00
Fe	2.90	2.42	2.22	2.35	2.62	2.52	5.14	5.20	5.22	5.05	3.15	3.20	3.34	3.31	3.11	3.12	3.13	3.10	4.24	4.34	4.61	2.06
Mn	0.01	0.01	0.01	0.00	0.03	0.01	0.02	0.03	0.01	0.01	0.01	0.01	0.01	0.01	0.01	0.01	0.01	0.01	0.00	0.00	0.01	0.01
Mg	7.33	7.26	7.32	7.42	7.33	7.03	4.67	4.56	4.88	4.55	6.74	6.77	6.62	6.61	6.81	6.75	6.73	6.62	5.95	6.06	5.37	7.48
Zn	0.00	0.00	0.00	0.00	0.00	0.00	0.00	0.00	0.00	0.00	0.00	0.00	0.00	0.00	0.00	0.00	0.00	0.00	0.00	0.00	0.00	0.00
Ca	0.03	0.02	0.00	0.04	0.05	0.00	0.00	0.00	0.00	0.00	0.01	0.00	0.01	0.00	0.00	0.02	0.01	0.00	0.01	0.00	0.02	0.01
Na	0.01	0.01	0.00	0.01	0.02	0.01	0.03	0.00	0.00	0.01	0.02	0.00	0.03	0.00	0.01	0.02	0.01	0.02	0.00	0.00	0.00	0.02
K	0.01	0.01	0.00	0.00	0.01	0.00	0.08	0.01	0.02	0.31	0.02	0.00	0.01	0.02	0.00	0.01	0.00	0.01	0.05	0.02	0.06	0.00
Ba	0.00	0.00	0.00	0.00	0.00	0.00	0.00	0.00	0.00	0.01	0.00	0.00	0.00	0.00	0.00	0.00	0.00	0.00	0.00	0.00	0.00	0.00
V	0.01	0.01	0.01	0.01	0.01	0.00	0.00	0.00	0.00	0.02	0.00	0.00	0.00	0.01	0.00	0.01	0.00	0.01	0.01	0.01	0.00	0.01
Ni	0.04	0.07	0.05	0.06	0.05	0.09	0.03	0.03	0.03	0.03	0.01	0.02	0.02	0.01	0.01	0.01	0.02	0.02	0.02	0.02	0.01	0.09
F	0.07	0.00	0.00	0.00	0.05	0.00	0.07	0.00	0.00	0.00	0.00	0.02	0.01	0.00	0.00	0.00	0.00	0.00	0.07	0.09	0.07	0.04
Cl	0.00	0.00	0.01	0.00	0.00	0.01	0.01	0.03	0.02	0.02	0.02	0.01	0.02	0.00	0.01	0.02	0.01	0.01	0.00	0.01	0.00	0.01
OH	15.93	16.00	15.99	16.00	15.95	15.99	15.92	15.97	15.98	15.98	15.98	15.97	15.97	16.00	15.99	15.98	15.99	15.99	15.92	15.90	15.92	15.95
Cations	20.00	20.01	20.01	20.02	19.97	20.02	20.43	20.31	20.45	20.39	20.33	20.41	20.38	20.35	20.34	20.33	20.34	20.30	20.34	20.44	20.29	20.05

Tabela 6A. (Cont). Resultados analíticos de microssonda em clorita.

Rock Type	GRN	GRN	GRN	GRN	GRN	GRN	Bt-Chl	Bt-Chl	Bt-Chl	Bt-Chl	Bt-Chl	Bt-Chl	Bt-Chl	Bt-Chl	Bt-Chl	Bt-Chl	Bt-Chl	Bt-Chl	Bt-Chl	Bt-Chl	Bt-Chl
Sample	MFO22	MFO22	MFO22	MFO22	MFO22	MFO22	MFO27	MFO27	MFO27	MFO27	MFO31	MFO31	MFO31	MFO31	MFO31	MFO31	MFO31	MFO31	MFO31	MFO31	MFO31
Analysis (wt%)	C1_chl4	C1_chl5	C2_chl1	C2_chl2	C2_chl3	C2_chl4	C3_chl4	C2_chl5	C2_chl6	C2_chl7	C1_chl1.1	C1_chl2.2	C1_chl2.1	C1_chl2.2	C3_chl1.1	C3_chl1.2	C3_chl1.3	C3_chl2.1	C3_chl2.2	C3_chl2.3	C4_chl1.1	C4_chl1.2
SiO2	25.56	26.69	25.30	25.96	26.80	26.60	26.75	26.30	26.62	26.69	26.99	26.68	27.08	27.32	27.06	26.61	27.40	26.29	26.45	27.20	27.31	26.72
TiO2	0.00	0.06	0.21	0.08	0.12	0.01	0.00	0.24	0.20	0.19	0.07	0.09	0.07	0.08	0.23	0.13	0.09	0.25	0.05	0.00	0.13	0.19
Al2O3	16.91	17.22	18.48	17.11	17.28	17.65	21.06	21.52	22.02	19.16	20.71	20.92	20.63	20.48	20.60	20.79	19.91	19.97	20.21	21.07	20.69	20.69
Cr2O3	0.64	0.51	0.33	0.50	0.45	0.74	0.00	0.04	0.01	0.00	0.05	0.04	0.07	0.13	0.08	0.10	0.00	0.20	0.00	0.00	0.00	0.11
FeO	23.14	22.80	23.36	24.21	23.38	24.48	17.55	16.96	17.44	18.48	16.31	16.30	16.86	16.59	16.72	16.43	17.89	16.03	16.29	16.61	16.09	15.81
MnO	0.08	0.00	0.00	0.00	0.07	0.00	0.21	0.06	0.02	0.07	0.09	0.11	0.20	0.20	0.05	0.00	0.14	0.17	0.12	0.12	0.09	0.10
MgO	18.93	19.19	18.33	19.23	19.06	17.07	22.48	21.59	21.81	20.98	22.29	22.48	22.35	22.16	21.85	22.15	21.57	20.58	22.21	22.06	22.58	22.40
BaO	0.00	0.04	0.00	0.03	0.05	0.04	0.00	0.00	0.00	0.00	0.05	0.00	0.00	0.00	0.03	0.00	0.05	0.02	0.08	0.04	0.00	0.07
CaO	0.04	0.03	0.10	0.03	0.02	0.13	0.00	0.01	0.00	0.02	0.05	0.01	0.04	0.01	0.02	0.00	0.02	0.03	0.02	0.00	0.00	0.00
Na2O	0.03	0.02	0.01	0.00	0.00	0.05	0.01	0.00	0.03	0.01	0.03	0.02	0.01	0.00	0.01	0.05	0.01	0.02	0.00	0.00	0.01	0.00
K2O	0.04	0.24	0.07	0.04	0.04	0.05	0.06	0.01	0.02	0.03	0.02	0.01	0.01	0.03	0.00	0.03	0.02	0.18	0.02	0.01	0.00	0.00
V2O3	0.06	0.00	0.01	0.00	0.07	0.05	0.08	0.04	0.07	0.09	0.04	0.02	0.03	0.04	0.01	0.00	0.03	0.00	0.04	0.00	0.00	0.00
NiO	0.11	0.20	0.07	0.10	0.17	0.14	0.13	0.06	0.06	0.08	0.18	0.16	0.19	0.22	0.37	0.32	0.37	0.26	0.16	0.23	0.26	0.22
F	0.07	0.28	0.08	0.12	0.19	0.16	0.06	0.04	0.03	0.05	0.00	0.00	0.01	0.00	0.00	0.00	0.00	0.00	0.00	0.00	0.08	0.00
Cl	0.02	0.03	0.01	0.00	0.02	0.00	0.02	0.02	0.02	0.04	0.01	0.04	0.03	0.02	0.05	0.07	0.03	0.04	0.03	0.03	0.02	0.02
Total	85.62	87.31	86.35	87.41	87.72	87.15	88.41	86.88	88.34	85.90	86.89	86.87	87.58	87.27	87.08	86.69	87.53	84.03	85.67	87.37	87.26	86.32
Number of cations per 28 oxygens																						
Si	5.53	5.66	5.41	5.52	5.65	5.67	5.38	5.36	5.34	5.56	5.48	5.42	5.47	5.53	5.50	5.43	5.57	5.53	5.46	5.49	5.51	5.45
Al (IV)	2.47	2.34	2.59	2.48	2.35	2.33	2.62	2.64	2.66	2.44	2.52	2.58	2.53	2.47	2.50	2.57	2.43	2.47	2.54	2.51	2.49	2.55
Al (VI)	1.83	1.96	2.07	1.80	1.94	2.10	2.37	2.52	2.54	2.26	2.43	2.42	2.38	2.41	2.43	2.42	2.34	2.48	2.37	2.50	2.44	2.42
Ti	0.00	0.01	0.03	0.01	0.02	0.00	0.00	0.04	0.03	0.03	0.01	0.01	0.01	0.01	0.04	0.02	0.01	0.04	0.01	0.00	0.02	0.03
Cr	0.11	0.09	0.05	0.08	0.08	0.12	0.00	0.01	0.00	0.00	0.01	0.01	0.01	0.02	0.01	0.02	0.00	0.03	0.00	0.00	0.00	0.02
Fe	4.18	4.04	4.18	4.30	4.12	4.36	2.95	2.89	2.92	3.22	2.77	2.77	2.85	2.81	2.84	2.80	3.04	2.82	2.81	2.80	2.72	2.70
Mn	0.01	0.00	0.00	0.00	0.01	0.00	0.04	0.01	0.00	0.01	0.02	0.02	0.03	0.03	0.01	0.00	0.02	0.03	0.02	0.02	0.02	0.02
Mg	6.10	6.06	5.84	6.09	5.99	5.42	6.74	6.55	6.52	6.51	6.74	6.80	6.73	6.68	6.62	6.73	6.54	6.46	6.83	6.64	6.80	6.81
Zn	0.00	0.00	0.00	0.00	0.00	0.00	0.00	0.00	0.00	0.00	0.00	0.00	0.00	0.00	0.00	0.00	0.00	0.00	0.00	0.00	0.00	0.00
Ca	0.01	0.01	0.02	0.01	0.00	0.03	0.00	0.00	0.00	0.00	0.01	0.00	0.01	0.00	0.00	0.00	0.00	0.01	0.00	0.00	0.00	0.00
Na	0.01	0.01	0.00	0.00	0.00	0.02	0.00	0.00	0.01	0.00	0.01	0.01	0.00	0.00	0.00	0.02	0.00	0.01	0.00	0.00	0.00	0.00
K	0.01	0.06	0.02	0.01	0.01	0.01	0.02	0.00	0.01	0.01	0.00	0.00	0.00	0.01	0.00	0.01	0.00	0.05	0.00	0.00	0.00	0.00
Ba	0.00	0.00	0.00	0.00	0.00	0.00	0.00	0.00	0.00	0.00	0.00	0.00	0.00	0.00	0.00	0.00	0.00	0.00	0.01	0.00	0.00	0.01
V	0.01	0.00	0.00	0.00	0.01	0.01	0.01	0.01	0.01	0.02	0.01	0.00	0.00	0.01	0.00	0.00	0.00	0.00	0.01	0.00	0.00	0.00
Ni	0.02	0.03	0.01	0.02	0.03	0.02	0.02	0.01	0.01	0.01	0.03	0.03	0.03	0.04	0.06	0.05	0.06	0.04	0.03	0.04	0.04	0.04
F	0.05	0.19	0.05	0.08	0.13	0.11	0.04	0.02	0.02	0.03	0.00	0.00	0.01	0.00	0.00	0.00	0.00	0.00	0.00	0.00	0.05	0.00
Cl	0.01	0.01	0.01	0.00	0.01	0.00	0.01	0.01	0.01	0.01	0.00	0.01	0.01	0.01	0.02	0.02	0.01	0.01	0.01	0.01	0.01	0.01
OH	15.94	15.80	15.94	15.92	15.87	15.89	15.96	15.97	15.98	15.95	16.00	15.99	15.98	15.99	15.98	15.98	15.99	15.99	15.99	15.99	15.94	15.99
Cations	20.36	20.47	20.30	20.42	20.35	20.22	20.19	20.07	20.07	20.13	20.04	20.09	20.08	20.02	20.03	20.10	20.05	19.98	20.10	20.02	20.09	20.04

Tabela 6A. (Cont). Resultados analíticos de microssonda em clorita.

Rock Type	Bt-Chl	Bt-Chl	Bt-Chl	Bt-Chl	Bt-Chl	Bt-Chl	Bt-Chl	Bt-Chl	Bt-Chl	Bt-Chl	Bt-Chl	Bt-Chl	Bt-Chl	Bt-Chl	Bt-Chl	Bt-Chl	Bt-Chl	Bt-Chl	Bt-Chl	Bt-Chl	Bt-Chl	Bt-Chl
Sample	MFO31	MFO31	MFO31	MFO31	MFO23	MFO23	MFO23	MFO23	MFO23	MFO23	MFO23	MFO23	MFO23	MFO27	MFO27	MFO27	MFO27	MFO27	MFO27	MFO27	MFO27	MFO27
Analysis (wt%)	C4 chl 1.3	C4 chl 2.1	C4 chl 2.2	C4 chl 2.3	C4 chl 1	C4 chl 2	C4 chl 3	C4 chl 4	C3 chl 1.1	C3 chl 1.2	C1 chl 1	C1 chl 2	C1 chl 3	C1 chl 1	C1 chl 2	C1 chl 3	C1 chl 4	C2 chl 1	C2 chl 3	C2 chl 4	C3 chl 1	C3 chl 2	C3 chl 3
SiO2	27.03	26.70	27.17	27.04	26.68	26.57	25.91	27.62	26.60	26.12	26.79	25.83	26.08	25.96	26.12	25.85	25.74	26.30	27.40	26.34	26.66	26.66	26.42
TiO2	0.00	0.17	0.31	0.00	0.00	0.00	0.02	0.12	0.04	0.15	0.04	0.15	0.23	0.32	0.03	0.19	0.11	0.00	0.28	0.12	0.06	0.07	0.17
Al2O3	20.99	20.76	20.23	20.73	21.07	20.04	20.51	19.09	21.02	20.44	19.38	20.64	20.25	19.83	20.37	20.24	20.53	20.69	19.04	20.29	20.52	20.67	20.28
Cr2O3	0.00	0.06	0.07	0.01	0.05	0.01	0.06	0.00	0.02	0.02	0.07	0.00	0.00	0.00	0.03	0.00	0.06	0.00	0.00	0.03	0.00	0.04	0.00
FeO	16.05	17.13	16.28	16.48	17.85	17.49	18.10	17.21	17.95	17.93	17.64	17.87	17.68	17.46	16.95	16.89	16.95	16.98	16.20	17.35	17.05	17.21	16.86
MnO	0.10	0.08	0.11	0.12	0.04	0.14	0.17	0.07	0.08	0.08	0.05	0.18	0.06	0.02	0.00	0.09	0.13	0.04	0.00	0.10	0.01	0.09	0.10
MgO	23.02	21.98	22.05	22.97	20.98	21.16	20.43	22.32	21.17	21.15	21.76	20.52	20.37	20.80	21.16	21.01	21.34	21.20	22.07	21.05	21.72	21.58	21.82
BaO	0.00	0.00	0.00	0.00	0.06	0.00	0.00	0.05	0.00	0.10	0.00	0.00	0.05	0.01	0.00	0.17	0.08	0.00	0.00	0.00	0.10	0.00	0.00
CaO	0.03	0.03	0.02	0.03	0.00	0.00	0.01	0.03	0.00	0.00	0.00	0.03	0.01	0.01	0.02	0.02	0.03	0.02	0.03	0.02	0.02	0.00	0.01
Na2O	0.02	0.02	0.01	0.04	0.00	0.00	0.07	0.05	0.01	0.02	0.00	0.03	0.00	0.08	0.00	0.02	0.00	0.02	0.01	0.01	0.01	0.02	0.04
K2O	0.04	0.07	0.02	0.04	0.04	0.04	0.11	0.04	0.04	0.03	0.02	0.05	0.04	0.07	0.04	0.01	0.04	0.08	0.12	0.06	0.06	0.00	0.18
V2O3	0.04	0.04	0.00	0.06	0.00	0.01	0.00	0.04	0.00	0.00	0.01	0.05	0.02	0.05	0.08	0.03	0.02	0.07	0.09	0.06	0.08	0.07	0.04
NiO	0.18	0.26	0.11	0.15	0.34	0.22	0.27	0.27	0.15	0.18	0.25	0.19	0.12	0.03	0.01	0.04	0.05	0.10	0.01	0.09	0.09	0.06	0.07
F	0.00	0.00	0.00	0.03	0.11	0.18	0.01	0.10	0.10	0.09	0.12	0.04	0.11	0.01	0.04	0.03	0.00	0.05	0.13	0.04	0.07	0.02	0.00
Cl	0.03	0.01	0.03	0.03	0.02	0.06	0.05	0.08	0.02	0.04	0.07	0.05	0.04	0.06	0.04	0.02	0.04	0.02	0.02	0.07	0.01	0.04	0.04
Total	87.53	87.30	86.41	87.73	87.23	85.92	85.72	87.08	87.20	86.35	86.20	85.63	85.06	84.71	84.88	84.62	85.12	85.56	85.39	85.62	86.46	86.52	86.03
Number of Cations per 28 Oxygens																							
Si	5.44	5.42	5.54	5.44	5.45	5.52	5.41	5.64	5.43	5.41	5.55	5.39	5.47	5.46	5.45	5.43	5.37	5.45	5.67	5.47	5.47	5.46	5.44
Al (IV)	2.56	2.58	2.46	2.56	2.55	2.48	2.59	2.36	2.57	2.59	2.45	2.61	2.53	2.54	2.55	2.57	2.63	2.55	2.33	2.53	2.53	2.54	2.56
Al (VI)	2.41	2.39	2.40	2.36	2.53	2.43	2.45	2.24	2.49	2.39	2.28	2.46	2.48	2.37	2.47	2.43	2.42	2.50	2.31	2.44	2.43	2.45	2.37
Ti	0.00	0.03	0.05	0.00	0.00	0.00	0.00	0.02	0.01	0.02	0.01	0.02	0.04	0.05	0.00	0.03	0.02	0.00	0.04	0.02	0.01	0.01	0.03
Cr	0.00	0.01	0.01	0.00	0.01	0.00	0.01	0.00	0.00	0.00	0.01	0.00	0.00	0.00	0.00	0.00	0.01	0.00	0.00	0.00	0.00	0.01	0.00
Fe	2.70	2.91	2.78	2.77	3.05	3.04	3.16	2.94	3.07	3.10	3.06	3.12	3.10	3.07	2.96	2.96	2.96	2.94	2.80	3.01	2.93	2.95	2.91
Mn	0.02	0.01	0.02	0.02	0.01	0.02	0.03	0.01	0.01	0.01	0.01	0.03	0.01	0.00	0.00	0.02	0.02	0.01	0.00	0.02	0.00	0.02	0.02
Mg	6.90	6.65	6.70	6.89	6.39	6.56	6.35	6.80	6.45	6.53	6.72	6.38	6.37	6.52	6.59	6.57	6.64	6.55	6.81	6.52	6.64	6.59	6.70
Zn	0.00	0.00	0.00	0.00	0.00	0.00	0.00	0.00	0.00	0.00	0.00	0.00	0.00	0.00	0.00	0.00	0.00	0.00	0.00	0.00	0.00	0.00	0.00
Ca	0.01	0.01	0.00	0.01	0.00	0.00	0.00	0.01	0.00	0.00	0.00	0.01	0.00	0.00	0.00	0.00	0.01	0.00	0.01	0.00	0.00	0.00	0.00
Na	0.01	0.01	0.00	0.02	0.00	0.00	0.03	0.02	0.00	0.01	0.00	0.01	0.00	0.03	0.00	0.01	0.00	0.01	0.00	0.00	0.00	0.01	0.02
K	0.01	0.02	0.00	0.01	0.01	0.01	0.03	0.01	0.01	0.01	0.01	0.01	0.01	0.02	0.01	0.00	0.01	0.02	0.03	0.02	0.02	0.00	0.05
Ba	0.00	0.00	0.00	0.00	0.00	0.00	0.00	0.00	0.00	0.01	0.00	0.00	0.00	0.00	0.00	0.01	0.01	0.00	0.00	0.00	0.01	0.00	0.00
V	0.01	0.01	0.00	0.01	0.00	0.00	0.00	0.01	0.00	0.00	0.00	0.01	0.00	0.01	0.01	0.00	0.00	0.01	0.01	0.01	0.01	0.01	0.01
Ni	0.03	0.04	0.02	0.02	0.06	0.04	0.04	0.04	0.02	0.03	0.04	0.03	0.02	0.01	0.00	0.01	0.01	0.02	0.00	0.01	0.02	0.01	0.01
F	0.00	0.00	0.00	0.02	0.07	0.12	0.01	0.06	0.07	0.06	0.08	0.02	0.07	0.01	0.03	0.02	0.00	0.03	0.08	0.02	0.04	0.01	0.00
Cl	0.01	0.00	0.01	0.01	0.01	0.02	0.02	0.03	0.01	0.02	0.02	0.02	0.01	0.02	0.02	0.01	0.01	0.01	0.01	0.02	0.00	0.01	0.01
OH	15.99	16.00	15.99	15.97	15.92	15.86	15.97	15.91	15.93	15.92	15.89	15.96	15.91	15.97	15.96	15.97	15.99	15.96	15.91	15.95	15.95	15.98	15.99
Cations	20.10	20.08	20.00	20.15	20.13	20.24	20.13	20.19	20.14	20.20	20.23	20.12	20.13	20.10	20.10	20.09	20.11	20.09	20.11	20.11	20.11	20.07	20.12